Università degli Studi di Napoli Federico II

Dottorato di Ricerca in
Ingegneria Strutturale, Geotecnica e Rischio Sismico

THESIS FOR THE DEGREE OF DOCTOR OF PHILOSOPHY

Design procedure for Intermediate Isolation Systems (IIS): application for existing building retrofit

by

FRANCESCO ESPOSITO

Advisor: Prof. Elena Mele

Co-advisor: PhD, Diana Faiella

SCUOLA POLITECNICA E DELLE SCIENZE DI BASE
DIPARTIMENTO D STRUTTURE PER L'INGEGNERIA E L'ARCHITETTURA

To my family, Enzo, Gilda, Sissy and
to my girlfriend, Marika

Design procedure for Intermediate Isolation Systems (IIS): application for existing building retrofit

Ph.D. Thesis presented

for the fulfillment of the Degree of Doctor of Philosophy

in Ingegneria Strutturale, Geotecnica e Rischio Sismico

by

FRANCESCO ESPOSITO

March 2024

Approved as to style and content by

Prof. Elena Mele, Advisor

PhD, Diana Faiella, Co-advisor

Università degli Studi di Napoli Federico II

Ph.D. Program in Ingegneria Strutturale, Geotecnica e Rischio Sismico

XXXVI cycle - Chairman: Prof. Iunio Iervolino

www.dist.unina.it/dottorati-di-ricerca/dottorati

Candidate's declaration

I hereby declare that this thesis submitted to obtain the academic degree of Philosophiæ Doctor (Ph.D.) in Ingegneria Strutturale, Geotecnica e Rischio Sismico is my own unaided work, that have not used other than the sources indicated, and that all direct and indirect sources are acknowledged as references.

Parts of this dissertation have been published in international journals and/or conference proceedings (see list of the author's publications at the end of the thesis).

Napoli, March 09, 2024

Francesco Esposito

Abstract

In this thesis work, the vibration control strategy of intermediate isolation system (IIS) is investigated. Such system has special dynamic characteristics: the structure above the isolation system (US) can function as a huge mass damper for the structure below the isolation system (LS). Due to this type of dynamic behaviour, IIS has become very widespread and popular in Japan, where specific guidance for the design of buildings with IIS can be found in the national standards. On the other hand, in Europe, IIS is almost completely unknown, although it is an ideal solution when intervening on existing buildings located within major urban centres in medium or high seismic risk zones. In fact, IIS can be achieved by placing an isolated structure on the roof of existing buildings, thus simultaneously increasing the volume of the building, and reducing, or at most not increasing, the seismic demand in the existing building. Therefore, to facilitate the deployment and application of the IIS for the extension and seismic retrofitting of existing buildings, a detailed design procedure divided into 5-block is defined in this thesis. The key tool of the whole design procedure is the IIS design spectrum, derived by means of parametric response spectrum analysis (RSA), allows to predict the maximum seismic response of the lower structure (LS) as the isolation period varies. Thus, it allows to identify the design solution that maximises the mass-damping effect on the LS. The design procedure is first applied to a real case study for evaluating the effectiveness of IIS working as a nonconventional Tuned Mass Damper (TMD) for the existing construction and then applied to several case studies to verify the accuracy of the response prediction offered by the *IIS design spectra*. In the latter case, it is shown that the IIS design spectra can also be used when the existing building exhibits inelastic behaviour. However, in this case, a *stepwise procedure* should be followed, which leads to the definition of a so-called inelastic behaviour zone for IIS, bounded by two IIS design spectra. Finally, a closed-form relationship based on the application of the pole allocation method is proposed as an alternative to the parametric RSA for deriving the IIS design spectra.

Keywords: Intermediate Isolation System, mass damping, seismic retrofit, vertical extension, existing buildings, nonlinear behaviour.

Sintesi in lingua italiana

In questo lavoro di tesi viene studiata la strategia di controllo dell'isolamento a livello intermedio (IIS). Tale sistema presenta peculiari caratteristiche dinamiche, in quanto la struttura al di sopra del sistema di isolamento (US) può funzionare come un enorme smorzatore di massa per la struttura posta al di sotto del sistema di isolamento (LS). Grazie a questo tipo di comportamento dinamico l'IIS è diventato molto diffuso e popolare in Giappone, dove in ambito normativo è possibile trovare specifiche indicazioni per la progettazione di edifici con IIS. Di contro, in Europa l'IIS è quasi del tutto sconosciuto, pur essendo una soluzione ideale quando bisogna intervenire su edifici esistenti collocati all'interno di grandi centri urbani in aeree a medio o alto rischio sismico. Infatti, l'IIS può essere ottenuto collocando una struttura isolata sul tetto di un edificio esistente, riuscendo contemporaneamente ad incrementare il volume dell'edificio e ridurre, o al limite non aumentare, la domanda sismica sulla struttura esistente. Pertanto, al fine di facilitare la diffusione e l'applicazione dell'IIS per l'ampliamento e adeguamento sismico degli edifici esistenti, in questa tesi viene definita una dettagliata procedura di progetto articolata in cinque Blocchi. Strumento chiave dell'intera procedura di progetto è *lo spettro di progetto per IIS* che, ricavato attraverso analisi parametriche con spettro di risposta (RSA), consente di prevedere la risposta sismica massima della struttura inferiore (LS) al variare del periodo di isolamento, e quindi, di individuare la soluzione progettuale che massimizza l'effetto di smorzamento di massa sulla LS. L'intera procedura di progetto viene prima applicata ad un caso studio reale per valutare l'efficacia dell'IIS come smorzatore di massa accordato (TMD) non convenzionale per la costruzione esistente; successivamente viene applicata a diversi casi studio per testare l'affidabilità della previsione della risposta offerta dagli *spettri di progetto per IIS*. In particolare, in quest'ultimo caso si dimostra che *gli spettri di progetto per IIS* possono essere impiegati anche quando l'edificio esistente mostra un comportamento inelastico. In tal caso occorre seguire una procedura a cinque passi che porta alla definizione di una *zona di comportamento inelastico per IIS*, compresa tra due *spettri di progetto per IIS*. Infine, viene proposta una relazione in forma chiusa basata sull'applicazione del

metodo di allocazione dei poli come alternativa alla RSA parametrica per derivare lo spettro di progetto per IIS.

Parole chiave: Sistema con isolamento intermedio, smorzamento di massa, adeguamento sismico, sopraelevazione, edifici esistenti, comportamento non lineare.

Contents

Acknowledgements

I would like to express my gratitude to my tutor, Professor Elena Mele, for her support and encouragement throughout my PhD career. Her deep scientific knowledge and passion for research have been a valuable source of inspiration for my work.

I would also like to thank my co-tutor, Research Fellow Diana Faiella, for her constant help throughout these years of study and research; her support has been fundamental in deepening various aspects of the research topic.

I would also like to express my sincere gratitude to Professor Yoshiki Ikeda for hosting me at the Disaster Prevention Research Institute (DPRI) of Kyoto University and sharing with me his vast knowledge on structural design and vibration system control; the long discussions and days spent in his company have been a source of strong inspiration and motivation to continue and expand my scientific research.

I would further like to thank all the members of the Ikeda & Kurata laboratory who brightened my working days during my stay in Japan. I would like to make special mention of Professor Masahiro Kurata, who made me feel at home and shared insights for the future development of my research activities, and PhD candidate Kun-Sian Lin, who supported me in all laboratory activities and showing me fantastic places.

I would like to thank the “Programma di scambi internazionali tra l’Università degli Studi di Napoli Federico II ed Istituti di ricerca stranieri per la mobilità di breve durata di docenti, studiosi e ricercatori - DR/2020/2375 del 16/07/2020” for partially supporting my study period in Japan.

I am very grateful to Professor Iunio Iervolino, coordinator of the PhD course I attended, for his excellent organisation.

Furthermore, I want to thank the Department of Structures for Engineering and Architecture (DIST) of the Federico II University and all the people working here that I have met during these years. In particular, I want to thank the Professor, Giuseppe Brandonisio, Beatrice Faggiano and colleagues, Mario Argenziano, Dante

Marranzini, Giacomo Iovane, Giovanna Laura Guidi for their kind support.

I would like to thank my family for their encouragement and support.

Last but not least, I would like to sincerely thank my girlfriend, Marika, for her great patience in standing by me and always making me feel her support and approval. She has been an irrepressible source of motivation to complete this PhD course, giving me all her energy and determination to achieve my professional goals.

List of Acronyms

The following acronyms are used throughout the thesis.

3D IIS FEM Three Dimensional Finite Element Model for Intermediate Isolation System

3D Three Dimensional

3DOF IIS Three Degree Of Freedom Intermediate Isolation System

AS-IS Existing building in as is configuration

CBF Concentric Braced Frame

CFT Concrete Filled Tube

CQC Complete Quadratic Combination

DCR Demand to Capacity Ratio

$DMF_{ug,\ 2DOF\ BIS}$ Dynamic Magnification Factor for 2DOF BIS model under harmonic support excitation

$DMF_{ug,\ 2DOF\ IIS}$ Dynamic Magnification Factor for 2DOF IIS model under harmonic support excitation

$DMF_{ug,\ SDOF\ LS}$ Dynamic Magnification Factor for SDOF LS model under harmonic support excitation

$DMF_{FE,\ 2DOF\ IIS}$ Dynamic Magnification Factor for 2DOF IIS model under first mass force excitation

$DMF_{FE,\ SDOF\ LS}$ Dynamic Magnification Factor for SDOF LS model under first mass force excitation

DOF Degree Of Freedom

ESB Elastomeric Slider Bearings

FE Finite Element

FEM Finite Element Model

ff-3DOF IIS free-free 3DOF IIS model

GF	Ground Floor
HDRB	Hight Damping Rubber Bearing
IDA	Incremental Dynamic Analyses
***i*-IIS**	Inelastic Intermediate Isolation System
IIS	Intermediate Isolation System
ISO	Isolation
IT	Intervention Type
LD	Lead Dampers
L-DOF LS	fixed-base L-DOF lower structure
LS	Lower Structure
LTHA	Linear Time History Analysis
MD	Mass Damped structure
MDOF	Multi-Degree Of Freedom
MRF	Moment Resisting Frame
NDOF	N-Degree Of Freedom
NTHA	Non-linear Time History Analysis
PAM	Pole Allocation Method
PGA	Peak Ground Acceleration
RC	Reinforced Concrete
RSA	Response Spectrum Analysis
SD	Steel Damper
SDOF LS	Single Degree Of Freedom Lower Structure
SRC	Steel Reinforced Concrete
SW	Shear Wall
THA	Time History Analysis

TMD	Tuned Mass Damper
TOD	Transit Oriented Development
URM	UnReinforced Masonry
US	Upper Structure
US+ISO	Isolated vertical extension
U-SD	U-shaped Steel Dampers
VDW	Viscous Damping Wall

List of Figures

List of Tables

List of Symbols

The following symbols are used within the thesis

$\boldsymbol{0}$	zero-array matrix
$\boldsymbol{A}$	state matrix
A_f	floor area
A_{floors}	floor area
a_g	peak ground acceleration
$a_{g,0}$	reference peak ground acceleration
a_s	absolute acceleration
$\boldsymbol{b}$	input vector
b	shape factor for shear resistance of masonry wall
B_i, B_j	real-valued participation factors in complex modal analysis
$\tilde{c}_{LS}$	damping constant of equivalent SDOF LS
C_C	soil category coefficient
ce_{ij}	correlation effect of the phase difference between the mode *i* and *j*.
c_{LS}, c_{ISO}, c_{US}	damping coefficient of LS, ISO and US
c_{P0}, $c_{P\infty}$	damping coefficient of P_0 and P_∞ model
d_1 x d_2	maximum floor plan dimensions
E_h	cumulated hysteretic energy
E_i	seismic input energy
e_X, e_Y	eccentricity along X and Y direction between mass and stiffness centroids
F	shear force in the isolation device

F_0 dynamic spectral amplification

f_d compressive strength

F_E external force

f_i *i-th* frequency

f_{td} diagonal cracking tensile strength

f_{yd} design yield stress

f_{yk} characteristic yield stress

G mass centroid

G shear modulus of the elastomer

$G_{2DOF\ BIS}$ frequency response of 2DOF BIS model

$G_{2DOF\ IIS}$ frequency response of 2DOF IIS model

H building height

H_{ISO} height above ground level of the ISO system

$\boldsymbol{I}$ identical matrix

I isolation period ratio

L_X, L_Y external plan length along X and Y direction

$\tilde{k}_{ISO}$ equivalent stiffness of the isolation system in reduced single degree of freedom model

$\tilde{k}_{LS}$ equivalent stiffness of the lower structure in reduced single degree of freedom model for a real case study

$\tilde{k}_{US}$ equivalent stiffness of the upper structure in reduced single degree of freedom model

K stiffness ratio

k_1 initial stiffness in bilinear model of ISO

k_2 post-yield stiffness in bilinear model of ISO

k_{eff} effective secant stiffness in bilinear model of ISO

$\mathbf{K}_{ISO}$, $\mathbf{K}_{US}$ stiffness centroid of ISO and US

k_{ISO} global secant stiffness of ISO system

k_{LS}, k_{ISO}, k_{US} stiffness of LS, ISO and US

k_x, k_y, k_z shear stiffness values in x, y and z direction for two-joint linear links

l length of masonry wall

$\widetilde{M}_{ISO}$ equivalent mass of isolated vertical extension in reduced single degree of freedom model for a real case study

$\widetilde{m}_{ISO}$ equivalent mass of the isolation system in reduced single degree of freedom model

$\widetilde{m}_{LS}$ equivalent mass of the lower structure in reduced single degree of freedom model for a real case study

$\widetilde{m}_{US}$ equivalent mass of the upper structure in reduced single degree of freedom model

M bending moment

M_{ISO} mass of isolated vertical extension

$\boldsymbol{M}$, $\boldsymbol{K}$, $\boldsymbol{C}$ mass, stiffness and damping matrices

m_1, m_2, m_3 mass at first, second and third level

m_{LS}, m_{ISO}, m_{US} mass of LS, ISO and US

m_{P0}, $m_{P\infty}$ mass of P_0 and P_∞ model

n_{ef} number of extension floors

n_{floors} number of floors

n_{ISO} number of isolator

P'_0 limit point of $T_{ISO} \rightarrow 0$ for damaged LS

P'_∞ limit point of $T_{ISO} \rightarrow 0$ for damaged LS

P_0 limit point of $T_{ISO} \rightarrow 0$

P_∞ limit point of $T_{ISO} \rightarrow \infty$

Q characteristic strength in bilinear model of ISO

R maximum system response in complex modal analysis

R_i, R_j spectral displacements in complex modal analysis

R_m total mass ratio

S soil coefficient

S_a code spectral acceleration

ScF scaling factor

S_d spectral design displacement

T period

t thickness of masonry wall

T_1 fundamental period

T_B period at the start of constant spectral velocity range

T_C period at the start of constant spectral velocity range

T_C* period at the end of constant spectral velocity range for Soil Type A

T_{eq} equivalent reduced period of LS

$T_{eq,0}$ equivalent period of damaged LS at P'_0 limit point

$T_{eq,\infty}$ equivalent period of damaged LS at P'_∞ limit point

T_{LS}, T_{ISO}, T_{US} period of LS, ISO and US

T_r Higher mode coupling periods ratio

$\bar{u}_{3D}$ displacement ratio for 3D FEM

$\bar{u}$ displacement ratio

$\mathbf{u}$ state vector

u_{AB} displacement of Absorber in SDOF+TMD model

$u_{AS\text{-}IS}$ displacement of AS-IS in SDOF AS-IS model

$u_{AS\text{-}IS1}$, $u_{AS\text{-}IS2}$ displacement at first and second floor of 3D AS-IS FEM

u_g ground displacement

u_{ISO} displacement of ISO system in lumped mass IIS model

u_{LS} displacement of LS in lumped mass IIS model

u_{LS1}, u_{LS2} displacement at first and second floor of LS in 3D IIS FEM

u_{MS} displacement of Main System in SDOF+TMD model

u_{st} static displacement of the main mass in 2DOF+TMD model

u_{top} top building displacement

$u_{top,y}$ top building displacement at yielding

u_{US} displacement of US in 3DOF IIS model

U_x, U_y, R_z participating mass in X, Y and rotational direction

U_{LS}, U_{ISO}, U_{US} Laplace transformed displacement of LS, ISO and US

$\bar{v}$ base shear ratio

V shear in masonry walls

V_b base shear

V_y base shear strength

w unit structural weight

W seismic weight

$y_{AS\text{-}IS}$, y_{IIS} seismic response of AS-IS and IIS building

α_1, α_2, β_1, β_2, η_{Pivot} Pivot model parameters

α_s, α'_s	volume of the damper
β_h	higher mode coupling parameter
β_{ij}	ratio between the frequencies at modes *i* and *j*
Γ	participation mass ratio of reduced-order model
Δ	percentage change
$\bar{\bar{\delta}}_{ISO}$	average of peak displacements value of ISO system
δ_{ISO}	peak displacements value of ISO
$\delta_{ISO,u}$	ISO displacement demand
$\delta_{ISO,y}$	yield displacement in bilinear model of ISO
η_i	modal damping ratios at *i*-th mode
κ	BIS mass ratio
λ	forced frequency ratio for LS
λ_U	forced frequency ratio for US
λ_i	*i-th* complex eigenvalue
λ_i^*	*i*-th conjugate complex eigenvalue
λ_P, λ_P	forced frequency ratio at fixed point P and Q.
μ	mass ratio
ξ	spectral damping
ξ_1, ξ_2	first and second modal damping ratio
ξ_{AB}	absorber damping ratio
ξ_{LS}, ξ_{ISO}, ξ_{US}	damping ratio of LS, ISO and US
ξ_{LS}, ξ_{ISO}, ξ_{US},	damping ratio of LS, ISO and US
ρ_E	hysteretic adsorption ratio
$\rho_{ij,mod}$	real-valued modal correlation coefficients
σ_0	compression stress of masonry wall

$\boldsymbol{\Phi_i}$ *i-th* complex eigenvector

ω_{AB} natural circular frequency of absorber in SDOF+TMD model.

$\omega_{AB}, \omega_{ISO}, \omega_{US}$ natural circular frequency of equivalent single degree of freedom for LS, ISO and US.

ω_{MS} natural circular frequency of Main System in SDOF+TMD model.

$\omega_{n\text{-}DOF\ BIS,h}$ *h-th* higher frequency of the *n*-DOF BIS model

Chapter 1

Introduction

If architects can be compared to novelists, who tell a sweeping story, then engineers surely are poets, finding beauty in economy.

Ahmad Rahimian, WSP, NYC,
designer of One World Trade Center

The Intermediate (or Inter-story or Mid-story) Isolation System (IIS) derives from the Base Isolation System (BIS) by shifting the position of the isolation layer upward. Therefore, the building can be ideally subdivided in two sub-structures, the lower and upper, respectively placed below and above the isolation (ISO) interface. Due to the flexibility of the lower structure (LS), the IIS dynamic behaviour is more complex and less intuitive than the BIS. The IIS, indeed, is characterized by a twofold dynamic behaviour that combines two strategies of passive control: the isolation of the upper structure (US) and the mass damping on the lower structure. In particular, the isolated upper structure (ISO+US) behaves as a base isolated structure on the roof of the lower structure and, at the same time, as a mass damper for the lower structure [1 – 8]. Mass Damping is a well-known passive strategy for mitigating structural vibrations in buildings and improving serviceability and occupant comfort [9]. In fact, Tuned Mass Dampers (TMDs) with relatively small mass are widely applied for reducing wind-induced response, particularly in tall buildings; the same devices, however, are not equally effective under seismic input [9 – 11]. In the IIS, unlike *conventional* tuned mass dampers (TMD), in which the mass of the absorber is an added mass of only few per cent of the structural mass, a part of the building is converted into a huge mass damper, with a mass that can be comparable to, or even larger than, the mass of the LS. For this reason, the IIS is also termed as *non-conventional mass damper*, *building mass damper*, or *inhabited mass* *damper* [1, 5, 12], where the LS and the isolated US represent the main system and the dynamic vibration absorber, respectively. By increasing the mass of the TMD, the robustness of the system increases; consequently, the seismic response is less sensitive to variations of the design parameters, and to the frequency content and impulsive character of the seismic input [12]. By exploiting this robustness, some actual IIS buildings have been designed in Japan as *"untuned"* mass dampers [7, 13, 14].

It is worth observing that, though some analogies can be found between isolation and mass damping, the rationale behind them is profoundly different, if not opposite. The seismic isolation aims at the dynamic decoupling, as perfect and total as possible, of the building motion from the vibration source, that is the ground (by separating the prevailing frequencies of building and ground motion); in other words, isolation means making dynamic interaction minimal, if not null. The mass damping, instead, aims at the dynamic coupling, as perfect and total as possible, of the structure mass and an added mass. When the natural frequency of the added mass is tuned to the prevailing frequency of the main structure, it vibrates out of phase of the main mode of the structure, attenuating its amplitude; in other words, tuned mass damping means making dynamic interaction maximum, complete.

However, in IIS, the seismic isolation and mass damping are related because the ISO system is utilised for activating and controlling the relative motion between the two substructures, thus giving rise to the mass damping effect.

1.1 Motivation of the research activity

The world population within urbanised areas is growing rapidly and is estimated to reach 7 billion people by 2050 [15]; therefore, the need arises to create new living spaces within the current extremely high complexity and high-density urban environment. The vertical extension of existing buildings could be a good strategy because, in addition to preserving the existing building heritage, it saves the carbon footprint required for the demolition and subsequent reconstruction of existing buildings [16, 17]. This strategy is being adopted in several major European cities as a means of sustainable recovery and growth with almost no land take [2, 13, 14, 18 – 23]. Vertical extensions are also very useful in responding to the demand, born after the COVID-19 pandemic, for new living and working spaces that allow safe social distancing. In England, new laws have been issued in 2020 to encourage the construction of new living space by adding up to 2 storeys to existing buildings without any application [17]. Upper extensions are arising in Geneva, Milan, Rotterdam, Vienna, London, New York City; this strategy is worth of spreading, because, based on the concept of circular economy, it is more sustainable than the common approach of demolition/reconstruction of existing buildings, which consumes more energy and materials [16]. Furthermore, within the current urban planning trend of Transit Oriented Development (TOD), the realization of over-track buildings for exploiting the space above rail infrastructure is becoming quite popular in Japan. A very interesting example is the Daiya Gate Ikebukuro, in Tokyo, an over-track tall building with mid-story isolation, constructed over the Ikebukuro railway station [24], or the Kintetsu Hotel built over the tracks of Kyoto Station [25 – 27].

Given the above advantages, a non-conventional technique for vertical extension in urban context characterized by high seismic hazard can be proposed, i.e., connecting the existing structure with the new vertical extension through an isolation layer (Figure 1.1a). Indeed, as briefly mentioned in the previous section, IIS can prevent any increase of seismic effects, despite the mass increase due to the vertical extension. Further, even a non-negligible reduction of the seismic response can be obtained, if proper design procedures are followed for the new extension and the isolation system, based on the properties of the existing one.

However, this is not the only way to use IIS for existing buildings; in fact, several buildings in Japan are retrofitted using the IIS strategy, by subdividing the existing building into two parts, and interconnected through an ISO system. In particular, two different cases can be distinguished. The first one, shown in Figure 1.1b, where the existing building has a regular shape along the height and the ISO system is generally placed at the lower floors, avoiding the need for realisation of the clearance around the building, as in the case of BIS. The second one, shown in Figure 1.1c, where the existing building is characterised by an abrupt change in geometry along the height, which is the ideal location for the ISO system. It is evident that the dynamic behaviour of retrofitting solutions represented by the scheme of Figure 1.1b is very close to the BIS but since the ISO system is not at the base it is still identified as IIS.

The application of IIS strategy in Japan is not limited to existing buildings: it is widely used also for new tall buildings (Figure 1.1d). Indeed, as reported in [7]: *"In the case of intermediate isolation, the building is ideally subdivided in two main structural portions, i.e. an upper structure (US) and a lower structure (LS), respectively above and below the isolation system (ISO). This subdivision strongly enhances the feasibility of the isolation strategy in several situations, like in the case of densely populated areas [28], when the planning and urban restraints at the base of a building do not allow for the introduction of the seismic gap, as required in the case of classical base isolation systems. Furthermore, the IIS is an advantageous solution for mixed-use buildings: different occupancies along elevation give rise to different architectural plans and structural systems, also with grid layouts staggered one from the other, thus identifying a level of structural discontinuity that can be ideally utilized for placing the isolation system [13, 29, 30]. Finally, tall buildings can become good candidates for seismic isolation thanks to the introduction of an optimally placed IIS [31], that can remarkably improve the response of both structural parts above and below the isolation system."*

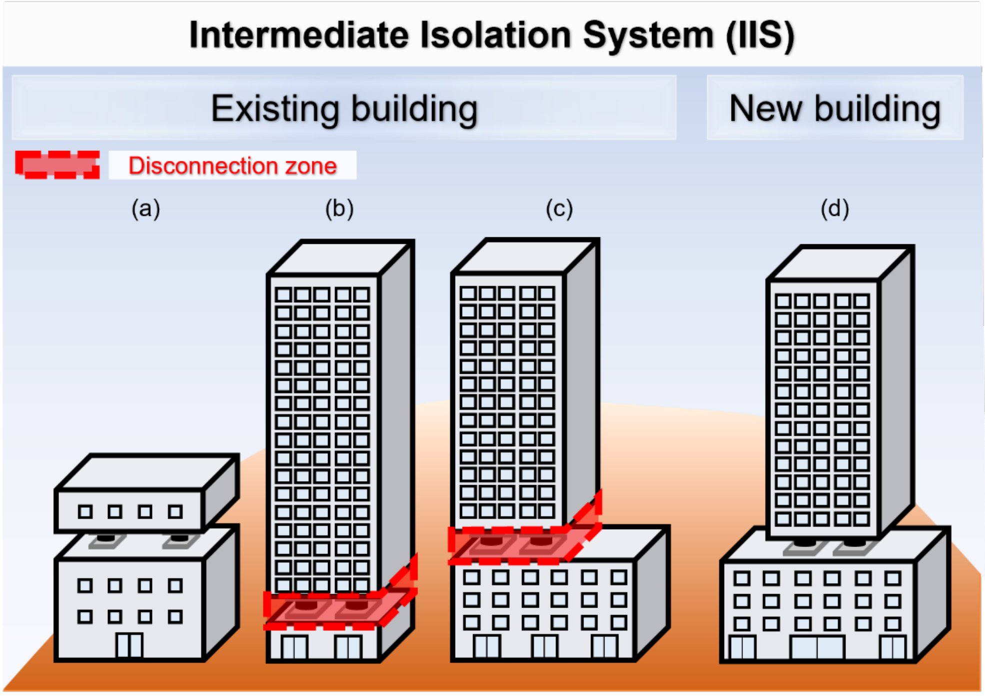

Figure 1.1. Intervention types with IIS: (a) existing building with vertical extension; (b) existing building with regular building shape; (c) existing building with irregular building shape; (d) new building.

In Japan, more than 60 buildings with IIS had been realized as of 2009 [32]. The first applications date back to the 90s and concern the seismic retrofitting of existing buildings, such as the Personnel Training Center of Taisei Corporation (1996) in Shizuoka prefecture [33 – 35] (see Appendix A.1), and the Kudan, Post Office and Housing (1998) in Tokyo [36, 37] (see Appendix A.3). Afterwards, IIS has been mainly used for new (often tall) buildings, such as: Iidiabashi 1st Building, Shiodome Sumitomo Building, Nakanoshima Festival Tower, Tekko Building, Fukuoka Financial Group Head Office, Roppongi Ground Tower, Kyobashi Edogrand and Ikebukuro DaiyaGate [13, 14, 29, 30, 38 – 45]. However, cases of IIS for the vertical extension of existing buildings there are only two cases: one in Japan, the Musashino City Disaster Prevention and Safety Centre in Tokyo [13, 14], and the other one in USA, at 185 Berry Street, in the China Basin area of San Francisco [18, 19] (Details on twenty examples of real buildings with IIS are reported in Tables A.1 – A.7 of Appendix A).

The growth of IIS buildings in Japan, in addition to being supported by extensive research of the scientific community, is the result of a clear regulatory framework [46, 47] that explicitly considers the possibility of placing the ISO system along the height of the building (i.e. IIS).

1.1.1 Japanese standard framework

In Japan, the Design Recommendations for Seismically Isolated Buildings [46] explicitly allow the adoption of isolation systems at the intermediate level, even stating that: *"… intermediate-level seismic isolation is one of the most favorable methods for improving the current extremely high-complexity and high-density urban environment"*.

In particular, subsection 4.6.3 of [46] contains: (i) description of the IIS strategy and its differences compared to the BIS strategy; (ii) summary of the advantages of IIS; (iii) scenarios in which it may be desirable to choose IIS; (iv) description of the design problems that typically affect IIS, i.e. *"the mode coupling effect, which produces amplification of the superstructure response due to the coupling effect between the vibration modes of the superstructure and the lower structure"* [46]; (v) indications about the method to be used for the IIS design. On this last aspect, the standard states that: *"To determine these vibration and seismic response characteristics, a simple response prediction method that does not require time history response analysis is effective* [48, 49]*. It is considered that a more rational design method is to simply evaluate the response reduction effect of the dampers of the seismic isolation level and the response amplification due to the mode coupling action, set parameters that are effective for response control, predict the response, and based on this, perform a detailed analysis using the time history response analysis"*. Therefore, it is suggested to follow in a first design phase the recommendations given in [48, 49], where it is provided a method for assessing the reduction of the IIS response obtained for a certain value of damping in the ISO system and the response amplification due to the mode coupling effect; then non-linear time-history analyses (NTHAs) should be executed to assess more accurately the IIS response. Finally, in order to preserve the structural integrity after an earthquake, the following measures are deemed necessary: isolation devices must be protected with fireproof coating, fire prevention compartmentalization of ISO level, and *ad hoc* design of elevator shafts and stairs that cross ISO level.

Regarding the later aspects, more information are given in *"the construction procedure standard for seismic isolation structure"* of the Japan Society of Seismic Isolation [47]: here practical details are given for several IIS construction aspects, such as: installation of the isolation device on the upper part of the column; connection between two parts of external walls at the ISO level to provide water and fire protection; structural design criteria for the stairs and elevator passing through the ISO level; fire protection system to be applied around the isolation devices. Similar indications are also given in [34].

In contrast, the European seismic design code, in the part 8 devoted to seismic isolation [50], does not provide any guidance on the design of IIS, although it does not explicitly prohibit it. The absence of specific design guidelines for IIS limits the deployment of this vibration control strategy in Europe, where the IIS could be widely applied for vertical extension and seismic retrofit of existing buildings.

Therefore, the research activity on IIS reported in this thesis work is aimed at identifying a specific IIS design procedure that could be useful to fill this gap.

1.2 IIS literature review

In the last decade, several researchers have studied IIS in order to understand its dynamic behaviour, identify the governing mechanical parameters, and derive design indications that ensure good seismic performance.

Important contributions, of course, come from Japan; in particular, some researchers [13, 14, 29, 38] deal with the IIS as a "concentrated energy dissipation" design problem, considering that most of the seismic energy input is absorbed by isolator and damper devices installed in the isolation layer. Other Japanese researchers [49, 51, 52] adopt two-degree-of-freedom (2DOF) models and have proposed a seismic response prediction method in which the natural mode functions are incorporated into the energy-balance method, firstly suggested by Akiyama [53], to derive the seismic response of the system.

Other contributions are basically related to two major conceptual approaches, namely the isolation and mass damping. Researchers generally study the IIS dynamics by focusing on either the isolation or mass damping approach [6, 7, 54].

The research contributions regarding the isolation approach mainly investigate the dynamic interaction between the lower and upper structure in IIS and the effect of the potential coupling of the higher modes on the structural response. In some papers [55 – 57], the impact of the dynamic interaction between upper and lower structures and the effect of the possible coupling of the higher modes are examined by adopting simplified three-degree-of-freedom (3DOF) models; the results of the analyses are also compared to the outcomes of experimental campaigns [28, 58]. In other papers [6, 23, 57], instead, multi-degree-of-freedom (MDOF) models are adopted to better describe the interaction of the structural portions. Ryan and Earl [23] have studied the IIS effectiveness by varying the location of the isolation layer along the height of the building; Faiella and Mele [6] have examined the IIS vibration characteristics by varying both the location of the isolation layer and the mass and stiffness distributions of upper and lower structures.

Research contributions related to the mass-damping approach consider the beneficial effect of dynamic interaction between the LS and the isolated US, with the latter working as a giant mass damper for the former. The main research contributions related to this approach are described as follows. In [59], the effect of absorber damping on the IIS seismic response is analysed through a 2DOF model, showing that the optimum IIS performance is obtained when damping values are equal for the first two complex modes of vibration. The validity of this control procedure has been extended in [60], by searching the TMD design parameters for which the two complex modes of vibration show equal damping ratios and equal frequencies. The methodology proposed in [60] has gained great interest in the scientific community; in fact, this procedure has been applied by many researchers [2, 61] or utilized for comparative purposes [1, 5, 12]. Chey et al. [2] have evaluated the IIS effectiveness as a seismic retrofit strategy for existing buildings with reinforced concrete frames. De Angelis et al [12] and Reggio and De Angelis [5] have investigated the dynamic behaviour of nonconventional TMD by adopting both multi and two-degree of freedom models and by modelling the seismic input as a stationary Gaussian stochastic process with zero mean; the control criterion suggested in [12] is the minimization of the root-mean-square displacement response of the damped main structure; in [5], instead, such criterion is the maximization of an energy performance index, defined as the ratio between the energy dissipated in the isolation system and the input energy globally transferred to the model. An experimental campaign on multi-story frame structure equipped with nonconventional TMD has also been reported in [62], with white noise, sine sweep, and natural earthquakes as input motion conditions.

Other researchers [31, 63] utilized a combined approach, and cover the design range of both design approaches, i.e. isolation and mass damping. Zhou et al. [31] and Tan et al. [63] developed an optimisation procedure based on minimising the variance of the base shear through the adoption of a 2DOF model. Based on the outcome provided in [60], an optimization procedure has been also proposed in [3, 64], by adopting 3DOF models to enhance the seismic performance of both upper and lower structure. Donà et al. [65, 66] have considered IIS made by fluid viscous dampers and have derived the optimal parameters for minimizing the isolation drift and simultaneously controlling the superstructure performance. These optimal parameters have been then used in [67, 68] to derive IIS design solutions, by selecting as case studies an existing masonry building and a reinforced concrete school building. Bernardi et al. [69] have proposed a multi-objective optimization approach applied to a 2DOF model, representing an IIS working as a TMD. The objective functions are the minimization of the variance of the substructure drift and the variance of the isolation drift (or of the superstructure acceleration), with the seismic input modelled as a stationary Gaussian stochastic process with zero mean. Ikeda [70] has recently suggested the pole allocation method applied to 3DOF models for analysing the dynamic characteristics of intermediate isolation systems and elaborating a mathematical solution in closed form. In a subsequent paper [71], the method has been generalized for including any passive control strategy (base isolation, inter-story isolation, tuned mass dampers, viscous dampers).

Further research contributions, devoted to classical TMD systems (i.e. TMDs characterised by small mass ratio - few units percent), can be mentioned below as they cover some design features that are also common to non-conventional TMD systems (i.e. TMDs characterised by large mass ratios) for retrofit applications. In fact, when earthquakes occur, the inelastic behaviour of the lower structure (i.e., the existing building) in IIS cannot be excluded and should be accounted for in the analyses. This problem has been already faced by several scholars for classical TMDs and some noteworthy contributions can be found within the scientific literature.

The problem has been firstly investigated by Soto-Brito and Ruiz [11]; by examining the influence of the ground motion intensity on the seismic effectiveness of TMDs, the authors have accounted for the inelastic behaviour and consequent damage in the main system. In particular, the lumped mass model of a 22-story nonlinear frame, considered as the main system, has been analysed. The results have revealed that the TMD effectiveness in limiting the peak response of the structure is greatly reduced for systems exhibiting highly nonlinear behaviour caused by high-intensity ground motions.

However, it is well-known that the peak response is not an exhaustive measure of the cyclic nonlinear behaviour of structures under seismic events. As firstly suggested by Lukkunaprasit and Wanitkorkul [72], the effects of accumulated damage, i.e. the hysteretic energy absorption, is another important performance index to be considered in the assessment of TMD performance. Therefore, in the last two decades, the nonlinear behaviour of the TMD-controlled structure has been investigated by considering both peak response parameters and accumulated damage indexes. Pinkaew et al. [73] have analysed a single-degree-of-freedom (SDOF) system, equivalent to an inelastic concrete building, equipped with a TMD, and have found that, though the TMD's effectiveness in reducing the maximum response gradually decreases as the structure experiences inelastic deformations, a significant reduction of structural damage occurs. In fact, several studies have demonstrated that the use of TMD on inelastic structures decreases the plastic energy dissipation [74 – 78]. Among them, Wong and Johnson [77] have examined the ability of single or multiple TMDs to improve the seismic response of inelastic structures. So-called "tuned mass spectra" have been proposed to determine the best tuning period of the TMD under a specific ground motion, while the exact location of the absorber has been individuated as the one corresponding to the minimum plastic energy dissipation. Sgobba and Marano [78] have proposed a TMD optimization for reducing the nonlinear response of a SDOF system through a stochastic linearization. Both the hysteretic dissipated energy and the displacement of the main structure are minimized, revealing that TMD effectiveness increases in structures with medium to long periods. An equivalent linearization has been also adopted by Zhang and Balendra [79] to reduce the nonlinear response of a SDOF-TMD system under narrow-band seismic excitation; the study also accounted for the effect of the stroke length, showing that its increase reduces structural damage, and that a limited stroke length can be compensated by increasing the TMD mass ratio.

All the studies on the topic find more or less explicitly that the optimal values of the TMD design parameters are very sensitive to the characteristics of the earthquake ground motion. Moreover, several scholars (e.g. [72, 73, 80]) establish that TMDs are effective in reducing the seismic response of inelastic structures only in the case of far-field ground motions, characterised by narrow-band frequency and long duration. Notwithstanding, Quaranta et al. [81] have studied the case of TMD installed on inelastic structures under pulse-like ground motions. In particular, by adopting optimum design procedures based on the elastic properties of the protected structure, the authors have found that TMDs are not effective for the displacement control of buildings undergoing significant inelastic deformations, while they are marginally useful for acceleration mitigation. Also Domizio et al. [82] have investigated different TMD configurations for controlling the seismic response of nonlinear SDOF structures under both far-field records and near-fault pulse-like ground motions. For this aim, the authors have developed optimization procedures for both single and multiple TMDs; two objective functions have been considered, namely the minimization of the frequency response magnitude of the undamaged structure and the maximization of the robustness of the TMD against stiffness degradation scenarios. A lower TMD effectiveness has been observed under near-fault records, especially for short-period structures.

1.3 Thesis overview

The thesis has been organised into the following chapters and appendices:

Chapter 2: *“Dynamic behaviour of IIS”*. In this chapter, the dynamic behaviour of IIS buildings is explored, starting with the definition of the reduced-order model that can reproduce the effective behaviour of the IIS building, i.e. the 3DOF model. From the equations of motion written for such a system, it can be clearly seen that the two vibration control strategies, seismic isolation at the base and mass damping, are interconnected in IIS. Then, it is shown that, under appropriate assumptions, the representative model of IIS can be reduced to a 2DOF model. Finally, the main design parameters for IIS are identified and their influence on the IIS dynamic response is assessed by considering two different types of excitations, namely harmonic motion of the support with constant acceleration amplitude, and harmonic force applied to the mass of the LS.

Chapter 3: *“General 5-Block design procedure for IIS in existing building retrofit”*. The IIS strategy is proposed for the vertical extension of an aggregate of masonry buildings located in the town of Pozzuoli, Italy, and a general design procedure is defined for this purpose. The effectiveness of IIS working as nonconventional TMD for the existing construction is assessed in terms of reduction of seismic demand and damage in the masonry structure undergoing inelastic deformation. First, the characterization of dynamic behaviour and seismic capacity of the building aggregate is addressed through modal and push over analyses, respectively. Elastic parametric analyses are then carried out on lumped mass models to derive the so-called *nonconventional TMD design spectrum* and to define the design configurations of the isolated vertical addition that minimize the global seismic response of the overall structure. Finally, the effectiveness of the retrofit solutions is evaluated through nonlinear time history analyses and its performance is compared to the one of the as-is building structure (i.e. the existing structure in its uncontrolled configuration); structural performance indexes accounting for both peak response and accumulated damage are defined and utilised for this purpose.

Chapter 4: *“Influence of LS and ISO nonlinear behaviour on IIS response”*. The key point of the design procedure defined and illustrated in the chapter 3 is the parametric response spectrum analyses performed on lumped mass models by varying the mechanical properties of the building extension. As a result, so-called *IIS design spectra* are derived and used for selecting design solutions of the vertical extension that do not alter or reduce the response of the existing lower structure. In this chapter, with reference to the real case study already presented in chapter 3, the IIS design procedure is improved by considering the nonlinear behaviour of the masonry structure of the existing building and of the isolation system, made of High Damping Rubber Bearings. Therefore, the effect of nonlinearities in structural complex with IIS is here assessed; basically, the idea is to check the accuracy and reliability of IIS design spectra as a tool for the preliminary design of the isolated vertical extension. For this purpose, several IIS configurations are analysed, and the results are discussed and compared in terms of peak response. In the light of the obtained analysis results, the effectiveness and robustness of IIS applications for vertical extensions and the response prediction offered by IIS design spectra are discussed. Finally, the results of Nonlinear Time History Analyses (NTHAs) obtained for the three-dimensional finite element model (3D FEM) of the IIS building are compared to the corresponding results obtained on the reduced order model (i.e. 2DOF model), demonstrating the representativeness and validity of non-linear 2DOF model to replicate the non-linear response of the IIS building.

Chapter 5: *"A diagram-based design procedure for IIS in existing buildings with inelastic behaviour"*. The *IIS design spectrum* allows for a complete evaluation of all design configurations that can be obtained varying the value of isolation period. It provides indications on the optimum value, the one that gives rise to the maximum reduction of the response of the existing structure; however, when such solution is not applicable for any reason, possible sub-optimum alternatives can be individuated in the *spectrum*. The *IIS spectrum* is constructed from parametric Response Spectrum Analysis (RSA) with the code spectrum specified for the site of interest and does not account for the inelastic behaviour that possibly arises in existing buildings. However, when earthquakes occur, the inelastic behaviour of existing (masonry or concrete) structures cannot be excluded and should be considered in the analyses. For this purpose, a design procedure is here proposed to supply the *IIS design spectrum* for existing buildings that exhibit nonlinear behaviour, without executing several nonlinear time history analyses for different models by varying the isolation period, but only examining in the inelastic field two limit behaviours of the extended building. Essential for this procedure are a series of diagrams derived from parametric RSA; as a result, two curves are identified as IIS design spectra and the region bounded by them, appointed as *inelastic IIS behaviour zone* (*i-IIS zone*), represents the nonlinear response prediction of the existing structure varying the isolation period of the vertical extension. The outlined design procedure is applied to some case studies and validated through the comparison with the results of nonlinear time history analyses. This *stepwise procedure* is employed to generalise the 5-block design procedure developed in the chapter 3. In fact, it allows to consider the inelastic behaviour, possibly occurring in the existing structure, from the first phases of the design process of vertical extension of existing buildings trough IIS.

Chapter 6: *"Generalization of the 5-Block design procedure for IIS"*. In this chapter, the design procedure presented in chapter 5 to derive the response of the isolated vertical addition has been extended and generalised to consider both the cases of elastic and inelastic behaviour of the existing building. Once selected the value of the isolation period corresponding to the required/desired (e.g., minimum) displacement of the existing building (elastic or inelastic) through *IIS design spectra*, *ISO displacement spectra* are defined and utilised to identify the displacement for the design of the isolation system. Furthermore, to avoid the complex RSA on simplified lumped mass model of IIS, design charts are also provided, varying the shape of code design spectra and the seismic hazard through a scaling factor. Making use of these design charts, the procedure is validated by developing some case studies and by comparing the RSA predictions to the numerical results of nonlinear time history analyses.

Chapter 7: *"IIS and ISO design spectrum: close-form relationship through Pole Allocation Method (PAM)"*. The *IIS design spectrum* utilised in the previous chapters is derived through complex response spectrum analysis (RSA) of non-classically damped IIS lumped mass model. In this chapter, an alternative, analytical approach is suggested for deriving the *IIS design spectrum*. For this aim, the Pole Allocation Method (PAM) is applied to a 2DOF IIS model; a useful closed-form relationship is derived, which links the modal damping ratios of the system to the values of natural circular frequency and damping ratio of the single degrees of freedom of the 2DOF system. Then, known the values of the damping ratio for the two vibration modes, closed form relationships for the *IIS design spectrum* and the *ISO design spectrum* (*or, isolator displacement spectrum*) are derived. For a case study, both design spectra are traced according to the closed form relationships and compared to the spectra obtained through complex RSA. In addition, time-history analyses are carried out and the results in terms of response of the lower structure and isolation system are compared, respectively to the predictions obtained by means of the relevant *design spectra*.

Chapter 8: *"IIS for existing irregular buildings"*. In this chapter, the possibility of regularizing, as well as reducing, the dynamic response of the existing structure through an appropriate design of the isolation system is examined. For this purpose, an existing masonry building, with eccentricity between the stiffness and mass centroids, is selected and analysed as a case study. A parametric study is developed to better clarify the regularizing potentials of IIS deriving from the dynamic interaction between the two structural portions. Some IIS design configurations, with different isolation systems, are designed and analysed. Analyses results and preliminary design implications are discussed.

Appendix A: *"Examples of IIS"*. In this appendix, a description of 20 new or existing IIS buildings is provided.

Appendix B: *"The non-proportional damped system"*. In this appendix, the method proposed by Sinha and Igusa [83] to deal with system characterised by non-proportional damping is illustrated. A system with intermediate isolation, indeed, exhibits very different damping values at different storeys and therefore its dynamic response must be evaluated considering damped frequency values and modal shapes. Hence, the IIS must be considered as a non-classically damped system, i.e. it is not possible to consider the hypothesis of damping proportional to masses and/or stiffnesses.

Appendix C: *"The Pole Allocation Method (PAM)"*. In this appendix, after introducing the open-loop and closed-loop controlled system, the Pole Allocation Method (PAM) is briefly described. The PAM has been used in chapter 7 for the IIS lumped mass model (i.e. an open-loop system) to obtain the closed-form relationships for the *IIS* and *ISO design spectrum*. A classical application of this method to closed-loop systems is shown for comparison.

Appendix D: *"Suggested value of ISO damping ratio"*. In the IIS applications developed in this thesis, the damping value of the ISO system has been assumed to be fixed, in accordance with the isolator type; however, this design parameter has a strong influence on the structural response. Therefore, in this appendix, the influence of the ISO damping ratio (ξ_{ISO}) on the dynamic response of a 2DOF IIS model is analysed; then a value of ξ_{ISO} for which the dynamic response of the system becomes approximately insensitive to the dominant frequency of the harmonic input is identified. Finally, the ISO damping value above individuated is compared to the optimal damping values identified by other authors for classical TMD [84 – 86].

Chapter 2

Dynamic behaviour of IIS

2.1 Simplified models

The intermediate isolation system (IIS) derives from the better-known base isolation system (BIS). In the IIS, the isolation (ISO) layer, which is located at an intermediate level along the height of the building, subdivided the whole system into two separate parts, i.e. the Lower Structure (LS) and the Upper Structure (US), each one with its mechanical properties. The IIS combines the strategies of isolation and mass damping: on one hand, the ISO filters the inertial forces transmitted from the LS to the US, on the other hand, the LS response is reduced thanks to the mass damping effect exerted by the isolated US. As reported in chapter 1, while the design practice for BIS and systems with tuned mass dampers (TMDs) is well consolidated and accepted, numerous approaches can be found in the literature for IIS, both with reference to the formulation of the problem and the definition of the design objectives and parameters. As reported in [6, 7, 54] and in chapter 1, two approaches can be clearly identified: the isolation and mass damping. The research works related to the first approach analyse the effect of the dynamic interaction between LS and US on the IIS response. In particular, either three Degrees Of Freedom (3DOF) models are used to grasp the global behaviour of IIS, or Multi Degrees Of Freedom (MDOF) models to evaluate the influence of the mass and stiffness distribution and of the location of the ISO level along elevation on the IIS response [6, 23, 57]. The research works related to the second approach consider the mass damping effect that the isolated US exerts on the LS and the models used are two Degrees Of Freedom (2DOF) models [5, 31, 59, 60, 87 – 90]. However, it is worth pointing out that 2DOF models can be adopted only if the response amplification effect due to the dynamic interaction between LS and US is avoided and if the US is much stiffer than the ISO system; in this case, the US contributes only in terms of mass. As a result, the main features of the IIS dynamic behaviour can be investigated by referring to a 3DOF IIS model [6, 28, 55 – 58], in which at the first, second and third degree of freedom are respectively assigned the mass (*m*), stiffness (*k*) and damping (*c*) properties of the Single Degree Of Freedom (SDOF) model equivalent to lower structure (m_{LS}, k_{LS} and c_{LS}), ISO system (m_{ISO}, k_{ISO} and c_{ISO}) and upper structure (m_{US}, k_{US} and c_{US}) (Figure 2.1a). The relative displacements of the three masses with respect to the base are denoted by u_{LS}, u_{ISO}, and u_{US} for m_{LS}, m_{ISO}, and m_{US}, respectively; the absolute displacement of the support is indicated by u_g; the single over-dot and the double over-dot denote the terms of velocities and accelerations, respectively. An external force, applied to the first degree of freedom, is denoted by F_E.

The equations of motion for the 3DOF IIS are:

$$m_{US}\,\ddot{u}_{US} + c_{US}\left(\dot{u}_{US} - \dot{u}_{ISO}\right) + k_{US}\left(u_{US} - u_{ISO}\right) = -m_{US}\,\ddot{u}_g \tag{2.1}$$

$$\begin{aligned} &m_{ISO}\,\ddot{u}_{ISO} + c_{ISO}\left(\dot{u}_{ISO} - \dot{u}_{LS}\right) + k_{ISO}\left(u_{ISO} - u_{LS}\right) = -m_{ISO}\,\ddot{u}_g \\ &+c_{US}\left(\dot{u}_{US} - \dot{u}_{ISO}\right) + k_{US}\left(u_{US} - u_{ISO}\right) \end{aligned} \tag{2.2}$$

$$\begin{aligned} &m_{LS}\,\ddot{u}_{LS} + c_{LS}\,\dot{u}_{LS} + k_{LS}\,u_{LS} = -m_{LS}\,\ddot{u}_g + F_E + c_{ISO}\left(\dot{u}_{ISO} - \dot{u}_{LS}\right) \\ &+k_{ISO}\left(u_{ISO} - u_{LS}\right) \end{aligned} \tag{2.3}$$

which in matrix form become:

$$\begin{aligned} &\begin{bmatrix} m_{LS} & 0 & 0 \\ 0 & m_{ISO} & 0 \\ 0 & 0 & m_{US} \end{bmatrix} \cdot \begin{Bmatrix} \ddot{u}_{LS} \\ \ddot{u}_{ISO} \\ \ddot{u}_{US} \end{Bmatrix} + \begin{bmatrix} c_{ISO}+c_{LS} & -c_{ISO} & 0 \\ -c_{ISO} & c_{ISO} & c_{US} \\ 0 & c_{US} & -c_{US} \end{bmatrix} \cdot \begin{Bmatrix} \dot{u}_{LS} \\ \dot{u}_{ISO} \\ \dot{u}_{US} \end{Bmatrix} \\ &+ \begin{bmatrix} k_{ISO}+k_{LS} & -k_{ISO} & 0 \\ -k_{ISO} & k_{ISO} & k_{US} \\ 0 & k_{US} & -k_{US} \end{bmatrix} \cdot \begin{Bmatrix} u_{LS} \\ u_{ISO} \\ u_{US} \end{Bmatrix} = - \begin{bmatrix} m_{LS} & 0 & 0 \\ 0 & m_{ISO} & 0 \\ 0 & 0 & m_{US} \end{bmatrix} \cdot \begin{Bmatrix} 1 \\ 1 \\ 1 \end{Bmatrix} \ddot{u}_g + \begin{Bmatrix} 1 \\ 0 \\ 0 \end{Bmatrix} F_E \end{aligned} \tag{2.4}$$

To grasp the dynamic behaviour of the IIS, it is interesting to compare the equations of motion of 3DOF IIS (Eqs. (2.1) – (2.3)) to the equations of motion of a base isolated system (BIS) and a mass damped (MD) structure. From several research contributions [84 – 86, 91 – 93], base isolated and mass damped structures can be analysed through 2DOF models, respectively shown in, respectively shown in Figure 2.1b and Figure 2.1c.

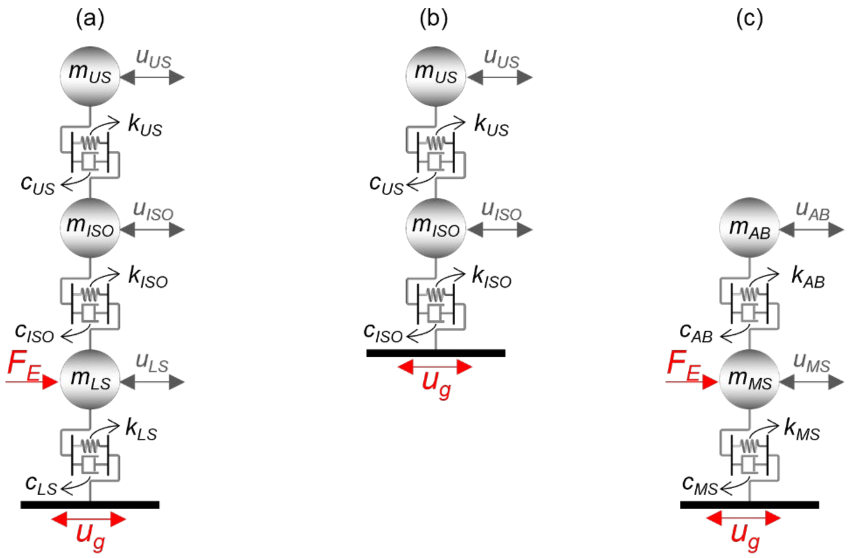

Figure 2.1. Concentrated mass models: (a) 3DOF IIS; (b) 2DOF BIS; (c) 2DOF MD.

In the 2DOF BIS model shown in Figure 2.1b, the first degree of freedom represents the isolation system (ISO) and the second degree the structure (also appointed as US). The equations of motion are:

$$m_{US}\,\ddot{u}_{US} + c_{US}\left(\dot{u}_{US} - \dot{u}_{ISO}\right) + k_{US}\left(u_{US} - u_{ISO}\right) = -m_{US}\,\ddot{u}_g \tag{2.5}$$

$$\begin{aligned} &m_{ISO}\,\ddot{u}_{ISO} + c_{ISO}\,\dot{u}_{ISO} + k_{ISO}\,u_{ISO} = -m_{ISO}\,\ddot{u}_g \\ &+c_{US}\left(\dot{u}_{US} - \dot{u}_{ISO}\right) + k_{US}\left(u_{US} - u_{ISO}\right) \end{aligned} \tag{2.6}$$

In the 2DOF MD shown in Figure 2.1c, the first degree of freedom represents the Main System (MS) with mass, stiffness, and damping constants equal to m_{MS}, k_{MS}, and c_{MS}, and the second degree represents the *vibration absorber* with dynamic properties equal to m_{AB}, k_{AB}, and c_{AB}. In particular, in classical applications with TMD, the vibration absorber is characterised by an added mass considerably smaller than the mass of the main system. The equations of motion are:

$$m_{AB}\,\ddot{u}_{AB} + c_{AB}\left(\dot{u}_{AB} - \dot{u}_{MS}\right) + k_{AB}\left(u_{AB} - u_{MS}\right) = -m_{AB}\,\ddot{u}_g \tag{2.7}$$

$$m_{MS}\,\ddot{u}_{MS} + c_{MS}\,\dot{u}_{MS} + k_{MS}\,u_{MS} = -m_{MS}\,\ddot{u}_g + F_E + c_{AB}\left(\dot{u}_{AB} - \dot{u}_{MS}\right) + k_{AB}\left(u_{AB} - u_{MS}\right) \tag{2.8}$$

From Eqs. (2.1) – (2.3), it can be observed that, if the stiffness of LS is assumed significantly larger than the stiffness of ISO, the relative displacement of LS tends to zero, i.e. $k_{LS} \gg k_{ISO} \Rightarrow u_{LS} \approx 0$. Consequently, the equations of motion of the 3DOF IIS (Eqs. (2.1) – (2.3)) correspond to Eqs. (2.5) and (2.6) of the 2DOF BIS [91, 93] (Figure 2.1b).

However, from Eqs. (2.1) – (2.3) it can also be seen that, if the US is much stiffer than the ISO system, the relative displacement between US and ISO tends to zero (i.e. $k_{US} \gg k_{ISO} \Rightarrow u_{US} \approx u_{ISO}$). Hence, the system of three equations of motion can be reduced to a system of two equations:

$$M_{ISO}\,\ddot{u}_{ISO} + c_{ISO}\left(\dot{u}_{ISO} - \dot{u}_{LS}\right) + k_{ISO}\left(u_{ISO} - u_{LS}\right) = -M_{ISO}\,\ddot{u}_g \tag{2.9}$$

$$m_{LS}\,\ddot{u}_{LS} + c_{LS}\,\dot{u}_{LS} + k_{LS}\,u_{LS} = -m_{LS}\,\ddot{u}_g + F_E + c_{ISO}\left(\dot{u}_{ISO} - \dot{u}_{LS}\right) + k_{ISO}\left(u_{ISO} - u_{LS}\right) \tag{2.10}$$

which in matrix form become:

$$\begin{bmatrix} m_{LS} & 0 \\ 0 & M_{ISO} \end{bmatrix}\begin{Bmatrix} \ddot{u}_{LS} \\ \ddot{u}_{ISO} \end{Bmatrix} + \begin{bmatrix} c_{ISO}+c_{LS} & -c_{ISO} \\ -c_{ISO} & c_{ISO} \end{bmatrix}\begin{Bmatrix} \dot{u}_{LS} \\ \dot{u}_{ISO} \end{Bmatrix} + \begin{bmatrix} k_{ISO}+k_{LS} & -k_{ISO} \\ -k_{ISO} & k_{ISO} \end{bmatrix}\begin{Bmatrix} u_{LS} \\ u_{ISO} \end{Bmatrix} = -\begin{bmatrix} m_{LS} & 0 \\ 0 & M_{ISO} \end{bmatrix}\begin{Bmatrix} 1 \\ 1 \end{Bmatrix}\ddot{u}_g + \begin{Bmatrix} 1 \\ 0 \end{Bmatrix}F_E \tag{2.11}$$

Eqs. (2.9) and (2.10) (or similarly Eq. (2.11)) represent the equations of motion of the 2DOF IIS (Figure 2.2b) in which the first degree of freedom still represents the LS and the second degree represent the whole isolated upper structure with mass M_{ISO} – i.e. the summation of the masses of ISO and US, M_{ISO} = m_{US} + m_{ISO} – and stiffness and damping constants of the ISO, k_{ISO} and c_{ISO}. These equations correspond to the counterparts of the 2DOF MD (Eqs. (2.7) and (2.8)), by considering the upper structure as the vibration absorber, the lower structure as the main system and the mass of the adsorber equal to the total isolated mass.

The simplified analytical formulation of the IIS system through lumped mass models highlights that the isolation layer represents an isolation system for the upper structure, and, in turn, the isolated upper structure can work as a mass damper for the lower structure. However, a most specific physical phenomenon can be observed only in intermediate isolation, as suggested by Ikeda in [70]: *"the seismic response of the upper substructure may be amplified by the modal coupling behaviour between the lower and upper substructures, and the seismic response of the lower substructure may be suppressed by the TMD effect of the upper substructures"*.

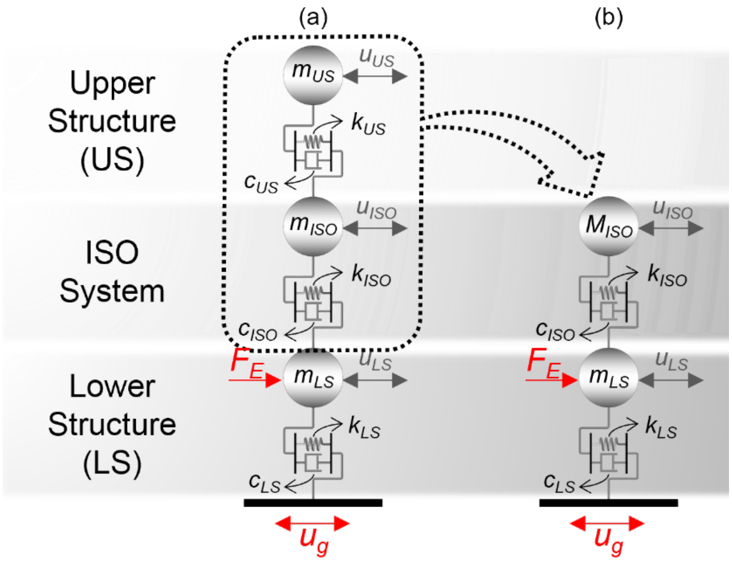

Figure 2.2. reduced order IIS model: (a) 3DOF IIS; (b) 2DOF IIS.

2.1.1 Design Parameters

To grasp the IIS dynamic behaviour, different design parameters governing the problem are adopted, as reported in the following.

Three parameters are defined by considering the 3DOF IIS, namely I, β_h, and T_R (Figure 2.1a).

The parameter I represents the ratio between the natural period of the ISO system, T_{ISO}, and the natural period of the US considered as fixed-base, T_{US}, i.e.:

$$I = T_{ISO}/T_{US} \tag{2.12}$$

This parameter gives information about the flexibility of the US with respect to the isolation system. It is defined in analogy with the case of BIS [91, 93]. Many standards [50, 94] suggest to adopt for BIS values of I greater than 3 in order to consider the structure above the isolation level as a rigid block, i.e., the structure moves together with the ISO system without relative displacements [91, 93, 95, 96].

The mode coupling parameter β_h deals with the higher mode coupling effect, which gives information about the dynamic interaction between LS and US [6, 28, 57]. In 3DOF IIS, the first mode mainly involves deformations in the isolation system while the two higher modes involve deformations either in LS or in US. However, when the higher mode coupling occurs, the higher modes involve deformations in both LS and US. This detrimental effect can lead to an amplification of the response of the US, as suggested by [6, 20, 28, 54, 57, 70]. Since the mode coupling is independent on the isolation period [6, 28, 57], the parameter β_h can be calculated by adopting a *free-free* 3DOF IIS model, characterised by an infinitely flexible isolation layer (k_{ISO} = 0 in Figure 2.1a) [6, 20, 28, 54, 57]. Hence, by assuming k_{ISO} = 0, the US and LS become perfectly separated from each other and two sub-systems can be identified and analysed separately. The first sub-system is the free-free base isolated upper structure (k_{ISO} = 0) and the second one is the fixed-base lower structure. Therefore, the dynamic behaviour of the IIS solution can be evaluated by analysing the dynamic behaviour of the two independent sub-systems.

The solution of the eigenvalue problem for the two separate parts of ff-3DOF IIS model leads to the definition of the parameter β_h:

$$\beta_h = \omega_{US}\sqrt{1 + m_{US}/m_{ISO}}\Big/\omega_{LS} \tag{2.13}$$

In the Eq. (2.13) the parameters ω_{LS} and ω_{US} are the circular frequency of SDOF model of LS and US, respectively.

$$\omega_{LS} = \sqrt{k_{LS} / m_{LS}} \tag{2.14}$$

$$\omega_{US} = \sqrt{k_{US} / m_{US}} \tag{2.15}$$

As reported in the literature [6, 7, 57], the higher mode coupling effect arises when the mode coupling parameter is close to one, i.e., β_h = 1±0.15. Consequently, from Eq. (2.13) it is possible to assert that the mode coupling effect is avoided if the frequency of the free-free base isolated upper structure model (i.e., $\omega_{US}\cdot(1+m_{US}/m_{ISO})^{0.5}$) is far from the frequency of the fixed-base lower structure model (i.e., ω_{LS}). By carefully designing US and LS, the mode coupling effect can be avoided. Since in real applications the mass ratio is generally set, the mode coupling can be prevented by modifying only the stiffness of US and LS.

As mentioned in sub-section 1.1.1, the Japanese standard [47] recommends a careful control of higher modes coupling effect in the IIS design.

However, it is interesting to note that Eq. (2.13) can be rewritten in terms of the periods of lower and upper structure (i.e. T_{LS}, T_{US}):

$$\beta_h = T_{LS}/T_{US}\sqrt{1+m_{US}/m_{ISO}} \tag{2.16}$$

$$T_{LS} = 2\pi/\omega_{LS} \tag{2.17}$$

$$T_{US} = 2\pi/\omega_{US} \tag{2.18}$$

Therefore, it is possible to introduce a further design parameter, the ratio T_r, equal to:

$$T_r = T_{LS}/T_{US} \tag{2.19}$$

An extensive parametric analysis carried out in [20] shows that if T_r is greater than 0.5, β_h is always greater than 1.15 and therefore the effect of the amplification response due to the higher mode coupling does not occur.

As reported above, the 3DOF IIS model is able to describe the main features of the IIS dynamic behaviour. However, as suggested by several authors [6, 20, 28, 57, 97], if the coupling effects of the higher modes can be neglected and the US can be considered as a rigid block standing on the ISO system, a 2DOF model can be adopted. These aims can be achieved by considering a value of the modal coupling parameter β_h different from 1±0.15, or similarly T_r >

0.5 and a value of the isolation ratio $I > 3$. Hence, the 3DOF IIS model in Figure 2.1a can be further reduced in the 2DOF IIS model (Figure 2.2b) considering only the mass contribution from the US.

Additional six parameters can be defined, by considering both the 3DOF and 2DOF models, i.e.: natural circular frequency of LS (i.e., ω_{LS}) and of ISO system (i.e., ω_{ISO},); damping ratios of the LS (i.e., ξ_{LS}) and of ISO system (i.e., ξ_{ISO}); mass ratio (μ) between the masses of the isolated upper structure and lower structure; ratio f between the circular natural frequencies of the isolated upper structure and lower structure, usually appointed in literature [84 – 86] as *tuning ratio* between the absorber (i.e. the isolated vertical addition, ISO+US) and the main system (i.e. the lower structure, LS). The value of ω_{LS} is provided by Eq. (2.14), while the remaining design parameters are provided by the following relationships:

$$\omega_{ISO} = \sqrt{k_{ISO}/M_{ISO}} \tag{2.20}$$

$$\xi_{LS} = \frac{c_{LS}}{2m_{LS}\omega_{LS}} \tag{2.21}$$

$$\xi_{ISO} = \frac{c_{ISO}}{2M_{ISO}\omega_{ISO}} \tag{2.22}$$

$$\mu = \frac{m_{ISO} + m_{US}}{m_{LS}} = \frac{M_{ISO}}{m_{LS}} \tag{2.23}$$

$$f = \frac{\omega_{ISO}}{\omega_{LS}} = \frac{T_{LS}}{T_{ISO}} \tag{2.24}$$

The damping ratio ξ_{LS} is usually fixed, once defined the structural material of the lower structure; the damping ratio ξ_{ISO} varies as a function of the devices - dampers and/or isolators - utilised in the isolation layer (see Appendix D for major details); the period T_{LS} is set by adopting an existing building as lower structure; the period T_{ISO} generally varies in a wide range for exploring possible design solutions in the light of the mass damping and isolation approaches; the mass ratio μ, which implicitly defines the position of the ISO layer along the height of the building, is generally set; the tuning ratio f generally varies as a function of T_{ISO}, by assuming T_{LS} has a fixed value.

All design parameters here defined are necessary to explore the IIS dynamics by means of parametric analyses. The main goal of this research is to control the dynamic response of the lower structure (i.e. the existing building) in order to limit, or even counteract, its engagement in the inelastic field (see chapters 3). Set μ and ξ_{ISO}, the parameter that controls the dynamic response of the lower structure (e.g. its maximum displacement) is the isolation period, T_{ISO}.

Once the design value of T_{ISO} has been chosen, it is possible to design the ISO system, i.e. to calculate the displacement demand for the isolation system. Unlike BIS, in IIS this displacement is strongly affected by the dynamics of the lower structure. Therefore, a specific design tool, the so-called ISO design spectrum introduced in chapter 6, is defined and utilised for predicting the value of the isolation displacement demand in the preliminary design phase.

For the sake of clarity, the design parameters identified for the 3DOF IIS and 2DOF IIS model are shown in Table 2.1.

Table 2.1. Main design parameter of IIS lumped mass model.

Model	Design parameters								
3DOF IIS	ξ_{LS}	ξ_{ISO}	T_{LS} (ω_{LS})	T_{ISO} (ω_{ISO})	μ	f	T_{US} (ω_{US})	T_r (β_h)	I
2DOF IIS	ξ_{LS}	ξ_{ISO}	T_{LS} (ω_{LS})	T_{ISO} (ω_{ISO})	μ	f	-	-	-

2.2 Influence of design parameters on 2DOF IIS model response

The influence of the design parameters on the IIS response is here evaluated considering only the 2DOF IIS model. For this purpose, a frequency response analysis is developed by adopting harmonic excitations.

2.2.1 Support excitation

To study the steady-state response of the 2DOF IIS model under a harmonic excitation of the support with a fixed value of the acceleration amplitude and independent of frequency, Eqs. (2.14), (2.20) – (2.24) are substituted into Eqs. (2.9) and (2.10) setting $F_E = 0$:

$$\begin{aligned}&\ddot{u}_{LS}+\dot{u}_{LS}\omega_{LS}\left(2\xi_{LS}+2\mu\xi_{ISO}f\right)+u_{LS}\omega_{LS}^2\left(1+\mu f^2\right)=-\ddot{u}_g\\&+\dot{u}_{ISO}2\mu\xi_{ISO}f\omega_{LS}+u_{ISO}\mu f^2\omega_{LS}^2\end{aligned} \tag{2.25}$$

$$\begin{aligned}&\ddot{u}_{ISO}+\dot{u}_{ISO}\omega_{LS}\left(2\xi_{ISO}f\right)+u_{ISO}f^2\omega_{LS}^2=-\ddot{u}_g\\&+\dot{u}_{LS}2\xi_{ISO}f\omega_{LS}+u_{LS}f^2\omega_{LS}^2\end{aligned} \tag{2.26}$$

For analytical convenience we use the Laplace transformation on Eqs. (2.25) and (2.26) in order to leave the time domain in favour of a complex domain, or often referred to as the Laplace domain [98].

$$\begin{aligned}&s^2U_{LS}(s)+sU_{LS}(s)\omega_{LS}\left(2\xi_{LS}+2\mu\xi_{ISO}f\right)+U_{LS}(s)\omega_{LS}^2\left(1+\mu f^2\right)\\&=-\ddot{U}_g(s)+sU_{ISO}(s)2\mu\xi_{ISO}f\omega_{LS}+U_{ISO}(s)\mu f^2\omega_{LS}^2\end{aligned} \tag{2.27}$$

$$\begin{aligned}&s^2U_{ISO}(s)+sU_{ISO}(s)2\xi_{ISO}f\omega_{LS}+U_{ISO}(s)f^2\omega_{LS}^2\\&=-\ddot{U}_g(s)+sU_{LS}(s)2\xi_{ISO}f\omega_{LS}+U_{LS}(s)f^2\omega_{LS}^2\end{aligned} \tag{2.28}$$

In Eqs. (2.27) and (2.28) all initial conditions have been omitted as they are assumed equal to zero, and with s has been indicated in general a complex quantity defined as a *subsidiary variable* [99]. In addition, it can be seen that, through the Laplace transformation a system of differential equations in the time domain (Eqs. (2.25) and (2.26)) has been transformed into a system of algebraic expressions in the Laplace domain (or s-plane); because a differentiation in the time domain is equivalent to multiplying by s in the Laplace domain.

However, writing the equations of motion in the Laplace domain, it is particularly interesting to study the relationship between the transformed response and the transformed input ($\ddot{U}_g(s)$). In particular, considering the displacement of the lower structure in the 2DOF IIS model (Figure 2.2c) as the transformed response parameter ($U_{LS}(s)$), we have:

$$\frac{U_{LS}(s)}{\ddot{U}_g(s)}=G_{ug,2DOF\,IIS}(s) \tag{2.29}$$

$G(s)$ is known as the *system transfer function*, and is equal to:

$$G_{ug,2DOF\,IIS}(s) = -\frac{s^2 + s2\xi_{ISO} f\omega_{LS}(1+\mu) + f^2\omega_{LS}^2(1+\mu)}{s^4 + a_1 s^3 + a_2 s^2 + a_3 s + \omega_{LS}^2\omega_{ISO}^2}$$
$$a_1 = 2\omega_{LS}(\xi_{LS} + \xi_{ISO} f + \mu\xi_{ISO} f)$$
$$a_2 = \omega_{LS}^2(\mu f^2 + 1 + f^2 + 4\xi_{LS}\xi_{ISO} f)$$
$$a_3 = 2\omega_{LS}^3(\xi_{ISO} f + \xi_{LS} f^2) \tag{2.30}$$

As reported in [98], it can be demonstrated that the *transfer function*, $G_{ug,2DOF\ IIS}$ (s), is simply the *frequency response*, $G_{ug,2DOF\ IIS}$ ($i\omega$), with $i\omega$ substituted to s; where i is the imaginary part and ω is the circular natural frequency of a harmonic input. For this reason, to derive a briefer form for $G_{ug,2DOF\ IIS}$ ($i\omega$), it is useful to introduce the following parameters to be replaced in Eq. (2.30):

$$s = i\omega \tag{2.31}$$

$$\lambda = \frac{\omega}{\omega_{LS}} \tag{2.32}$$

In Eq. (2.32), the parameter λ is the *forced frequency ratio* and has been defined as the ratio between the circular natural frequency of a harmonic input (i.e. ω) and the circular natural frequency of the lower structure (i.e. ω_{LS}). Thus, this parameter is indicative of the resonance effect that leads to an increase in the response of lower structure.

Substituting Eqs. (2.24), (2.31) and (2.32) into Eq. (2.30), yields:

$$G_{ug,2DOF\,IIS}(i\omega) = -\frac{2\xi_{ISO}\lambda f + 2\mu\xi_{ISO}\lambda f - \mu f^2 i - f^2 i + \lambda^2 i}{\omega_{LS}^2\left(b_1 f^2 + b_2 f + \lambda^2 i - \lambda^4 i - 2\lambda^3\xi_{LS}\right)}$$
$$b_1 = \left(2\xi_{LS}\lambda - i + \lambda^2 i + \mu\lambda^2 i\right)$$
$$b_2 = \left(-2\xi_{ISO}\lambda^3 + 2\xi_{ISO}\lambda - 2\mu\xi_{ISO}\lambda^3 + 4\xi_{LS}\xi_{ISO}\lambda^2 i\right) \tag{2.33}$$

as stated in [100, 101], if the ground motion is reported as a harmonic excitation, it is possible to identify a *Dynamic Magnification Factor* (*DMF*) equal to the modulus of the *frequency response function* (or *admittance function*), i.e. G ($i\omega$), which for the 2DOF IIS model with harmonic support excitation is equal to:

$$DMF_{ug,2DOF\,IIS} = \left|G_{ug,2DOF\,IIS}(i\omega)\right| = \frac{1}{\omega_{LS}^2}\left|\frac{\overline{\mathrm{Re}}(\lambda)+i\overline{\mathrm{Im}}(\lambda)}{\mathrm{Re}(\lambda)+i\mathrm{Im}(\lambda)}\right|$$
$$= \frac{1}{\omega_{LS}^2}\sqrt{\frac{\overline{\mathrm{Re}}^2(\lambda)+\overline{\mathrm{Im}}^2(\lambda)}{\mathrm{Re}^2(\lambda)+\mathrm{Im}^2(\lambda)}} \tag{2.34}$$

where:

$$\overline{\mathrm{Re}}(\lambda) = 2\xi_{ISO}\lambda f + 2\mu\xi_{ISO}\lambda f \tag{2.35}$$

$$\overline{\mathrm{Im}}(\lambda) = \lambda^2 - f^2(1+\mu) \tag{2.36}$$

$$\mathrm{Re}(\lambda) = -2\xi_{LS}\lambda f^2 + 2\xi_{LS}\lambda^3 - 2\xi_{ISO}\lambda f + 2\xi_{ISO}\lambda^3 f(1+\mu) \tag{2.37}$$

$$\mathrm{Im}(\lambda) = -\lambda^2 + \lambda^4 + f^2 - \lambda^2 f^2(1+\mu) - 4\xi_{LS}\xi_{ISO}\lambda^2 f \tag{2.38}$$

In addition, to compare the response of the model with IIS versus the response of the model without IIS, the $DMF_{ug,\,SDOF\,LS}$ for the Single Degree Of Freedom model of LS (SDOF LS) is also evaluated:

$$DMF_{ug,SDOF\,LS} = \frac{1}{\omega_{LS}^2}\cdot\frac{1}{\left|1+2i\xi_{LS}-\lambda^2\right|} \tag{2.39}$$

Figure 2.3 shows four DMF_{ug} vs. λ graphs associated with four different values of the mass ratio μ, i.e. 0.05, 0.1, 0.5 and 1. In each graph, two curves are shown, a black curve for the 2DOF IIS model and a dashed grey curve for the SDOF LS model. The results are obtained for fixed values of ξ_{LS}, ξ_{ISO} and f, respectively equal to 0.05, 0.15 and 1. A comparison between the curves for the 2DOF IIS model and the curves for the SDOF LS model shows that the operating range - or controlled bandwidth [6, 54] - i.e. the range of λ values in which the curves intercept, increases as μ increases. Consequently, as μ increases, the efficiency of the model with IIS and its robustness to variations of the input frequency (ω) increase.

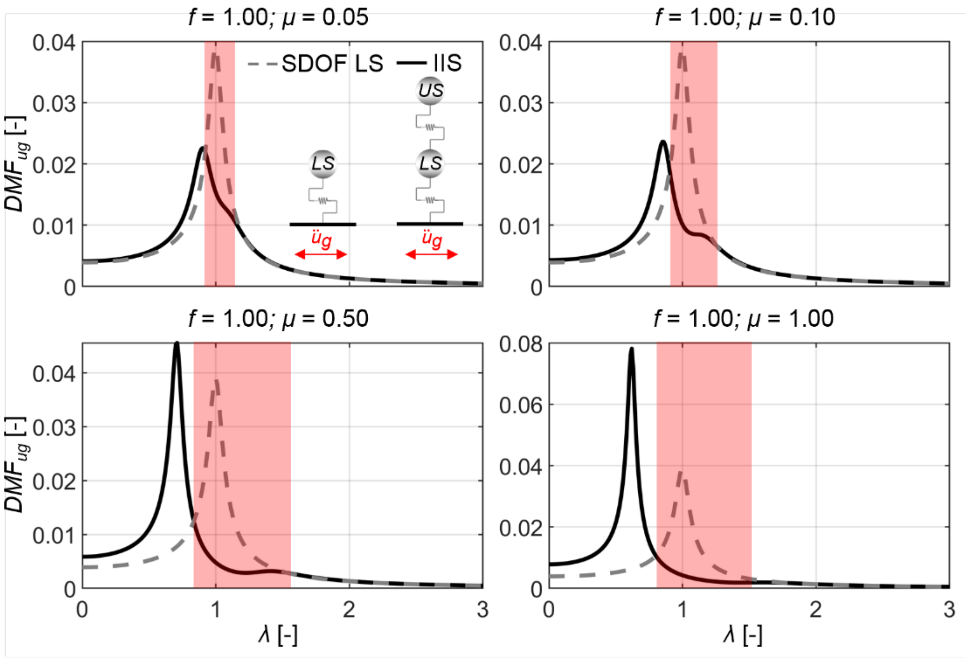

Figure 2.3. DMF_{ug}-λ plots for λ = [0 - 3], ξ_{LS} = 0.05, ξ_{ISO} = 0.15, f = 1, μ = [0.05, 0.10, 0.50, 1.00].

However, if on the one hand the increase of μ expands the operative range, on the other hand it also tends to increase the DMF_{ug} value at the first peak of the black curve which corresponds to the frequency of the isolated US (the second peak is relative to the frequency of the LS). Therefore, to reduce this peak value of the DMF_{ug}, the tuning ratio f can be varied. In fact, in Figure 2.4, the same graphs as in Figure 2.3 have been replicated by varying only f from 1 to 0.5, and it can be seen that for high values of mass, the DMF_{ug} peak value goes down while for low values of mass, it goes up. This type of relationship between f and μ, i.e. as μ increases optimal f increases, can be observed in several optimal relationships provided in the literature [84 – 86].

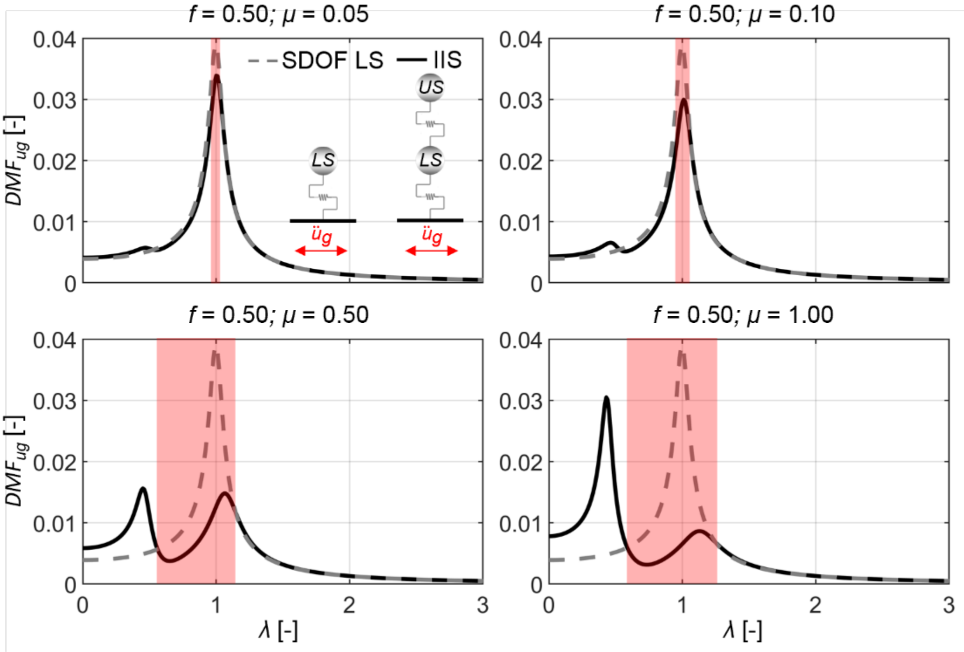

Figure 2.4. DMF_{ug}-λ plots for λ = [0 - 3], ξ_{LS} = 0.05, ξ_{ISO} = 0.15, f = 0.5, μ = [0.05, 0.10, 0.50, 1.00].

In addition, it is interesting to note that by rewriting the equations of motion for the 2DOF BIS model (Eq. (2.5) and (2.6)) in terms of relative displacements of US with respect to LS (δ_{US}), i.e. by substituting the displacement u_{US} with the term u_{US} = (δ_{US} + u_{ISO}), it is possible to evaluate the *frequency response,* $G_{ug,2DOF\ BIS}$ $(i\omega)$, for the 2DOF BIS model in terms of δ_{US}:

$$G_{ug,2DOF\,BIS}(i\omega)=\frac{\delta_{US}(i\omega)}{\ddot{u}_g(i\omega)}=\frac{l^2+2l^2\lambda_U\xi_{ISO}\mathrm{i}}{\omega_{US}{}^2\left(+b_1l^2+b_2l-\lambda_U^4+2\lambda_U^3\xi_{ISO}\mathrm{i}+\lambda_U^2\right)}$$

$$b_1=\left(-1+\lambda_U^2+\lambda_U^2\left(\frac{\kappa}{1-\kappa}\right)-2\lambda_U\xi_{ISO}\mathrm{i}\right) \tag{2.40}$$

$$b_2=\left(4\lambda_U^2\xi_{ISO}\xi_{US}+2\lambda_U^3\xi_{US}\mathrm{i}-2\lambda_U\xi_{US}\mathrm{i}+2\lambda_U^3\left(\frac{\kappa}{1-\kappa}\right)\xi_{US}\mathrm{i}\right)$$

where λ_U is the *forced frequency ratio* and has been defined as the ratio between the circular natural frequency of a harmonic input (i.e. ω) and the circular natural frequency of the upper structure (i.e. ω_{US}),

κ *is* the ratio between m_{US} and (m_{US} + m_{ISO}). The modulus of the *frequency response function* is the *Dynamic Magnification Factor* ($DMF_{ug,\ 2DOF\ BIS}$):

$$DMF_{ug,2DOF\,BIS} = \left|G_{ug,2DOF\,BIS}(i\omega)\right| = \frac{1}{\omega_{US}^2}\left|\frac{\overline{\mathrm{Re}}(\lambda)+i\overline{\mathrm{Im}}(\lambda)}{\mathrm{Re}(\lambda)+i\mathrm{Im}(\lambda)}\right|$$
$$= \frac{1}{\omega_{US}^2}\sqrt{\frac{\overline{\mathrm{Re}}^2(\lambda)+\overline{\mathrm{Im}}^2(\lambda)}{\mathrm{Re}^2(\lambda)+\mathrm{Im}^2(\lambda)}} \tag{2.41}$$

Figure 2.5 shows a comparison between a fixed-base and a base-isolated system in which the isolation ratio I is assumed to be 3, the damping ratios of ISO and US are respectively assumed to be 0.15 and 0.05, and the ratio $\kappa = m_{US} / (m_{US} + m_{ISO})$ is assumed to be 0.6. Therefore, it can be seen that the operative range of the isolation is very wide, and the controlled system significantly reduces the displacement response of the US.

Comparing Figure 2.3, Figure 2.4 and Figure 2.5, it can be observed that, when the mass ratio is less than 1 the isolated US works as a TMD for the LS, while when μ becomes greater than 1 the model with IIS tends to behave like the BIS model [54].

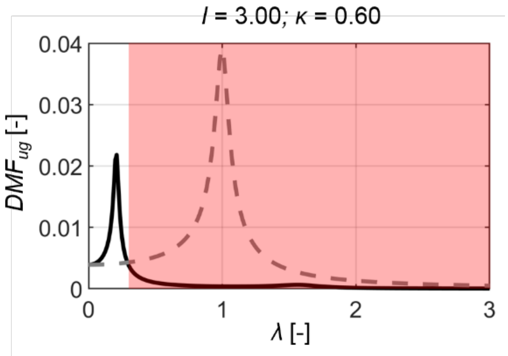

Figure 2.5. *DMF_{ug}-λ* plots of BIS for λ = [0 - 3], ξ_{US} = 0.05, ξ_{ISO} = 0.15, I = 3, κ = 0.6.

2.2.2 LS mass excitation

Now let us analyse the response of the 2DOF IIS model assuming a harmonic force applied to the mass of the LS rather than a support motion. Hence, in Eqs. (2.9) and (2.10) let us consider $\ddot{u}_g = 0$ and, for the sake of brevity, let us also consider $\xi_{LS} = 0$. The external force, F_E, applied on the main system mass, is of the kind $P_0 \sin(\omega t)$, where P_0 is the constant amplitude of the force and is independent of the input circular frequency, i.e., ω.

The corresponding equations of motion are given below:

$$m_{LS}\ddot{u}_{LS} + k_{LS}u_{LS} - k_{ISO}\left(u_{ISO} - u_{LS}\right) - c_{ISO}\left(\dot{u}_{ISO} - \dot{u}_{LS}\right) = P_0 \sin\left(\omega t\right) \quad (2.42)$$

$$m_{AB}\ddot{u}_{AB} + k_{AB}\left(u_{AB} - u_{MS}\right) + c_{AB}\left(\dot{u}_{AB} - \dot{u}_{MS}\right) = 0 \quad (2.43)$$

From Eqs. (2.42) and (2.43), only the forced vibration response is addressed, so the values of $\ddot{u}_{LS}, \dot{u}_{LS}, u_{LS}$ and $\ddot{u}_{ISO}, \dot{u}_{ISO}, u_{ISO}$ can be represented in the so-called *phasor plane* [102], where these vectors rotate with constant angular velocity equal to ω and keep the angles between them unchanged. Then, it is possible to solve these equations by writing the vectors as complex numbers (note that the same result can also be achieved by performing the Laplace transformation as done in the previous subsection).

$$\left(-m_{MS}\omega^2 + k_{MS} + k_{AB} + i\omega c_{AB}\right)u_{MS} - \left(k_{AB} + i\omega c_{AB}\right)u_{AB} = P_0 \quad (2.44)$$

$$-\left(k_{AB} + i\omega c_{AB}\right)u_{MS} + \left(-m_{AB}\omega^2 + k_{AB} + i\omega c_{AB}\right)u_{AB} = 0 \quad (2.45)$$

From these equations, after some analytical manipulation, it is possible to derive the amplitude of the motion of the LS mass, i.e., the *Dynamic Magnification Factor* ($DMF_{FE,\ 2DOF\ IIS}$) for a 2DOF IIS model excited with a harmonic force at the LS mass [84].

$$DMF_{F_E,2DOF\,BIS} = \left|\frac{u_{LS}}{u_{st}}\right|$$
$$= \sqrt{\frac{\left(2\xi_{ISO}\lambda^2\right)^2 + \left(\lambda^2 - f^2\right)^2}{\left(2\xi_{ISO}\lambda\right)^2\left(\lambda^2 - 1 + \mu\lambda^2\right)^2 + \left[\mu f^2\lambda^2 - \left(\lambda^2 - 1\right)\left(\lambda^2 - f^2\right)\right]^2}} \quad (2.46)$$

where u_{st} is the static displacement of the main system equal to P_0/k_{LS}.

Again, to compare the response of the model with IIS versus the response of the model without IIS, the $DMF_{FE,\,SDOF\,LS}$ for the undamped SDOF LS is also evaluated:

$$DMF_{F_E,SDOF\,LS} = \frac{1}{1-\lambda^2} \tag{2.47}$$

The Eq. (2.46) is a function of four design parameters, ξ_{ISO}, λ, f, and μ. In order to evaluate the influence of these design parameters on the structural response of the 2DOF IIS model, similar graphs to those in Figure 2.3 and Figure 2.4 are shown in Figure 2.6 and Figure 2.7, respectively. Figure 2.6 shows four DMF_{FE} vs. λ graphs associated with four different values of the mass ratio μ = [0.05, 0.1, 0.5, 1] and for a fixed value of ξ_{ISO} and f equal to 0.15 and 1, respectively. As already observed from Figure 2.3 and Figure 2.4, it can also be seen from Figure 2.6 and Figure 2.7 that the operative range increases as the mass ratio increases and the maximum peak value of the black curve for the 2DOF IIS model decreases as f decreases for large values of the mass ratio.

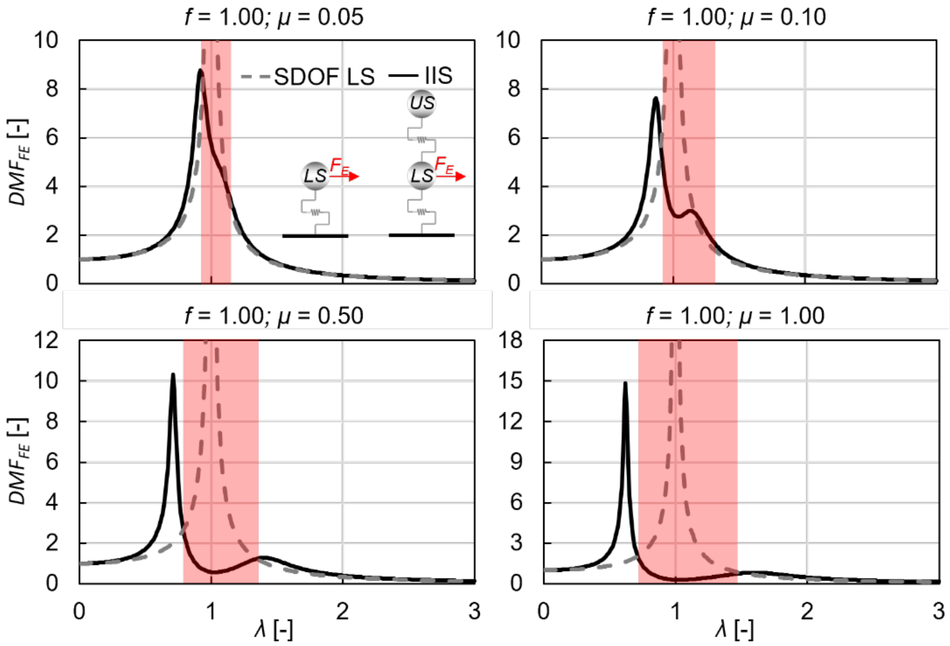

Figure 2.6. DMF_{FE}-λ plots for λ = [0 - 3], ξ_{ISO} = 0.15, f = 1, μ = [0.05, 0.10, 0.50, 1.00].

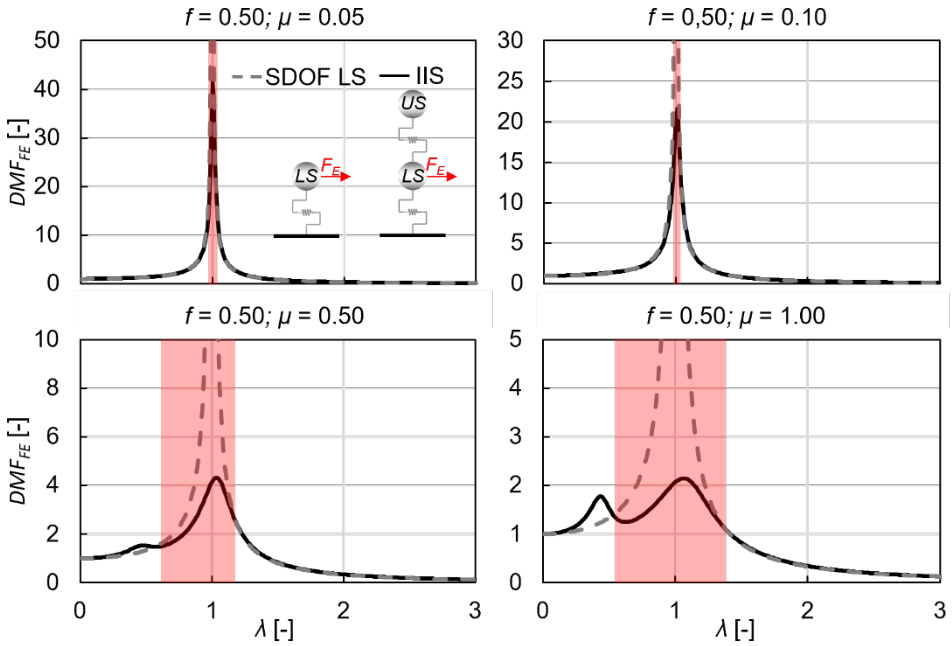

Figure 2.7. DMF_{FE}-λ plots for λ = [0 - 3], ξ_{ISO} = 0.15, f = 0.5, μ = [0.05, 0.10, 0.50, 1.00].

Chapter 3

5-Block design procedure for IIS in existing building

In this chapter, the strategy of Intermediate Isolation System (IIS) is proposed for the vertical extension of an aggregate of masonry buildings located in Pozzuoli, south Italy. The effectiveness of IIS working as a nonconventional Tuned Mass Damper (TMD) for the existing construction is assessed in terms of reduction of seismic demand and damage in the masonry structure undergoing inelastic deformation under seismic input. For this aim, a so-called *5-Block design procedure* is first defined and then applied to the case study building.

First, the characterization of dynamic behaviour and seismic capacity of the building aggregate is addressed through modal and push over analyses, respectively. Elastic parametric analyses are then carried out on lumped mass models to derive the so-called *nonconventional TMD design spectrum* (or *IIS design spectrum*) and to define the design configurations of the isolated vertical addition that minimize the global seismic response of the overall structure. Finally, the effectiveness of the retrofit solutions is evaluated through nonlinear time history analyses (NLTHAs) and its performance is compared to the one of the AS-IS building structure (i.e. the existing structure in its uncontrolled configuration); structural performance indexes accounting for both peak response and accumulated damage are defined and utilised for this purpose.

3.1 5-Block design procedure

A procedure is here proposed for designing IIS and assessing its effectiveness in realizing isolated extension of existing masonry building that can work as nonconventional TMD for the original structure. The proposed method is described step-by-step in the following sub-sections; special focus is on the inelastic response of the existing structure, thus extending and generalizing the results presented in references [20, 21], where a linear behaviour was considered for the LS. The flowchart of the proposed procedure is schematised in Figure 3.1 and is divided into five blocks, which are thoroughly discussed in the following sub-sections.

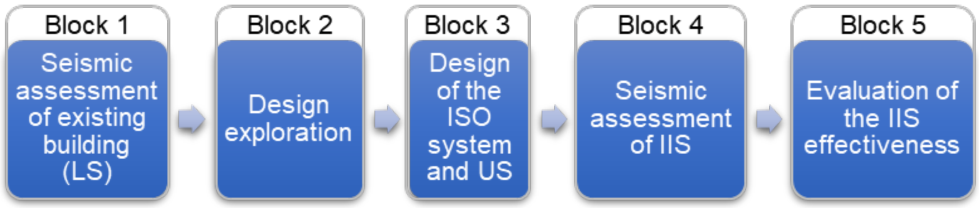

Figure 3.1. 5-Block IIS design procedure.

3.1.1 Block 1: seismic assessment of existing building

The block 1 of the proposed design procedure is the dynamic characterisation and seismic assessment of the existing building in the as-is configuration (in the following this model will be denoted as "AS-IS") (Figure 3.2); the masonry building model is also appointed as LS (Lower Structure) when it is part of the design configuration with upper extension. A 3D FE (finite element) model of the masonry structure is created utilising the equivalent frame model approach, and both linear and nonlinear analyses are performed.

For the nonlinear static (or pushover) analysis, a lumped plasticity model is adopted for the bending and shear behaviour of the masonry piers; in particular, flexural plastic hinges are assigned at both top and bottom of each pier, while one shear hinge is assigned at pier mid-height. The plastic hinge properties are defined by using the capacity models suggested by the Italian seismic code [94, 103] for yielding and ultimate limit states (Figure 3.3). Two loading patterns, with forces proportional respectively to the fundamental mode shape (triangular pattern) and to the masses (uniform pattern), are adopted in each direction. According to [94], the collapse of the structure is conventionally assumed when the capacity curve exhibits a peak strength reduction of 20%.

Through the well-known N2 method [104], the equivalent reduced order single-degree-of-freedom model of the existing building is derived. Hence, the equivalent mass, equivalent stiffness, and equivalent damping constant - $m_{AS\text{-}IS}$, $k_{AS\text{-}IS}$, and $c_{AS\text{-}IS}$ - are obtained.

The 3D FEM used for the nonlinear time history analyses is the same as the one used for the pushover analyses, enriched by the additional description of the hysteretic response of the flexural and shear hinges, here represented by a Pivot-type model [105] (Figure 3.4). The shape of the hysteresis loop and the stiffness and strength degradation of the model are controlled by the parameters α_1, α_2, β_1, β_2, and η. In particular, α_1 and α_2 locate the *primary pivot points* P_1, P_2 and P_3, P_4 for unloading to zero from positive and negative force, respectively; β_1 and β_2 locate the *pinching pivot points* PP_1 and PP_2 for reverse loading from zero toward positive and negative force, respectively; the parameter η, finally, determines the amount of degradation of the elastic slopes after plastic deformation. According to [106 – 108], appropriate values to be assigned to the parameters for modelling the cyclic behaviour of masonry walls are 0.45 for α_1, α_2, β_1, β_2, while η can be set equal to zero.

For existing buildings that experience inelastic deformations under a certain intensity level of ground motion, a parameter that accounts for the damage accumulation in the structure can be calculated.

Since the seismic damage is strictly related to the hysteretic energy absorbed by the system during the cyclic loading [72 – 78], a hysteretic energy absorption ratio, $\rho_{E,\,AS\,IS}$, is introduced for the AS-IS configuration, i.e.:

$$\rho_{E,AS-IS} = \frac{E_{h,AS-IS}}{E_{i,AS-IS}} \tag{3.1}$$

where $E_{h,\,AS\,IS}$ is the cumulated hysteretic energy dissipated during the inelastic cycling and $E_{i,\,AS\,IS}$ is the seismic input energy.

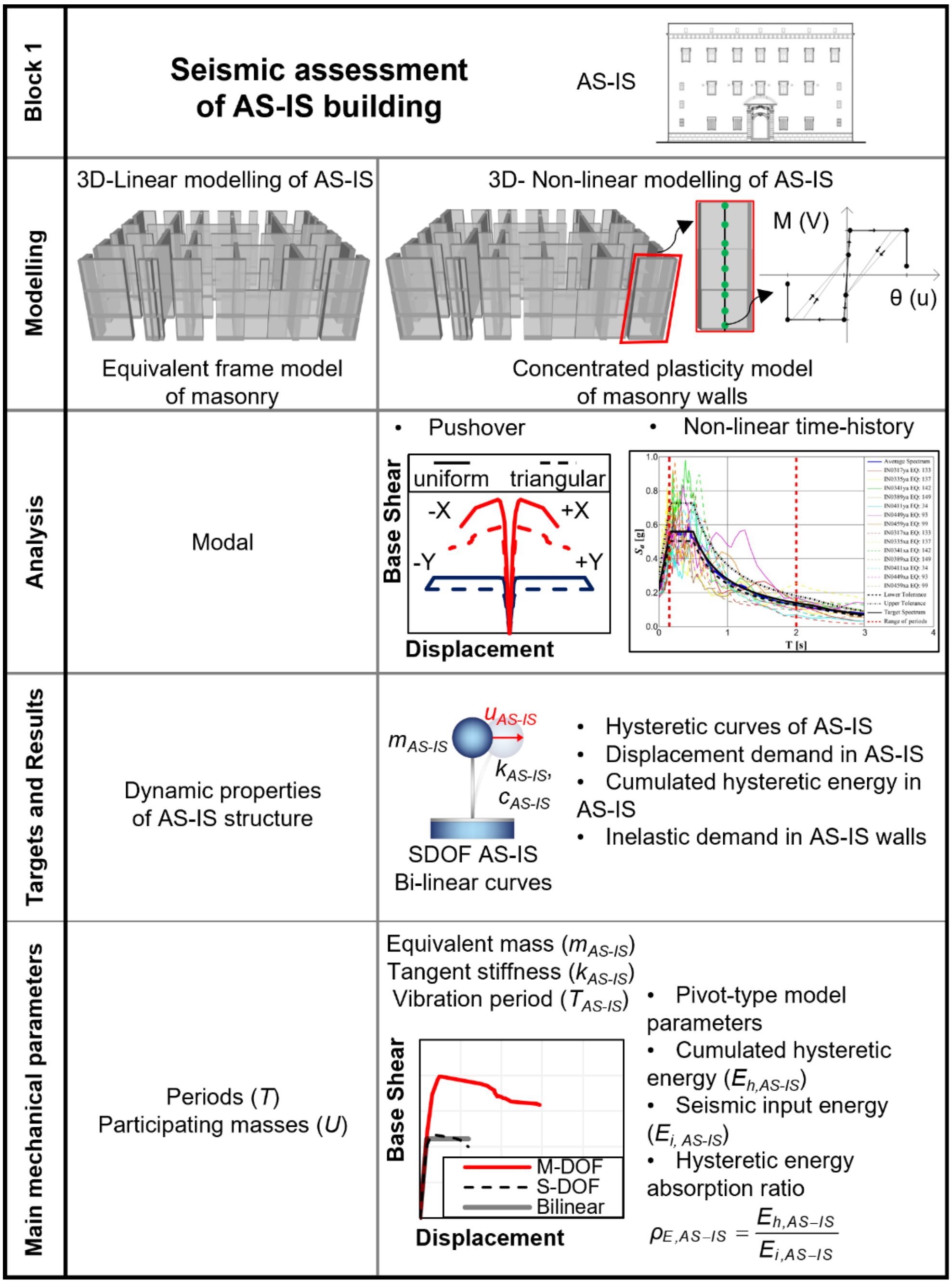

Figure 3.2. Block 1 - IIS design procedure: seismic assessment of existing building.

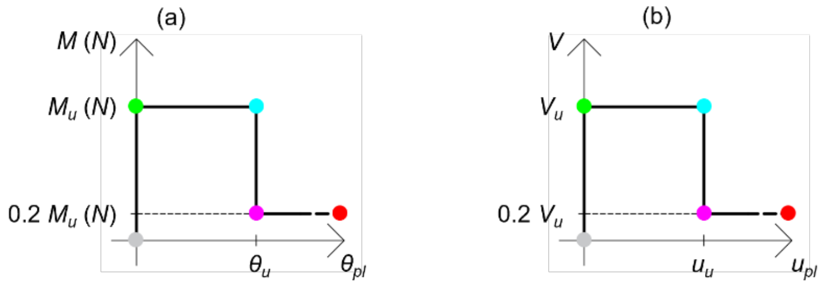

Figure 3.3. Plastic hinge model of masonry walls: (a) moment-plastic chord rotation response, (b) shear force-displacement response.

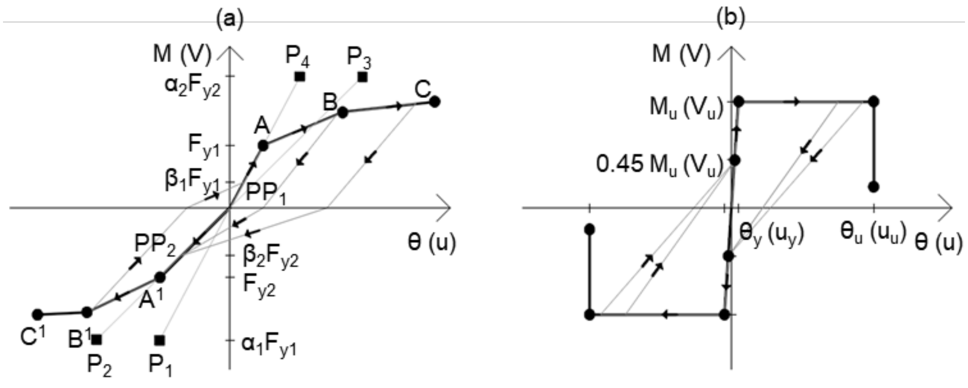

Figure 3.4. Pivot-type model: (a) general model, (b) model adopted for the plastic hinges of masonry walls.

3.1.2 Block 2: selection of the IIS design configuration

The Block 2 of the proposed design procedure consists in the selection of the design configuration of the intermediate isolation system (IIS) (Figure 3.5).

For this aim, two reduced-order models, respectively characterised by a single degree of freedom (SDOF) and by three degrees of freedom (3DOF), are utilised. The SDOF model represents the existing structure, AS-IS, with equivalent properties derived from push over curve through the N2 method (block 1). The 3DOF model describes the structural complex with intermediate isolation system, IIS, i.e. the masonry building (LS) extended by means of a vertical addition in structural steelwork (US), equipped with seismic isolation system at its base (ISO). It is worth underlining that, the dynamic properties of the LS correspond to the dynamic properties of the AS-IS, i.e.: $m_{AS\text{-}IS} = m_{LS}$, $k_{AS\text{-}IS} = k_{LS}$, $c_{AS\text{-}IS} = c_{LS}$.

For the definition of the design parameters of the building extension (US and ISO), a parametric analysis is carried out on the 3DOF IIS model by means of linear response spectrum analyses (RSA); the same analyses are also performed on the SDOF LS model for comparative purpose. In the parametric analysis, the mass, stiffness, and damping constants of the ISO and US degrees of freedom are varied.

The parameters introduced for this aim are:

$M_{ISO} = m_{US} + m_{ISO}$ total isolated mass, sum of upper structure mass, m_{US}, and isolation system mass, m_{ISO};

$\mu = M_{ISO} / m_{LS}$ ratio between the isolated (or added) and existing mass values, M_{ISO} and m_{LS};

$K = k_{US} / k_{LS}$ ratio between the stiffness values of upper and lower structure, k_{US} and k_{LS};

$I = T_{ISO} / T_{US}$ ratio between nominal periods of isolation system and upper structure, T_{ISO} and T_{US}.

The natural frequencies of the three portions are defined as follows:

$$\omega_{LS} = \sqrt{\frac{k_{LS}}{m_{LS}}};\ \omega_{ISO} = \sqrt{\frac{k_{ISO}}{M_{ISO}}};\ \omega_{US} = \sqrt{\frac{k_{US}}{m_{US}}}$$

In [20, 21] it has been found that the stiffness ratio K does not significantly affect the dynamic response when is larger than 1, therefore here it is set at 1.25; also the mass ratio α, which was varied in a wide range in [20, 21], in this example is set at the value of 0.25. Therefore, the major design parameter examined in the present study is the isolation ratio I; to give maximum generality to this study, the values of I are varied in the range [0.1 - 50]. It is worth recalling that the parameter I is also defined for base isolated buildings, and several design codes (e.g. [94]) recommend a minimum value for I equal to 3.

The damping constants for the three degrees of freedom, c_{LS}, c_{ISO}, c_{US}, are obtained from the values of the equivalent viscous damping ratios usually adopted for the corresponding structure types, i.e.: ξ_{LS} =

0.05 for the LS made of tuff masonry piers; ξ_{ISO} = 0.15 for the isolation system made of high damping rubber bearings; ξ_{US} = 0.02 for the upper structure made of steel concentric braced frames. Adopting different values of damping ratios within the same structure leads to a system characterized by non-proportional damping that does not satisfy the Caughey and O' Kelly identity: $\boldsymbol{CM}^{-1}\boldsymbol{K}=\boldsymbol{KM}^{-1}\boldsymbol{C}$ (with $\boldsymbol{M}$, $\boldsymbol{K}$ and $\boldsymbol{C}$ the mass, stiffness and damping matrices) and shows complex-valued natural modes [83, 109, 110] (see Appendix B).

For a better understanding of the analysis results obtained for the 3DOF IIS, a dimensionless response parameter, $\bar{u}$, is introduced and plotted as a function of the isolation period T_{ISO}. It is defined as the ratio between the displacement of the first DOF in the 3DOF IIS model, i.e. u_{LS}, and the SDOF AS-IS model counterpart, i.e. $u_{AS\text{-}IS}$. When $\bar{u}$ is less than one, the displacement in the masonry structure in the IIS configuration is smaller than in the AS-IS configuration; in these cases ($\bar{u}$ < 1), the isolated vertical extension works as a nonconventional TMD, thus reducing the seismic demand on the existing structure despite the increase of the seismic mass due the vertical extension. By plotting such results as a function of the isolation period T_{ISO}, a design spectrum is obtained, i.e. a *nonconventional TMD design spectrum* in terms of displacement.

One or more design configurations, such that the displacement ratio $\bar{u}$ is smaller than, or almost equal to one ($\bar{u}$ < 1), can be chosen for the isolated upper structure from the so-called *nonconventional TMD design spectrum*.

It is worth observing that some additional aspects may affect the final choice of the design configurations above identified, namely: 1) urban planning restraints on number of stories, floor area, total height; 2) construction feasibility of the new addition in terms of additional gravity load transferred to the existing masonry structure; 3) construction feasibility of the new addition in terms of structural system; 4) technical feasibility of the isolation system for the target design period. The above issues are dealt with in the block 3.

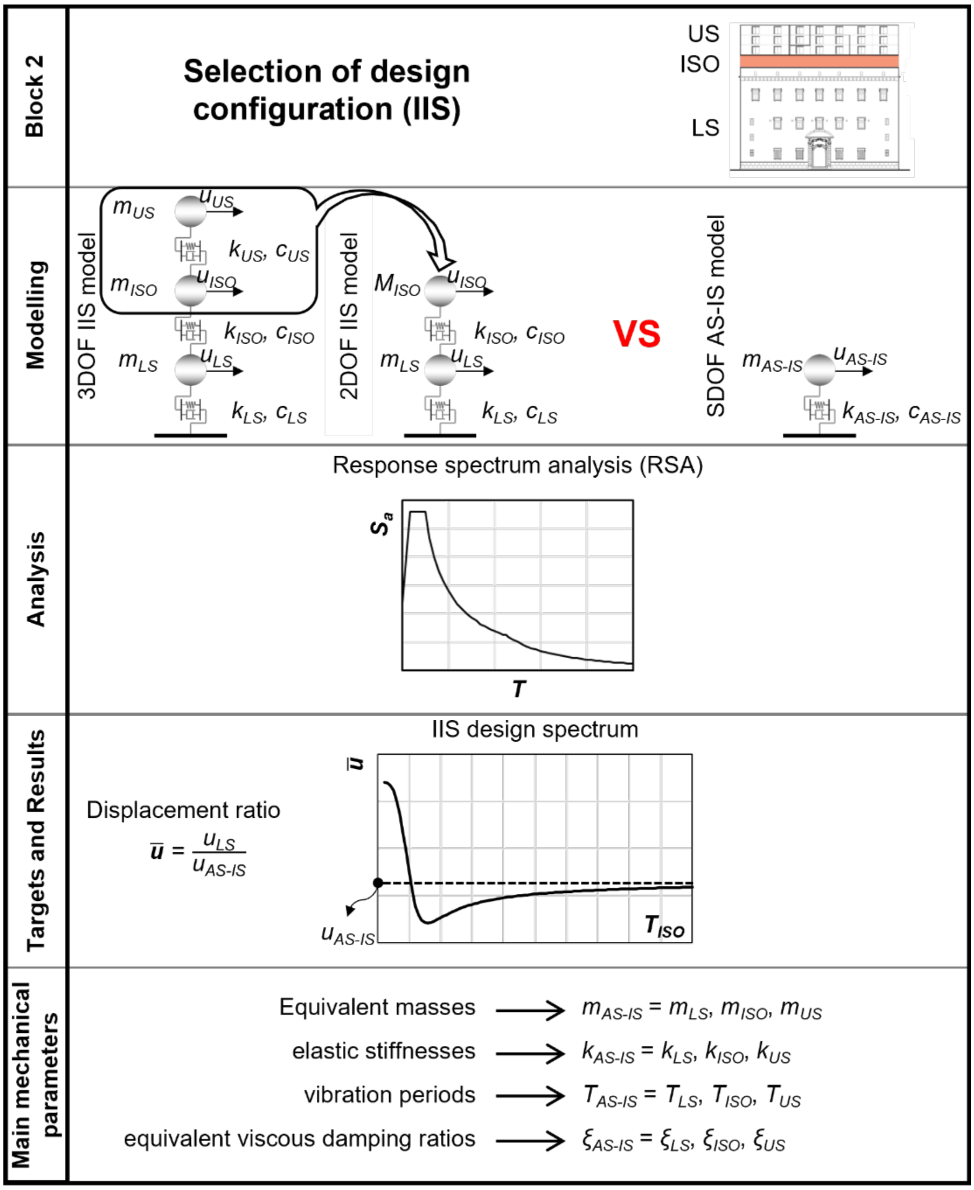

Figure 3.5. Block 2 - IIS design procedure: selection of the IIS design configuration.

3.1.3 Block 3: design of ISO system and US

The Block 3 of the proposed design procedure consists in the design of the ISO and US system (Figure 3.6).

For the isolation system, the isolators, e.g. high damping rubber bearings (HDRBs), should be placed at the intersections of perpendicular walls in the LS. For design purpose, the behaviour of HDRBs can be assumed linear elastic with equivalent damping ratio ξ_{ISO} equal to, say, 0.15. In the design process of the isolators, the global stiffness required for the isolation system k_{ISO} is derived from T_{ISO} and M_{ISO}, while the displacement demand δ_{ISO} is evaluated from the displacement response spectrum defined for the specific site at the corresponding isolation period T_{ISO}.

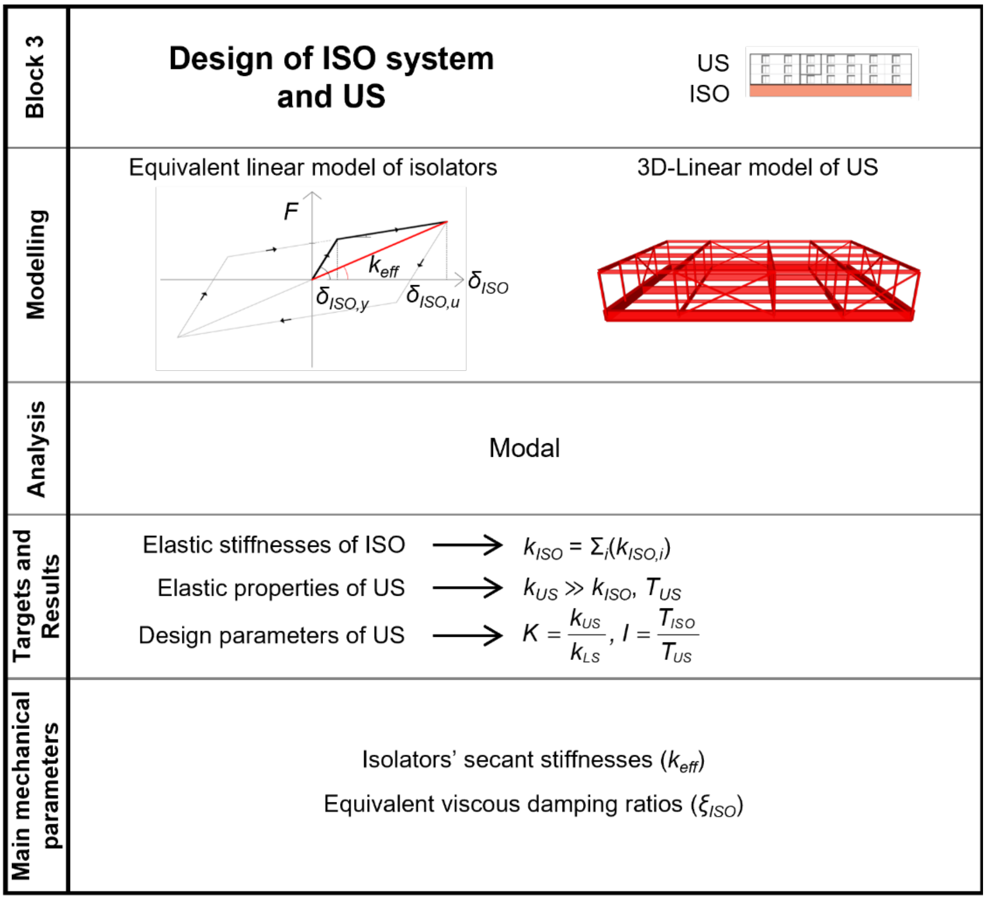

Figure 3.6. Block 3 - IIS design procedure: design of ISO system and US.

Steel structures are adopted for the US, since they are characterized by rigidity and lightness and allow for easy assembly and erection, with almost no disruptions for the activities hosted in the existing structure. Furthermore, by selecting a structural steelwork for the extension, the floors to rebuild are lighter than masonry or concrete floors. Finally, braced frame solutions are particularly suitable due to the possibility of tuning the lateral stiffness k_{US} as a function almost uniquely of the diagonal cross sections [111, 112]. The design solution of the US should be such to satisfy the selected value of $K = k_{US} / k_{LS}$ and $I = T_{ISO} / T_{US}$.

3.1.4 Block 4: seismic assessment of IIS

The Block 4 of the design procedure consists in the seismic assessment of the IIS design configurations (Figure 3.7). For this aim, 3D finite element models of the IIS design configurations (3D FEMs IIS) are developed and used for FE analyses through the software SAP2000 [113]. Spectrum compliant ground motion records are utilised for defining seismic inputs in nonlinear time history analyses. In the 3D IIS models, only masonry nonlinearities are considered, according to the same modelling approach utilised in the block 1.

As already done for the AS-IS configuration (block 1), it is possible to calculate the hysteretic energy absorption ratio, $\rho_{E,\,IIS}$, for the IIS configuration, i.e.:

$$\rho_{E,IIS} = \frac{E_{h,IIS}}{E_{i,IIS}} \tag{3.2}$$

where $E_{h,\,IIS}$ is the cumulated hysteretic energy dissipated during the inelastic cycling and $E_{i,\,IIS}$ is the seismic input energy.

Block 4	**Seismic assessment of IIS**	US ISO LS 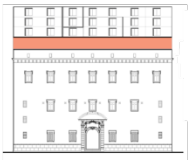
Modelling	3D modelling of IIS 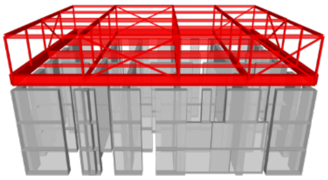 US → linear ISO → linear LS → linear	3D-modelling of IIS 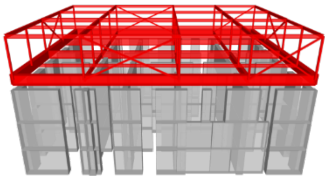 US → linear ISO → linear LS → nonlinear
Analysis	Modal	Nonlinear time-history 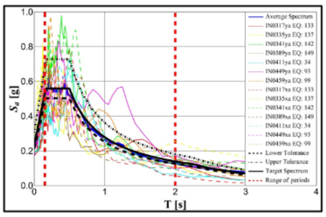
Targets and Results	• Dynamic properties of IIS • Displacement demand of LS • Base shear of IIS (V_{IIS}) • ISO system displacement value ($\delta_{ISO,IIS}$)	• Hysteretic curves of LS • Displacement demand of LS • Cumulated hysteretic energy of LS • Inelastic demand of LS walls • ISO system displacement value ($\delta_{ISO,IIS}$)
Main mechanical parameters	Elastic Periods (T) Participating masses (U)	• Pivot-type model parameters • Cumulated hysteretic energy ($E_{h,IIS}$) • Seismic input energy ($E_{i,IIS}$) • Hysteretic energy absorption ratio $\rho_{E,IIS} = \frac{E_{h,IIS}}{E_{i,IIS}}$

Figure 3.7. Block 4 - IIS design procedure: seismic assessment of IIS design configuration.

3.1.5 Block 5: Evaluation of the IIS effectiveness

The effectiveness of IIS is evaluated through the comparison between the seismic response of the existing building in the AS-IS configuration (Block 1) and the counterpart in the IIS configurations (Block 4) (see Figure 3.8). The seismic response of the same existing building with a conventional vertical extension, i.e. with the US fully connected to the LS without the intermediate isolation system (appointed as LS+US configuration), can also be considered for highlighting the effectiveness of IIS in terms of seismic response. The performance parameters derived from the non-linear analyses and adopted for the assessment are: the story and inter-story drifts, in particular the drift at the top level of the existing structure; the cumulated hysteretic energy; the inelastic deformation demand in the plastic hinges of masonry walls. Instead, in the case of linear analyses, the performance parameters adopted for the assessment are: the story and inter-story drifts and the base shear demand. Both time histories and peak values, as well as average of peak values, of the performance parameters are considered.

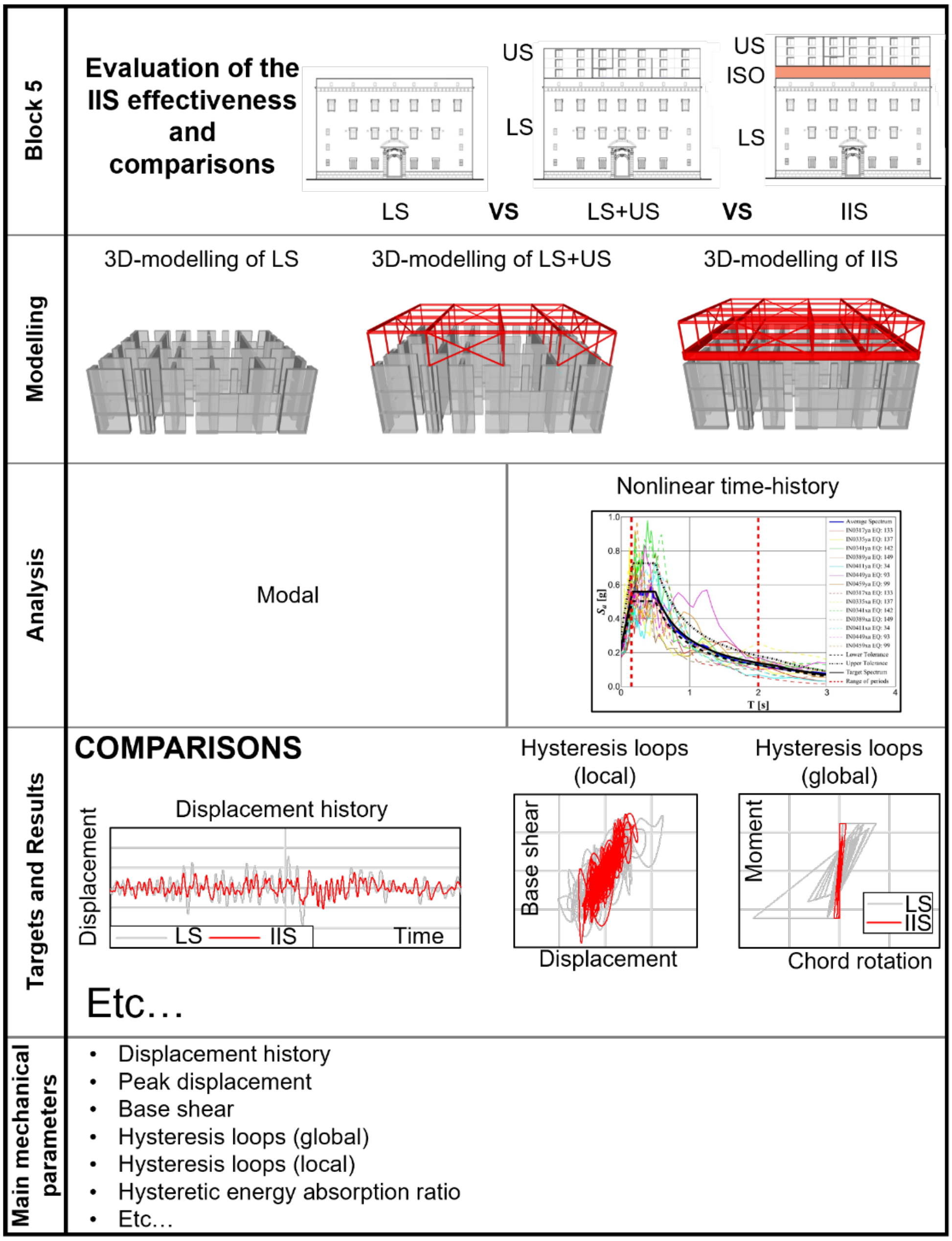

Figure 3.8. Block 5 - IIS design procedure: evaluation of the IIS effectiveness and comparisons.

3.2 Application of 5-Block design procedure to a real case study

In this section, the general 5-block design procedure for the IIS is applied by selecting as case study an aggregate of masonry buildings located in the city of Pozzuoli (Italy). This aggregate is listed in the study [21], where a large-scale application of the IIS strategy is proposed for the vertical extension of several masonry buildings in the historical centre of Pozzuoli. In particular, the effectiveness of IIS working as nonconventional TMD for the existing construction assessing the reduction of seismic demand and damage in the masonry structure undergoing inelastic deformation. First, the characterization of dynamic behaviour and seismic capacity of the building aggregate is addressed through modal and push over analyses, respectively. Elastic parametric analyses are then carried out on lumped mass models to derive the so-called *nonconventional TMD design spectrum* and to define the design configurations of the isolated vertical addition that minimize the global seismic response of the overall structure. Finally, the effectiveness of the retrofit solutions is evaluated through nonlinear time history analyses and its performance is compared to the one of the AS-IS building structure (i.e. the existing structure in its uncontrolled configuration); structural performance indexes accounting for both peak response and accumulated damage are defined and utilised for this purpose.

3.2.1 Brief description of the real case study

The case study considered in this chapter is an aggregate of four unreinforced masonry (URM) buildings (Figure 3.9a) located in Pozzuoli (Naples, Italy), where a recently issued Urban Implementation Plan [114] provides the reconstruction of rooftop volumes, demolished during the 1980s, of several buildings in the historic centre.

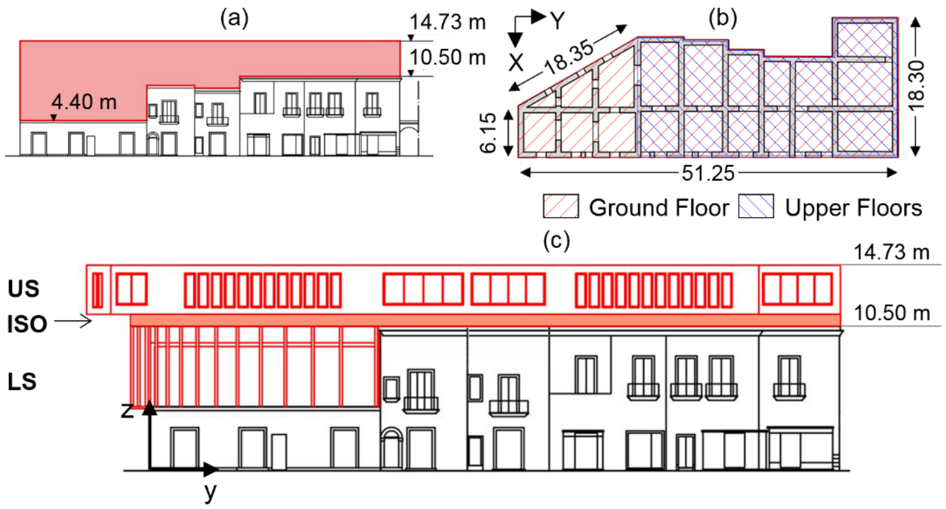

Figure 3.9. Case study building: (a) AS-IS configuration (the red portion is the demolished volume, to rebuild), (b) floor plans, (c) IIS configuration.

In Figure 3.9a the original size of the case of study, a three stories construction of the 16th century, is provided; at present, however, the aggregate is constituted by one or two-story, lacking the red portion depicted in Figure 3.9a. It has a discontinuous profile of elevations, with the first building on the left formed by a single story, with a total height of 4.4 m, and the other buildings of two-story, with a total height of 10.5 m. Therefore, the floor plan is 51.25 m x 18.30 m (floor area 820 m^2) at ground level, and 35.25 m x 18.30 m (floor area 610 m^2) at the upper floor.

Tuff masonry walls in the transversal direction, 75 cm thick, are spaced at quite regular intervals, of 5-6 m (Figure 3.9b), except for the last span, of 8.40 m. The masonry structure is well preserved and does not display any evident damage due to past earthquakes, such as cracks in the walls and detachments between walls and floors. The mechanical properties assumed for the tuff masonry material are: average weight 16 kN/m^3, Young modulus 1080 MPa, shear modulus 360 MPa, compression strength 3.0 MPa [103].

A preliminary evaluation of the compression stress state at the base of the walls has been carried out, to assess the reserve of bearing capacity and, in turn, the feasibility of the building vertical extension. As expected, considering the original construction size, the average compressive stress due to gravity loads (at Ultimate Limit

State loading condition) is equal to or less than 8% of the compression strength capacity for all masonry piers.

The idea for this case study is to rebuild the demolished portion (Figure 3.9c) as a base isolated extension, with the seismic isolation system located on the roof of the masonry aggregate and at the base of the new structure, realizing the extended structural complex with an intermediate isolation system. As displayed in Figure 3.9c, the isolation layer subdivides the extended building into three parts, i.e.: the LS, the ISO and the US. For realizing the one-story isolated addition (Figure 3.9c), a unique and continuous level for the isolation interface is required. Therefore, to compensate the altitude difference of 6.30 m (Figure 3.9a) between the roofs of the buildings in the aggregate, a "*filling*" frame structure is designed to be erected on the roof of the shorter building.

3.2.2 Application of Block 1: seismic assessment of the AS-IS configuration

The structural system of the unreinforced masonry (URM) building is made of vertical walls connected by horizontal spandrels and a rigid floor. As reported in Section 3.1.1, the 3D FEM of the AS-IS configuration (appointed as 3D AS-IS) is the equivalent frame model (EFM) with weak spandrels [115], which is a simplified approach very common in engineering practice [115 – 117]. Neglecting the flexural contribution of the spandrels, the model is composed of vertical cantilevers beams (the piers) connected at floor levels through rigid diaphragm. The masonry piers contribute to the global response along each principal direction only with their in-plane behaviour; therefore, the out-of-plane contribution of each single pier is assumed negligible. The total mass of the building is 3932 kNs^2/m, concentrated at floor levels (m_1= 2033 kNs^2/m and m_2=1899 kNs^2/m).

As observed in Figure 3.9a, the masonry buildings in aggregate shows vertical setbacks that are removed to provide the same rooftop level, corresponding to the isolation layer. For this aim, a "*filling*" steel structure has been added on the roof of the first building on the left side; furthermore, the masonry walls of the second and third buildings have been extended with the same masonry material for reaching all the same height (Figure 3.9c and Figure 3.10b).

The “*filling*” structure is a two-story steel Moment Resisting Frame (MRF, Figure 3.10a) that has been designed to not alter the dynamics of the existing masonry aggregate. It has inter-story height of 3.15 m, beams IPE 240 and IPE 360, columns CHS 219.1x16; the steel grade is S275 (f_{yk} = 275 MPa, f_{yd} = 262 MPa). The total MRF mass is 269.2 kNs^2/m, concentrated at floor levels (m_1 = 134.6 kNs^2/m and m_2 = 134.6 kNs^2/m). The masonry aggregate (AS-IS model) plus the “*filling*” MRF represents the LS in the IIS structural complex; the relevant FE model is appointed as the 3D LS model and is depicted in Figure 3.10b.

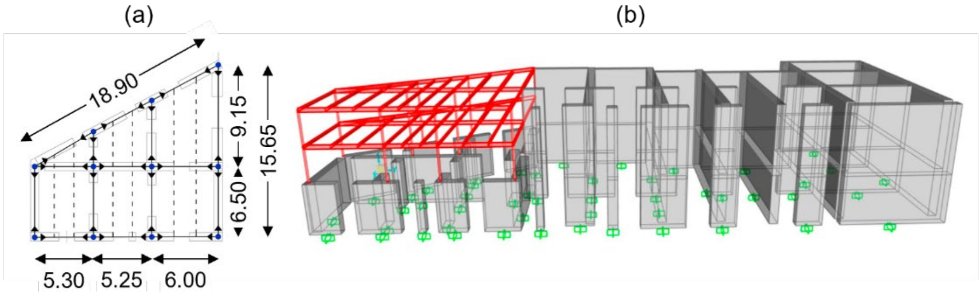

Figure 3.10. (a) Schematic floor structure of the “*filling*” MRF, (b) 3D LS model, masonry structure plus “*filling*” MRF.

The nonlinear modelling adopted for the aggregate of masonry buildings has been already described in Section 3.1.1. A concentrated plasticity model is used for describing the flexural and shear nonlinear behaviour of masonry piers [106, 107, 115, 118]. Two flexural hinges are assigned at both ends of each pier, while one shear hinge is assigned at the centre of each pier (Figure 3.3). Only the diagonal cracking (Eq (3.3)) has been considered as possible shear failure mechanism [108] since it is the most likely failure mode for URM with irregular blocks, as also suggested by the Italian code [103]. The sliding shear failure, which is related to the un-cracked section, thus, in turn, to the flexural behaviour, has not been considered in the model. For this reason, the shear-flexure interaction in the plastic hinges is neglected. The diagonal shear and flexural resistances are calculated using the formulas reported in the Italian code [94, 103] and recalled below:

$$V_U = l \cdot t \cdot \frac{f_{td}}{b} \sqrt{1 + \frac{\sigma_0}{f_{td}}} \tag{3.3}$$

$$M_U = \left(l^2 \cdot t \cdot \frac{\sigma_0}{2} \right) \cdot \left(1 - \frac{\sigma_0}{0.85 \cdot f_d} \right) \tag{3.4}$$

where: l, t and σ_0 are respectively the length, the thickness and the stress compression due to gravity load of the masonry piers; b is a factor that takes into account the shear stress distribution in the cross section and is related to aspect ratio of the wall [119].

The plastic hinge properties at yielding and ultimate limit states are given in Figure 3.3, while the general and adopted Pivot-type hysteretic model for the AS-IS are reported in Figure 3.4.

3.2.2.1 Linear dynamic analysis of LS

For evaluating the dynamic behaviour of the case study, modal analyses are carried out on the 3D AS-IS and 3D LS models using the computer code SAP2000 [113]. Periods (T) and participating mass ratios of the first three vibration modes are given in Table 3.1, where U_x, U_y and R_z are the values of translational participating mass in x, y and rotational direction respectively. For both models, it can be observed that the first mode is purely translational in the direction Y, while the other two modes couple translation in the direction X and rotation around the vertical Z axis.

Table 3.1. Periods and participating masses of the first three vibration modes of the AS-IS and LS models.

	AS-IS model				LS model			
Mode	T [s]	U_x [%]	U_y [%]	R_z [%]	T [s]	U_x [%]	U_y [%]	R_z [%]
1	0.39	0.35	72.37	0.83	0.39	0.34	72.54	0.80
2	0.28	46.26	1.38	20.15	0.28	47.57	1.29	19.45
3	0.24	32.92	0.22	49.86	0.24	31.72	0.22	50.93

The results in Table 3.1 confirm that the "*filling*" MRF does not modify the building dynamics; indeed, the periods of the LS and AS-IS models are identical, and the participating mass ratios differ less than 7%. Therefore, the two 3D models, 3D AS-IS and 3D LS, which only differ for the "*filling*" MRF, can be considered equivalent from the dynamic point of view. In the following, the model LS is utilised indifferently for representing both the lower structure of the extended construction and the original AS-IS configuration of the building aggregate.

3.2.2.2 Pushover analysis of 3D LS and definition of reduced-order SDOF model

The masonry building capacity is assessed by means of push over analyses on the 3D LS model subjected to both triangular and uniform horizontal loading patterns.

The exam of the push over curves obtained under the two loading patterns suggests that the triangular distribution gives rise to the smallest strength, for both the principal directions. Therefore, these curves are selected for deriving the dynamic properties of the reduced-order SDOF models equivalent to the masonry structure, according to the N2 method [104] (Figure 3.11). In particular, the equivalent mass, stiffness, and period in each principal direction are:

$\tilde{m}_{LS,X}$ = 1077.20 kNs^2/m $\qquad$ $\tilde{m}_{LS,Y}$ = 2472 kNs^2/m

$\tilde{k}_{LS,X}$ = 1.37x10^6 kN/m $\qquad$ $\tilde{k}_{LS,Y}$ = 639883 kN/m

$T_{LS,X}$ = 0.176 s $\qquad$ $T_{LS,Y}$ = 0.39 s

These dynamic properties are assigned to the degree of freedom representing the LS in the 3DOF model utilized for the parametric analysis, as reported in subsection 3.2.3. In fact, the ~ symbol refers to the reduced order model derived from the 3D FEM LS

The damping constant in X and Y direction, $\tilde{c}_{LS,X}$ and $\tilde{c}_{LS,Y}$, are equal to:

$$\tilde{c}_{LS,X}=2\xi_{LS}\omega_{LS,X}\tilde{m}_{LS,X} = 3846 \text{ kNs/m}$$

$$\tilde{c}_{LS,Y}=2\xi_{LS}\omega_{LS,Y}\tilde{m}_{LS,Y} = 3983 \text{ kNs/m}$$

in which the equivalent viscous damping ratio is ξ_{LS} = 0.05 and fundamental circular frequencies are $\omega_{LS,X} = 2\pi/T_{LS}$ = 35.70 rad/s and $\omega_{LS,Y} = 2\pi/T_{LS}$ = 16.11 rad/s for X and Y direction, respectively.

Furthermore, the results of pushover analyses for Y direction is showed in Figure 3.12, where the failure of piers aligned along Y direction is due to the attainment of the ultimate bending capacity (see

Figure 3.3). while the piers along X direction (not depicted in figure for the sake of brevity) fail for the attainment of both ultimate bending and shear capacities.

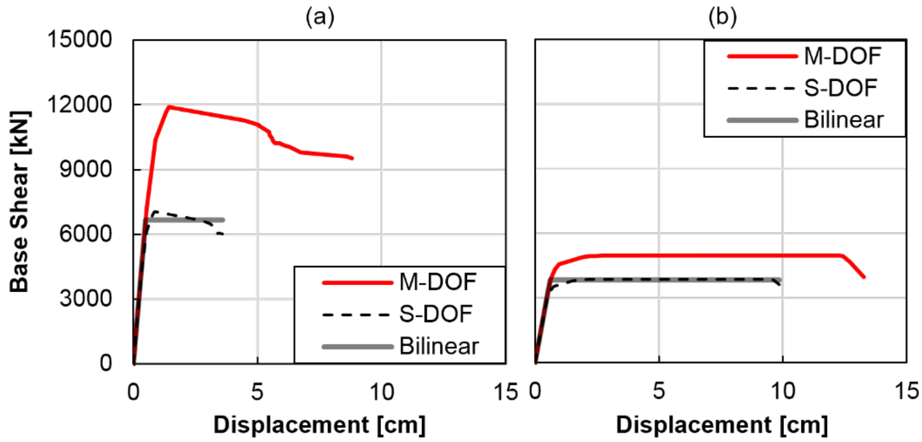

Figure 3.11. Capacity curves: (a) X direction, (b) Y direction.

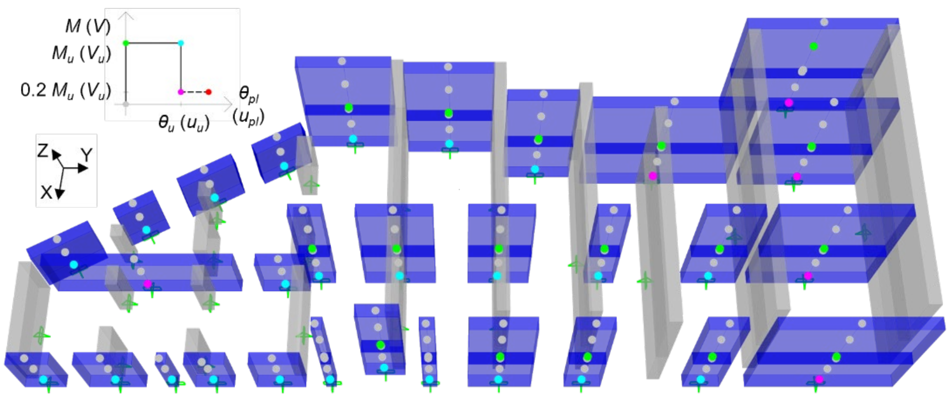

Figure 3.12. 3D LS model: plastic hinges in the walls (Y direction).

3.2.2.3 Nonlinear time history of LS

For a thorough assessment of masonry LS, nonlinear time history analyses are also performed on the relevant 3D model, by adopting seven pairs of acceleration records of real ground motions [94]. The software REXEL v 3.5 [120] is used to select records such that their average response spectrum is close to the target response spectrum, with upper and lower tolerance of 30% and 10%, respectively. In particular, the target spectrum is the elastic acceleration response spectrum defined by the Italian seismic design code [94] for the site of

Pozzuoli at the Design Basis Earthquake (DBE) level, characterised by 10% probability of exceedance in 50 years (return period of 475 years). The ground motion records are selected from the SIMBAD database (Selected Input Motions for displacement-Based Assessment and Design) [121], considering a peak ground acceleration (PGA) between 0.1 g and 0.3 g in the period range of 0.15 - 2 s. The major data of the ground motion records are provided in Table 3.2, while the Figure 3.13 shows the response spectra of the selected acceleration records and compares the average spectrum to the target spectrum of Pozzuoli.

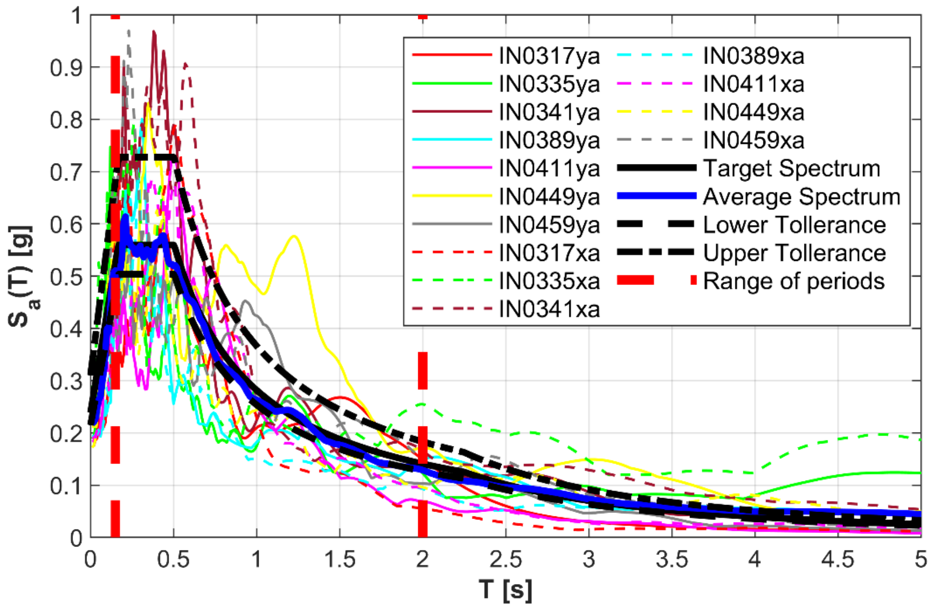

Figure 3.13. Set of seven pairs of averagely spectrum-compatible acceleration response spectra.

In Figure 3.14 the push over curves obtained for each direction with the two types of loading pattern (triangular and uniform), are compared to the global hysteretic response of the existing building (Figure 3.14a and Figure 3.14b). In particular, the base shear vs. top displacement of the LS model resulting from two-time history analyses are provided. The selected time histories correspond to the minimum and maximum displacement demand, i.e. the records 449 and 341 for X direction, and the records 389 and 449 for Y direction. From the plots it can be observed that the push over curves represent the backbones of the cyclic responses; furthermore, the wider hysteresis loops in the

Y direction testify that the response of the structure in this direction becomes significantly nonlinear, due to the much lower strength capacity with respect to the X direction.

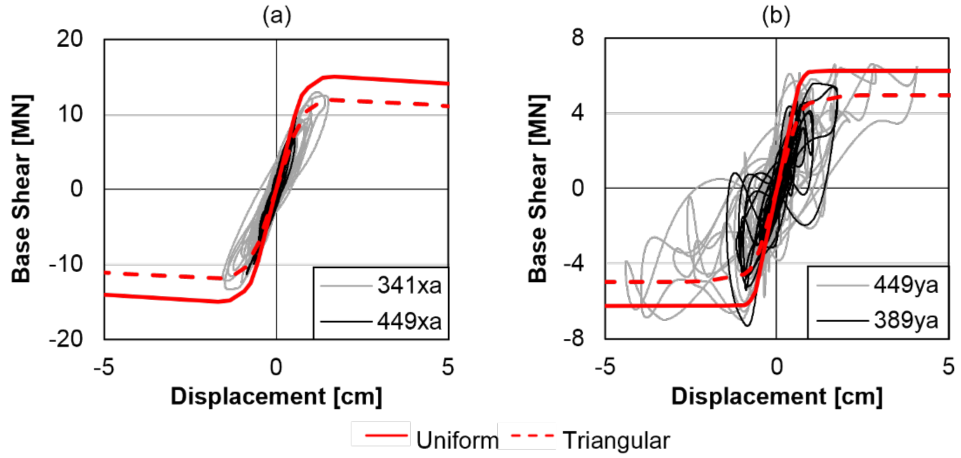

Figure 3.14. LS: push over curves and global hysteretic loops under selected time histories: (a) X direction, (b) Y direction.

Table 3.2. Major data of seven pairs of spectrum-compatible acceleration records.

Earthquake name	EN1	EN2	EN3	EN3	EN4	EN5	EN6
Date	29/05/ 2012	03/09/ 2010	21/02/ 2011	13/06/ 2011	16/01/ 1995	24/11/ 1987	17/01/ 1994
W. ID	317	335	341	389	411	449	459
E. ID	133	137	142	149	34	93	99
S. ID	MOG0	TPLC	RHSC	RHSC	TKS	WSM	ST_243 89
F. M.	reverse	strike-slip	reverse	reverse	strike-slip	strike-slip	reverse
Epi. Dist [km]	16.43	23.58	13.73	14.76	17.45	19.5	20.19
PGAx [g]	0.24	0.28	0.29	0.19	0.19	0.17	0.26
PGAy [g]	0.17	0.19	0.25	0.19	0.18	0.21	0.22
EC8 S. C.	C*	C*	C*	C*	C*	C	C
$v_{s,30}$ [m/s]	n.a.	n.a.	n.a.	n.a.	n.a.	194	278

***Note**: site class with * is based on geological information alone.*
Key: EN1 = Emilia Pianura Padana; EN2 = Darfield; EN3 = Christchurch; EN4 = Hyogo - Ken Nanbu; EN5 = Superstition Hills; EN6 = Northridge; W. ID = Waveform ID; E. ID = Earthquake ID; S. ID = Station ID; F. M = Fault Mechanism; Epi. Dist = Epicentral Distance; S.C. = Site Class; n.a. = not available.

In addition, the average values of the maximum plastic rotation demand to capacity ratios (DCR), calculated for the seven acceleration records in the walls at the base floor of the 3D LS model, are depicted in Figure 3.15. Analogously to what observed in Figure 3.12, in which the piers collapse for the attainment of the ultimate bending capacity in Y direction, the most stressed piers show values of plastic rotation DCR in the range of 0.15 – 0.20.

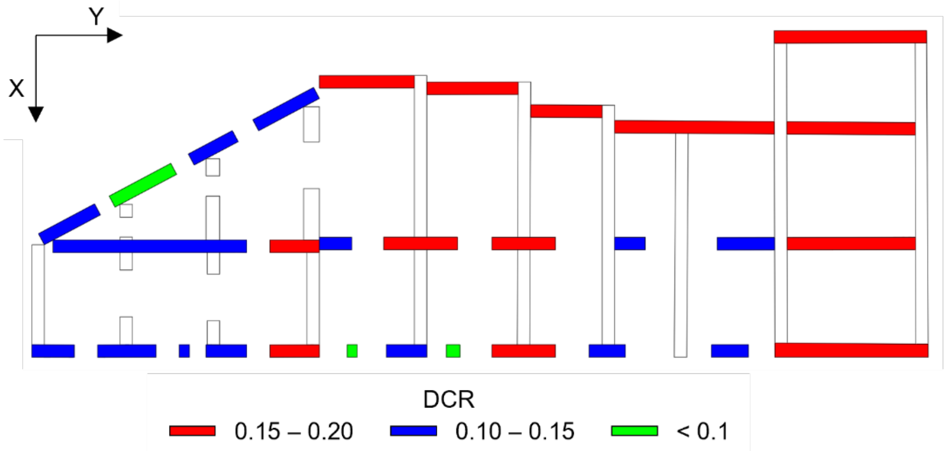

Figure 3.15. DCR in terms of chord rotation for the piers at the base floor of the 3D LS model.

3.2.3 Application of Block 2: design of IIS

3.2.3.1 Parametric analysis on reduced-order models

The dynamic properties of the reduced-order model of the existing building are derived from the push over analyses carried out in the previous sub-section; referring to the weakest (Y) direction of the LS configuration, they are: mass $\tilde{m}_{LS,Y}$ = 2472 kNs^2/m, stiffness $\tilde{k}_{LS,Y}$ = 639883 kN/m, period $T_{LS,Y}$ = 0.39 s. By adopting average values of the seismic weight (dead plus reduced live loads) equal to 20 kN/m^2 and 7 kN/m^2, respectively for the masonry and steel structures, and by considering the constraints of the urban reconstruction plan [114] in terms of floor areas and number of stories to rebuild, as reported in [21, 122], the value of the mass ratio $\mu = M_{ISO}/(m_{1,LS}+m_{2,LS})$ for the case study is assumed approximately equal to 0.25. In the same way, for the reduced-order lumped mass model, the mass ratio $\tilde{\mu}=\tilde{M}_{ISO}/\tilde{m}_{LS}$ is approximately equal to 0.38. While the total isolated mass M_{ISO} ($\approx\tilde{M}_{ISO}$) is derived from the mass ratio μ, the masses m_{US} and m_{ISO} can be separately evaluated by using the ratio $\gamma = m_{US}/M_{ISO}$, defined within the linear theory of base isolation [92, 93]. By assuming γ = 0.6, the ratio m_{US}/m_{ISO} is equal to 1.5. The stiffness ratio $K=k_{US}/k_{LS}$ is assumed equal to 1.25. The period of the isolated extension $T_{ISO}=2\pi\left(\tilde{M}_{ISO}/\tilde{k}_{ISO}\right)^{0.5}$ varies in the range of values [0.05 - 5] s.

By selecting a steel braced frame structure for the addition, an equivalent viscous damping ratio ξ_{US} = 0.02 is adopted for the US, while for the isolation system made of High Damping Rubber Bearings (HDRB), equivalent viscous damping ratio ξ_{ISO} = 0.15 is considered.

With these assumptions, the values of mass, stiffness and damping constants of the isolated vertical addition are provided in Table 3.3; the values of the fundamental period and circular frequency of the standalone (not-isolated) upper structure, T_{US} and ω_{US}, and of the isolation system, T_{ISO} and ω_{ISO}, are provided as well.

Table 3.3. Dynamic properties of the upper structure and isolation system in the 3DOF IIS.

UPPER STRUCTURE	ISOLATION SYSTEM
$\tilde{m}_{US}=0.6\cdot\tilde{M}_{ISO}$ =371 kNs²/m	$\tilde{m}_{ISO}=\tilde{M}_{ISO}-\tilde{m}_{US}$ = 247 kNs²/m
$\tilde{k}_{US}=K\cdot\tilde{k}_{LS}$ = 799854 kN/m	$\tilde{k}_{ISO}=4\pi^2\tilde{M}_{ISO}/T_{ISO}^2$ = [976, 9759065] kN/m
$\tilde{c}_{US}=2\xi_{US}\omega_{US}\tilde{m}_{US}$ = 689 kNs/m	$\tilde{c}_{ISO}=2\xi_{ISO}\omega_{ISO}\tilde{M}_{ISO}$ = [233, 23298] kNs/m
$T_{US}=2\pi\cdot\left(\tilde{m}_{US}/\tilde{k}_{US}\right)^{0.5}$ = 0.135 s	$T_{ISO}=2\pi\left(\tilde{M}_{ISO}/\tilde{k}_{ISO}\right)^{0.5}$ = [0.05, 5] s
$\omega_{US}=\left(\tilde{k}_{US}/\tilde{m}_{US}\right)^{0.5}$ = 46.43 rad/s	$\omega_{ISO}=\left(\tilde{k}_{ISO}/\tilde{M}_{ISO}\right)^{0.5}$ = [1.26, 126] rad/s

3.2.3.2 Response spectrum analyses (RSA) on reduced order models

Linear dynamic analyses are carried out on the 3DOF IIS and SDOF LS models considering the elastic acceleration response spectrum for the Design Basis Earthquake (DBE) level, defined within the Italian seismic code [94] for the site of Pozzuoli, and characterized by 10% probability of exceedance in 50 years (return period of 475 years). The spectrum is depicted in Figure 3.16a, for a_g = 0.162 g, site ground acceleration, F_0 = 2.347, maximum value of the amplification factor for horizontal acceleration, T_C* = 0.333 s, reference value to calculate the period corresponding to the starting point of the constant velocity branch, S = 1.472, factor depending on the soil and topographic categories, C_C = 1.509, factor depending on the soil category, ξ = 0.05, viscous damping ratio. As already stated, the parametric response spectrum analysis (RSA) is aimed to assess the feasibility of retrofitting masonry buildings with intermediate isolation system and to define the optimal configurations for the isolated vertical extension.

As mentioned in the subsection 3.1.2, the eigenvalue complex problem is solved in the state space for deriving the modal damping factors, by accounting for the effect of the non-proportional damping, and RSA is carried out by considering complex modal superposition methods [83] (see Appendix B). The results of this analysis can be plotted in terms of different global response parameters (absolute acceleration, a_s; base shear, V_b; drift of the first DOF, u_{LS}), as a function of T_{ISO}/T_{LS} (i.e. the inverse of the tuning ratio, $1/f$), which is the major design parameter, once the size (and the mass) of the vertical extension has been set. The typical trend of the RSA results has been shown in Figure 3.16b which refers to the IIS made by the LS here chosen as an example and the steel vertical extension plus the HDRB isolation system. The graph represents the so called "*nonconventional TMD design spectrum*" or "*IIS design spectrum*", in terms of displacement ratio $\bar{u} = u_{LS}/u_{AS\text{-}IS}$, i.e. drift of LS, in the 3DOF IIS model (design configuration) divided by the counterpart in the SDOF AS-IS (as-is configuration).

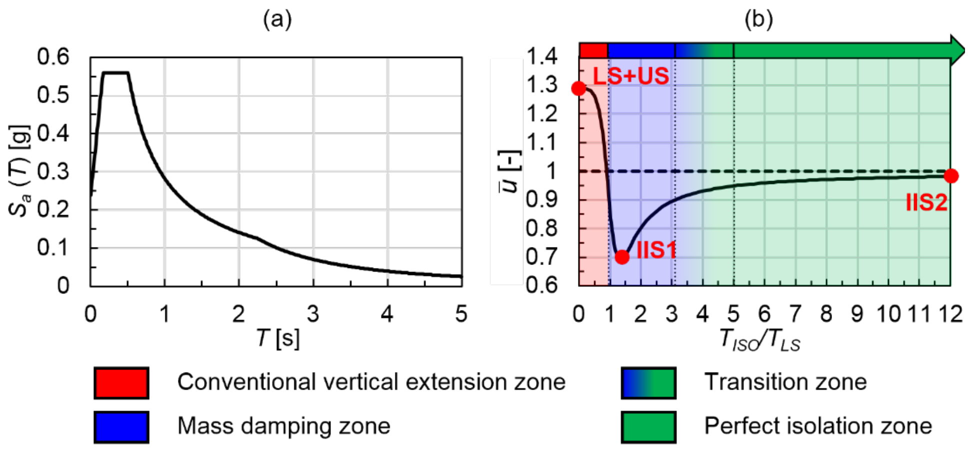

Figure 3.16. (a) DBE Elastic Acceleration Response Spectrum - site Pozzuoli (Italy), damping 5%; (b) graph of displacement ratio $\bar{u} = u_{LS}/u_{AS\text{-}IS}$ as a function of the period ratio T_{ISO}/T_{LS}, considered as *IIS design spectrum*.

From the IIS design spectrum in Figure 3.16b it is possible to identify three plus one regions, i.e.: zone 1, characterised by displacement ratio values $\bar{u}$ larger than 1; zone 2, characterised by displacement ratio values $\bar{u}$ smaller than 1; zone 3, characterised by displacement ratio values $\bar{u}$ almost equal to 1; *transition zone*, between zones 2 and 3, characterised by displacement ratio values $\bar{u}$ gradually approaching to 1.

The zone 1, where $T_{ISO}/T_{LS} < 1$ and $\bar{u} > 1$, exemplifies the case of existing buildings expanded with vertical additions rigidly connected to the substructure (*conventional vertical extension zone*). The solutions that fall into the zone 3, where $T_{ISO}/T_{LS} > 5$ and $\bar{u}$ is close to 1(i.e. $\bar{u} > \approx 0.95$), correspond to a nearly perfect disconnection between vertical extensions and substructure (*perfect isolation effect zone*). In this case, the isolated upper structure works as a structure isolated at its base (BIS), with values of T_{ISO} enough long to exclude any dynamic interaction with the substructure.

For period ratios T_{ISO}/T_{LS} approximately in the range 1 – 3, the ratio $\bar{u} < 1$ and an advantageous dynamic interaction arises between the two structural parts. The isolated upper structure, in fact, acts as a TMD for the lower structure, thus reducing the displacement response of the system (*mass damping effect zone*). It is worth observing that the range of period ratios T_{ISO}/T_{LS} =1 – 3 identifies the zone 2, conventionally defined for $\bar{u} \leq 0.9$; then, in the range T_{ISO}/T_{LS} = 3 – 5, the displacement ratio $\bar{u}$ goes from 0.9 to ≈0.95.

Hence, in brief, the results provided in Figure 3.16b lead to the following remarks:

- the seismic demand on the LS of the IIS building can be almost the same of the existing construction if the isolation system (ISO) is designed to disconnect upper and lower structure; or, even better, the seismic demand can be reduced if the isolation system is designed to connect appropriately the two portions, thus converting the isolated extension into a mass damper with large mass ratio.
- For ratios T_{ISO}/T_{LS} not much larger than 1 (zone 2), the *mass damping effect* arises, and the isolated upper structure (US+ISO) works as a nonconventional (tuned or un-tuned) mass damper (TMD) for the lower structure (LS), leading to a reduced top displacement in the masonry lower structure as compared to the original building.

- For ratios T_{ISO}/T_{LS} much larger than 1 (zone 3), the *isolation effect* is emphasized, with almost no variation of the top displacement of the existing lower structure with respect to value registered in the AS-IS configuration.

Based on the above discussion, the value of 0.5 s for T_{ISO}, which corresponds to the minimum displacement ratio, 0.692, is selected as the optimal period, and the relevant design configuration is appointed as IIS 1. A further design solution, characterised by a very long period, is also considered: T_{ISO} = 5.0 s, $\bar{u}$ = 0.983, appointed as IIS 2. The two design solutions IIS 1 and IIS2, falling in the *mass damping effect zone* and *perfect isolation zone* of the plot in Figure 3.16b, represent configurations of the isolated vertical addition that maximize the *mass damping effect* and the *isolation effect*, respectively

3.2.4 Application of Block 3: design of the isolation system and vertical extension

For all design configurations (IIS 1-2, LS+US), the upper structure is a single-story steel CBF structure, with two and four braced bays along X and Y direction, respectively (Figure 3.17a). Circular hollow section CHS 219.1x16 mm is adopted for the columns and IPE cross sections (240, 360) are adopted for the beams. The diagonal cross sections are HEB 120B and HEB 160B, respectively for the braced frames x1-y1 and x2 - y2. A foundation grillage is realized on the roof of the existing building, composed by beams with rectangular hollow sections and wide flange sections (900 x 450 x 40 mm, HE 900B and 700B, IPE 400 and 550). The global mass of the isolation grillage and upper structure is equal to 940 kNs^2/m. For all structural members, steel grade S275 (f_{yk} = 275 MPa, f_{yd} = 261 MPa) is utilized.

The average compressive stress in the walls due to gravity loads, evaluated at the ultimate limit state [94] in the AS-IS configuration, is equal to 10% of the compression strength. An average increase of compression equal to 3% is obtained in the IIS configuration with respect to the AS-IS counterpart.

In both the IIS configurations, the isolation system is composed of 10 high damping rubber bearings (HDRBs), placed at the intersections of perpendicular walls of the lower structure, as depicted in Figure 3.17a, and characterised by equivalent viscous damping ratio ξ_{ISO} equal to 0.15. The properties of the isolation system and the design parameters of the isolated vertical addition are reported in Table 3.4 for IIS1 and IIS2 configurations. In detail, the table reports: the isolation period T_{ISO}, the isolators' design displacement $\delta_{ISO,u} = S_d$ at the isolation period in the base displacement response spectrum for Pozzuoli, the isolators' secant stiffness k_{eff}, the stiffness and isolation ratios, K and I, and the fundamental period of the standalone upper structure, T_{US}, for each direction.

The HDRBs have been modelled in SAP 2000 [113] through two-joint linear links with infinite vertical (axial) stiffness (k_z), and horizontal (shear) stiffness values in both direction ($k_x = k_y$) depending on the target vibration period (T_{ISO}). In the case of $T_{ISO} = 0.5$ s, a horizontal stiffness of 14844 N/mm has been assigned to each linear link, which corresponds to the secant shear stiffness of circular seismic isolators characterized by hard rubber (G = 1.4MPa), 900 mm diameter and 60 mm total rubber thickness [123]. Instead, to reach of $T_{ISO} = 5.0$ s, the stiffness assigned in SAP 2000 to the linear links is $k_x = k_y = 148$ N/mm and corresponds to circular seismic isolators with soft rubber (G = 0.4 MPa), 200 mm diameter and 85 mm total rubber thickness.

Table 3.4. Characteristics of isolation system and design parameters of the isolated vertical addition for IIS configurations.

Config.	Characteristics of Isolation system				Design parameters of the isolated vertical addition					
					X dir.			Y dir		
	T_{ISO} [s]	S_d [mm]	k_{eff} [N/mm]	ξ_{ISO} [-]	T_{US} [s]	K [-]	I [-]	T_{US} [s]	K [-]	I [-]
3D IIS 1	0.5	36	14844	0.15	0.24	0.34	2.1	0.14	1.28	3.6
3D IIS 2	5.0	160	148				21.2			36.2

3.2.5 Application of Block 4: seismic assessment of IIS

For assessing the dynamic behaviour of the design solutions and for evaluating the accuracy of the preliminary parametric analyses carried out on 3DOF IIS models, 3D models have been developed and used for FE analyses through the software SAP2000 [113]. In particular, three different 3D models are considered, i.e. the IIS structure in the two design configurations (3D IIS 1 and 3D IIS 2, Figure 3.17b and Figure 3.17c), and the LS plus the conventional extension (3D LS+US).

Moreover, in the 3D models of the IIS design solutions, the values of the ultimate bending moment for the flexural plastic hinges at the ends of masonry piers are updated to consider the compression due to the gravity load of the vertical extension. This additional compression has a general stabilizing effect for the LS, which reflects in a reduction of the tensile stress arising in the walls for lateral load.

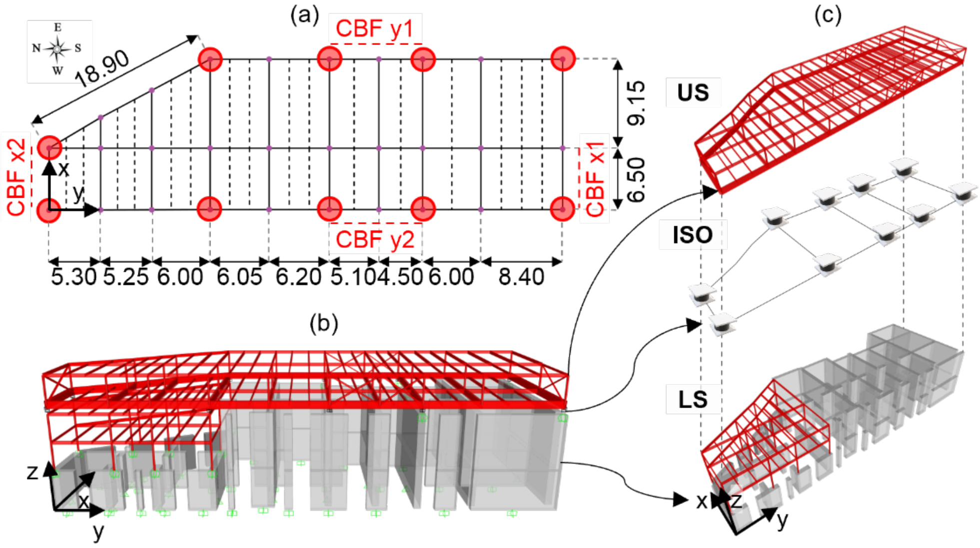

Figure 3.17. (a) floor system of US and isolation system; (b) 3D FEM of the IIS; (c) exploded axonometric view of IIS.

Nonlinear time history analyses are performed on the 3D models, by adopting the same seven pairs earthquake records used for the LS (see Figure 3.13 and Table 3.2). As already discussed in section 3.1.2, the three parts of the IIS complex show very different damping ratios, leading to a system characterized by non-proportional damping. For this reason, direct-integration time history analyses are developed by means of SAP2000 [113], with the IIS models accounting for the full damping matrix. Direct-integration time history analyses are also performed for the LS and LS+US models.

3.2.6 Application of Block 5: evaluation of IIS Effectiveness and comparisons AS-IS vs. LS+US vs. IIS

In the following, the main results of the nonlinear time history analyses obtained for the existing and the design configurations are only discussed for the weakest Y direction. The seismic response of the different models is compared and the effectiveness of the isolated vertical addition in reducing the seismic demand on the existing structure is evaluated (Figures 3.18 – 3.23).

The Figure 3.18 provides the plots of story (Figure 3.18a) and inter-story (Figure 3.18b) drifts obtained considering the average of the peak values for the seven input waves. The AS-IS masonry building (3D LS model), the conventional vertical extension (LS+US model), and the two solutions realized with intermediate isolation systems (IIS 1 and IIS 2 models), are directly compared. In the case of IIS 1 and IIS 2 models, the drifts at the top story of LS, as well as the LS_1-LS_2 inter-story drifts, are reduced with respect to the model of the lower structure as standalone. As expected, a greater reduction of drifts can be observed for the solution IIS 1 than the IIS 2 one. For the isolated upper structure, the displacements are mainly concentrated into the isolation system, thus confirming that this structural portion behaves as a base isolated structure.

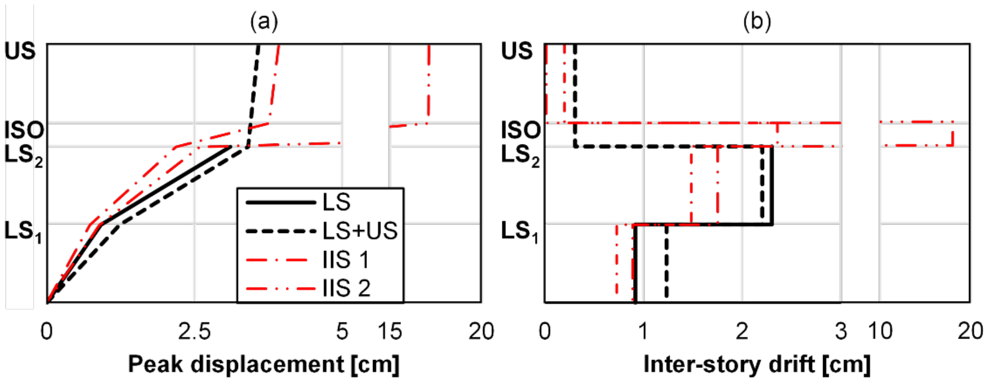

Figure 3.18. average values from nonlinear analyses of: (a) peak story displacements; (b) inter-story drift.

Recognizing that reduction of the peak response is not sufficient for estimating the effectiveness of the isolated vertical extension as TMD, a parameter is here defined which accounts for the damage accumulation in the existing building. Since the seismic damage is strictly related to the hysteretic energy absorbed by the system during the cyclic loading [72 – 78], a hysteretic energy absorption ratio, ρ_E, has been introduced in section 3.1.1 for AS-IS, or equivalently for LS ($\rho_{E,LS}$), and in section 3.1.4 for IIS ($\rho_{E,IIS}$), calculated by Eq. (3.1) and (3.2), respectively.

The ratio ρ_E is calculated for the different configurations (LS, LS+US, IIS 1, IIS 2) under each ground motion. The choice of examining this parameter in non-dimensional form is related to the fact that varying the dynamic characteristics of the four building configurations, the input energy is different in each of them, therefore the comparison only in terms of hysteretic energy would not be fair. In other words, for evaluating the ability of the isolated vertical extension in reducing the damage in the existing building by working as a TMD, the percentage of energy that is dissipated via hysteretic cycling with respect to input energy is a better measure than the hysteretic energy in absolute terms.

The hysteretic energy absorption ratio ρ_E calculated for the four configurations under the seven acceleration records is depicted in Figure 3.19. The average values of the ratios, $\rho_{E,ave}$, are also provided in the figure. The energy dissipated in the masonry elements is almost equal for the LS and LS+US models while it decreases by considering the isolated models. In particular, the minimum values are obtained for the IIS 1 model, characterised by an average value of the ratio ρ_E equal to 0.16; quite larger, as expected, the average ratio for the IIS 2 model, equal to 0.41.

Additional results, which confirm the differences of performance between the four cases, are provided in terms of: time histories of the top displacement of the existing structure (u_{LS2}) (Figure 3.20), cyclic response in terms of base shear (V) vs. displacement at the top of the existing structure (u_{LS2}) (Figure 3.21), hysteresis loops moment-plastic rotation in the masonry walls (Figure 3.22); these results are here reported only for one seismic input, i.e. the Darfield record (Table 3.2, 335 ya - input).

From Figure 3.20 it can be noted that the LS+US model shows displacements at the top of the existing building greater than the LS counterparts; the peak displacement ratio $\bar{u}$, indeed, is equal to 1.21. Instead, the IIS models show reduction of top displacement, with peak displacement ratios $\bar{u}$ respectively equal to 0.56 and to 0.89 for the IIS1 and IIS2 configurations.

The global cyclic response, base shear (V) vs. top displacement of masonry structure (u_{LS2}), under the same ground motion is shown in Figure 3.21. Each plot compares one of the three extension solutions (red lines) to the AS-IS configuration (gray line). It can be observed that in the case of conventional extension (LS+US model) the loops are nearly overlapped to the ones of the LS model. On the contrary, in the case of the solution IIS 1 the cycles appear less wide than in the LS case, though some peak values of displacement are comparable to the LS counterparts. An intermediate behaviour is observed for the solution IIS2.

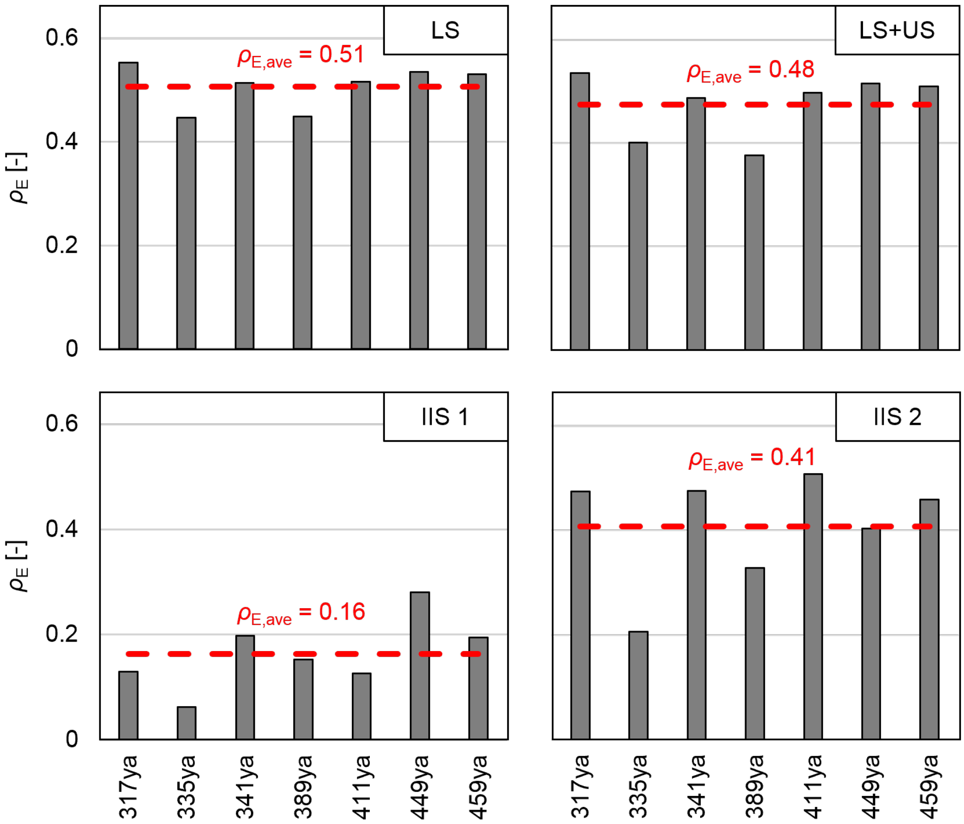

Figure 3.19. Cumulated hysteretic energy normalised to input energy - LS, LS+US, IIS 1, IIS 2 models.

Similar considerations can be made in terms of parameters describing the local behaviour of the masonry walls. For instance, a focus is provided on the structural wall indicated by the blue arrow in Figure 3.22. Being relatively slender, the failure mode of the wall is governed by the flexural response, thus the four plots depicted in Figure 3.22 represent the moment rotation cyclic response. It can be observed that the wall working conditions significantly worsen, with respect to the AS-IS configuration, in the model with the conventional vertical extension, while the inelastic engagement seems almost cancelled in the case IIS1.

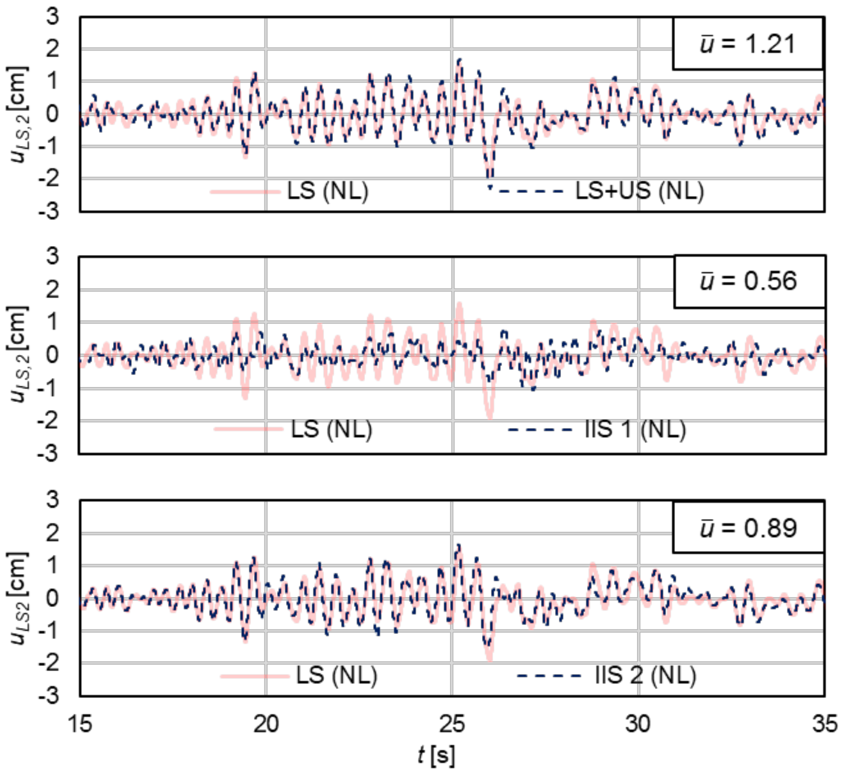

Figure 3.20. Time history of masonry structure top drift ($u_{LS,2}$) - 335ya-input: (a) LS vs. LS+US, (b) LS vs. IIS1, (c) LS vs. IIS2.

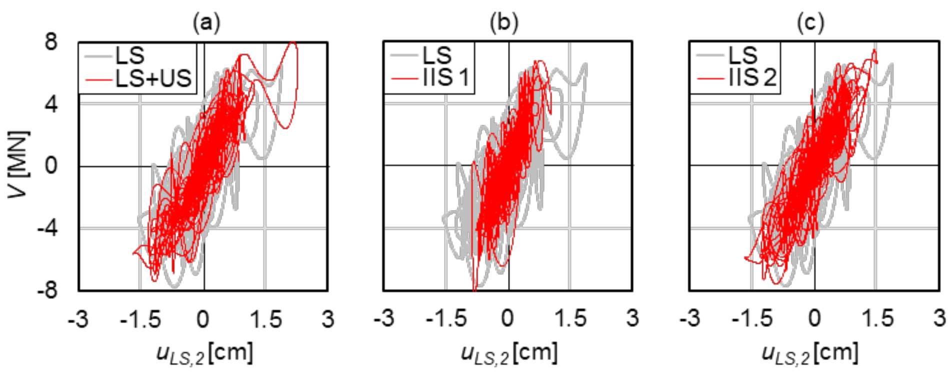

Figure 3.21. Nonlinear analyses - hysteresis loops for 335ya-input wave: (a) LS vs. LS+US, (b) LS vs. IIS1, (c) LS vs. IIS2.

In addition, for comparing the plastic rotation in the different configurations, the Figure 3.23 depicts the ratio between DCRs (demand to capacity ratios); in particular, DCR calculated for the masonry walls in the LS+US and IIS models are normalized to the DCRs in the reference LS model (Figure 3.15). The figure highlights that the minimum engagement of the masonry structure is obtained by adopting the IIS1 design solution (Figure 3.23b); instead, the plastic rotation demand to capacity ratios in the LS+US model are larger than in the LS model (Figure 3.23a), while in the IIS2 model, the DCRs are almost equal to the counterparts in the LS model (Figure 3.23c).

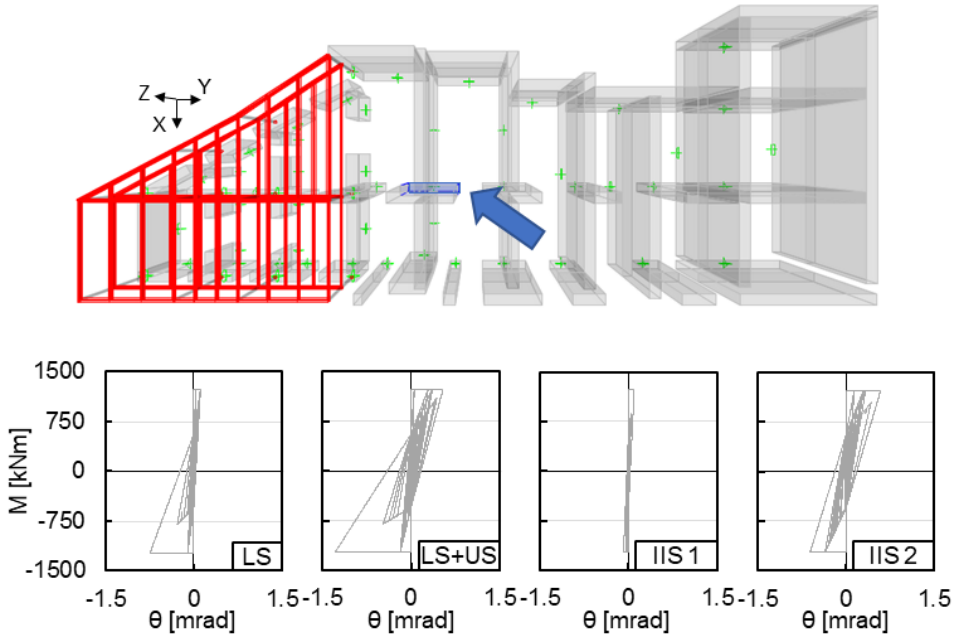

Figure 3.22. Inelastic flexural response of single wall - LS, LS+US, IIS1, IIS2 models - 335ya-input wave.

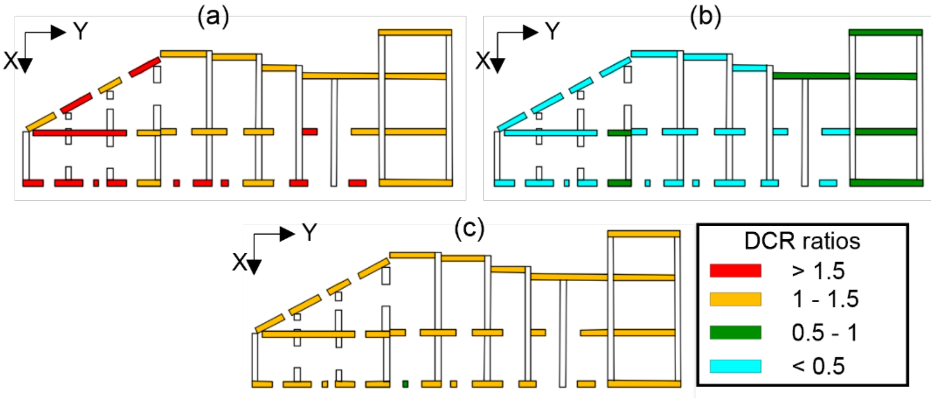

Figure 3.23. Demand to capacity ratios in terms of chord rotation of the piers at the base floor in the 3D models: (a) LS+US; (b) IIS1; (c) IIS2.

Chapter 4

Influence of LS and ISO nonlinear behaviour on IIS response

In previous chapters, the dynamic problem of IIS application for building extensions has been deeply examined, with the aim of promoting the diffusion of this strategy, both sustainable and effective in earthquake prone zones. In chapter 3 a three-storey masonry building is selected as case study and extended by means of different two-storey steel structures, isolated at the base and erected on the top of the existing building and finally, a design procedure has been defined and illustrated. Key point of this procedure is the parametric response spectrum analyses performed on lumped mass models by varying the mechanical properties of the building extension. As a result, so called *IIS design spectra* are derived and used for selecting design solutions of the vertical extension that do not alter or reduce the response of the existing lower structure.

In this chapter, the procedure described in chapter 3 is improved by considering the nonlinear behaviour of the masonry structure of the existing building and of the isolation system, made of High Damping Rubber Bearings. Hence, the assessment of the effect of nonlinearities in structural complexes with IIS is investigated with the aim to check the accuracy and reliability of *IIS design spectra* as a tool for the preliminary design of an isolated vertical extension. For this purpose, nonlinear time history analyses (NTHA) are performed on the 3D FE models of the same real case study selected in chapter 3 and of several IIS design solutions, characterized by the same upper structure and by different isolation systems. The results of NTHA are then compared to the previsions of the *IIS design spectra*.

4.1 Selection of several IIS design solution

As shown in Figure 3.16b of chapter 3, two different IIS design solutions have been selected, one falling in the *mass damping effect zone* (IIS 1, T_{ISO} = 0.5 s) and one falling in the *perfect isolation zone* (IIS 2, T_{ISO} = 5 s). This choice has been justified by the intent to investigate two different structural behaviours of the IIS with the aim to prove the effectiveness of the isolated vertical extension in working as an unconventional TMD. Since the aim of this chapter is to assess the accuracy of the *IIS design spectrum* in predicting the IIS response, two further IIS design solutions are considered by varying the isolation period, i.e. T_{ISO} = 1 s and T_{ISO} = 1.5 s. The response of the LS+US configuration is also considered for comparison.

Therefore, four different IIS design solutions designated with B, C, D, E in Figure 4.1 are chosen and explored. The solution B (IIS 1 solution in chapter 3) corresponds to the minimum response, thus it can be considered as one of the *optimal* solution, according to the modelling approach and analysis methods adopted herein (3DOF model, linear RSA). The solution C also falls in the zone 2, where a non-negligible response reduction is expected, while the solution D is on the edge between zone 2 and transition zone; finally, the solution E (IIS 2 solution in chapter 3) corresponds to almost perfect isolation, with values of the response parameters very close to the one of the existing building in the AS-IS configuration. A conventional vertical extension, consisting of US without isolation system, designated as solution A in Figure 4.1, is also considered for comparison.

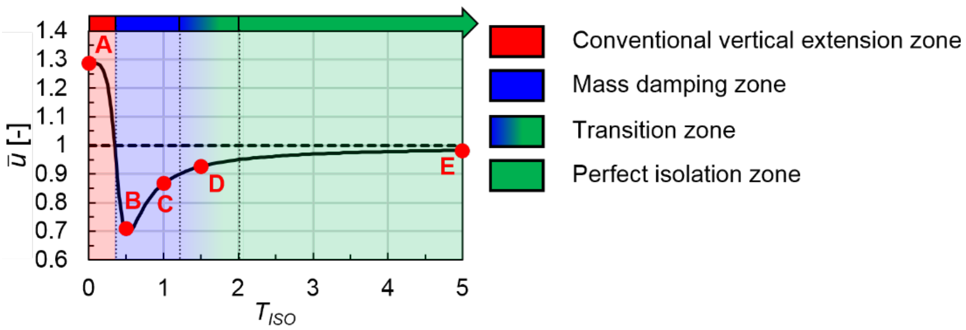

Figure 4.1. graph of displacement ratio $\bar{u} = u_{LS}/u_{AS\text{-}IS}$ as a function of the isolation period T_{ISO}, considered as *IIS design spectrum.*

Both the ISO system and the upper structure of each structural solutions have been designed. The upper structure, a steel structure with braced frames, described in the section 3.2.4, remains the same in all solutions A, B, C, D, E. Characterized in weakest direction (i.e. y-direction) by $K = 1.28$ and $T_{US} = 0.14$ s with $T_{US} < T_{ISO} / 3$ and $\beta_h = 2.79$, it has been designed to avoid higher mode coupling with the lower structure and to be sufficiently stiffer than the isolation system. The isolation system, which governs the dynamic behaviour of the extended building, is made by High Damping Rubber Bearings (HDRBs), with equivalent viscous damping ratio $\xi_{ISO} = 0.15$. It has been designed to provide a global secant stiffness k_{ISO} such that the selected values of T_{ISO} (T_{ISO} = 0.5 s; 1.0 s; 1.5 s; 5.0 s) are obtained as: $T_{ISO} = 2\pi(M_{ISO}/k_{ISO})^{0.5}$, with M_{ISO} = 940 kNs^2/m the total isolated mass of the steel superstructure plus the isolation system.

The schematic representation of the isolation system, composed by 10 HDRBs placed at the intersection of orthogonal masonry walls, is provided in Figure 3.17 from section 3.2.5.

4.2 Time history analyses on 3D models and comparison to IIS design spectrum

4.2.1 Modelling approaches and analysis types

The results on IIS behaviour discussed above have been derived from linear response spectrum analyses. As next step, some simplified assumptions and limitations are removed in order to assess the effectiveness of IIS through more accurate models and methods. Hence, the three-dimension (3D) FE models of the selected solutions (Figure 4.1) are built in the SAP2000 computer code [113] and analysed through linear and nonlinear Time History Analyses (THA). The cases of standalone lower structure and of conventional vertical extension, consisting of US attached to the existing building without any isolation system (designated as A in Figure 4.1), have also been considered.

In the nonlinear THA, the 3D FE model of the LS already utilized for the NTHA analyses in the previous chapter (see section 3.1.1 and section 3.2.2) is retained. In addition, as reported in section 3.2.5, in the 3D IIS FEM the values of the ultimate bending moment for the flexural plastic hinges at the ends of masonry piers are updated to consider the compression due to the gravity load of the vertical extension. The Pivot-type hysteretic model [105] is adopted for describing the cyclic response of both hinges in bending and shear (Figure 3.4b), with the values of the parameters α_1, α_2, β_1, β_2, and η_{Pivot} defined to control the shape of the hysteresis loops and the stiffness and strength degradation. According to [106 – 108], the model parameters α_1, α_2, β_1, β_2, are here set equal to 0.45, while the parameter η_{Pivot} is set equal to zero.

Concerning the isolation system (Figure 3.17c), the hysteretic behaviour of HDRBs can be reasonably described by the bilinear constitutive model calibrated as follows [93] (Figure 4.2). Known the values of: global secant stiffness k_{ISO}, design displacement $\delta_{ISO,u} = S_d$ (from the base displacement design spectrum at T_{ISO}), equivalent viscous damping ratio ξ_{ISO}, number of isolators n_{ISO}; then, the values of: secant stiffness k_{eff}, initial stiffness k_1, post-yield stiffness k_2, intersection between the prolongation of post-yield branch and the y-axis Q, yield displacement $\delta_{ISO,y}$, are derived according the following formulae:

$$k_{eff} = \frac{k_{ISO}}{n_{ISO}} \tag{4.1}$$

$$\xi_{ISO} = 2 \cdot Q \cdot \frac{\left(\delta_{ISO,u} - \delta_{ISO,y}\right)}{\pi k_{eff} \delta_{ISO,u}^2} \tag{4.2}$$

$$Q^{(1)} = \frac{\pi}{2} \cdot k_{eff} \cdot \delta_{ISO,u} \cdot \xi_{ISO}, \quad k_2^{(1)} = k_{eff} \frac{Q^{(1)}}{\delta_{ISO,u}}, \quad k_1^{(1)} = 10 k_2^{(1)} \tag{4.3}$$

$$\delta_{ISO,y} = \frac{Q^{(1)}}{k_1^{(1)} - k_2^{(1)}} \tag{4.4}$$

$$Q = \frac{\pi \cdot k_{eff} \cdot \delta_{ISO,u}^2 \cdot \xi_{ISO}}{2\left(\delta_{ISO,u} - \delta_{ISO,y}\right)}, \quad k_2 = k_{eff} \frac{Q}{\delta_{ISO,u}}, \quad k_1 = 10 k_2 \tag{4.5}$$

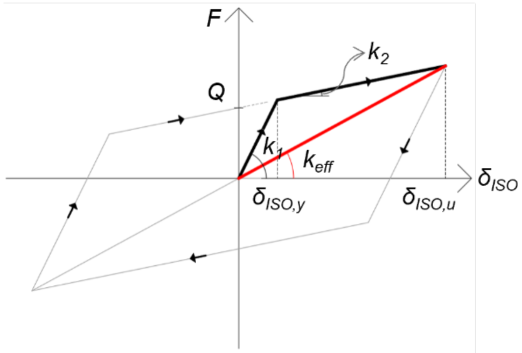

Figure 4.2. Bilinear model of HDRB isolator.

The secant stiffness k_{eff} (Eq.(4.1) is obtained by dividing the global secant stiffness k_{ISO} for the number of isolators (n_{ISO} = 10). Specified the value of equivalent viscous damping ratio (Eq. (4.2), ξ_{ISO} = 0.15) and neglecting $\delta_{ISO,y}$, we can calculate a first estimate for $Q^{(1)}$, $k_2^{(1)}$ and $k_1^{(1)}$ from Eq. (4.3). From these values, we can derive the value of D_y through Eq. (4.4) and recalculate Q, k_2, and k_1 (Eq. (4.5)).

Data of the bilinear constitutive model of the isolators utilized in the design solutions B, C, D, E are reported in Table 4.1.

Table 4.1. Data of the bilinear constitutive model of the isolators utilized in the IIS design solutions.

	T_{ISO} [s]	k_{eff} [N/mm]	k_1 [N/mm]	k_2 [N/mm]	Q [N]	S_d [mm]
B	0.5	14844	112223	11222	128343	36
C	1	3711	28056	2806	64506	71
D	1.5	1649	12469	1247	43004	107
E	5	148	1122	112	5800	160

For the sake of simplicity, the spectral displacements obtained from the code design spectrum at the base for T = T_{ISO} are here assumed as design displacements of the different ISO systems. More accurate values of the design displacement of the ISO system can be calculated through floor spectra, i.e. the roof spectra accounting for the mass damping effect of the upper structure (the so-called *ISO Design Spectrum*, presented in detail in chapter 6).

The seismic isolators can be preliminarily sized from data sheets of producers [e.g. [123]], as done in the section 3.2.4. However, in the case of IIS design solutions with a long isolation period, such as the configuration E (T_{ISO} = 5 s), a solution with quite small isolators (200 mm diameter, 75 mm total rubber thickness) is derived even considering a soft rubber (G = 0.4 MPa); so, a mixed solution (isolators plus sliders) could be a better choice.

Because the design solutions are non-classically damped systems (see section 3.1.2 and section 3.2.3), the fully populated damping matrix, which lead to coupled equation of motions, is accounted for through direct-integration THA [113]. Direct-integration THA are also developed for the 3D FE model of the AS-IS configuration. The method of superposition of modal damping matrices [113, 124] has been used for constructing the viscous damping matrix, as recommended by [125]. In both model types, representing the AS-IS configuration and the design configurations (A-E), energy dissipation sources other than that associated with the yielding of structural elements have been accounted for through viscous damping. For the existing masonry building in the AS-IS configuration, a single value of the modal damping ratio is specified, equal to 5%. For the IIS configurations, different values of modal damping ratios have been attributed to the modes based on the structural portion (LS, ISO, US) that contributes more significantly to structural response. Therefore, a modal damping ratio equal to 0 is attributed to the first three modes, which manly involves the isolated upper structure, since the energy dissipating mechanisms usually accounted through viscous damping do not arise either at the isolated level or in the US (which follows the isolation system almost rigidly). For the modes from the fourth to the twelfth, mainly involving the LS, the values of the modal damping ratios are 5%. Higher modes involving the US are not present, due to its high stiffness.

Seven earthquake records are selected by means of the software REXEL v 3.5 [120] from the SIMBAD database [121] (same records adopted in subsection 3.2.2.3); the record set is selected to derive an average spectrum close to the response spectrum of the site (Figure 3.16a), with upper and lower tolerance of 30% and 10% in the range of periods 0.15 - 2 s (Figure 3.13). The major data of the ground motion records are provided in Table 3.2.

The horizontal component of the ground motion has been applied only in the weakest direction (i.e. Y-direction) and only the nonlinear behaviour of in-plane masonry piers, in Y-Direction, has been considered. Moreover, the possible couplings between the two horizontal components and between the horizontal and vertical components of the ground motion have been neglected. Soil-structure interaction, as well, has been neglected.

The results of LTHA and NTHA are compared to the RSA results.

The object of comparison is threefold, and concerns:

- modelling of the AS-IS and retrofitted building configurations: lumped mass (3DOF IIS and SDOF AS-IS) vs. three-dimensional (3D FE IIS and 3D FE AS-IS) models;
- assumption on the mechanical behaviour of the existing structure and of the ISO system: equivalent linear vs. nonlinear behaviour;
- seismic input and analysis type: code elastic spectrum and Response Spectrum Analysis (RSA) vs. ground motion acceleration records averagely matching the elastic spectrum and Time History Analyses (linear and nonlinear THA).

All in all, the final aim is the evaluation of Block 2 design procedure, i.e. parametric RSA on lumped mass model and resulting *IIS design spectrum*, as a reliable prediction of the actual response of IIS. That is, though some slight scatters between the values of response parameters could be allowable, the behaviour trend should be confirmed.

In the following, LTHA on 3D FE building models are first carried out, in order to establish the effects of modelling (lumped mass vs. three-dimensional models) and seismic input (Figures 4.3 – 4.6). Nonlinear analyses only consider the hysteresis of either the substructure or the ISO system are then performed. Fully nonlinear analyses accounting for both mechanical nonlinearities (in the LS and ISO) are finally executed.

The results in Figures 4.3 – 4.6 are shown as a function of the fundamental period of the IIS (masonry structure plus isolated addition), T_1, while the results of the RSA on lumped mass models, in Figure 4.1, had been plotted as a function of the ratio T_{ISO}/T_{LS}.

4.2.2 LTHA

A preliminary comparison is given in Figure 4.3a, where the *IIS design spectrum* (displacement ratio vs. fundamental period of the IIS) is contrasted to the blue markers, representing the results of LTHAs carried out on the 3D FE models of the six design solutions (A - E). The markers are obtained as the ratio of average values of the peak displacements ($\bar{\bar{u}}$) exhibited under the seven seismic inputs from LS and AS-IS (i.e., $\bar{u}_{3D} = \bar{\bar{u}}_{LS2} / \bar{\bar{u}}_{AS-IS2}$) and are plotted as a function of the fundamental period T_1 of the structural complex after addition. The markers are almost coincident with the curve derived from RSA on lumped mass models. Therefore, it seems that, when the LS of the IIS complex remains in the elastic field, the *IIS design spectrum* provides a very good estimate of the expected behaviour in terms of displacement demand.

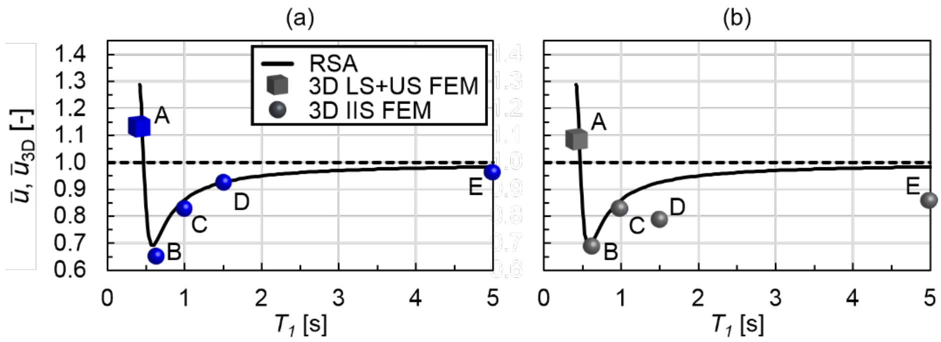

Figure 4.3. RSA on lumped mass models vs. THA on 3D FE models with (a) linear and (b) nonlinear LS behaviour.

4.2.3 NTHA: Nonlinearity in the lower structure

A comparison analogous to the one in in Figure 4.3a is given in Figure 4.3b, where the markers provide the result of NTHA on 3D FE models of IIS, with the LS described through the Pivot-type model, as reported in section 3.1.1. For both the US and the isolation system, linear modelling is adopted. The results seem in agreement with RSA curve for cases B (T_{ISO} = 0.5 s, T_1 = 0.63 s) and C (T_{ISO} = 1 s, T_1 = 1.06 s); some scatters are observed for the cases D (T_{ISO} = 1.5 s, T_1 = 1.54 s) and E (T_{ISO} = 5 s, T_1 = 5.01 s). However, it is worth observing that these displacement ratios are smaller than the RSA counterparts. Therefore, even when the lower structure has nonlinear behaviour, the *IIS spectrum* can be used for the preliminary design of IIS, since it provides an estimate *on the safe side* of the expected behaviour.

4.2.4 NTHA: Nonlinearity in the isolation system

Further analyses on 3D FEMs have also been performed by accounting for the nonlinear response of the isolation system, made of HDRBs, as discussed in section 4.2.1. Linear behaviour for the lower structure is considered in these analyses, while subsequently nonlinear behaviour of both isolation system and lower structure is considered.

In Figure 4.4a, the RSA curve is contrasted to the results of NTHA on the 3D FEMs only accounting for the nonlinearity in the isolation system. A substantial correspondence of nonlinear analysis results with RSA is found for the cases B and E, while the values of displacement ratio derived from nonlinear THA for the design solutions C and D are slightly lower than the RSA counterparts. Therefore, also accounting for the hysteretic behaviour of the isolation devices, the RSA provides an estimate of the expected behaviour *on the safe side*.

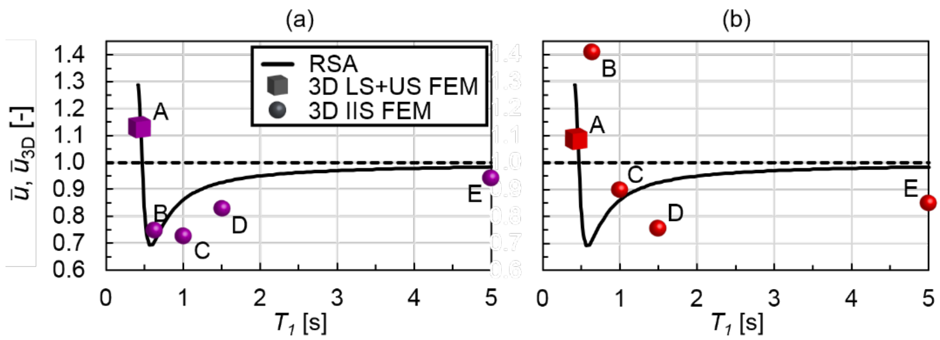

Figure 4.4. RSA on lumped mass models vs. THA on 3D FE models with (a) nonlinear ISO behaviour and (b) nonlinear behaviour of both LS and ISO.

4.2.5 NTHA: Nonlinearity in the lower structure and isolation system

Finally, both the lower structure and the isolators are modelled accounting for their hysteretic response, as reported in the previous section 4.2.1.

In Figure 4.4b, the relevant results of the NTHA on the 3D FEMs are compared to the *IIS design spectrum*. The case C and the RSA curve show similar values of displacement ratio; instead, a displacement demand larger than one, thus much larger than the value predicted from RSA, is obtained for the design solution B. The value of the displacement ratio larger than one implies an increase, rather than a reduction, of displacement compared to the reference LS model, which, in turn, implies that *IIS spectrum* derived by means of RSA seems nor accurate neither safe as design tool for solution maximizing the mass damping effect.

Therefore, when the nonlinear behaviour of both the isolation devices and the lower structure are considered, the RSA provides an estimate of the expected behaviour *on the safe side* for isolation periods falling in the transition zone or longer. Indeed, for the cases D and E, significant differences can be observed between the RSA curve and the NTHA results; however, the latter ones are smaller than the former. Hence, the RSA-based predictions of seismic demand remain *on the safe side*, though not accurate.

Comparing the IIS solutions to the conventional extension (point A, T_1 = 0.43 s), in most cases the IIS counterparts exhibit lower displacement demand. However fully nonlinear analyses, accounting for the hysteretic behaviour of both masonry structure and isolation system, have highlighted that design solutions that maximize the mass damping effect (design zone 2, case B in Figure 4.4b), can exhibit an amplification, rather than a reduction of the seismic response.

Since the solution B is the only one that does not follow, more or less closely, the trend predicted through linear RSA and confirmed by linear THA, it must be analysed in detail. Considering that NTHA response is particularly sensitive to the modelling assumptions, additional analyses are developed, modifying the values of the modal damping ratios (η_i) attributed to the masonry structure modes (i.e., to all modes, for the LS in the AS-IS configuration; from the fourth to the twelfth modes, for the IIS configurations). In addition to the value of 5%, already adopted in previous analyses, also the value 2% has been specified for η_i. The results obtained from analyses with η_i = 2% are compared to the ones with η_i = 5% in terms of displacement ratio in Figure 4.5. Here it can be observed that the results for the design solutions A (conventional extension) and E (perfect isolation) are very close varying η_i. For the solutions B, C, D, instead, larger scatters can be observed, particularly for the solution B. These preliminary analyses results highlight that the modal damping value strongly influences the structural response in NTHA.

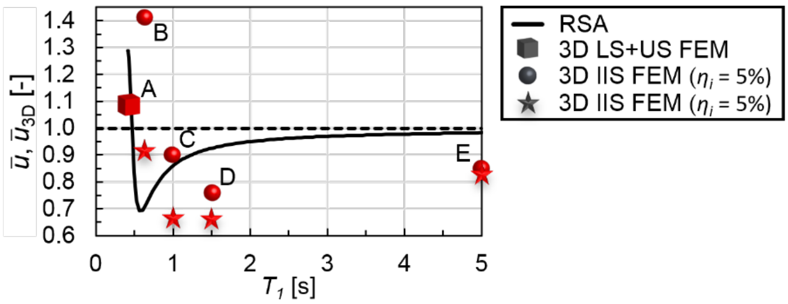

Figure 4.5. RSA on lumped mass models vs. THA on 3D FEMs with η_i = 5% vs. THA on 3D FEMs with η_i = 2%.

4.2.6 Linear and Nonlinear THA: the base shear ratio

In Figure 4.6, the *IIS design spectrum* is compared to markers, representing the average peak results of the seven THA on the design solutions in the case of masonry structure and isolation system both assumed elastic (Figure 4.6a), or masonry structure elastic and isolation system inelastic (Figure 4.6b). In particular, the markers are depicted both in terms of displacement ratio and base shear ratio, and the RSA curves for $\bar{u}$ and $\bar{v}$ are overlapped since they represent results in normalized form. As can be seen in Figure 4.6, the THA values of the base shear ratio are slightly larger than the displacement ratio counterparts, both neglecting and considering the nonlinear behaviour of the isolation system.

This comparison is only reported for the analyses where the LS is linear, since the base shear ratio is not indicative of the IIS response when the hysteretic behaviour of the masonry structure is considered. As shown in [22], by comparing the push over curves and the global hysteretic loops under selected seismic inputs, it clearly appears that the former are the backbones of latter. Exceeding the elastic limit of the masonry structure, the top displacement increases under an almost constant value of base shear. For this reason, when the existing structure undergoes inelastic deformations, in the AS-IS configuration and/or in the design solution, the base shear ratio is not representative of the seismic response of the IIS.

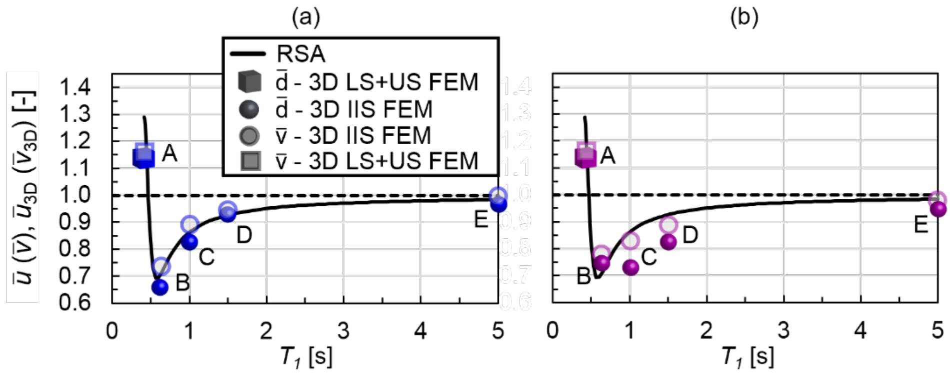

Figure 4.6. RSA on lumped mass models vs. THA on 3D FEMs with (a) linear behaviour of both LS and ISO and (b) nonlinear ISO behaviour.

4.3 Accuracy of reduced-order lumped mass models

In the previous sections of this chapter, it has been shown that previsions with the parametric RSA on lumped mass models can simulate with a good approximation the results of THAs on 3D IIS FEM, except for the case in which both the ISO and the LS exhibit a strong nonlinear behaviour. In this subsection, to investigate the accuracy of the simplified one-dimensional 2DOF IIS model in the first stage of the design process, a comparison between the simplified and more refined models is here proposed in terms of LS displacements by carrying out NTHAs on the 2DOF IIS model (Figure 4.7) with the same record set utilized for the 3D analyses of the A-E configurations (section 3.1.4). To describe the nonlinear behaviour of the 2DOF models, the modelling approach described in section 3.1.1 is adopted for the LS, while the bilinear isolator model described in section 4.2.1 is used for the ISO by assuming k_{ISO} = k_{eff}.

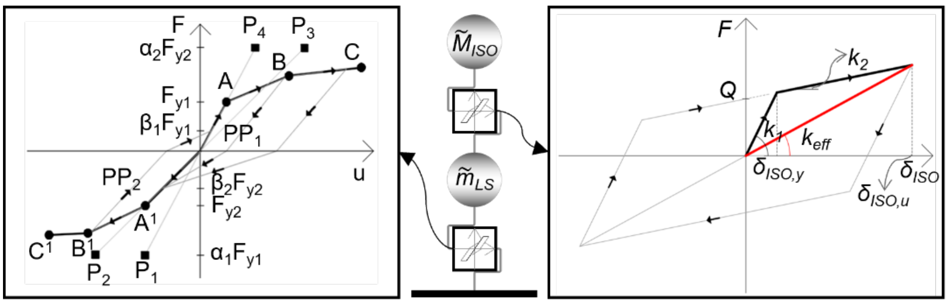

Figure 4.7. 2DOF IIS for NTHA.

Figure 4.8 shows the average values of the peak displacements obtained from the NTHA for 3D IIS FEM ($\bar{\bar{u}}_{LS2}$) and 2DOF IIS ($\bar{\bar{u}}_{LS}$). Values of $\bar{\bar{u}}_{LS2}$ and $\bar{\bar{u}}_{LS}$ are quite close, and the percentage variation (Δ) of $\bar{\bar{u}}_{LS}$ with respect to $\bar{\bar{u}}_{LS2}$ does not exceed 20% in any of the cases analysed. Therefore, the 2DOF IIS model - if correctly defined - can simulate the behaviour of the corresponding 3D IIS FEM, with considerably reduced computational effort.

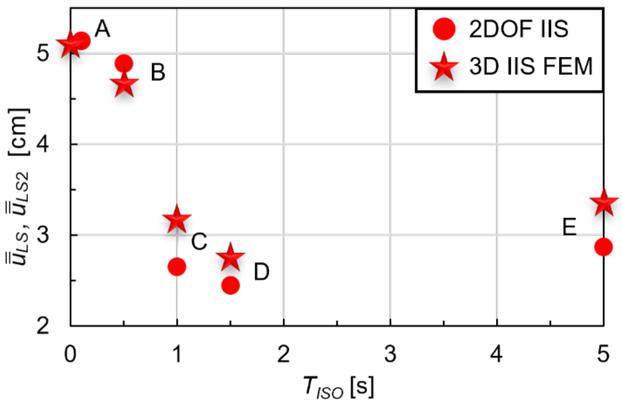

	$\bar{\bar{u}}_{LS}$ [cm]	$\bar{\bar{u}}_{LS2}$ [cm]	Δ [%]
IIS B	4.9	4.7	4.8
IIS C	2.7	3.2	-16.1
IIS D	2.4	2.7	-10.8
IIS E	2.9	3.4	-14.7

Figure 4.8. Comparison of displacement results for 3D IIS FEM vs. 2DOF IIS.

Chapter 5

A diagram-based design procedure for IIS in existing buildings with inelastic behaviour

In chapter 3 and chapter 4, the *IIS spectrum* has been utilised for a complete evaluation of all design configurations that can be obtained varying the value of isolation period. It provides indications on the optimum value, the one that gives rise to the maximum reduction of the response of the existing structure; however, when such solution is not applicable for any reason, possible sub-optimum alternatives can be individuated in the *IIS spectrum*. The *IIS spectrum* is constructed from parametric response spectrum analysis (RSA) with the code spectrum specified for the site of interest and does not account for the inelastic behaviour that possibly arises in existing buildings.

However, when earthquakes occur, the inelastic behaviour of existing (masonry or concrete) structures cannot be excluded and should be considered in the analyses. For this purpose, a *stepwise procedure* is here proposed to supply the *IIS design spectrum* for existing buildings that exhibit nonlinear behaviour, without executing several nonlinear time history analyses for different models by varying the isolation period, but only examining in the inelastic field two limit behaviours of the extended building. Essential for this procedure are a series of diagrams derived from parametric RSA; as a result, two curves are identified as IIS design spectra and the region bounded by them, appointed as *inelastic IIS behaviour zone*, represents the nonlinear response prediction of the existing structure varying the isolation period of the vertical extension. The outlined design procedure is applied to some case studies and validated through the comparison with the results of nonlinear time history analyses.

This procedure can be also employed to generalise the design framework developed in chapter 3. In fact, in chapter 3, the design configuration of the isolated vertical addition is selected on the base of the trend of the *IIS design spectrum*. In this chapter, instead, the inelastic behaviour, possibly occurring in the existing structure, is considered from the first phases of the design process.

5.1 Parametric RSA for construction of IIS design spectra

In Block 2 of the 5-Block design procedure (chapter 3), a key design tool has been introduced: the *IIS design spectrum*. To derive the *IIS design spectrum*, it is possible to refer either to the 3DOF IIS model or to the 2DOF IIS model. In the following, the procedure for calculating the *IIS design spectra* is provided considering the 2DOF IIS model depicted in Figure 2.2b, which well grasps the IIS dynamic behaviour, as demonstrated in section 2.1 and suggested by several authors [6, 20, 28, 57, 97].

The 2DOF IIS model describes the structural complex made of the existing building, the vertical extension, and the intermediate isolation system (IIS). The first degree of freedom represents the structure of the existing building (lower structure, LS), while the second one represents the isolated vertical extension (ISO+US) (Figure 2.1c). Recalling that, mass, stiffness, and damping constant of the first degree of freedom are appointed as: m_{LS}, k_{LS}, c_{LS}. While, for the second degree of freedom the mass, appointed as M_{ISO}, is the whole isolated mass and is given by the summation of the masses of the upper structure m_{US} and isolation system m_{ISO}, i.e. $M_{ISO} = m_{US} + m_{ISO}$. The stiffness and damping are the ones of the isolation system and are appointed as k_{ISO} and c_{ISO}. It is worth reminding that the 2DOF model can be adopted for describing the main dynamic characteristics of IIS provided that the upper structure is very rigid with respect to the isolation system and higher modes of the lower and upper structures are not coupled [6, 28, 57].

Being u_{LS} and u_{ISO} the displacements of the two oscillators relative to the ground, and u_g the displacement of the ground, the equations of motion of the 2DOF IIS model are given in chapter 2 by the Eqs. (2.9) and (2.10). Which for simplicity are rewritten here:

$$M_{ISO}\,\ddot{u}_{ISO} + c_{ISO}\left(\dot{u}_{ISO} - \dot{u}_{LS}\right) + k_{ISO}\left(u_{ISO} - u_{LS}\right) = -M_{ISO}\,\ddot{u}_0 \tag{2.9}$$

$$m_{LS}\,\ddot{u}_{LS} + c_{LS}\,\dot{u}_{LS} + k_{LS}\,u_{LS} = -m_{LS}\,\ddot{u}_0 + c_{ISO}\left(\dot{u}_{ISO} - \dot{u}_{LS}\right) + k_{ISO}\left(u_{ISO} - u_{LS}\right) \tag{2.10}$$

The design parameters of the model can be derived from the dynamic properties of the two oscillators (i.e. LS and ISO+US) as follows:

- period of the standalone lower structure T_{LS}, being $T_{LS} = 2\pi(m_{LS}/k_{LS})^{0.5}$;
- period of the isolated vertical addition T_{ISO}, being $T_{ISO} = 2\pi(M_{ISO}/k_{ISO})^{0.5}$;
- mass ratio μ, being $\mu = M_{ISO}/m_{LS} = 0.05 – 2$;
- damping ratio of the lower structure ξ_{LS}, being $\xi_{LS} = c_{LS}/[2(k_{LS}m_{LS})^{0.5}]$;
- damping ratio of the isolation system ξ_{ISO}, being $\xi_{ISO} = c_{ISO}/[2(k_{ISO}M_{ISO})^{0.5}]$.

The values assumed for the above parameters in the parametric study here reported are:

- $T_{LS} = 0.39 – 1.23$ s;
- $T_{ISO} = 0.1 – 5$ s;
- $\mu = 0.05 – 2$;

The damping ratios are not been varied and are assumed as: $\xi_{LS} = 0.05$ and $\xi_{ISO} = 0.15$. The value of ξ_{LS} is the one usually adopted for concrete or masonry structures, while the value of ξ_{ISO} is typical of high damping rubber bearings. As discussed in the previous chapters and with more accuracy in Appendix B, such difference between damping ratios leads to a *non-proportionally* (or *non-classically*) damped system, for which a fully populated damping matrix should be considered to provide an accurate response prediction [90]. The full damping matrix gives rise to coupled equations of motion in the system composed of Eqs. (2.9) and (2.10), thus involving complex modal coordinates and complex eigenvalues and eigenvectors [109, 110].

5.1.1 IIS design spectrum

The dynamic characteristics of the isolated vertical addition that minimize the seismic demand on the overall structure are derived through a parametric response spectrum analysis (RSA) on the 2DOF IIS model (Figure 2.2b) (see Appendix B).

A schematic representation of a typical curve reporting the results of RSA is shown in Figure 5.1, where, set the values of the parameters T_{LS} and μ, the displacement of the lower structure varies as a function of the period T_{ISO}. The displacement of the SDOF model of the existing building in the AS-IS configuration, $u_{AS\text{-}IS}$, is taken as a term of comparison and is also provided in the figure as a horizontal dashed line.

The chart in Figure 5.1 exemplifies the so called *nonconventional TMD design spectrum* or *IIS design spectrum* [22, 126] in which, as reported in subsection 3.2.3.2, four zones can be identified: the red zone, the *conventional vertical extension zone;* (characterised $T_{ISO}/T_{LS} \ll 1$ and $u_{LS} > u_{AS\text{-}IS}$); The blue zone is the so-called *mass damping zone:* it is characterized by $T_{ISO}/T_{LS} \approx 1$ (or larger, depending on the mass ratio) and $u_{LS} < u_{AS\text{-}IS}$, i.e. displacement in the design configuration lower than the original configuration counterpart. This behaviour emerges thanks to the beneficial dynamic interaction between the two structural parts, with isolated vertical additions acting as a TMD for the existing building. Finally, the green zone individuates the *perfect isolation* behaviour, characterized by $T_{ISO}/T_{LS} \gg 1$ and $u_{LS} \approx u_{AS\text{-}IS}$, and by isolated vertical additions almost perfectly disconnected from the existing building, thanks to the very flexible isolation system that allows the upper structure moving independently from the lower one. A fourth zone, the *transition zone* between the mass damping and perfect isolation zones, can also be defined, where u_{LS} gradually tends to $u_{AS\text{-}IS}$.

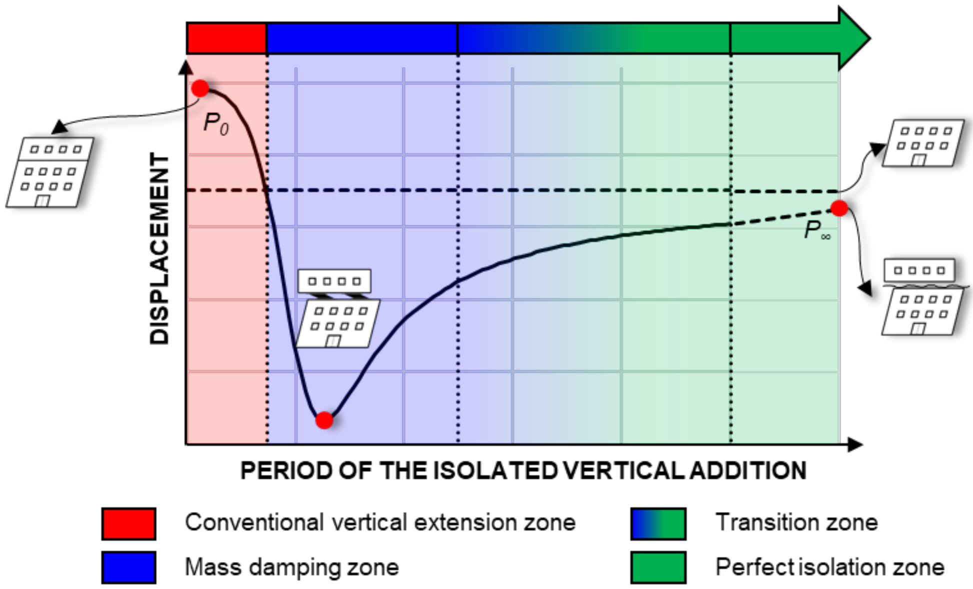

Figure 5.1. Typical IIS design spectrum.

On this chart, two limit points can be defined: the point P_0, corresponding to T_{ISO} that tends to zero, and the point P_∞, corresponding to T_{ISO} that tends to infinity. The point P_0 represents the first point of the RSA curve: when T_{ISO} tends to zero, the spring stiffness of the isolation system tends to infinite; therefore, the corresponding 2DOF IIS model is, in fact, a SDOF model having mass equal to the total mass of the system, i.e.: $m_{P0} = m_{LS} + M_{ISO}$, and stiffness is equal to the existing building counterparts, i.e.: k_{LS}, while the damping constants is equal to $c_{P0}= \xi_{LS} \{2[k_{LS}(m_{LS} + M_{ISO})]^{0.5}\}$;. The point P_∞ represents the end point of the RSA curve: when T_{ISO} tends to infinity, the spring stiffness of the isolation system tends to zero, and the building extension is fully decoupled from the existing structure; therefore, the 2DOF IIS model coincides with the SDOF model of the existing building, having mass, stiffness, and damping constants equal to m_{LS}, k_{LS}, and c_{LS}.

In order to show some numerical results of the parametric RSA and the influence of the aforementioned IIS design parameters, in this section, the RSA is developed with the horizontal elastic response spectrum in acceleration of Type 1, prescribed by the Eurocode 8 [50]; for the ground type A, with spectral shape defined by the following parameters: a_g = 0.1 g, S = 1, T_B = 0.15 s, T_C = 0.4 s, T_D = 2 s.

Surface plots provided in Figure 5.2a and Figure 5.2b show the influence of the design parameters T_{LS} and μ on the *IIS design spectrum*. In particular, *IIS design spectra* are plotted either by varying T_{LS} for a fixed value of the mass ratio (μ = 0.25, Figure 5.2a), or by varying μ for a fixed value of the period of the LS (T_{LS} = 0.39 s, Figure 5.2b). From Figure 5.2a it can be observed that, by increasing T_{LS}, the displacements of the lower structure increase in the whole range of T_{ISO}, the mass damping zone becomes wider, and the minimum values of displacement are reached at longer values of T_{ISO}. The plot in Figure 5.2b shows the effect of the mass ratio μ: by increasing μ, the displacement of the lower structure at the minimum value of T_{ISO} (T_{ISO} = 0.1 s) increases linearly, while, at the maximum value of T_{ISO} (T_{ISO} = 5.0 s), it decreases very slightly; further, the mass damping zone becomes wider by increasing μ, and the minimum displacement values are reached for longer values of T_{ISO}. Therefore, the larger the values of both parameters T_{LS} and μ, the wider the mass damping zone, i.e., the IIS effectiveness.

In Figure 5.3 the same RSA curves as the ones of Figure 5.2b are provided, here obtained with the minimum and the maximum values of T_{ISO} respectively equal to 0.01 s and 50 s. The range of T_{ISO} has been widened to define the limit points, P_0 (representative of conventional vertical extension) and P_∞ (representative of the existing structure as standalone), as the initial and end points of each RSA curve. By connecting all initial points of the curves, an almost straight line is obtained for the displacement of P_0 as a function the mass ratio, as already observed from Figure 5.2b. Analogously, by connecting the end points, an almost constant value for the displacement of P_∞ is obtained varying the mass ratio, as expected, due to the almost complete disconnection between the two masses. Finally, surface plots depicting the displacement of the limit points P_0 and P_∞ by varying T_{ISO} and μ are provided in Figure 5.4.

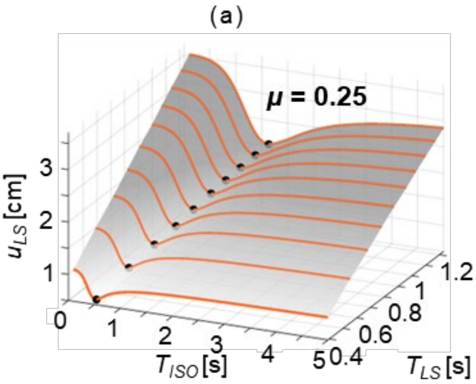

Figure 5.2. Surface plots of the IIS design spectra: (a) mass ratio $\mu = 0.25$; (b) period $T_{LS} = 0.39$ s.

All these charts are obtained from parametric analyses and are used to appreciate the behaviour of IIS in a very wide range of isolation period, varying the main design parameters T_{LS} and μ; however, the charts can also be employed as simplified tools within a design procedure for vertical extension of existing buildings through intermediate isolation system, as proposed in the following section. For this purpose, the 2D versions of the charts in Figure 5.2a, Figure 5.4a, and Figure 5.4b are traced and utilized in the next sections (Figures 6.5 – 6.7).

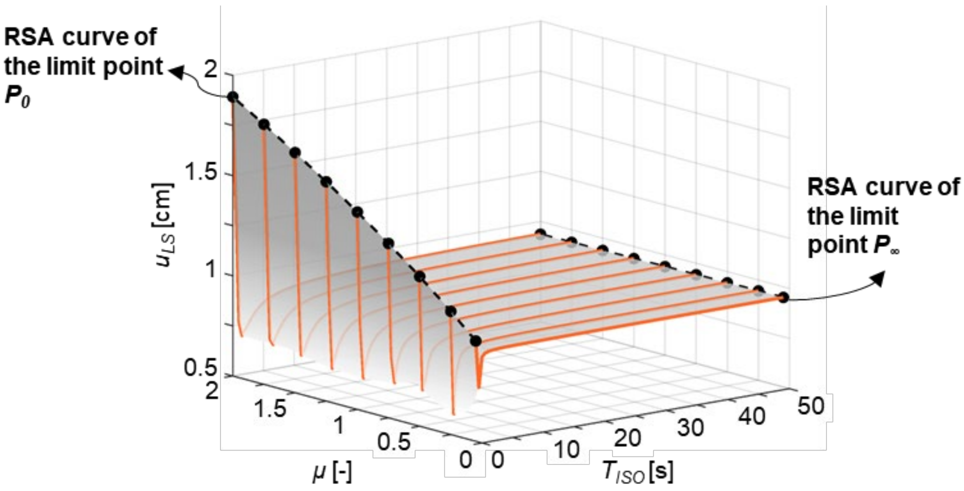

Figure 5.3. Surface plots of the IIS design spectra for periods $T_{LS} = 0.39$ s and $T_{ISO} = 0.01 – 50$ s.

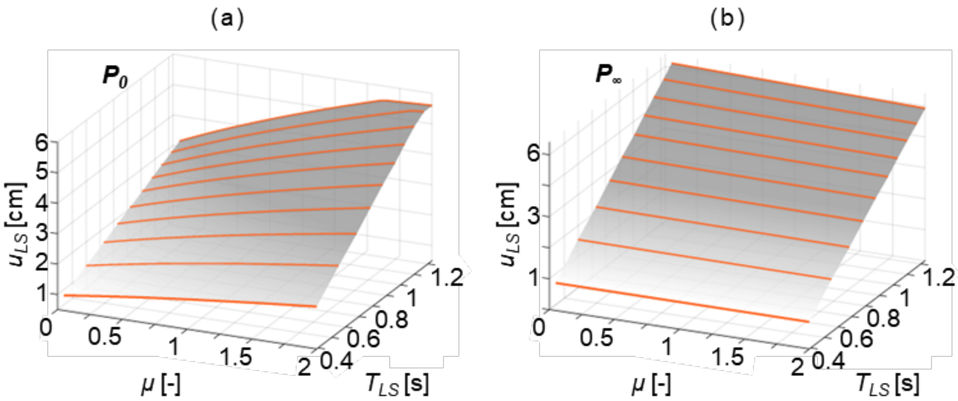

Figure 5.4. Surface plots of the IIS design spectra for the limit points: (a) point P_0; (b) point P_∞.

5.2 Stepwise procedure to predict the nonlinear response of LS

The IIS design displacement spectrum, that is the curve reporting the displacement of the lower structure obtained from RSA on the 2DOF IIS, having set the lower structure period T_{LS} and the mass ratio μ, and varying the isolation period T_{ISO}, is a very useful design tool for selecting the isolation period that allows the maximum reduction of the lower structure response. This design approach, based on *IIS spectrum*, assumes linear behaviour both in the lower structure and in the isolated upper structure. Since the lower structure is an existing structure, loss of linearity due to some damage under seismic actions cannot be excluded; in this case, the *IIS spectrum-based approach* can no longer provide accurate estimates of the building response. For this purpose, a design procedure is here defined that allows to use IIS spectrum also with nonlinear lower structure; the procedure, which also utilizes the charts depicted in the previous section, only requires nonlinear time history analyses (NTHAs) on the two SDOF models corresponding to the points P_0 and P_∞.

The design procedure is based on the empirical observation that when an existing structure experiences inelastic phenomena and structural damage, it exhibits a response softening, quantified by reduction of the global stiffness and elongation of the fundamental period. Basically, another RSA curve, characterised by a shift of the two points P_0 and P_∞ to P'_0 and P'_∞ (Figure 5.5), should be selected, thus defining the equivalent period $T_{eq} > T_{LS}$. However, the two points do not necessarily shift of the same quantity, since the nonlinearities arising in the lower structures are different in the two design configurations corresponding to the limit points. Therefore, not a single RSA curve should be defined, but two different curves, respectively passing through the points P'_0 and P'_∞, and corresponding to two equivalent periods $T_{eq,0} = T_{P'0}$ and $T_{eq,\infty} = T_{P'\infty}$. Since the points P'_0 and P'_∞ identify two limit behaviours that a given building with vertical extension exhibits in the inelastic field, the region bounded by the two RSA curves represents the prediction of the nonlinear response of the existing structure varying the isolation period of the vertical extension. For this reason, such zone in Figure 5.5 is called *inelastic IIS behaviour zone (i-IIS behaviour zone)*.

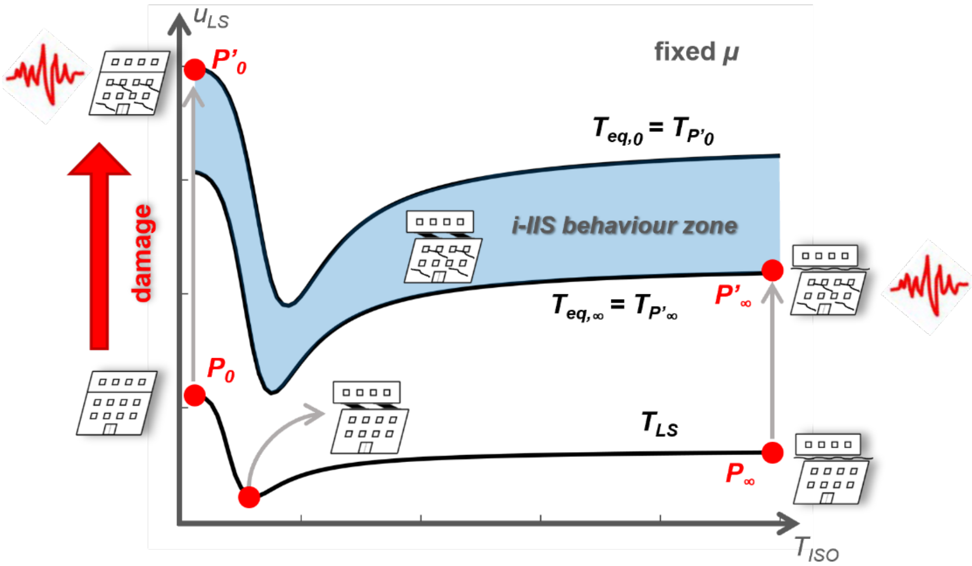

Figure 5.5. IIS design spectra and *i*-IIS behaviour zone to predict the nonlinear response of the existing building.

Key point of the procedure is to find the values of $T_{P'0}$ and $T_{P'\infty}$, and, in turn the two RSA curves corresponding to them. As will be shown in the following, some NTHAs should be carried out on two SDOF models P'_0 and P'_∞, respectively representing the existing building with a conventional vertical extension, and the existing building as a standalone structure. More in detail, the procedure is made of the five steps:

- step 1: definition of models SDOF P'_0 and SDOF P'_∞;
- step 2: NTHAs on SDOF P'_0 and SDOF P'_∞;
- step 3: identification of the periods $T_{P'0}$ and $T_{P'\infty}$;
- step 4: identification of the two RSA curves;
- step 5: definition of *i-IIS behaviour zone* and prediction of inelastic response.

A graphical representation of the proposed design procedure is provided in Figure 5.6, while the five steps are discussed in the following subsections. Some charts are used for facilitating the development of the procedure, namely: in the step 3, the 2D version of the plots of Figure 5.4a and Figure 5.4b, given in Figure 6.7; in the step 4, the 2D version of the chart in Figure 5.2a, given in Figure 6.5 and Figure 6.6.

5.2.1 Step 1: definition of SDOF P'_0 and SDOF P'_∞

Step 1 is devoted to the definition of the SDOF models corresponding to P'_0 and P'_∞, accounting for the inelastic behaviour of the existing structure in the two design configurations.

The mass of the SDOF model P'_0 is equal to the sum of the equivalent mass of the existing building, m_{LS}, and the added mass, $m_{P0} = m_{LS} + M_{ISO}$, while the mass of the SDOF model P'_∞ is equal to $m_{P\infty} = m_{LS}$. A bilinear relationship between the base shear and the top displacement is adopted for the nonlinear characterization of the SDOF models P'_0 and P'_∞, obtained, for example, according to the N2 method [104]. The hysteresis law selected to describe the inelastic dynamic response of the two models depends on the structural material of the existing building.

5.2.2 Step 2: NTHAs on SDOF P'_0 and SDOF P'_∞

Step 2 is devoted to the evaluation of the nonlinear response of the SDOF models P'_0 and P'_∞ through NTHAs, by adopting a set of original (un-scaled) accelerograms matching the target spectrum. The nonlinear response of the SDOF models P'_0 and P'_∞ is expressed in terms of average value of the peak displacements exhibited under the seismic records, namely $\bar{\bar{u}}_{P'_0}$ and $\bar{\bar{u}}_{P'_\infty}$.

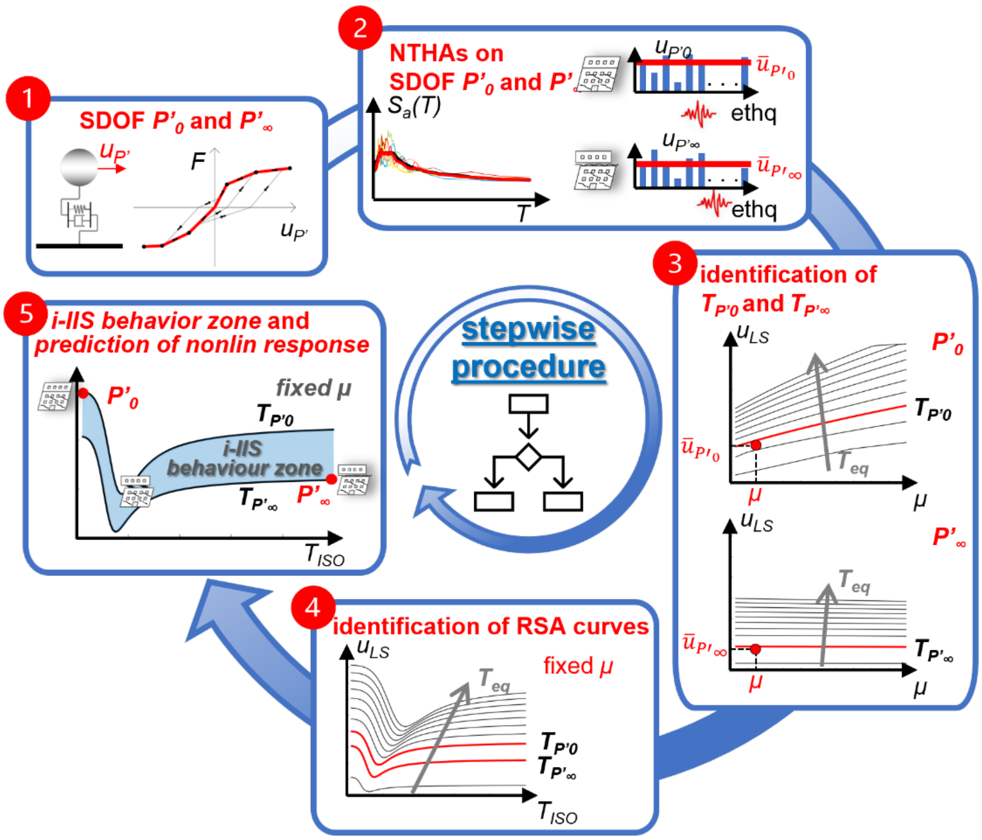

Figure 5.6. Design procedure.

5.2.3 Step 3: identification of the periods $T_{P'0}$ and $T_{P'\infty}$

Step 3 is devoted to the identification of the periods $T_{P'0}$ and $T_{P'\infty}$ i.e. the equivalent linear periods obtained from the peak inelastic response of NLTHAs. From the results of NTHAs on the SDOF models, and known the mass ratio μ, two couples of values (μ, $\bar{\bar{u}}_{P'_0}$) and (μ, $\bar{\bar{u}}_{P'_\infty}$) are used as coordinates in the plots of Figure 5.4a and Figure 5.4b, respectively, thus defining two points. The values $T_{P'0}$ and $T_{P'\infty}$ are given as the periods identifying the curve closest to the points (μ, $\bar{\bar{u}}_{P'_0}$) and (μ, $\bar{\bar{u}}_{P'_\infty}$), respectively.

5.2.4 Step 4: identification of the RSA design curves

Step 4 is devoted to the selection of the RSA design curves for the construction of the *i-IIS behaviour zone*. From the RSA curves of

Figure 5.2a, the ones corresponding to the values of $T_{P'0}$ and $T_{P'\infty}$ derived in the step 3, are selected.

5.2.5 Step 5: definition of *i-IIS behaviour zone* and prediction of nonlinear response

Step 5 is devoted to the definition of the *i-IIS behaviour zone* and the prediction of nonlinear response of the existing structure in the extended configuration. The region bounded by the curves defines the so called the *i-IIS behaviour zone*.

It is expected that the points describing the inelastic response of the 2DOF IIS model, varying the isolation period, fall within this zone. Since the 2DOF IIS model represents the existing structure in all possible design configurations of isolated vertical extension (set the mass ratio μ and varying the isolation period), the chart with the *i-IIS behaviour zone* can be used for choosing the optimal design configuration in a preliminary phase.

5.3 Validation of the *stepwise design procedure* through NTHAs

For validating the procedure, some 2DOF IIS models characterized by different configurations of both the existing building and the isolated vertical extension are considered. Nonlinear time history analyses are firstly carried out on the SDOF model for deriving the inelastic response of the existing building in the AS-IS configuration, i.e., without the vertical extension. The nonlinear response of the lower structure in the design configurations is then obtained according to the proposed design procedure. Nonlinear time history analyses are then carried out on the 2DOF models, and the results are compared to the predictions.

5.3.1 Case studies: SDOF and 2DOF IIS models

Three existing structures are considered as case studies and described by SDOF models. The structures are all characterized by the same normalized base shear strength V_y/W, equal to 0.13 (with W seismic weight), and by different values of the normalized top displacement at yielding $u_{top,y}/H$, respectively equal to 0.078%, 0.2%, and 0.35%, (with H building height). The corresponding bilinear curves are depicted in Figure 5.7a by normalizing the base shear to the seismic weight, V_b/W, and the top displacement to the total height of the building, u_{top}/H. For each existing structure, twenty-one configurations are adopted for the isolated vertical extension (Figure 5.7b); for all of them, the mass ratio μ has been assumed equal to 0.38, while the period of the isolated vertical extension T_{ISO} has been varied between 0.1 s and 5 s, with a step equal to 0.1 s in the range of values 0.4 – 2 s, and equal to 1 s for values larger than 2 s.

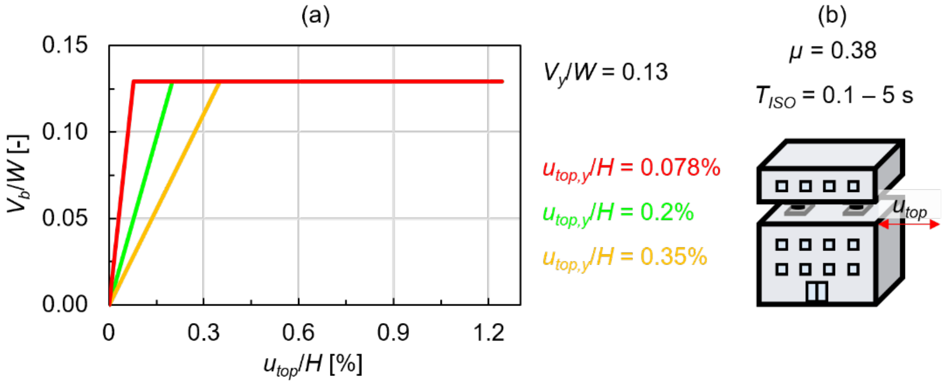

Figure 5.7. Case studies: (a) characterization of the inelastic behaviour of the existing buildings, (b) dynamic properties of the isolated vertical extension.

The lower structure of the 2DOF IIS model (e.g., the existing building) is characterized by the following dynamic properties: mass m_{LS}, and elastic stiffness $k_{LS} = 4\pi^2 m_{LS}/T_{LS}^2$, where T_{LS} is the period of the undamaged structure that varies as a function of the ratio $u_{top,y}/H$, i.e.: T_{LS} = 0.39 s, for $u_{top,y}/H$ = 0.078%; T_{LS} = 0.63 s, for $u_{top,y}/H$ = 0.2%; T_{LS} = 0.83 s, for $u_{top,y}/H$ = 0.35%. A multilinear plastic link is defined in SAP2000 [113] to describe the cyclic response of the existing building through a pivot-type model (Figure 3.4a). In such model, the shape of the hysteresis loops and the stiffness and strength degradation are controlled by the parameters α_1, α_2, β_1, β_2, and η_{Pivot} [105]. By considering, for example, existing buildings in unreinforced (URM) masonry structure, the parameters α_1, α_2, β_1, β_2 are assumed equal to 0.45 and the parameter η_{Pivot} equal to zero [22, 106 – 108, 126]. For the sake of simplicity, the three existing buildings are distinguished in the following according to the period T_{LS}.

The isolated vertical extension in the 2DOF IIS model is characterized by the following dynamic properties: mass $M_{ISO} = \mu \cdot m_{LS}$, and global secant stiffness $k_{ISO} = 4\pi^2 M_{ISO}/T_{ISO}^2$, which value varies as a function of the period T_{ISO}. By choosing an isolation system made of high damping rubber bearings, its hysteretic behaviour can be described by the bilinear constitutive model, depicted in Figure 4.2 and calibrated by means of the following parameters [93]: global secant stiffness $k_{eff} = k_{ISO}$; design displacement $\delta_{ISO,u} = S_d(T)$, with $S_d(T)$ the design spectral displacement at $T = T_{ISO}$; equivalent viscous damping ratio $\xi_{eq} = 2 \cdot Q(\delta_{ISO,u} - \delta_{ISO,y})/\pi \cdot k_{eff} \cdot \delta_{ISO,u}^2 = \xi_{ISO} = 0.15$; with Q the intersection between the prolongation of post-yield branch and the y-axis; the stiffness ratio between the post-yield and initial stiffnesses, i.e., $k_2/k_1 = 0.1$; displacement ratio between the yield and design displacements, i.e., $\delta_{ISO,y}/\delta_{ISO,u} = 0.034$.

It is worth observing that, the model here described is shown in Figure 4.7, with the only difference of replacing $\widetilde{m}_{LS}$ by m_{LS} and $\widetilde{M}_{ISO}$ by M_{ISO}, since the case studies here analysed are considered general and not directly related to real case studies.

5.3.2 NTHAs of the case studies

Nonlinear time history analyses are carried out on the 2DOF IIS models by means of a set of acceleration records matching to the target spectrum, that is Type 1 spectrum of Eurocode 8 defined at the Life Safety level, by 10% probability of exceedance in 50 years, and characterized by $a_g = 0.15$ g for ground type C.

Seven natural accelerograms are selected through the software REXEL v 3.5 [120] to match the target spectrum with a lower tolerance of 10%, for PGA values between 0.17 g and 0.25 g in the range of period between 0.01 and 5 s. The acceleration response spectra of the record set and the target spectrum are depicted in Figure 5.8, while the major data of the ground motions are provided in Table 5.1.

As discussed in subsection 5.1.1, the IIS is a non-classically damped system. For this reason, nonlinear direct-integration THA are performed by means of the software SAP2000 [113], in which the fully populated damping matrix is considered. The viscous damping matrix is constructed through the method of superposition of modal damping matrices each providing a fixed damping value in *i*-th vibration mode [113, 124]. In particular, a constant value of the modal damping ratio is assumed equal to 0.02 to include damping mechanisms that were not considered in the model, such as, for example, thermal effects from repeated elastic straining of structural materials, repeated straining of nonstructural elements, friction between the structure and nonstructural elements, and so on [125].

The inelastic response of the lower structure in the design configurations, varying the period T_{ISO}, is provided in Figure 5.9 for each existing building. The response parameter is the average values of the peak displacements obtained under the seven records ($\bar{\bar{u}}_{LS}$). It can be observed that the markers in Figure 5.9 display a trend similar to the IIS design spectra (Figure 5.1), reaching a minimum value in the zone of low-medium periods T_{ISO}, i.e., the *mass damping zone*.

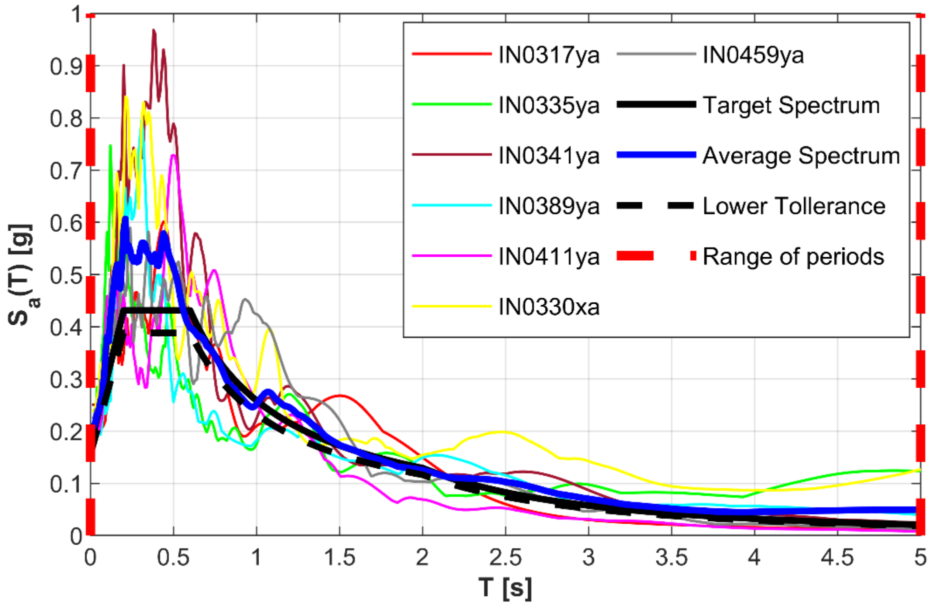

Figure 5.8. Set of spectrum-compatible acceleration records: acceleration response spectra.

Table 5.1. Major data of the set of spectrum-compatible acceleration records.

Earthquake name	EN1	EN2	EN3	EN3	EN4	EN5	EN6
Date	29/05/ 2012	03/09/ 2010	21/02/ 2011	13/06/ 2011	16/01/ 1995	3/09/ 2010	17/01/ 1994
W. ID	317	335	341	389	411	330	459
E. ID	133	137	142	149	34	137	99
S. ID	MOG0	TPLC	RHSC	RHSC	TKS	DSLC	ST_243 89
F. M.	reverse	strike-slip	reverse	reverse	strike-slip	strike-slip	reverse
Epi. Dist. [km]	16.43	23.58	13.73	14.76	17.45	13.31	20.19
PGA [g]	0.17	0.19	0.25	0.19	0.18	0.24	0.22
EC8 S.C.	C*	C*	C*	C*	C*	C*	C
$v_{s,30}$ [m/s]	n.a.	n.a.	n.a.	n.a.	n.a.	n.a.	278

***Note**: site class with * is based on geological information alone.*
Key: EN1 = Emilia Pianura Padana; EN2 = EN5 Darfield; EN3 = Christchurch; EN4 = Hyogo - Ken Nanbu; EN6 = Northridge; W. ID = Waveform ID; E. ID = Earthquake ID; S. ID = Station ID; F. M = Fault Mechanism; Epi. Dist = Epicentral Distance; S.C. = Site Class; n.a. = not available.

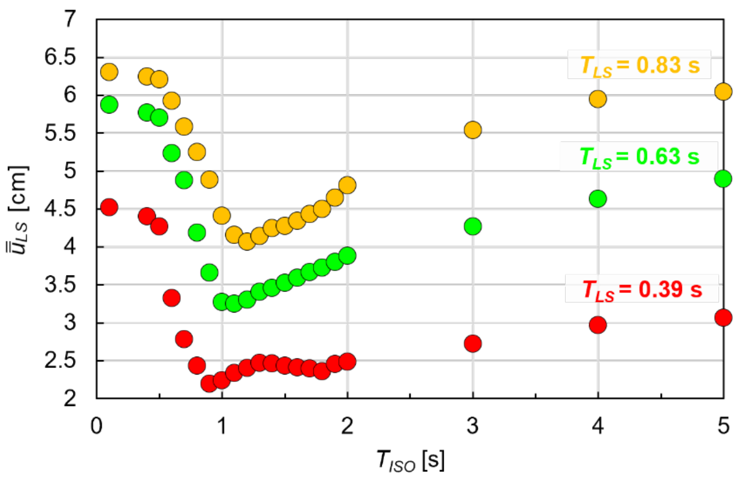

Figure 5.9. Average value of peak displacements as a function of the period T_{ISO}.

5.3.3 Application of the design procedure to the case studies

The nonlinear response of the lower structure in the 2DOF IIS models (Figure 5.9) is here compared to the design predictions obtained through IIS design spectra, according to the design procedure described in section 5.2.

Step 1: SDOF models P'_0 and P'_∞ (Figure 5.10). Mass of SDOF P'_0 is equal to $(1 + \mu)\cdot m_{LS}$, with μ = 0.38, and mass of SDOF P'_∞ is equal to m_{LS}. The same multilinear plastic link defined in SAP2000 [113] to describe the cyclic response of the lower structure in the 2DOF IIS models (Figure 3.4a) is here utilized, i.e., the pivot-type model with $\alpha_1 = \alpha_2 = \beta_1 = \beta_2 = 0.45$ and $\eta_{Pivot} = 0$.

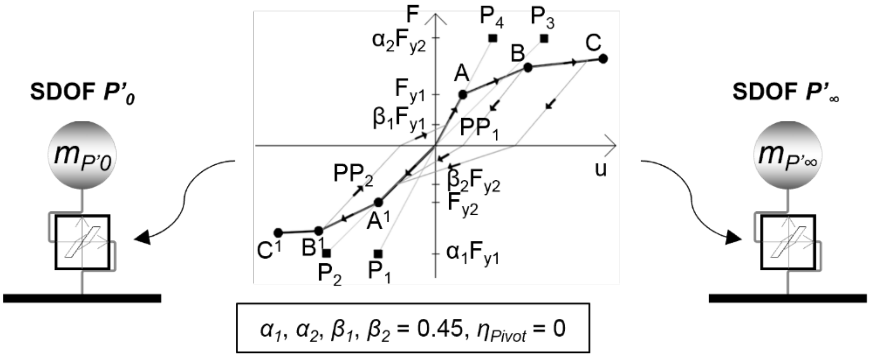

Figure 5.10. Step 1 of the design procedure: definition of SDOF P'_0 and SDOF P'_∞ models.

Step 2: NTHA of SDOF P'_0 and SDOF P'_∞. The record set in Figure 5.8 is used. The results are provided in Figure 5.11 in terms of peak displacements exhibited under each seismic input ($u_{P'0}$ and $u_{P'\infty}$); the average of the peaks, namely $\overline{\overline{u}}_{P'_0}$ and $\overline{\overline{u}}_{P'_\infty}$, is also provided in the figure. It can be observed that, by increasing the period T_{LS} of the lower structure, the average response increases. For the two smallest values of T_{LS}, the average displacement $\overline{\overline{u}}_{P'_0}$ is larger than $\overline{\overline{u}}_{P'_\infty}$; instead, for T_{LS} = 0.83 s, the average response of the limit points is almost equal.

Step 3: identification of $T_{P'0}$ and $T_{P'\infty}$. The charts of Figure 5.12 are used; these are the 2D version of the plots of Figure 5.4a and Figure 5.4b: mass ratio μ vs. displacement of the lower structure, with the different curves accounting for the different period of the lower structure T_{eq}. The points (μ, $\overline{\overline{u}}_{P'_0}$) and ($\mu$, $\overline{\overline{u}}_{P'_\infty}$) are also provided in the figure. By selecting the curves closest to the points (μ, $\overline{\overline{u}}_{P'_0}$) and ($\mu$, $\overline{\overline{u}}_{P'_\infty}$), from the figure, it can be derived that: $T_{P'0}$ = 0.68 s and $T_{P'\infty}$ = 0.55 s, for T_{LS} = 0.39 s; $T_{P'0} = T_{P'\infty}$ = 0.78 s, for T_{LS} = 0.63 s; $T_{P'0}$ = 0.87 s and $T'_{P\infty}$ = 1.03 s, for T_{LS} = 0.83 s. The configuration identified by T_{LS} = 0.63 s is a special case since the same curve is individuated for P'_0 and P'_∞.

Step 4: identification of RSA curves. The curves are selected among the ones built for $\mu = 0.38$ (Figure 5.13). As shown in the figure, for $T_{P'0}$ and $T_{P'\infty}$, two consecutive curves are selected for $T_{LS} = 0.39$ s, one curve for $T_{LS} = 0.63$ s, and two non-consecutive curves for $T_{LS} = 0.83$ s.

Step 5: definition of *i-IIS behaviour zone* and prediction of nonlinear response. The RSA curves (Figure 5.14) are considered as lower and upper bounds of the IIS response, for each value of T_{ISO}. The *i-IIS behaviour zones* are defined for $T_{LS} = 0.39$ s and $T_{LS} = 0.83$ s, while for $T_{LS} = 0.63$ s the behaviour zone collapses in one single design curve (*i-IIS curve*).

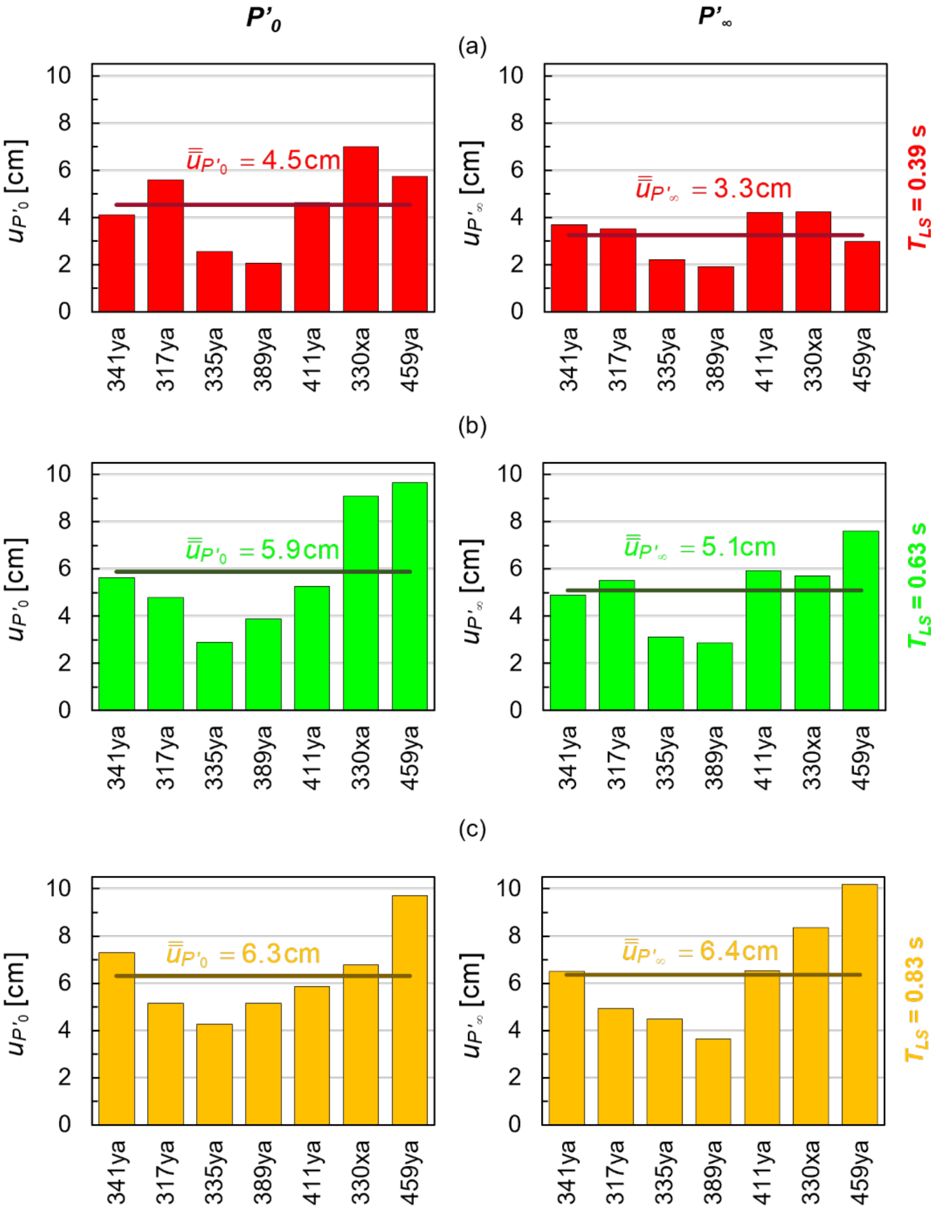

Figure 5.11. Step 2 of the design procedure: NTHAs on SDOF *P'₀* and SDOF *P'∞*.

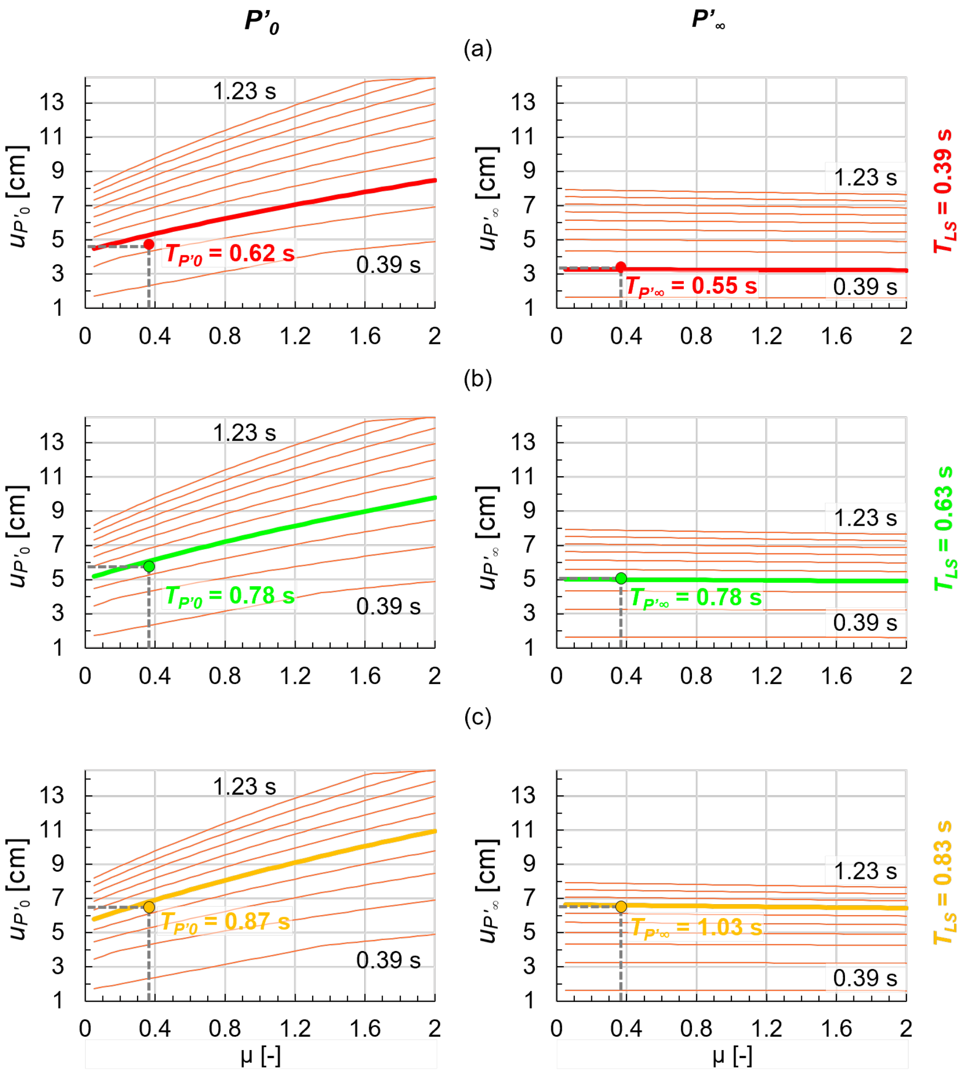

Figure 5.12. Step 3 of the design procedure - identification of the periods $T_{P'0}$ and $T_{P'\infty}$: (a) T_{LS} = 0.39 s, (b) T_{LS} = 0.63 s, (c) T_{LS} = 0.83 s.

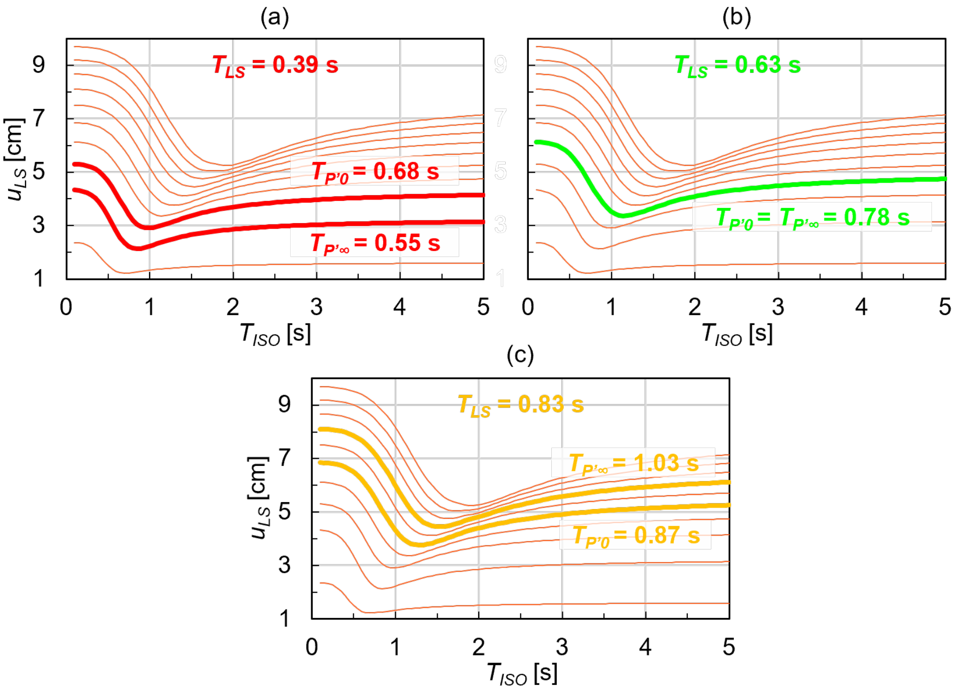

Figure 5.13. Step 4 of the design procedure - identification of the design curves: (a) T_{LS} = 0.39 s, (b) T_{LS} = 0.63 s, (c) T_{LS} = 0.83 s.

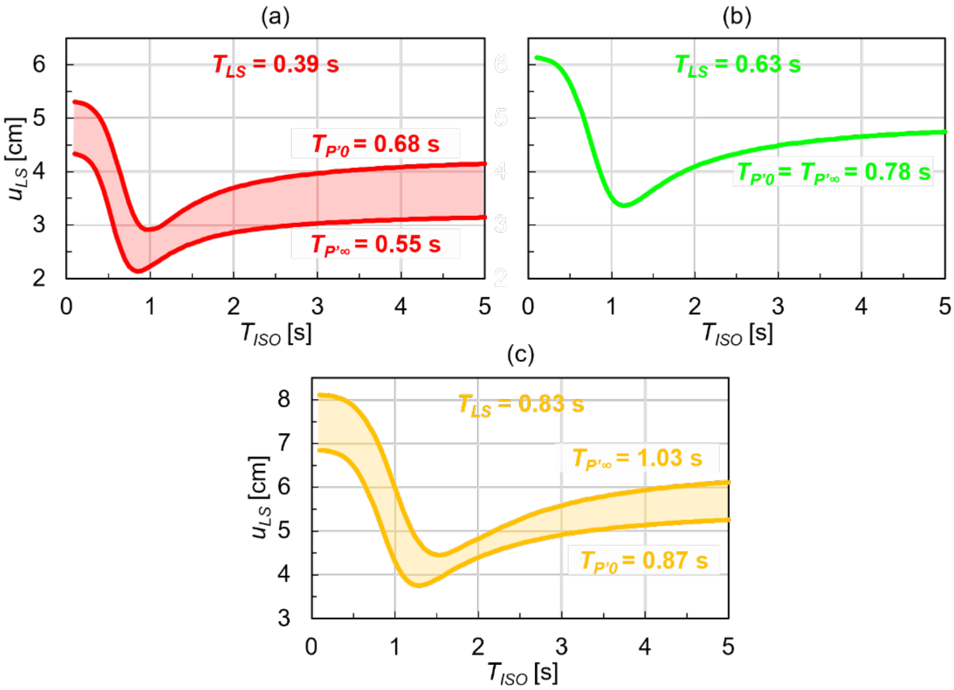

Figure 5.14. Step 5 - prediction of nonlinear response: (a) T_{LS} = 0.39 s, (b) T_{LS} = 0.63 s, (c) T_{LS} = 0.83 s.

5.3.4 Comparison between IIS design spectra and NTHAs

The Figure 5.15 compares the displacement response predicted according to the proposed procedure (Figure 5.14) to the displacement response of the first degree of freedom in the 2DOF IIS models obtained from NTHAs (Figure 5.9). For the sake of completeness, the results of the RSA obtained with the accelerograms' average spectrum (Figure 5.8) are also reported in the figure. From Figure 5.15, it can be observed that for T_{LS} equal to 0.39 s and 0.83 s the markers fall within or below the behaviour zone, for T_{LS} = 0.63 s the markers are almost equal to, or lower than, the values of the curve. This comparison testifies that the design procedure can be adopted in a preliminary design phase to estimate, in the entire range of periods, the inelastic response of structures to be vertically extended with IIS, and to select the isolation period that minimizes the building response and is compatible with the design requirements. The result curves obtained with the average spectrum are very close to the ones obtained with the target spectrum.

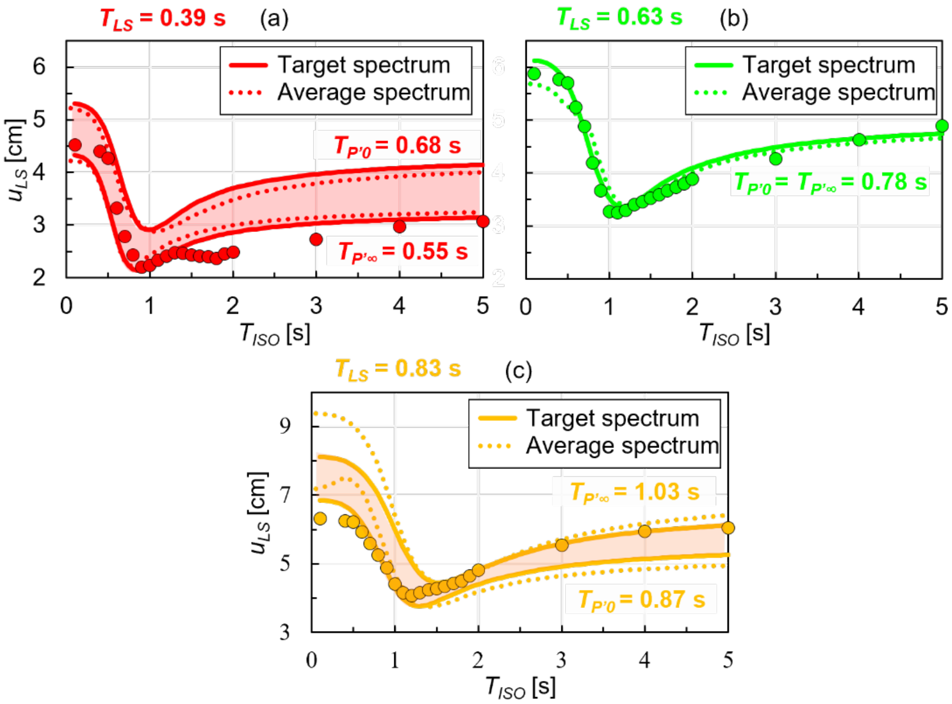

Figure 5.15. IIS design spectra vs. nonlinear THA: (a) T_{LS} = 0.39 s; (b) T_{LS} = 0.63 s; (c) T_{LS} = 0.83 s.

5.4 Application of *stepwise procedure* on real case study

In the previous sections of this chapter, the accuracy of the stepwise procedure has been demonstrated when LS exhibits nonlinear behaviour, by considering twenty-one IIS solutions for three different case studies. For comparative purposes, it is also interesting to apply the *stepwise procedure* to the real case study adopted in chapter 3 (an aggregate of masonry building located in Pozzuoli, Italy) and to the relevant IIS design configurations selected in chapter 4 (μ = 0.25 and T_{ISO} = {0.5, 1, 1.5, 5} s – A to E configurations). In fact, from Figure 4.5 it can be observed that the results of NTHAs on 3D IIS FEMs, independently of the modelling options adopted, show the typical trend of the IIS design spectrum. Hence, it is possible to identify the same four behaviour zones defined in section 5.1.1, by performing parametric RSA on 2DOF IIS models.

In particular, the *IIS design spectra* are here derived as described in section 5.4; the only differences refer to the adoption of the horizontal acceleration response spectrum defined in the Italian standard [94] and a value of a_g = 0.162 g, i.e. the one used in the RSA (see section 3.2.3.2).

Previsions through the *IIS design spectra* are then compared to the results of NTHAs performed on the 3D FEM of the IIS design configurations, obtained by adopting the same set of spectrum-compatible seismic records used in section 3.2.2.3.

5.4.1 Step 1: definition of SDOF P'$_0$ and SDOF P'$_\infty$

In step 1, the SDOF models of the points P'_0 and P'_∞ are defined, by accounting for the nonlinear hysteretic behaviour of LS.

As reported in section 5.2.1, the mass of the SDOF model P'_0 (Figure 5.16a) is equal to m_{LS} + M_{ISO} = 2472 + 940 = 3412 kNs^2/m; while the mass of the SDOF model P'_∞ (Figure 5.16b) is equal to m_{LS} = 2472 kNs^2/m. The nonlinear characterization of the SDOF models P'_0 and P'_∞ is obtained by adopting a bilinear relationship between the base shear and the top displacement. The corresponding bilinear curve is obtained from the Push-over analysis, by approximating the global push-over curve of the structure (for the multi-degree-of-freedom model) with a multi-linear bond (Figure 5.16c), as suggested in [127]. The hysteresis law selected to describe the inelastic dynamic response of the two models is the Pivot-type model already utilised to develop NTHAs on the 3D FEM of the AS-IS configuration (Figure 3.4b).

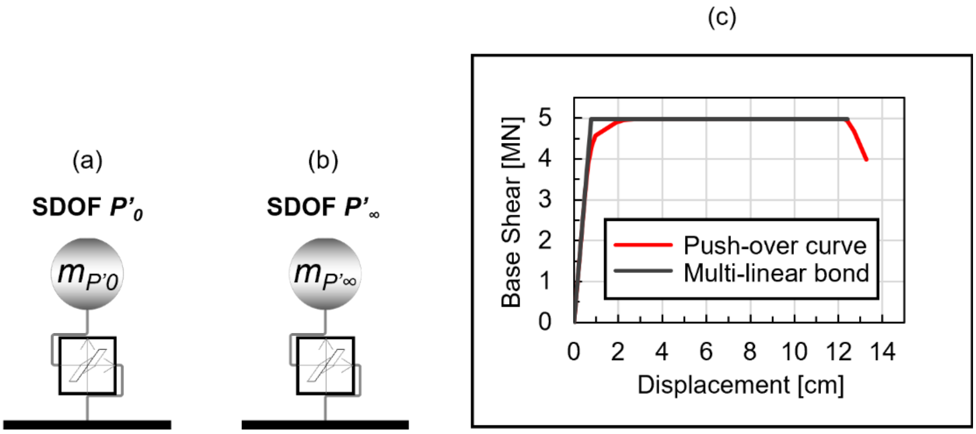

Figure 5.16. (a) SDOF P'_0 model; (b) SDOF P'_∞ model; (c) global push-over curve vs. multi-linear bond.

5.4.2 Step 2: NTHAs on SDOF P'₀ and SDOF P'∞

In step 2, NTHAs are performed on the SDOF P'_0 and SDOF P'_∞ models. The response of the SDOF P'_0 and SDOF P'_∞ models is plotted in terms of average value of the peak displacements exhibited under the seismic records in Figure 5.17a and Figure 5.17b, respectively.

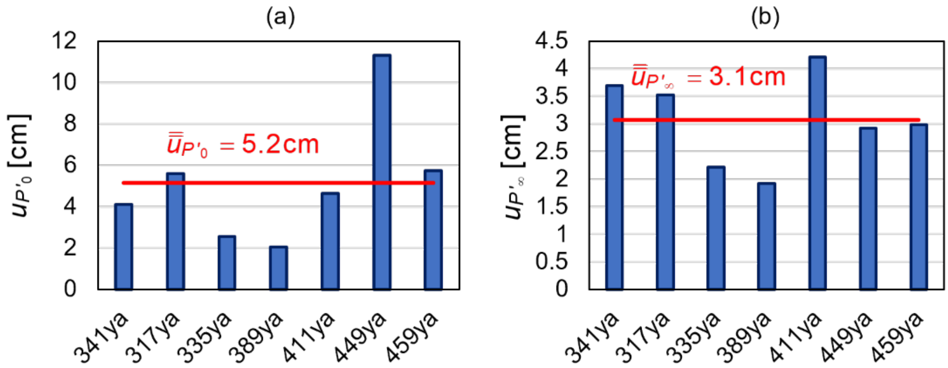

Figure 5.17. displacements response of: (a) SDOF P'_0; (b) SDOF P'_∞.

5.4.3 Step 3: identification of the periods $T_{P'0}$ and $T_{P'\infty}$

In step 3, $T_{P'0}$ and $T_{P'\infty}$ periods are identified as shown in Figure 5.18. In particular, the couples of values (μ, $\bar{\bar{u}}_{P'_0}$) and (μ, $\bar{\bar{u}}_{P'_\infty}$) are used as coordinates in the graph in Figure 5.18a and Figure 5.18b to respectively derive $T_{P'0}$ and $T_{P'\infty}$, i.e.: $T_{P'0}$ = 0.48 s and $T_{P'\infty}$ = 0.62 s.

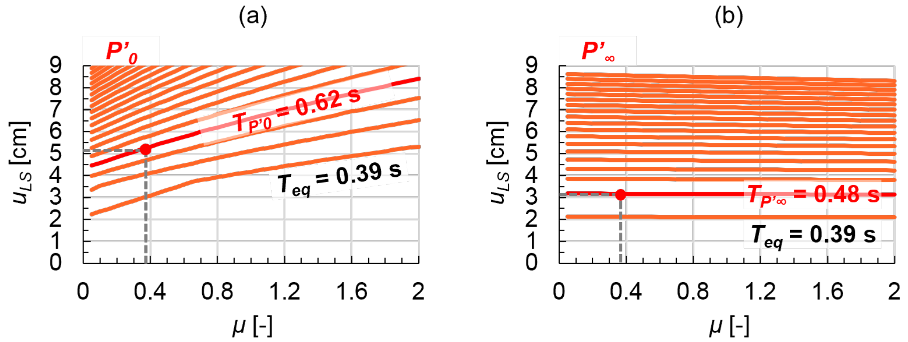

Figure 5.18. (a) graph of limit point P'0; (b) graph of limit point P'∞. T_{eq} = {0.39, 0,48, 0.55, 0.62, 0.68, 0.73, 0.78, 0.83, 0.87, 0.92, 0.96, 1.00, 1.03, 1.07, 1.10, 1.14, 1.17, 1.20, 1.23} s.

5.4.4 Step 4: identification of the RSA design curves

In step 4, the RSA design curves identifying the boundaries of the *i-IIS behaviour zone* are selected. Therefore, from the RSA curves in Figure 5.19a, those corresponding to the periods $T_{P'0}$ = 0.48 s and $T_{P'\infty}$ = 0.62 s are selected.

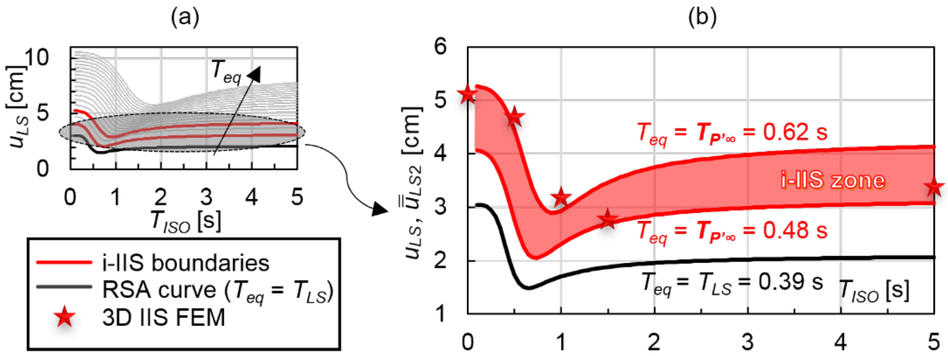

Figure 5.19. (a) RSA curves for T_{eq} = {0.39, 0,48, 0.55, 0.62, 0.68, 0.73, 0.78, 0.83, 0.87, 0.92, 0.96, 1.00, 1.03, 1.07, 1.10, 1.14, 1.17, 1.20, 1.23} s; (b) graph with *i-IIS zone*.

5.4.5 Step 5: definition of *i-IIS behaviour zone* and prediction of nonlinear response

In step 5, the *i-IIS behaviour zone* is identified, which provides the prediction of the LS nonlinear response.

Figure 5.19b also provides the average of peak displacements obtained with the NTHAs (red stars markers) carried out on the A – E configurations. Since the markers fall within or on the edge of the *i-IIS behaviour zone* in the whole range of isolation periods, *IIS design spectra* can be adopted in a preliminary design phase to select the isolation period corresponding to the required/desired response of the existing building that experiences inelastic behaviour. Therefore, the effectiveness and efficiency of the proposed design procedure also considering 3D FEM is here demonstrated.

From Figure 5.19b it can be further observed that the range of isolation periods corresponding to the minimum displacement ratios (in the mass-damping zone) are almost the same for all the periods T_{LS}, $T_{P'0}$, and $T_{P'\infty}$. Hence, the IIS design spectrum built for a period equal T_{LS} (undamaged structure) could be preliminary used to define the range of T_{ISO} that minimises the displacement ratio. However, as noted in subsection 5.1.1, this simplification is not recommended for small mass ratios for which the mass damping zone covers a small range of T_{ISO} values. In fact, in the case of IIS solution with a short isolation period, an amplification of the LS response could be achieved compared to the AS-IS configuration, i.e. the IIS configuration could belong to the zone of conventional vertical extensions.

Chapter 6

Generalization of the 5-Block design procedure for IIS

In this chapter, the 5-Block design procedure defined in chapter 3 has been extended and generalised to assess the effectiveness of IIS working as a nonconventional TMD by accounting for the possible inelastic behaviour of the existing structure from the first phases of the design process [128]. For this aim, the *stepwise procedure* developed in chapter 5 to predict the inelastic response of the existing building through *IIS design spectra* has been included in the block 2 of the generalised proposed procedure. So-called *ISO displacement spectra* are also developed and included in the block 2 to identify the displacement of the isolation system by varying the isolation period.

The flowchart of the generalised 5-block design procedure is depicted in Figure 6.1. More specifically: in block 1 the seismic behaviour of the LS is evaluated; in block 2 design solutions with IIS are explored by utilising simplified lumped mass models; in block 3, once selected the design configuration (one or more), the isolation system and the upper structure are designed; in block 4 the seismic behaviour of the IIS building is evaluated by adopting more refined 3D FE models; in block-5 the IIS effectiveness is evaluated by comparing the seismic response of the IIS configuration (one or more) to the counterpart of the reference AS-IS configuration.

Since the generalization of the procedure mainly deal with the block 2, the relevant flowchart is provided in Figure 6.2 and is subdivided in three main parts: (1) prediction of the elastic or inelastic displacement of the existing building through the *IIS design spectrum*; (2) selection of the IIS design configuration (one or more); (3) derivation of the displacement of isolators through the *ISO displacement spectrum*.

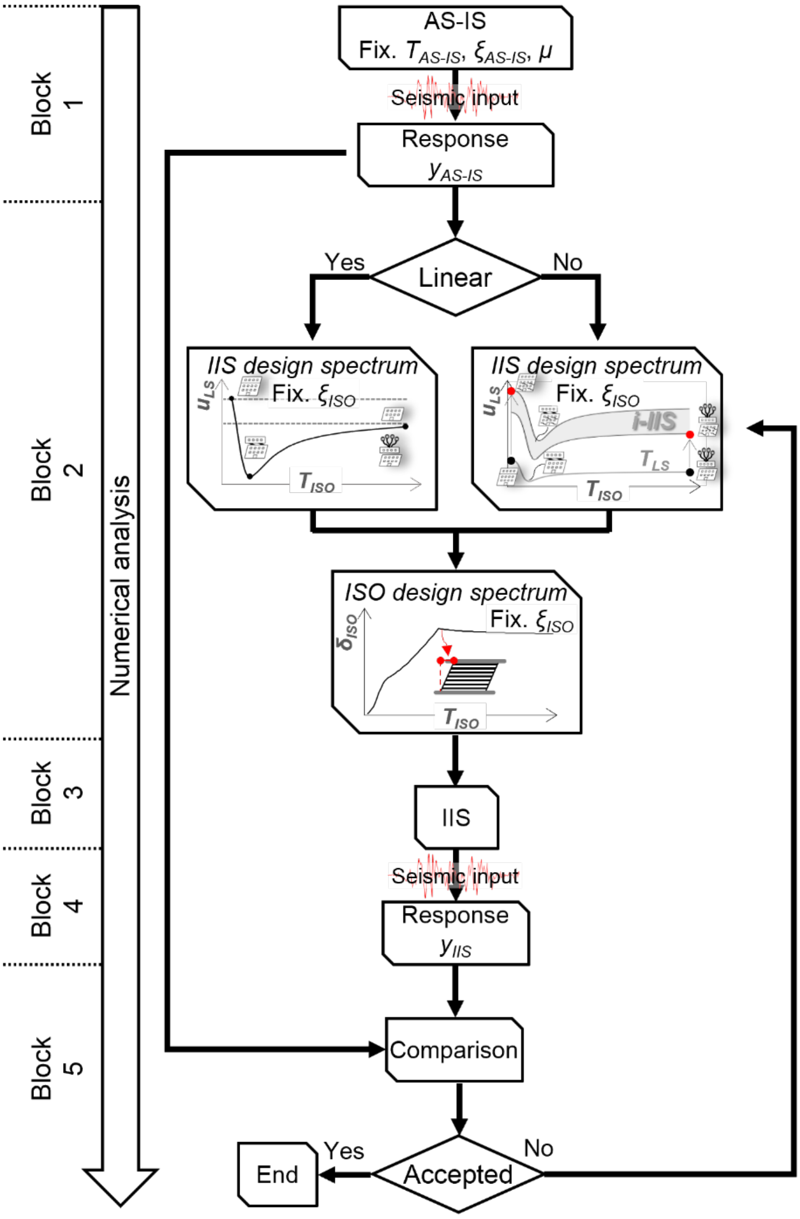

Figure 6.1. Flowchart of the generalised 5-Block design procedure.

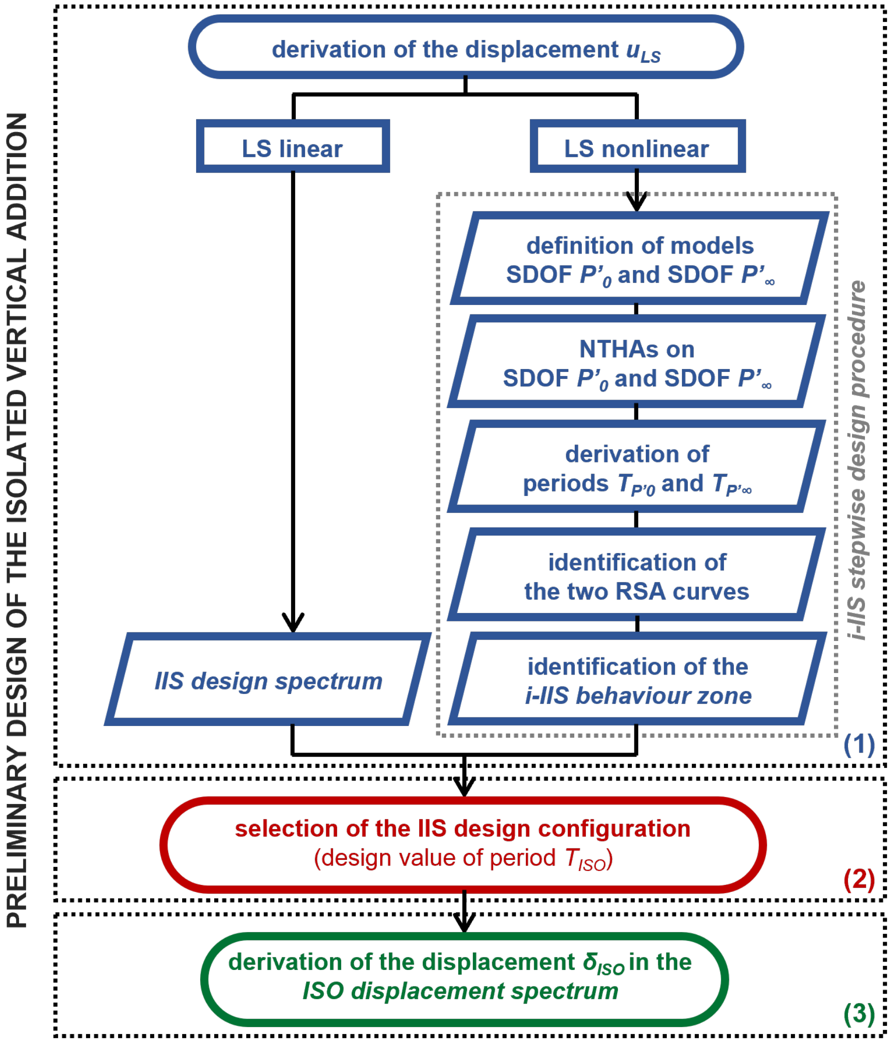

Figure 6.2. Flowchart of the Block 2 proposed design procedure.

In the following sections, after the definition of the *ISO displacement spectrum*, design charts are also provided, varying the shape of code design spectra and the seismic hazard through a scaling factor. Making use of these design charts, the procedure is validated by developing some case studies and by comparing the RSA previsions to the numerical results of nonlinear time history analyses.

6.1 ISO design spectrum

From the parametric RSA introduced in section 3.1.2, it is possible to obtain another useful design tool in chart form: the *ISO design spectrum*.

The *ISO displacement spectrum* depicts the displacement of the isolation device (δ_{ISO}), i.e., the difference between the relative displacement of the ISO mass (u_{ISO}) and the LS mass (u_{LS}) in the 2DOF IIS model (Figure 6.3a) by varying the isolation period. A typical curve, similar to the code displacement response spectrum, is plotted in Figure 6.3b.

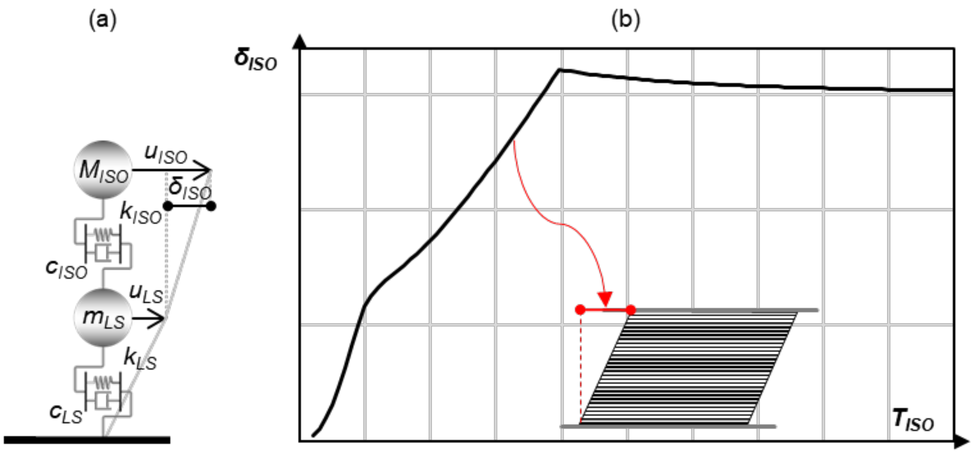

Figure 6.3. (a) 2DOF IIS model; (b) Typical *ISO design spectrum*.

6.2 Design charts

The *IIS* and *ISO spectrum* represented in plots of Figure 5.2, Figure 5.4, and Figure 6.3 can be used both to appreciate the behaviour of IIS in a wide range of isolation period, also varying the other design parameters T_{LS} and μ, and as simplified tools within the design procedure here proposed for IIS buildings with inelastic lower structure.

These plots have been obtained as results of a parametric RSA, carried out on the 2DOF IIS model, by assuming ξ_{LS} = 0.05 and ξ_{ISO} = 0.15, and by varying the major design parameters; in particular the lower structure period, T_{LS}, the isolation period, T_{ISO}, and the mass ratio, μ, have been varied within the following ranges: T_{LS} = 0.39 – 1.23 s; T_{ISO} = 0.1 – 5 s; μ = 0.05 – 2.

The range of values for T_{LS} is such to cover the periods of low-to medium rise existing buildings, with masonry or reinforced concrete structures, very common in European city; the value range chosen for T_{ISO} encompasses typical design values, while the values of μ account for the feasibility of vertical extensions of typical low-to-medium rise buildings.

As reported in section 5.1.1, the code design spectrum adopted for the RSA used for constructing the charts in Figure 5.2 and Figure 5.4 is the Type 1 spectrum of Eurocode 8 [50] at Life Safety level, characterized by 10% probability of exceedance in 50 years, and a_g = 0.1 g for soil type A. The CQC mode combination rule described by Sinha and Igusa in [83] is utilised to account for the nonproportional damping that characterises IIS configurations [22, 129] (see Appendix B).

Since the procedure is based on RSA curves, which, in turn, strongly depend on the shape of the code design spectrum, an extension of the parametric analyses is here provided, for including the effect of the spectral shape, i.e. the soil factor, therefore for a wider generalization. The elastic response spectrum $S_a(T)$ of Type 1, for which the surface-wave magnitude is larger than 5.5, varies as a function of: the seismic hazard, through the parameter a_g, (PGA on rock soil); the soil type, through the parameter S; and the damping ratio of the structure, through the parameter η. The spectral shapes for the five soil types defined in Eurocode 8 are shown in Figure 6.4, for a_g = 0.1 g and damping ratio equal to 0.05; the values of the soil factors for each type are also provided in the figure.

Recalling that all the spectral curves start from $S_a(T = 0) = a_g \times S$, the spectral shape can be scaled as a function of the seismic hazard through a scaling factor ScF equal to $a_g/a_{g,0}$, with the subscript 0 denoting a reference value of a_g, e.g. 0.1 g. Then, exploiting the linearity of the dynamic problem, the same scaling factor can be utilized to scale the response values obtained for a_g = 0.1 g.

Design charts to construct *IIS* and *ISO design spectra*, and the limit points curves are provided in the following two subsections.

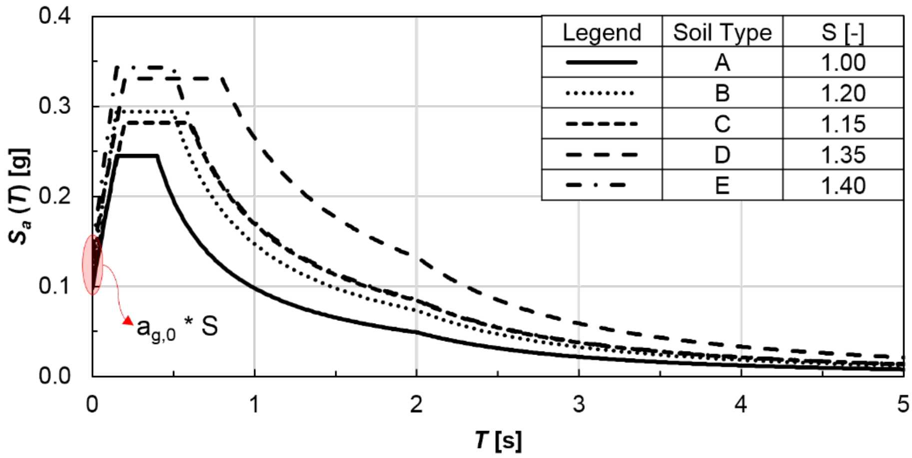

Figure 6.4. Type 1 elastic response spectra of Eurocode 8 for soil types A to E.

6.2.1 IIS design spectra and limit points curves

Regarding the *IIS design spectra*, design charts analogous to the ones of Figure 5.2a and Figure 5.4, are provided in Figure 6.5, Figure 6.6 and Figure 6.7, for the five soil types of Eurocode 8, by varying the period of the existing building, here appointed as T_{eq}, from 0.39 s to 1.23 s. In Figure 6.5 and Figure 6.6, the *IIS design spectra* (or RSA curves) are shown for the five soil types, A to E, and for mass ratio μ equal to 0.25, 0.5, 1, and 2. Limit points curves are depicted in Figure 6.7, for the same ranges of values of the design parameters. The surface plot previously reported in Figure 5.2a corresponds to the charts for Soil A and μ = 0.25 in Figure 6.5, while the surface plots previously reported in Figure 5.4 corresponds to the charts for Soil A in Figure 6.7.

When the existing building works in the elastic field, the period T_{eq} is equal to the period of the undamaged existing building, i.e., $T_{eq} = T_{LS}$, and the limit points are identified by the points P_0 and P_∞. When the existing building works in the inelastic field, the period T_{eq} is equal to the period of the damaged existing building, and the limit points are identified by the points P'_0 and P'_∞. The procedure can be applied to existing buildings that, once extended, are expected to work either in the elastic or in the inelastic field, as briefly described in the following.

Elastic building: For each couple of values T_{eq} - μ and soil type of the reference site, the design charts are utilized to derive the displacement of the lower structure both in the design configuration and as standalone. From the IIS design spectrum in Figure 6.5 and Figure 6.6, the designer can select the period T_{ISO} to derive the corresponding displacement of the lower structure. From the limit point curve P_∞ in Figure 6.7, the user can derive the displacement of the existing building as standalone structure. The comparison of these displacements gives information about the effectiveness of IIS to protect the lower structure from seismic actions.

Inelastic existing building: As discussed in the previous sections 5.2, the nonlinear response of the existing building in the extended configuration can be predicted through *IIS design spectra* according to the proposed design procedure. Set the mass ratio μ and the soil type, the periods $T_{P'0}$ and $T_{P'\infty}$ can be identified from Figure 6.7, by selecting the curves closest to the points (μ, $\bar{\bar{u}}_{P'_0}$) and (μ, $\bar{\bar{u}}_{P'_\infty}$) that, in turn, are derived from the results of nonlinear THA on the SDOF P'_0 and SDOF P'_∞ models. Then, the design curves can be identified from the *IIS design spectra* of Figure 6.5 and Figure 6.6, by selecting the RSA curves corresponding to $T_{eq} = T_{P'0}$ and $T_{eq} = T_{P'\infty}$.

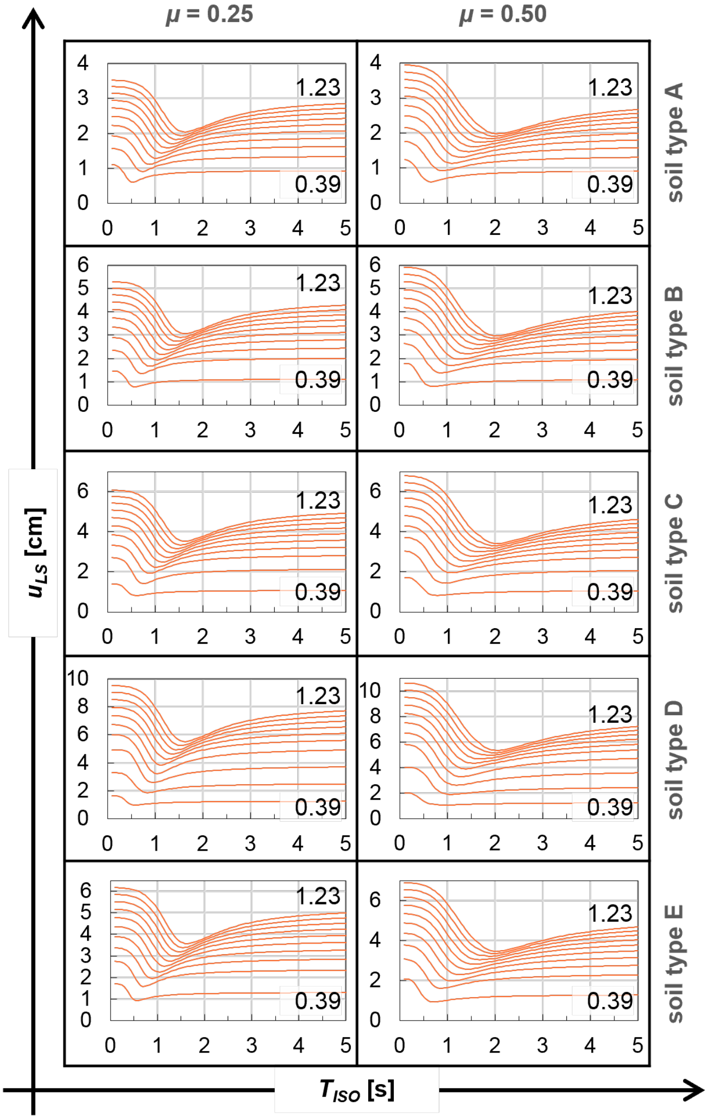

Figure 6.5. *IIS design spectra* for soil types A to E and mass ratios μ equal to 0.25, 0.5. Ordinate: u_{LS} [cm], abscissa: T_{ISO} [s]. Legend: T_{eq} = {0.39, 0.55, 0.68, 0.78, 0.87, 0.96, 1.03, 1.10, 1.17, 1.23} s.

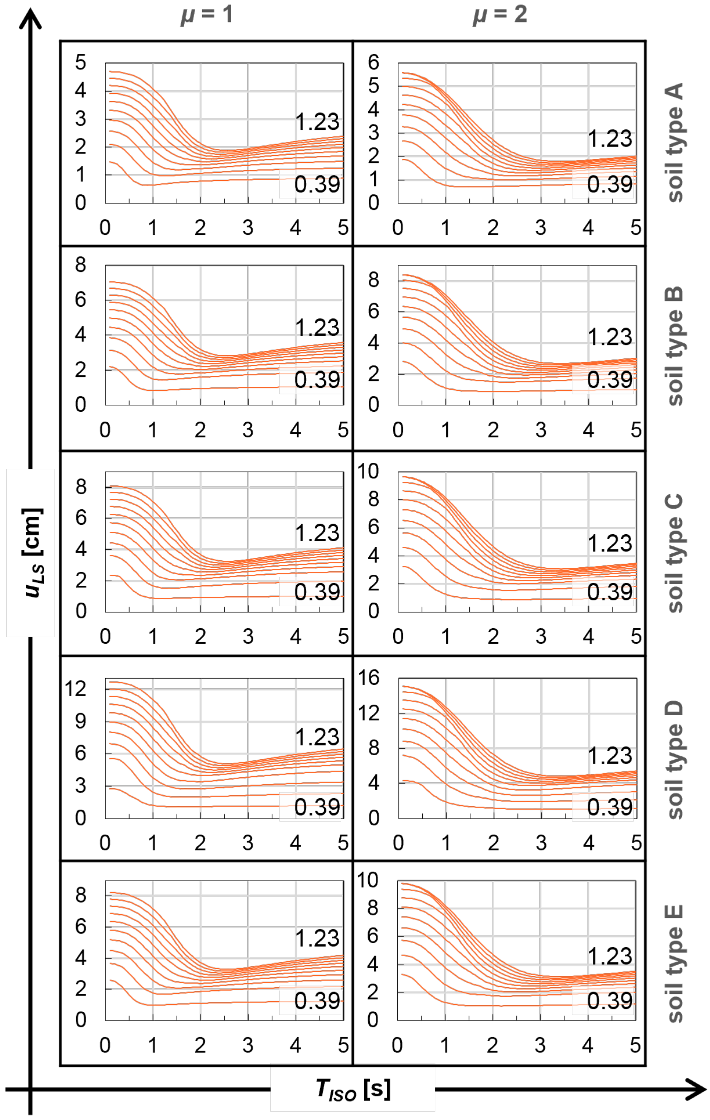

Figure 6.6. *IIS design spectra* for soil types A to E and mass ratios μ equal to 1, 2. Ordinate: u_{LS} [cm], abscissa: T_{ISO} [s]. Legend: T_{eq} = {0.39, 0.55, 0.68, 0.78, 0.87, 0.96, 1.03, 1.10, 1.17, 1.23} s.

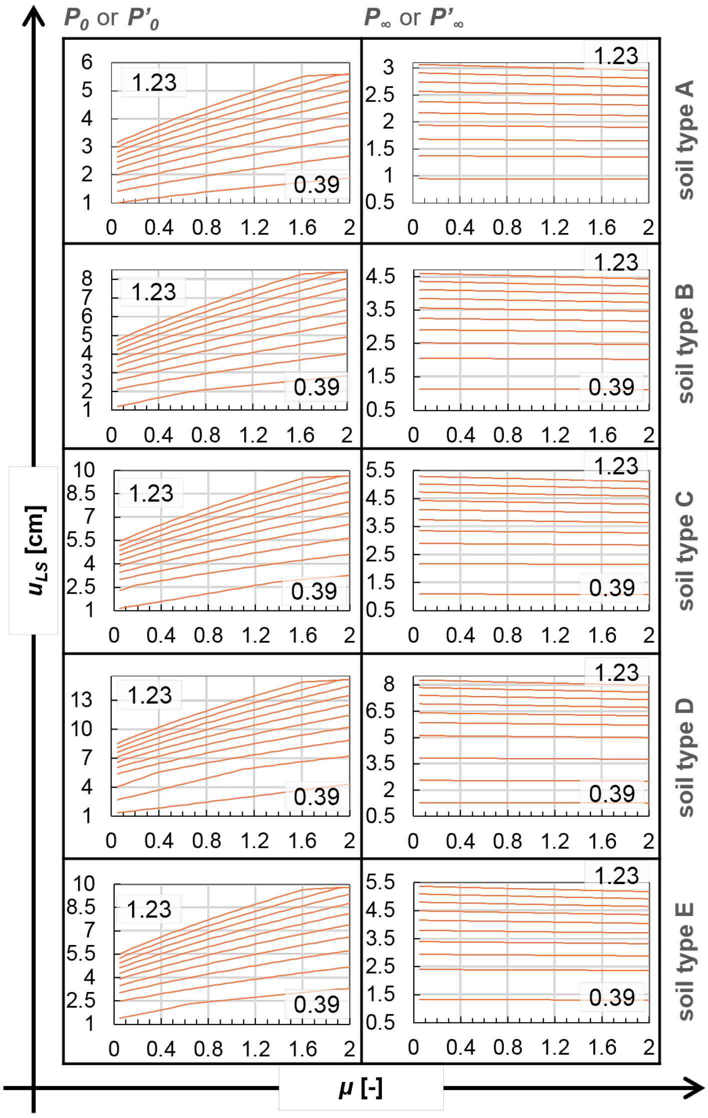

Figure 6.7. Limit points curves for soil types A to E: (a) point P_0; (b) Point P_∞. Ordinate: u_{LS} [cm], abscissa: μ [-]. Legend: T_{eq} = {0.39, 0.55, 0.68, 0.78, 0.87, 0.96, 1.03, 1.10, 1.17, 1.23} s.

6.2.2 ISO design spectra

As reported in section 6.1, from the parametric RSA results carried out to derive the *IIS design spectra* in Figure 6.5 and Figure 6.6, it is possible to derive the corresponding *ISO design spectra* (Figure 6.8 and Figure 6.9).

Also in this case, from the *ISO displacement spectra* (or *ISO design spectra*) traced in Figure 6.8 and Figure 6.9 (rows: soil types, columns: mass ratios), the influence of the design parameters T_{LS} and μ on the structural response can be noted. For example, still selecting the soil type A for $\mu = 0.25$, the displacement δ_{ISO} increases as T_{LS} (i.e. T_{eq}) increases in the range of T_{ISO} belonging to the mass damping zone; conversely, it decreases for longest values of T_{ISO} (i.e., in the perfect isolation zone). For the largest values of both T_{LS} and μ, this reduction is mitigated, and the curve shape follows the shape of the code displacement response spectrum, as previously observed (Figure 6.3b).

Once selected the design value of the isolation period T_{ISO} from the design charts of Figure 6.5 and Figure 6.6, the response δ_{ISO} is obtained and it can be derived from the design charts of Figure 6.8 and Figure 6.9.

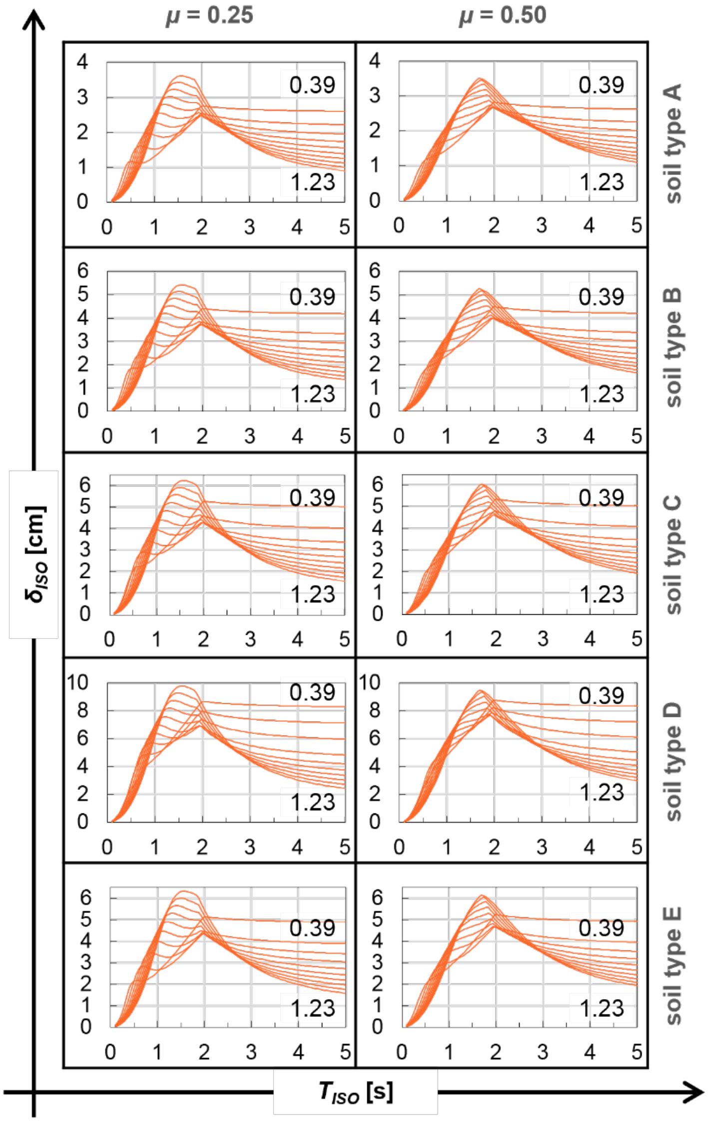

Figure 6.8. *ISO design spectra* for soil types A to E and mass ratios μ equal to 0.25, 0.5. Ordinate: δ_{ISO} [cm], abscissa: T_{ISO} [s]. Legend: T_{eq} = {0.39, 0.55, 0.68, 0.78, 0.87, 0.96, 1.03, 1.10, 1.17, 1.23} s.

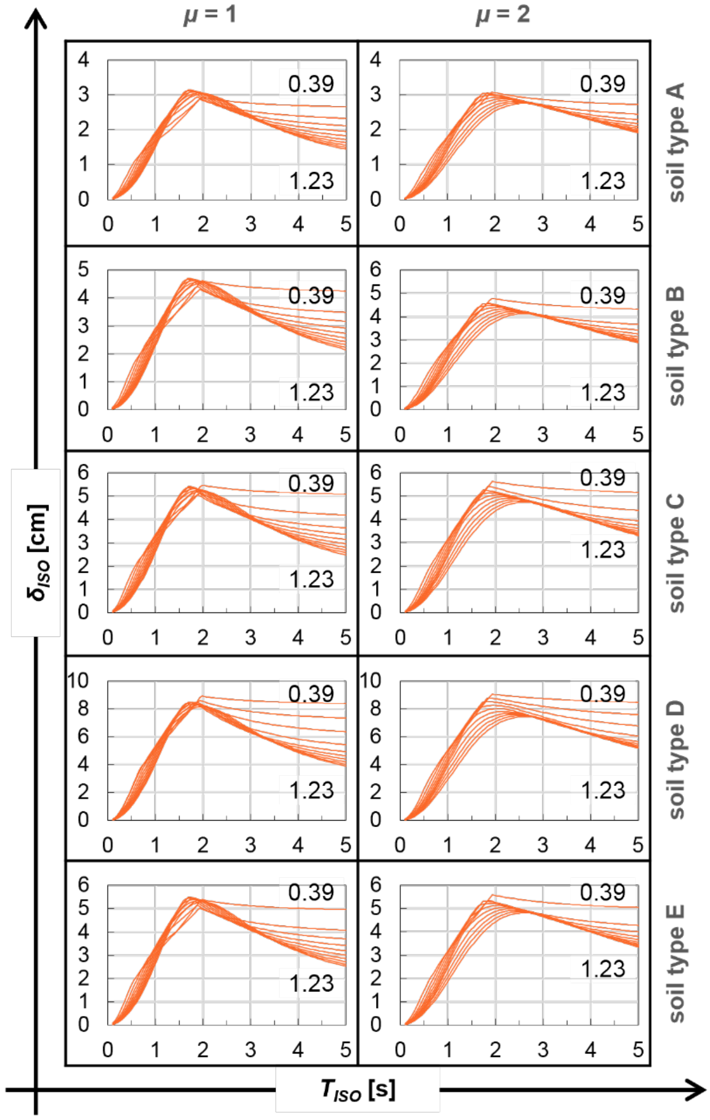

Figure 6.9. *ISO design spectra* for soil types A to E and mass ratios μ equal to 1, 2. Ordinate: δ_{ISO} [cm], abscissa: T_{ISO} [s]. Legend: T_{eq} = {0.39, 0.55, 0.68, 0.78, 0.87, 0.96, 1.03, 1.10, 1.17, 1.23} s.

6.3 Validation of the chart-based design procedure

Case studies are here adopted to validate the generalization of the proposed design procedure (Figure 6.2). Twenty-one 2DOF IIS models (Figure 6.10) characterised by the same lower structure (existing building with elastic or inelastic behaviour) and different configurations of the isolated vertical addition (μ = 0.5, $T_{ISO} \in \{0.05$ - $5\}$ s) are developed.

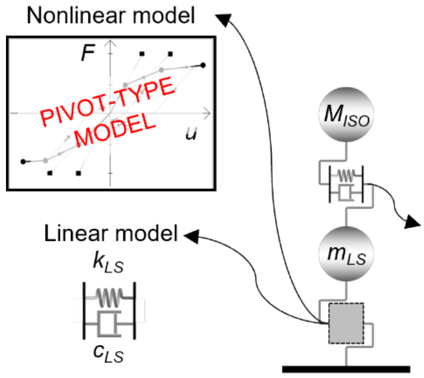

T_{ISO} [s]	k_{ISO} [kN/m]	c_{ISO} [kNs/m]
0.1	3710971.3	17718.6
0.4	231935.7	4429.6
0.5	148438.9	3543.7
0.6	103082.5	2953.1
0.7	75734.1	2531.2
0.8	57983.9	2214.8
0.9	45814.5	1968.7
1	37109.7	1771.9
1.1	30669.2	1610.8
1.2	25770.6	1476.5
1.3	21958.4	1363.0
1.4	18933.5	1265.6
1.5	16493.2	1181.2
1.6	14496.0	1107.4
1.7	12840.7	1042.3
1.8	11453.6	984.4
1.9	10279.7	932.6
2	9277.4	885.9
3	4123.3	590.6
4	2319.4	443.0
5	1484.4	354.4

Figure 6.10. 2DOF IIS model for LTHA and NTHA.

The RSA previsions derived from to proposed procedure are then compared to the results of linear or nonlinear THAs, depending on the behaviour of both degrees of freedom. The same spectrum adopted in the previous subsection is here chosen as target spectrum, i.e., Type 1 spectrum of EC8 at Life Safety level, characterised by 10% probability of exceedance in 50 years, and a_g = 0.15 g for soil type C. The set of seven spectrum-compatible ground motions defined in section 6.2 is here adopted for THAs.

Due to the nonproportional damping that characterises the IIS configuration, the full populated damping matrix is adopted. For this reason, direct-integration time history analyses (both linear and nonlinear) are developed in SAP2000 [113]. For the linear 2DOF IIS model, both degrees of freedom are modelled with a linear spring and a dashpot in parallel (Figure 6.10). For the nonlinear 2DOF IIS model, in which the nonlinearities are assumed only in the lower structure, the latter is modelled with a multilinear plastic link (Figure 6.10); in addition, the NTHAs are performed by assuming a constant modal damping ratio equal to 0.02 as described in subsection 5.3.2.

Dynamic properties of the 2DOF IIS model with elastic or inelastic lower structure, as well as the relevant analyses results, are provided in the following subsections 6.3.1 and 6.3.2.

6.3.1 Linear lower structure

By assuming a linear LS, the 2DOF IIS model is the model shown in Figure 6.10. The dynamic properties of the lower structure are mass m_{LS}, elastic stiffness $k_{LS} = 4\pi^2 m_{LS}/T_{LS}^2$, period T_{LS} = 0.39 s, and damping ratio ξ_{LS} = 0.05. The counterparts of the isolated vertical extension are mass $M_{ISO} = \mu \cdot m_{LS}$, secant stiffness $k_{ISO} = 4\pi^2 M_{ISO}/T_{ISO}^2$, period T_{ISO}, and damping ratio ξ_{ISO} = 0.15.

The *IIS design spectra* shown in Figure 6.11a are obtained from the design charts in Figure 6.5, by extracting the graph corresponding to the third row (soil type C) and the second column (μ = 0.5). Since the equivalent period of the existing building is $T_{eq} = T_{LS}$ = 0.39 s, the *IIS behaviour curve* is the black curve (i.e., RSA curve for T_{eq} = 0.39s). The twenty-one solutions are identified in Figure 6.11a with diamond markers, also showing the corresponding values of the displacement u_{LS} that are obtained for the reference value $a_{g,0}$ = 0.1 g. For a_g = 0.15 g, these values should be scaled through the scaling factor introduced in the section 6.2, i.e.: ScF = 0.15/0.1 = 1.5. As an example, for T_{ISO} = 1 s, u_{LS} = 0.86·1.5 = 1.29 cm. Similar operations are made in Figure 6.11b and Figure 6.11c to select the values of u_{P0} and $u_{P\infty}$ corresponding to μ = 0.5., i.e.: u_{P0} = 1.72·1.5 = 2.58 cm (limit point P_0) and $u_{P\infty}$ = 1.09·1.5 = 1.64 cm (limit point P_∞). Let's consider again T_{ISO} = 1 s, the ratio u_{LS}/u_{P0} = 0.50 and the ratio $u_{LS}/u_{P\infty}$ = 0.79; therefore, the vertical extension with IIS allows to reduce the displacement of the lower structure of the 50% than a conventional vertical extension and of the 21% than the AS-IS building.

The Figure 6.12 shows the comparison between the predicted displacements of the lower structure (black curve with diamond markers), derived from Figure 6.11a, and the average values of the peak displacements ($\bar{\bar{u}}_{LS}$) obtained from LTHAs with the seven records (blue circular markers). The lower tolerance and the RSA predictions obtained by assuming as response spectrum the average spectrum (average of the seven spectra of the seismic records, blue curve in Figure 5.8) are also considered. From Figure 6.12, the diamond markers are generally lower than the circular markers. Scatters between these markers depend upon the difference between the target spectrum and the average spectrum, and thus by the selection of the spectrum-compatible seismic records. In fact, the RSA previsions obtained with the average spectrum almost perfectly match the LTHAs results.

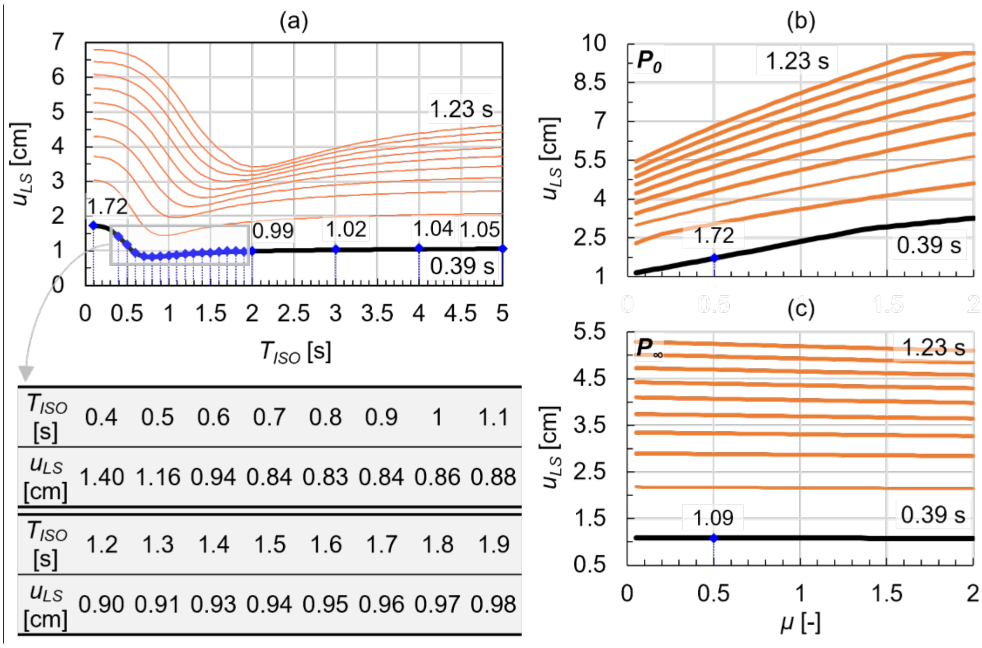

T_{ISO} [s]	0.4	0.5	0.6	0.7	0.8	0.9	1	1.1
u_{LS} [cm]	1.40	1.16	0.94	0.84	0.83	0.84	0.86	0.88
T_{ISO} [s]	1.2	1.3	1.4	1.5	1.6	1.7	1.8	1.9
u_{LS} [cm]	0.90	0.91	0.93	0.94	0.95	0.96	0.97	0.98

Figure 6.11. a) IIS design spectra for μ = 0.5 and Soil type C; b) Limit Points P_0; c) Limit Points P_∞.

As done for the graphs in Figure 6.11, the *ISO displacement spectrum* can be derived from Figure 6.8 by extracting the chart corresponding to the third row (soil type C) and the second column (μ = 0.5), and by scaling the ordinates of the first curve (T_{eq} = T_{LS} = 0.39 s) through the scaling factor *ScF* = 1.5. The resulting curve is depicted in black in Figure 6.13 and it is compared to the average values of the peak ISO displacements ($\overline{\overline{\delta}}_{ISO}$) obtained from LTHAs with the seven records (blue circular markers). The lower tolerance and the RSA predictions obtained by assuming as response spectrum the average spectrum are also considered. Similar observations as drawn from Figure 6.12 can be achieved.

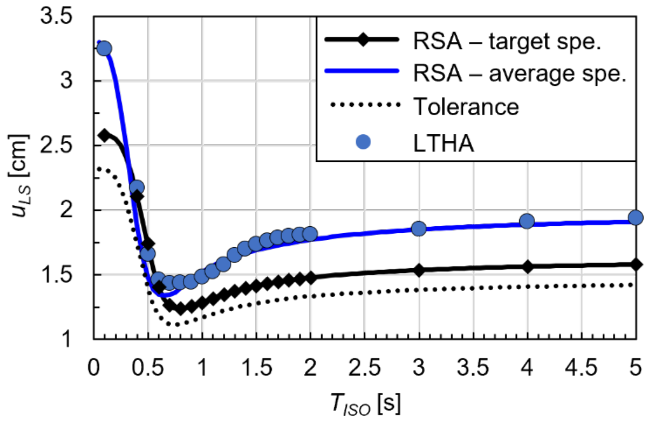

Figure 6.12. *IIS design spectra* vs LTHAs.

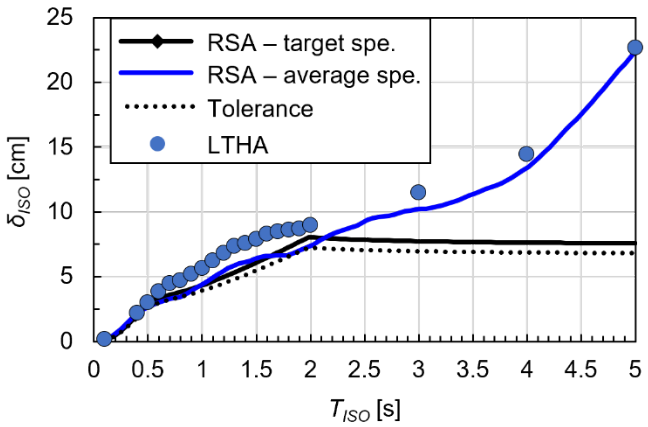

Figure 6.13. *ISO displacement spectra* vs LTHA.

6.3.2 Nonlinear lower structure

By accounting for the nonlinearity in the existing building, the first degree of freedom of the 2DOF IIS model is characterised by a bilinear behaviour, with normalized base shear strength V_y/W equal to 0.13 (with W seismic weight), and normalized top displacement at yielding dy/H equal to 0.078% (with H building height). The isolated vertical addition is characterised by the same dynamic properties adopted in the previous subsection (Figure 6.10).

The cyclic response of the existing building under seismic action is described by a pivot-type model [105] (for an unreinforced masonry structure, the control parameters are $\alpha_1 = \alpha_2 = \beta_1 = \beta_2 = 0.45$ and $\eta_{Pivot} = 0$ [106, 107]).

The nonlinear response of the existing building is predicted according to the *stepwise procedure* (section 5.2):

- Step 1: SDOF models P'_0 and P'_∞. Mass of models: for P'_0, $m_{P'0} = (1+\mu)\, m_{LS}$, for P'_∞, $m_{P'\infty} = m_{LS}$.
- Step 2: NTHAs of SDOF models P'_0 and P'_∞. Results in terms of average of the peak displacements, $\bar{\bar{u}}_{P'_0}$ = 5.46 cm and $\bar{\bar{u}}_{P'_\infty}$ = 3.61 cm.
- Step 3: identification of $T_{P'0}$ and $T_{P'\infty}$. Using charts μ - u_{LS} (third row in Figure 6.7), for different equivalent periods T_{eq}, the curves closest to the points $(\mu,\ \bar{\bar{u}}_{P'_0}/ScF) \equiv (0.5, 3.64)$ and $(\mu,\ \bar{\bar{u}}_{P'_\infty}/ScF) \equiv (0.5, 2.41)$ correspond to $T_{eq} = T_{P'0}$= 0.68 s and $T_{eq,\infty} = T_{P'\infty}$ = 0.55 s (Figure 6.14).
- Step 4: selection of RSA curves. Using charts T_{ISO} - u_{LS} (third row and second column in Figure 4), for different equivalent periods T_{eq}, the two curves corresponding to $T_{P'0}$= 0.68 s and $T_{P'\infty}$ = 0.55 s are selected (depicted in black in Figure 6.15a).
- Step 5: definition of *i-IIS behaviour zone* and prediction of nonlinear response. The *i-IIS behaviour zone* is obtained as the region bounded by the two RSA curves identified by equivalent periods $T_{P'0}$= 0.68 s and $T_{P'\infty}$ = 0.55 s; these curves are obtained by scaling the black curves in Figure 6.15a through the scaling factor *ScF* = 1.5 (Figure 6.15b).

The Figure 6.15b also shows the average of peak displacements obtained with the NTHAs (red circular markers). Since the markers fall within the *i-IIS behaviour zone* in the whole range of isolation periods, *IIS design spectra* can be adopted in a preliminary design phase to select the isolation period corresponding to the required/desired response of the existing building.

Charts T_{ISO} - δ_{ISO} (third row and second column in Figure 6.8) are used to select the *ISO displacement spectrum* built for T_{LS} = 0.39 s (Figure 6.16), which ordinates are scaled by *ScF* = 1.5. Other *IIS design spectra*, constructed with the average spectrum and different periods (T_{LS} = 0.39 s, $T_{P\infty}$ = 0.55 s, T_{P0} = 0.68 s) are also provided in the figure for comparative purposes. The *ISO displacement spectrum* with average spectrum built for T_{LS} = 0.39 s provides results that, though with some scatters, follows the trend outlined by markers. Furthermore, minor scatters are detected between the target spectrum and this average spectrum (e.g., for T_{LS} = 0.39 s) in the mass damping zone where the minimisation of the response of the existing building can be obtained. In general, these results prove that the *ISO displacement spectra* allow a good response prediction in a preliminary design phase.

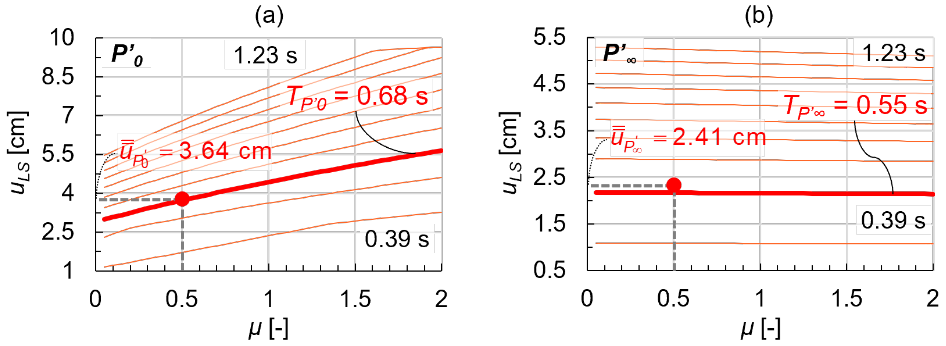

Figure 6.14. Step 3 of *i-IIS stepwise design procedure*: a) Limit point P'_0, a) Limit point P'_∞.

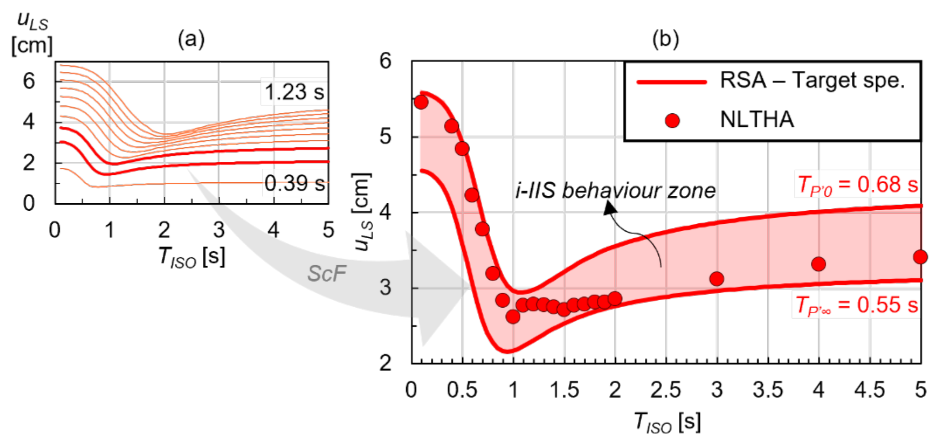

Figure 6.15. a) Step 4 of the *i-IIS stepwise design procedure*, b) step 5 of the *i-IIS stepwise design procedure* vs. NTHAs.

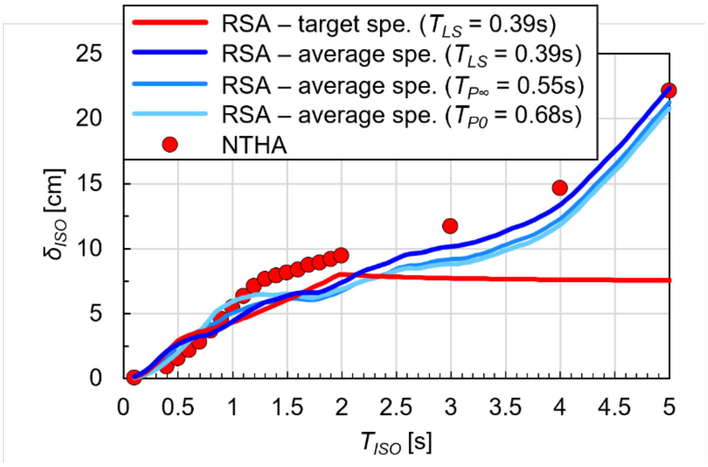

Figure 6.16. ISO displacement spectra vs. NTHAs.

6.4 Commentary on the design process for the vertical extension of existing buildings through IIS

The design process for vertically extending existing buildings through intermediate isolation is subject to the satisfaction of some requirements that are here discussed.

An essential requirement for the vertical extension of existing buildings is the check on an adequate overstrength of the structure for bearing the increase of gravity load due to extra-floors. Consequently, masonry structures are particularly suitable for this purpose for two main reasons: (i) relatively large compression capacity; (ii) stabilizing effect of the extra gravity under lateral actions. In well-designed masonry buildings, the compression strength demand to capacity ratio is usually quite low, between one fifth and one tenth [130, 131]; hence, this structural type is more than likely able to accommodate the additional compression forces due to the vertical extension. In prone-earthquake zones, masonry structures, which have poor tension resistance, can benefit from extra gravity loads; in fact, the local demand in terms of tensile stresses arising in the walls for bending and shear effects can be reduced or even counteracted. By erecting the new addition through intermediate isolation, a further improvement of the masonry behaviour can be obtained by exploiting the mass damping effect, for which the global seismic response on the existing structure can be also reduced. For these reasons, in the previous chapter is adopted an Italian masonry buildings as case studies to be extended through IIS, i.e.: an aggregate of three masonry buildings of two stories built in the 16th century.

The number of stories and the structural type of the new addition are generally known, therefore also the mass of the upper structure and, consequently, the mass ratio μ (initially neglecting the mass of the isolation system) are known. Hence, the period of the upper structure as standalone, T_{US}, only varies as a function of the stiffness of the structure. The stiffness can be derived to satisfy two design requirements: (i) upper structure rigid with respect to the isolation system; (ii) higher modes of lower and upper structures not coupled. As reported in section 2.1, these requirements, assumed *a priori* by adopting a 2DOF IIS model, can be satisfied by introducing some period ratios as design parameters. The first parameter is the ratio T_{ISO}/T_{US} that should be larger than 3 to satisfy the first requirement [92, 93]. The second parameter is β_h = (T_{LS}/T_{US}) (1 + m_{US}/m_{ISO})$^{0.5}$ that is a function of the period ratio T_{LS}/T_{US} [28, 57]. To satisfy the second requirement, the ratio β_h should differ from values between 0.85 and 1.15, or the ratio T_r = (T_{LS}/T_{US}) should be larger than 0.5 [20]. Once defined the isolation period, the only design variable in both ratios is the period T_{US} that can be modified by acting on the stiffness of the upper structure. For example, by considering T_{LS} between 0.3 and 0.5 s (typical range for 2-4 story masonry buildings) and T_{ISO} = 1 s, for T_{US} = 0.30 s the ratio T_{ISO}/T_{US} is equal to 3.33 (greater than 3) and the ratio T_{LS}/T_{US} varies between 1.00 and 1.67 (in both cases greater than 0.5). When the upper structure is not enough rigid with respect to the isolation system, say T_{US} = 0.5 s and T_{ISO}/T_{US} = 2, with a steel braced frame solution for the upper structure, the lateral stiffness can be easily increased by adjusting properly the diagonals' cross sections. The total mass of the isolated upper structure, M_{ISO} = m_{US} + m_{ISO}, can be approximately estimated as follows. The mass of the upper structure, m_{US}, can be calculated as a function of the unit structural weight (w), the number of extended storeys (n_{ef}), and the floor area (A_f), i.e. m_{US} = w x n_{sf} x A_f (e.g. for a steel US, w = 7 kN/m^2). Considering the values derived both from some actual isolated buildings [7] and from the relevant literature [91 – 93], the mass of the isolation system, m_{ISO}, can be assumed equal to two-thirds of the single floor mass of the fixed-base US, i.e. m_{ISO} = 2/3 $m_{US,n}$.

Chosen an isolation system made of high damping rubber bearings, the damping ratio ξ_{ISO} is almost set (it usually varies between 0.1 and 0.15); therefore, the properties of isolators vary only as a function of the isolation period T_{ISO}. In IIS applications for retrofit interventions, some aspects should be considered: tensile stresses in isolators and values of the isolation period quite small for maximizing the mass damping effect. The number of storeys to raise generally varies between 1 and 3, therefore the compression stress on each isolator could be not enough to counteract tensile stresses due to lateral actions. Short isolation periods (i.e. around 1 s) lead to quite rigid isolators. To overcome these issues, a smaller number of isolators could be adopted. For this aim, a transfer structure could be realized to collect the gravity load of different columns in few isolators. This is the trend usually followed in tall buildings with intermediate isolation [13, 30, 39, 132 – 135] as well as in base isolated buildings of new generation [95, 96]. At the same time, the adoption of few, highly loaded, isolators overcomes a further aspect not explicitly addressed in this thesis: since in IIS applications for retrofit the number of floors to be added is limited, the mass of the upper structure is relatively small, and it could lead to an increase in the sensitivity of the system's response to the vertical component of the earthquake.

Generally, the isolation system is composed by different types of devices, i.e. isolators and dampers (see Appendix A). Hence, the damping ratio cannot be set *a priori*. The optimal value of ξ_{ISO} could be chosen by considering several optimization procedures adopted in literature (e.g. [60]), or by adopting the simplified procedure suggested in Appendix D. The design displacement of the isolation system can be accurately predicted from the *ISO design spectrum*. However, this displacement can be also calculated – with a certain approximation – by adopting the Standard Design Spectrum at the base, as done in base isolated structures, or by a Standard floor Design Spectrum. In fact, in the common design practice for BISs, the design displacement of the ISO system ($\delta_{ISO,u}$) is initially assumed equal to the value obtained from the Standard Design Spectrum at the base (S_d) and is subsequently updated through more refined analyses on the 3D FEM of the whole BIS building ($\bar{\bar{\delta}}_{ISO}$). However, several standards [50, 94] suggest to adopt an iterative procedure until the difference between S_d

and $\bar{\bar{\delta}}_{ISO}$ does not exceed 5% of S_d. Hence, the more accurate the value of δ_{ISO} in the initial design phase, the smaller the number of iterations. To limit the number of iterations in the case of IIS configurations, it is suggested to use the *ISO design spectrum*, which is able to simultaneously grasp both the effects of mass damping and deformability of the lower structure. Hence, known the design value of the isolation period, the displacement of the isolation system can be estimated – on the safe side – as the maximum value among the displacement values obtained from the ISO *design spectra* built for equivalent periods equal to T_{LS}, $T_{P'0}$, and $T_{P'\infty}$.

Chapter 7

IIS and ISO design spectrum: close-form relationship through Pole Allocation Method (PAM)

In the previous chapters, a design procedure for IIS buildings was described based on the adoption of two key design tools, which are able to predict the IIS response through linear RSAs: the *IIS* and *ISO design spectra*.

However, due to the particularity of the IIS building, i.e. it is a non-classically damped system (see section 3.2), the RSA is performed in the complex field with the modified CQC modal superposition method [83, 109].

Consequently, these two design tools are not easily derived and their implementation in the current standard framework is very difficult.

Therefore, in this chapter in order to facilitate the dissemination of the *IIS* and *ISO design spectra*, i.e., of the proposed design procedure, closed-form relationships have been derived for them. These relationships are here derived through the application of the Pole Allocation Method (PAM) on a 2DOF IIS model in a similar way as done by Ikeda in [70, 71] on a 3DOF model. Through the PAM, the damping ratio values for the first two vibration modes are first obtained in closed-form and then through the RSA with the classical CQC modal superposition method the closed-form relationships for *IIS* and *ISO design spectrum* are obtained.

Consequently, the simplification of developing RSAs with the classical CQC instead of the modified CQC leads to a limitation in the use of the closed-form relationships. in fact, they can be used for ISO damping ratio values not too large.

7.1 PAM for IISs

Recently, as previously mentioned, Ikeda [70, 71] has also proposed the application of PAM to passive vibration control systems (i.e., open-loop systems) in order to derive useful closed-form relationships between modal and design parameters of the system. In fact, to allocate the poles of a system means to assign specific natural frequencies and damping ratios to each degree of freedom of controlled system, varying its modal characteristics consequently. Therefore, through this operation, Ikeda has derived the useful closed-form relationships between the dynamic parameters of the controlled system and the modal parameters.

In particular, since the system is open-loop in this case, feedback gains are absent. Consequently, target parameters for the whole structure (i.e., natural circular frequencies and damping ratios at each vibration mode of the system) must be defined that can be achieved by changing the structural design parameters (i.e., natural circular frequencies and damping ratios of each degree of freedom of the system).

In order to apply PAM to a system with passive vibration control, we consider the 2DOF IIS model in Figure 2.1c, the motion equations have already been written in the chapter 2 (Eq. (2.11)). However, for analytical convenience they are rewritten here in the state space:

$$
\begin{aligned}
&\begin{Bmatrix} \dot{u}_{LS} \\ \dot{u}_{ISO} \\ \ddot{u}_{LS} \\ \ddot{u}_{ISO} \end{Bmatrix} = \boldsymbol{A} \cdot \begin{Bmatrix} u_{LS} \\ u_{ISO} \\ \dot{u}_{LS} \\ \dot{u}_{ISO} \end{Bmatrix} - \begin{Bmatrix} 0 \\ 0 \\ 1 \\ 1 \end{Bmatrix} \ddot{u}_g \\
&\rightarrow \begin{Bmatrix} \dot{u}_{LS} \\ \dot{u}_{ISO} \\ \ddot{u}_{LS} \\ \ddot{u}_{ISO} \end{Bmatrix} = \begin{bmatrix} 0 & 0 & 1 & 0 \\ 0 & 0 & 0 & 1 \\ -\dfrac{k_{ISO}+k_{LS}}{m_{LS}} & \dfrac{k_{ISO}}{m_L} & -\dfrac{c_{ISO}+c_{LS}}{m_{LS}} & \dfrac{c_{ISO}}{m_{LS}} \\ \dfrac{k_{ISO}}{M_{ISO}} & -\dfrac{k_{ISO}}{M_{ISO}} & \dfrac{c_{ISO}}{M_{ISO}} & -\dfrac{c_{ISO}}{M_{ISO}} \end{bmatrix} \cdot \begin{Bmatrix} u_{LS} \\ u_{ISO} \\ \dot{u}_{LS} \\ \dot{u}_{ISO} \end{Bmatrix} - \begin{Bmatrix} 0 \\ 0 \\ 1 \\ 1 \end{Bmatrix} \ddot{u}_g
\end{aligned} \tag{7.1}
$$

Next, we can substitute Eqs. (2.14), (2.20) – (2.23) in Eq. (7.1) yielding:

$$
\begin{aligned}
&\begin{Bmatrix} \dot{u}_{LS} \\ \dot{u}_{ISO} \\ \ddot{u}_{LS} \\ \ddot{u}_{ISO} \end{Bmatrix} = \boldsymbol{A} \cdot \begin{Bmatrix} u_{LS} \\ u_{ISO} \\ \dot{u}_{LS} \\ \dot{u}_{ISO} \end{Bmatrix} - \begin{Bmatrix} 0 \\ 0 \\ 1 \\ 1 \end{Bmatrix} \ddot{u}_g \\
&\boldsymbol{A} = \begin{bmatrix} 0 & 0 & 1 & 0 \\ 0 & 0 & 0 & 1 \\ -\omega_{LS}{}^2 - \mu\,\omega_{ISO}{}^2 & \mu\,\omega_{ISO}{}^2 & -2\xi_{LS}\omega_{LS} - 2\mu\xi_{ISO}\omega_{ISO} & 2\mu\xi_{ISO}\omega_{ISO} \\ \omega_{ISO}{}^2 & -\omega_{ISO}{}^2 & 2\xi_{ISO}\omega_{ISO} & -2\xi_{ISO}\omega_{ISO} \end{bmatrix}
\end{aligned} \tag{7.2}
$$

To perform the PAM, it is convenient to rewrite the system of Eq. (7.2) applying the Laplace transformation (Eq. (2.31)), and setting the values of the initial conditions equal to zero as done in section 2.2:

$$
\dot{\mathbf{u}}(t) = \boldsymbol{A}\mathbf{u}(t) - \boldsymbol{b}\ddot{u}_g(t) \rightarrow \mathbf{s}\mathbf{U}(s) = \boldsymbol{A}\mathbf{u}(s) - \boldsymbol{b}\ddot{U}_g(s) \rightarrow (\boldsymbol{A} - s\boldsymbol{I})\mathbf{U}(s) = \boldsymbol{b}\ddot{U}_g(s) \tag{7.3}
$$

The characteristic equation of IIS can be calculated from Eq. (7.3), as also reported in [99]:

$$\det[s\boldsymbol{I}-\boldsymbol{A}]=0$$
$$\rightarrow\begin{vmatrix} -s & 0 & 1 & 0 \\ 0 & -s & 0 & 1 \\ -\omega_{LS}{}^2-\mu\omega_{ISO}{}^2 & \mu\omega_{ISO}{}^2 & -2\xi_{LS}\omega_{LS}-2\mu\xi_{ISO}\omega_{ISO}-s & 2\mu\xi_{ISO}\omega_{ISO} \\ \omega_{ISO}{}^2 & -\omega_{ISO}{}^2 & 2\xi_{ISO}\omega_{ISO} & -2\xi_{ISO}\omega_{ISO}-s \end{vmatrix}=0 \tag{7.4}$$

Eq. (7.4) is the characteristic equation of system matrix $\boldsymbol{A}$ and its roots are the poles of the transfer functions $G_{ug,\ 2DOF\ IIS}\ (s)$ (see section 2.2 and [99]). Considering the determinant in polynomial form, the Eq. (7.4) can be rewritten as follows:

$$\begin{aligned} & s^4+2\left(\xi_{ISO}\omega_{ISO}+\mu\xi_{ISO}\omega_{ISO}+\xi_{LS}\omega_{LS}\right)s^3 \\ & +\left\{\omega_{ISO}^2+\mu\omega_{ISO}^2+\omega_{LS}^2+4\xi_{ISO}\xi_{LS}\omega_{ISO}\omega_{LS}\right\}s^2 \\ & +2\left(\xi_{ISO}\omega_{ISO}\omega_{LS}^2+\xi_{LS}\omega_{LS}\omega_{ISO}^2\right)s+\omega_{ISO}^2\omega_{LS}^2=0 \end{aligned} \tag{7.5}$$

Eq. (7.5) is called the *characteristic equation of IIS* system and gives two sets of conjugate poles. In simplified and symbolic form, they can be rewritten as:

$$\left(s^2-\lambda_{1,D}\right)\cdot\left(s^2-\lambda_{2,D}\right)=0 \tag{7.6}$$

where $\lambda_{i,D}$ denotes i-th eigenvalue of $\boldsymbol{A}$ matrix.

Thus, through the PAM we can move the poles relative to eigenvalues $\lambda_{1,D}$ and $\lambda_{2,D}$ independently, i.e. we can define a system having two new eigenvalues, $\lambda_{1,M}$ and $\lambda_{2,M}$ (Figure 7.1).

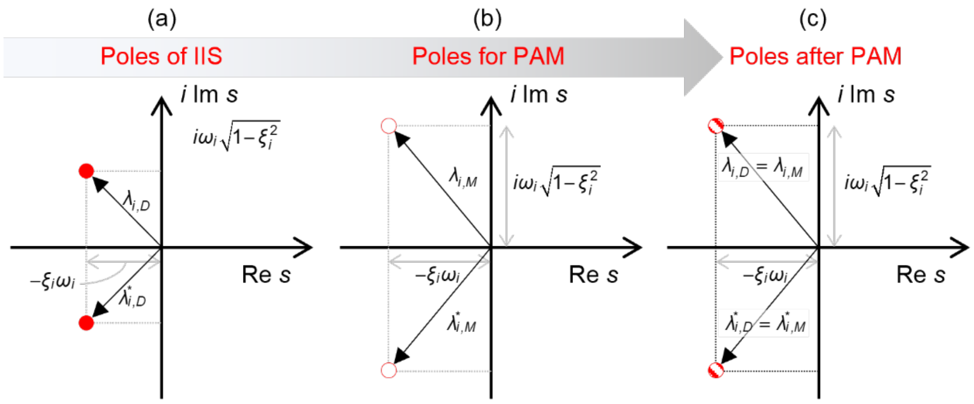

Figure 7.1. Poles in *s*-plane: (a) of IIS; (b) for PAM; (c) after PAM

The target equation will have the same form as Eq. (7.6) but the eigenvalues $\lambda_{1,D}$ and $\lambda_{2,D}$ are replaced by the eigenvalues $\lambda_{1,M}$ and $\lambda_{2,M}$ respectively:

$$\left(s^2-\lambda_{1,M}\right)\cdot\left(s^2-\lambda_{2,M}\right)=0 \tag{7.7}$$

Notably, in the first parenthesis of Eq (7.7) there is the eigenvalue associated with the first vibration mode of system, so the whole parenthesis can be considered as the characteristic equation of an SDOF system representative of the first vibration mode only. Therefore, the characteristic equation of this system, as reported in [99], is equal to the following expression:

$$s^2+s2\xi_1\omega_1+\omega_1^2=0 \tag{7.8}$$

In Eq. (7.8), ξ_1 and ω_1 denote the first-mode damping ratio and the first-mode circular natural frequency, respectively. The same consideration just made for the first vibration mode can be made for the second vibration mode, hence, Eq. (7.7) becomes:

$$\left(s^2+s2\xi_1\omega_1+\omega_1^2\right)\cdot\left(s^2+s2\xi_2\omega_2+\omega_2^2\right) \tag{7.9}$$

where ξ_2 and ω_2 are the second-mode damping ratio and the second-mode natural circular frequency, respectively.

Therefore, the two eigenvalues, $\lambda_{1,D}$ and $\lambda_{2,D}$, are a function of the IIS design parameters (i.e., ω_{LS}, ω_{ISO}, ξ_{LS}, ξ_{ISO} and μ), whereas the two eigenvalues, $\lambda_{1,M}$ and $\lambda_{2,M}$, are a function of the IIS modal properties (i.e., ω_1, ω_2, ξ_1 and ξ_2).

Eq. (7.9) is called the *target characteristic equation* (or *characteristic equation for Pole Allocation*), and in order to facilitate its comparison with the *characteristic equation of IIS* (Eq. (7.5)) it is rewritten below in extended form:

$$\begin{aligned} & s^4 + 2\left(\xi_1\omega_1 + \xi_2\omega_2\right)s^3 + \left(\omega_1^2 + 4\xi_1\xi_2\omega_1\omega_2 + \omega_2^2\right)s^2 \\ & +2\left(\xi_2\omega_1^2\omega_2 + \xi_1\omega_1\omega_2^2\right)s + \omega_1^2\omega_2^2 = 0 \end{aligned} \tag{7.10}$$

In order to apply the pole allocation method, we consider the poles of Eq. (7.5) in the complex eigenvalues plane should coincide with the poles of Eq. (7.10) (Figure 7.1c); under practical circumstances, this result is obtained by matching Eq. (7.5) and Eq. (7.10), which yields the following parameter relationships:

$$\xi_{ISO}\omega_{ISO} + \mu\xi_{ISO}\omega_{ISO} + \xi_{LS}\omega_{LS} = \omega_1\xi_1 + \omega_2\xi_2 \tag{7.11}$$

$$\omega_{ISO}^2 + \mu\omega_{ISO}^2 + \omega_{LS}^2 + 4\xi_{ISO}\xi_{LS}\omega_{ISO}\omega_{LS} = \omega_1^2 + 4\,\xi_1\xi_2\omega_1\omega_2 + \omega_2^2 \tag{7.12}$$

$$\xi_{ISO}\omega_{ISO}\omega_{LS}^2 + \xi_{LS}\omega_{LS}\omega_{ISO}^2 = \xi_2\omega_1^2\omega_2 + \xi_1\omega_1\omega_2^2 \tag{7.13}$$

$$\omega_{ISO}^2\omega_{LS}^2 = \omega_1^2\omega_2^2 \tag{7.14}$$

Dividing Eq. (7.13) by Eq. (7.14) yields the following trade-off relationship:

$$\frac{\xi_{ISO}}{\omega_{ISO}} + \frac{\xi_{LS}}{\omega_{LS}} = \frac{\xi_1}{\omega_1} + \frac{\xi_2}{\omega_2} \tag{7.15}$$

The same important trade-off relationship has been derived in [70] for a 3DOF IIS and with greater generality in [71] for a multi-lumped-mass stick-shape shear system.

From Eq. (7.15), it is possible to derive the value of ξ_2:

$$\xi_2 = \left(\frac{\xi_{ISO}}{\omega_{ISO}} + \frac{\xi_{LS}}{\omega_{LS}} - \frac{\xi_1}{\omega_1}\right)\omega_2 \tag{7.16}$$

Substituting Eq. (7.16) into Eq. (7.11), the value of ξ_1 is derived:

$$\xi_{ISO}\omega_{ISO} + \mu\xi_{ISO}\omega_{ISO} + \xi_{LS}\omega_{LS} = \omega_1\xi_1 + \omega_2^2\frac{\xi_{ISO}}{\omega_{ISO}} + \omega_2^2\frac{\xi_{LS}}{\omega_{LS}} - \omega_2^2\frac{\xi_1}{\omega_1} \tag{7.17}$$

$$\xi_1 = \frac{-(1+\mu)\xi_{ISO}\omega_{ISO} - \xi_{LS}\omega_{LS} + \omega_2^2\left(\frac{\xi_{ISO}}{\omega_{ISO}} + \frac{\xi_{LS}}{\omega_{LS}}\right)}{-\omega_1 + \frac{\omega_2^2}{\omega_1}} \tag{7.18}$$

From Eq. (7.18), it is possible to observe the dependence of ξ_1 upon seven parameters: ω_{ISO}, ω_{LS}, ξ_{ISO}, ξ_{LS}, ω_1, ω_2 and μ. However, considering that the values of natural circular frequencies for the two vibration modes are, even for large damping values, close to the natural circular frequencies of the undamped system, $\omega_{1,und}$ and $\omega_{2,und}$ for the first and second mode, respectively, it is possible to assume $\omega_1 \approx \omega_{1,und}$ and $\omega_2 \approx \omega_{2,und}$.

The values of the circular natural frequencies for the undamped 2DOF system are derived by solving the well-known eigenvalue problem given below:

$$\left(\boldsymbol{K} - \omega_{und}^2\boldsymbol{M}\right)\cdot\boldsymbol{\psi} = 0 \tag{7.19}$$

The matrices $\boldsymbol{M}$ and $\boldsymbol{K}$ shown in Eq. (7.19) are the mass and stiffness matrices of the undamped 2DOF system, respectively; and are equal to the corresponding mass and stiffness matrices for the damped 2DOF system reported in Eq. (2.11).

Then, from Eq. (7.19) it is possible to derive the characteristic equation for the undamped 2DOF system:

$$\begin{vmatrix} k_{ISO} + k_{LS} - m_{LS}\omega_{und}^2 & -k_{ISO} \\ -k_{ISO} & k_{ISO} - M_{ISO}\omega_{und}^2 \end{vmatrix} = 0 \tag{7.20}$$

Considering Eqs. (7.4), (7.8) and (7.11) it is possible to write Eq. (7.20) as follows:

$$\begin{vmatrix} \omega_{LS}^2 + \mu\omega_{ISO}^2 - \omega_{und}^2 & -\mu\omega_{ISO}^2 \\ -\mu\omega_{ISO}^2 & \mu\omega_{ISO}^2 - \mu\omega_{und}^2 \end{vmatrix} = 0 \tag{7.21}$$

Finally, it is possible to express Eq. (7.21) in polynomial form:

$$\left(\omega_{und}^2\right)^2 - \left(\mu\,\omega_{ISO}^2 + \omega_{LS}^2 + \omega_{ISO}^2\right)\omega_{und}^2 + \omega_{LS}^2\omega_{ISO}^2 = 0 \tag{7.22}$$

From Eq. (7.22), the closed-form relationships for $\omega_{1,und}$ and $\omega_{2,und}$ are easily derived for an undamped 2DOF system and are shown below:

$$\omega_{1,und} = \frac{\sqrt{2}\sqrt{d_1 - \sqrt{d_1^2 - 4\omega_{LS}{}^2\omega_{ISO}{}^2}}}{2} \tag{7.23}$$

$$\omega_{2,und} = \frac{\sqrt{2}\sqrt{d_1 + \sqrt{d_1^2 - 4\omega_{LS}{}^2\omega_{ISO}{}^2}}}{2} \tag{7.24}$$

$$d_1 = \mu\omega_{ISO}{}^2 + \omega_{LS}{}^2 + \omega_{ISO}{}^2 \tag{7.25}$$

Therefore, ξ_1 can be estimated as a function of five parameters, ω_{ISO}, ω_{LS}, ξ_{ISO}, ξ_{LS} and μ; but considering that the parameters of the lower structure and the mass ratio, ω_{LS}, ξ_{LS} and μ, are generally known in practical design, it is possible to reduce the number of design parameters to two, ω_{ISO} and ξ_{ISO}.

In the same way as the value of ξ_1, the value of ξ_2 can be derived:

$$\xi_2 = \frac{-(1+\mu)\xi_{ISO}\omega_{ISO} - \xi_{LS}\omega_{LS} + \omega_1^2\left(\frac{\xi_{ISO}}{\omega_{ISO}} + \frac{\xi_{LS}}{\omega_{LS}}\right)}{-\omega_2 + \frac{\omega_1^2}{\omega_2}} \tag{7.26}$$

7.2 Closed-form of IIS design spectrum

A design procedure for the vertical extension of existing buildings through intermediate isolation system is defined and applied in the previous chapter and in several papers [22, 126, 136 – 138]. The key tool of the procedure is the so-called "*IIS design spectrum*" (Figure 5.1).

In Figure 5.1 is shown the typical trend of the *IIS design spectrum*. The plot provides the results of Response Spectrum Analysis (RSA) in terms of displacement at the top of the lower structure (u_{LS}) in the IIS configuration varying the period of the isolation system (T_{ISO} = $2\pi/\omega_{ISO}$). In addition, in Figure 6.3 is depicted the typical trend of ISO design spectra, where the RSA results are plotted in terms of ISO displacement (δ_{ISO}) as the isolation period varies.

In particular, the *IIS* and *ISO design spectrum* can be derived by means of a linear response spectrum analysis (RSA) on the 3DOF model in Figure 2.1a or on the 3DOF model in Figure 2.1c, considering as a modal superposition method the classical CQC suggested by several standards [50, 94], or by adopting a modified CQC [83] as reported in the previous chapter and papers [22, 126, 136 – 138].

In this chapter, in order to derive the closed-form solution of the *IIS design spectra*, an RSA has been conducted on the 2DOF IIS model (Figure 2.1c). In the analysis, the modal amplitude at first DOF ($\psi_{i,LS}$) and participant mass factor (γ_i) values at *i*-th mode of the undamped system have been taken into account, as they are approximately equal to the corresponding values of the damped system.

The values of $\psi_{i,LS}$ and γ_i for the undamped 2DOF system, evaluated considering the modal amplitude at the second mass (ψ_{ISO}) equal to 1, are given as follows:

$$\psi_{i,LS} = -\frac{\omega_i^2 - \omega_{\mathrm{ISO}}^2}{\omega_{\mathrm{ISO}}^2} \tag{7.27}$$

$$\gamma_i = \frac{\mu\omega_{ISO}^4 + \omega_{ISO}^4 - \omega_i^2\omega_{ISO}^2}{\mu\omega_{ISO}^4 + \omega_i^4 + \omega_{ISO}^4 - 2\omega_i^2\omega_{ISO}^2} \tag{7.28}$$

In order to calculate the displacement of the first mass (u_{LS}) through CQC modal superposition method, it is necessary to introduce the spectral acceleration, $S_{a,i}$ (ω_i, ξ_i), and the corresponding spectral displacement, $S_{d,i}$ (ω_i, ξ_i). These two terms are a function of the natural circular frequency and the damping ratio of the *i*-th vibration mode.

$$S_{d,i,LS}\left(\omega_i,\xi_i\right) = \gamma_i\psi_{i,LS}\frac{S_{a,i}\left(\omega_i,\xi_i\right)}{\omega_i^2} \tag{7.29}$$

$$u_{LS} = \sqrt{\sum_{j=1}^{2}\sum_{i=1}^{2}\rho_{ij}S_{d,i,LS}S_{d,j,LS}} \tag{7.30}$$

where:

$$\rho_{ij} = \frac{8\sqrt{\xi_i\xi_j}\left(\beta_{ij}\xi_i + \xi_j\right)\beta_{ij}^{3/2}}{\left(1-\beta_{ij}^2\right)^2 + 4\xi_i\xi_j\beta_{ij}\left(1+\beta_{ij}^2\right) + 4\left(\xi_i^2+\xi_j^2\right)\beta_{ij}^2} \tag{7.31}$$

$$\beta_{ij} = \frac{\omega_i}{\omega_j} \tag{7.32}$$

From Eq. (7.30), it is possible to derive the *IIS design spectra* in terms of displacement, since ω_{LS}, ξ_{LS} and μ values are usually known in design applications. Moreover, if the isolation devices to be adopted are chosen, the value of the damping ratio for the isolation system is also fixed, and Eq. (7.30) becomes a function of ω_{ISO} only. Indeed, from Eq. (7.18) and Eq (7.26) it is possible to identify the damping value to be assigned to the isolation system in order to derive a target value for ξ_1 and ξ_2, respectively.

7.3 Closed-form of ISO design spectrum

As introduced in the previous subsection, similarly to the *IIS design spectrum*, it is possible to derive the *isolator displacement spectrum* (or *ISO design spectrum*) (Figure 6.3a), which provides the relative displacement between the masses of the 2DOF IIS (δ_{ISO}) (Figure 6.3a), representative of the isolator displacement demand. Indeed, considering that ψ_{ISO} = 1, it can be derived:

$$S_{d,i,ISO}\left(\omega_i,\xi_i\right) = \gamma_i\psi_{ISO}\frac{S_{a,i}\left(\omega_i,\xi_i\right)}{\omega_i{}^2} \tag{7.33}$$

$$u_{ISO} = \sqrt{\sum_{j=1}^{2}\sum_{i=1}^{2}\rho_{ij}S_{d,i,ISO}S_{d,j,ISO}} \tag{7.34}$$

$$\delta_{ISO} = u_{ISO} - u_{LS} \tag{7.35}$$

It is possible to note that the ISO design spectra, derived from Eq. (7.35), takes into account both the mass damping effect and the deformability of the lower structure.

7.4 Comparison of predicted response with design spectra and results of LTHA

The design spectra identified in the previous section provide a response prediction of both the lower structure and the isolation system in IIS. Therefore, they are useful support for the designer, particularly in the initial design phase, when it is necessary to select the optimum design parameters for the IIS.

In order to verify the accuracy of the 2DOF IIS model predicted response obtained through the close-form relationship for design spectra a case study is selected. For this case study, the following have been compared: the design spectrum by proposed closed-form (referred to as *closed-form RSA*) vs. the design spectrum by the complex RSA and modified CQC [83], i.e., as derived in the previous chapters (referred to as *complex RSA*) vs. the design spectrum by classical CQC for undamped system and fixed value of spectral damping, i.e., $\xi = 0.05$ (referred to as *classical RSA*) vs. the results of LTHAs.

For the selected case study, the values of the design parameters are as follows:

$T_{LS} = 0.39$ s

$\xi_{LS} = 0.05$

$\xi_{ISO} = 0.15$

$\mu = 0.38$

In particular, the LTHAs have been carried out on a 2DOF IIS model, with natural circular frequency equal to ω_{ISO} and damping ratio (ξ_{ISO}) equal to 15% adopted for the isolation system.

For the analyses, seven ground motion records have been selected from SIMBAD database [121] by means of the software REXEL v 3.5 [120] (Figure 7.2a, Table 7.1), the records are such that their average acceleration spectrum matches the target spectrum with tolerance +30% and -10% in the periods range 0.15 - 2 s. The target spectrum is the elastic acceleration response spectrum defined by the Italian seismic design code [94] for the site with peak ground acceleration equal to 1.62 m/s^2 and C soil class at the Design Basis

Earthquake (DBE) level, characterised by 10% probability of exceedance in 50 years (return period of 475 years) and 5% of damping ratio value. The Italian seismic design code [94] It states that: *"Spectra defined in this way can be used for structures with a fundamental period less than or equal to 4.0 s. For structures with higher fundamental periods, the spectrum must be defined by appropriate analyses or the seismic action must be described by means of time histories of ground motion.";* therefore, it provides indications for the construction of acceleration spectra up to T = 4 s. As a consequence, the same relationship between S_a and T valid for periods $T > T_D$ was chosen in the previous chapters, implying a constant spectral displacement value for $T > T_D$ up to 5s.

However, in this chapter, a constant value of the spectral acceleration has been assumed in the period range, 4 - 5 s, equal to the spectral acceleration at T = 4 s. This decision derives from the observation made on the *ISO design spectrum* in the previous chapter. In fact, if the spectral displacement value is constant for $T > T_D$, a high difference with the average spectrum is obtained; whereas, as can be seen in Figure 7.2b, by adopting this type of target spectrum, the distance between the average spectrum and the target spectrum is reduced.

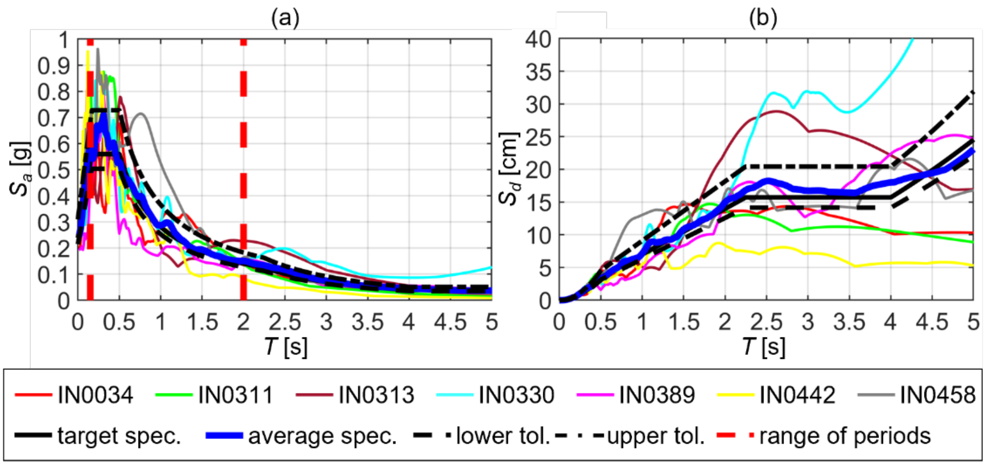

Figure 7.2. Set of seven response spectra in terms of: (a) acceleration; (b) displacement.

Table 7.1. Major data of seven spectrum-compatible acceleration records.

Earthquake name	EN1	EN2	EN3	EN4	EN5	EN2	EN6
Date	25/07/ 2003	29/05/ 2012	13/06/ 2011	15/10/ 1979	03/09/ 2010	20/05/ 2012	17/01/ 1994
W. ID	34	313	389	442	330	311	458
E. ID	15	133	149	89	137	132	99
S. ID	MYG01 0	SAN0	RHSC	AEP	DSLC	MRN	ST_240 87
F. M.	reverse	reverse	reverse	strike-slip	strike-slip	reverse	reverse
Epi. Dist. [km]	9.93	4.73	14.76	2.31	13.31	13.36	11.02
PGA [g]	0.20	0.22	0.19	0.26	0.24	0.26	0.34
EC8 S.C.	C	C*	C*	C	C*	C	C
$v_{s,30}$ [m/s]	279	n.a.	n.a.	274.5	n.a.	208	298

***Note**: site class with * is based on geological information alone.*
Key: EN1 = N Miyagi Prefecture; EN2 = EMILIA_Pianura_Padana; EN3 = Christchurch; EN4 = Imperial Valley; EN5 = Darfield; EN6 = Northridge; W. ID = Waveform ID; E. ID = Earthquake ID; S. ID = Station ID; F. M = Fault Mechanism; Epi. Dist = Epicentral Distance; S.C. = Site Class; n.a. = not available.

Figure 7.3 shows the comparison among: results of RSAs with classical CQC modal superposition method, obtained by Eq. (7.30) (dashed grey line); results of RSAs with modified CQC modal superposition method, obtained considering as input both the target spectrum (black line) and the average spectrum (blue line); results of classical RSAs for undamped system with 5% of spectral damping (brown line); and results of the LTHAs (orange circular marker). From the comparison, it can be seen that the *IIS design spectra* obtained with the closed-form relationship and the modified CQC modal superposition rules are identical, since with the application of the pole allocation method considers the full damping matrix and the isolation damping isn't very high.

Furthermore, considering the lower and upper bounds for the compatibility of the average spectrum with the target spectrum (dashed and dotdash black lines, respectively) or the same average spectrum (blue line) as input of the RSAs, the response prediction provided by the *IIS design spectrum* is quite good. In addition, the response spectrum analysis indicated with classical RSA shows a high difference with the remaining RSA curves in the short-to-medium period zone, whereas it matches the complex RSA curve by target spectrum for long period values.

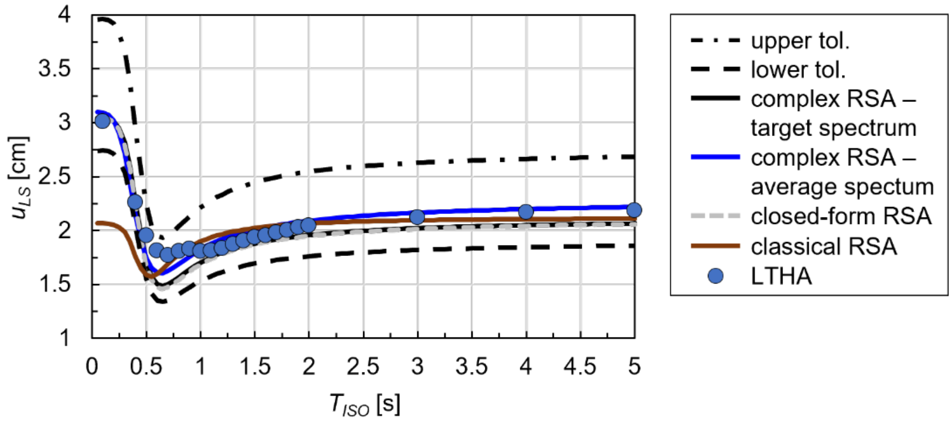

Figure 7.3. *IIS Design spectra* vs LTHA.

Figure 7.4 shows the comparison among the different *isolation displacement spectra* and the LTHAs results. Also in this case, the spectrum obtained with closed-form coincides with the spectrum obtained with complex CQC by target spectrum. The LTHAs results are close to the upper limit (target spectrum increased by 30%) for all structural configurations except for the case of T_{ISO} = 4 s, where a larger scatter is observed between the LTHA result and the upper limit. The RSA analysis with the average spectrum still provides a good estimate of the IIS structural response. The classical RSA is in agreement with the complex RSA by target spectrum for medium-long isolation periods.

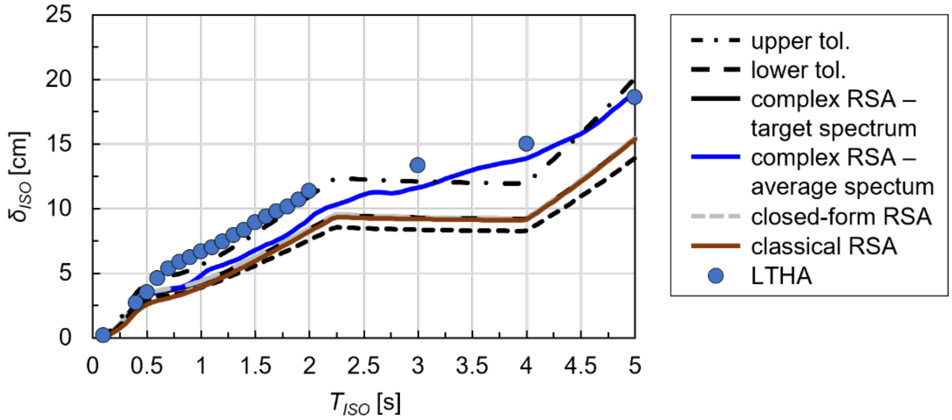

Figure 7.4. *Isolator displacement spectra* vs LTHA.

7.5 Comparison of RSA curves with classical CQC and modified CQC

The aim of the proposed procedure is to provide a simple tool for users to explore IIS design solution with small computational burden and time effort for deriving *IIS* and *ISO design spectrum*. Hence, although the IIS is characterised by non-proportional damping (see Appendix B), the classical CQC modal superposition method is utilised to derive the response u_{LS} and δ_{ISO} rather than the complex analysis, as done in the previous chapters. Nevertheless, for sake of completeness, the comparison between the IIS design spectrum obtained with the proposed closed-form relationship and with the complex analysis is provided in Figure 7.5 by adopting the following values of the design parameters: μ = 0.38, ξ_{LS} = 0.05, T_{LS} = 0.39, ξ_{ISO} = [0.15, 0.20, 0.25, 0.30, 0.35, 0.40, 0.45, 0.50]s.

As the value of ISO system damping ratio increases, from the Figure 7.5 it can be seen that the distance between the two RSA curves becomes greater in the mass-damping zone. The latter result was predictable since in the mass damping zone the period value at the first and second modes are close to each other and as reported in [83, 139] the modal coupling effect (see Eq. (B.2) in Appendix B) is maximum and consequently the analysis to be performed must take into account the whole damping matrix and the interaction effect between modes through the modified modal superposition rule.

In particular, if we compare the correlation coefficients proposed by the classical CQC (Eq. (7.31)) and the modified CQC provided by Eq. (B.8) in Appendix B and which is given below for brevity:

$$\rho_{ij,mod} = \rho_{ij} \cdot ce_{ij}$$
$$= \left[\frac{8\sqrt{\xi_i \xi_j}\left(\beta_{ij}\xi_i + \xi_j\right)\beta_{ij}^{3/2}}{\left(1-\beta_{ij}^2\right)^2 + 4\xi_i\xi_j\beta_{ij}\left(1+\beta_{ij}^2\right) + 4\left(\xi_i^2+\xi_j^2\right)\beta_{ij}^2} \right] \cdot \left[\frac{a_i a_j + \omega_i \omega_j c_i c_j}{B_i B_j} \right] \quad (7.36)$$

The only difference is the term ce_{ij} that takes into account the phase difference between the modal response coefficients and thus considers the correlation effect of the phase.

Therefore, in the closed-form relationship, the ce_{ij} term was assumed null, neglecting the correlation effect of the modes on the structural response. This approximation, as observed in Figure 7.5, leads to a prediction error in the IIS response that can be significant for high ξ_{ISO} values. However, in order to identify the error committed with classical CQC when the ISO damping ratio and mass ratio vary, i.e. what is the domain of the proposed closed-form relationship, Figure 7.6 shows the percentage change between the minimum points of the RSA curves with classical and modified CQC when the ISO damping ratio varies.

In addition, four different mass ratios have been considered, i.e. μ = [0.1, 0.38, 1, 2], where it can be observed that with the exception of the smallest mass ratio, μ = 0.1, the percentage change is approximately the same for the other mass ratios, i.e. μ = [0.38, 1, 2], when ξ_{ISO} is less than 0.35. Moreover, in the latter case, the percentage change is less than 12/13%. Therefore, we can conclude that the proposed closed-form relationship can be used up to values of ξ_{ISO} = 0.35, where the error in the prediction of the structural response is still small.

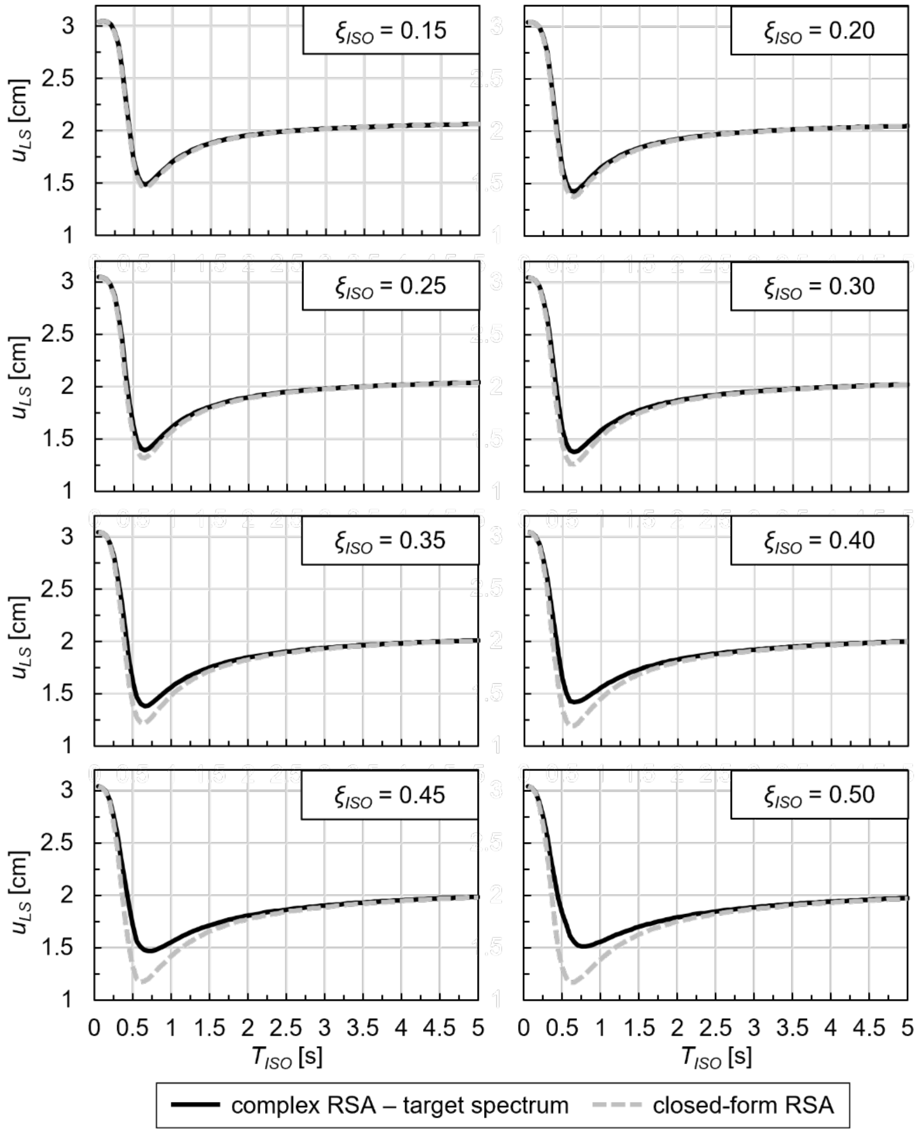

Figure 7.5. RSA curves obtained through complex analysis vs closed-form relationships for ξ_{ISO} = [0.15, 0.20, 0.25, 0.30, 0.35, 0.40, 0.45, 0.50].

From Figure 7.6 it can be seen that, the two RSA curves are almost overlapped for values of ξ_{ISO} smaller then 0.4; instead for greater values of ξ_{ISO} the gap between these curves increase and it is focused only in the mass damping zone. In this case the results provided with the proposed closed-form relationship are not on the safe side. However, the IIS application proposed in this thesis are characterized by ISO system composed of HDBR isolators, for which the damping ratio ξ_{ISO} is much smaller than 0.4 (say, 0.1 - 0.15).

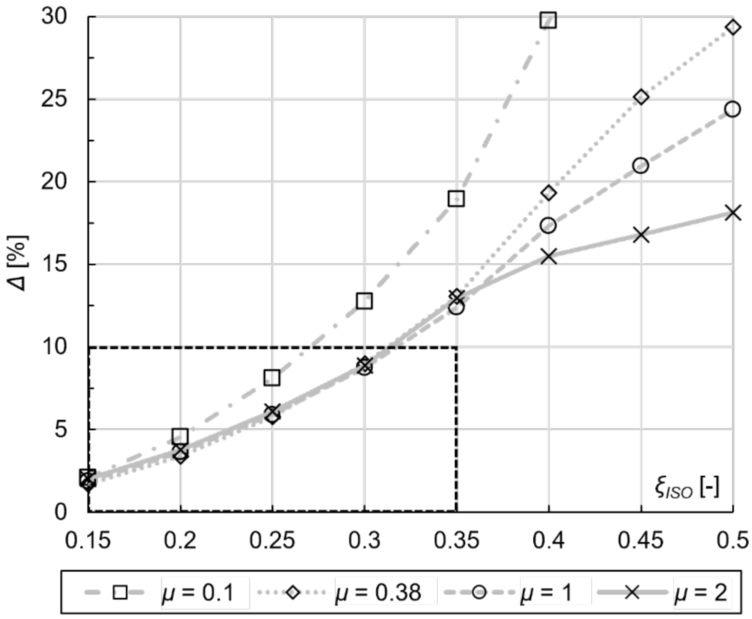

Figure 7.6. percentage change (*Δ*) between minimum values of complex RSA vs. closed-form relationship.

it is possible to observe that this result is also in agreement with the results reported in [83], where with reference to an eleven-storey base isolated building it is suggested to evaluate the system response with the modified CQC when the first-mode damping ratio exceeds 25%. In fact, considering the 2DOF IIS model with ξ_{ISO} = 0.38, Figure 7.7 shows its *IIS design spectrum* and the corresponding trend of modal damping ratios and modal periods. In this Figure, it can be seen that the greatest differences between the RSA curve obtained with classical CQC and the modified CQC occur when the values of the periods (or frequencies) of the two modes are close to each other, i.e. for T_{ISO} = 0.5 - 1s, and the damping ratio at the first mode is around 25%. Furthermore, it is also noticeable that the modal damping and period values evaluated with the closed formulae introduced in the previous sections, Eqs. (7.18), (7.26) and Eqs. (7.23), (7.24) respectively, are equal to the corresponding values evaluated through the complex analysis suggested by [83, 109]. Consequently, the difference between the RSA curves shown in the figures is a function of the different modal superposition method utilised.

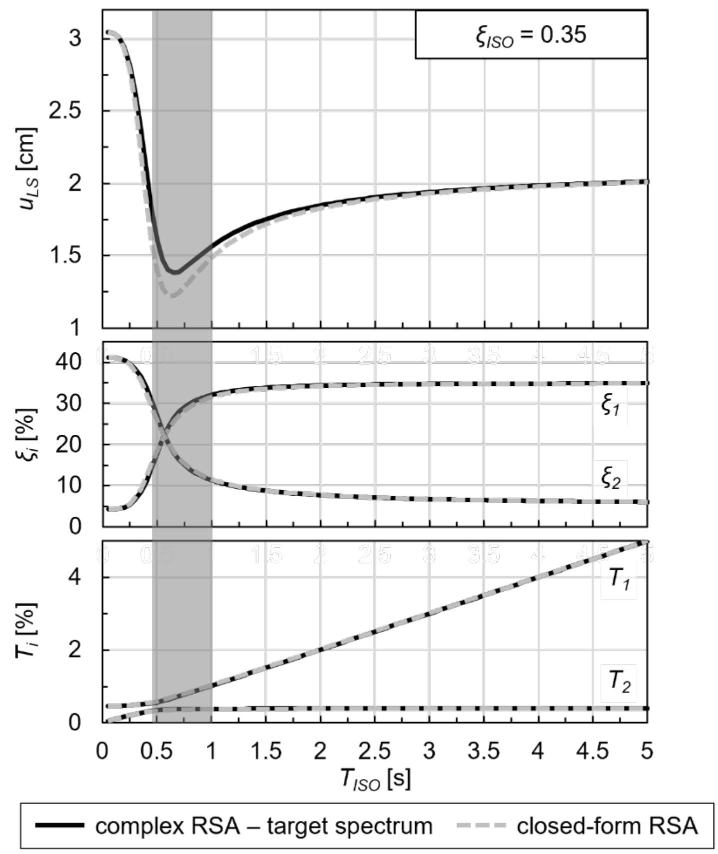

Figure 7.7. RSA curves and modal propriety of 2DOF IIS (μ = 0.38, ξ_{LS} = 0.05, T_{LS} = 0.39s, ξ_{ISO} = 0.38).

Chapter 8

IIS for existing irregular buildings

The retrofit of existing structures through Base Isolation System (BIS) has been suggested since the beginning of BIS history. It has been widely proposed for old reinforced concrete structures with poor seismic capacity [140], but also for monuments, historical churches and building cultural heritage [141, 142]. A noteworthy advantage of BIS is that, in addition to reducing the seismic demand on the existing structure up to levels comparable with poor capacities, a more regular behaviour can be obtained for structures characterised by stiffness distribution eccentric with respect to the masses [143]. Once introduced at the base of the building, indeed, the isolation system completely governs the dynamics of the isolated structure. Therefore, if the centre of the shear stiffnesses of the isolators matches the centroid of the floor masses of the building structure, then the behaviour of the system is regularized, being characterised by uncoupled modes, simple translation along each of the two orthogonal directions and rotation around the vertical axis. In the retrofit of existing structures through IIS, a vertical extension equipped with seismic isolation at its base is realised on the roof of the existing structure, thus working as a mass damper for the existing structure [13, 18]. IIS, therefore, appears as a promising strategy in cities' historic centres to expand and regenerate buildings for adaptive reuse. The approach has been widely discussed in general terms and considering some case studies [20, 21]; it has been observed that, in the case of existing buildings with stiffness eccentricity, a careful design of the isolated vertical addition can regularize the IIS response.

In this framework, a parametric study is here developed to better clarify the regularizing potentials of IIS deriving from the dynamic interaction between the two structural portions. Selected a case study building with eccentricity between mass and stiffness distributions, some IIS design configurations, with different isolation systems, are designed and analysed [144]. Analyses results and preliminary design implications are discussed.

8.1 Case study

The case study here considered is an Italian three-story masonry building of the 17th century (Figure 8.1a), still in use nowadays with office occupancy. The plan has a trapezoidal shape, with maximum dimensions along the two orthogonal directions X and Y of 26.4 m and 19.7 m. The inter-story height is 4.50 m. The wall thickness is between 80 and 65 cm. The building material is a mixed stones and bricks masonry with lime mortar; average weight is 20 kN/m^3, Young modulus is 2600 MPa, compression strength is 2.0 MPa; details can be found in [20]. The total mass of the building is 2900 t, concentrated at floor levels (m_1=1186 kNs^2/m, m_2=1030 kNs^2/m, m_3=684 kNs^2/m). The arrangement of masonry walls along X and Y, with different thickness and openings patterns, yields eccentricity between mass and stiffness centroids (Figure 8.1b), with non-dimensional eccentricities e_X/L_X=24%, e_Y/L_Y=16%.

The first six natural vibration modes obtained for the three-dimensional FEM building model (i.e. 3D FEM AS-IS), along with periods and mass participating ratios (namely U_x, U_y and R_z), are given in Figure 8.2. It can be clearly observed that, due to the eccentricity firstly detected, the first two modes couple translational motions in the two principal directions, resulting in a diagonal motion; the third mode is prevalently rotational, while the higher modes are purely translational or rotational modes. Globally, these natural modes provide a total participating mass equal to or greater than 85% along the directions X and Y and around the vertical axis Z.

Figure 8.1. Case study building: (a) front view; (b) plan of the ground floor.

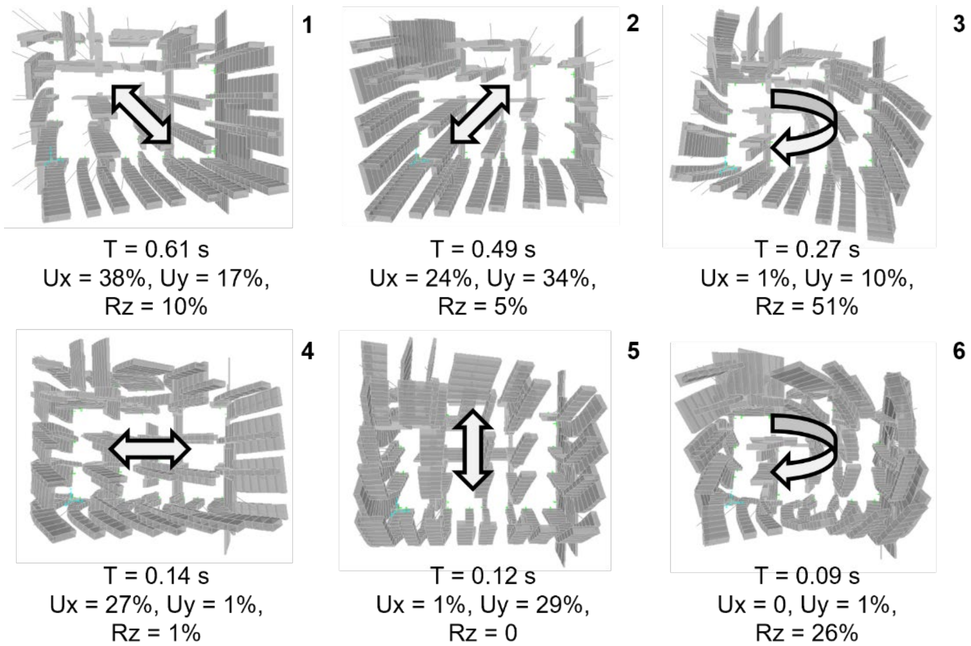

Figure 8.2. First six modes of vibration of the 3D AS-IS model.

8.2 IIS – parametric analysis

Vertical extension of the case study building is considered, with three added storeys realized in structural steelwork and equipped with seismic isolation system at the base, placed on the roof of the existing building. This IIS design configuration is made of a lower structure (LS), i.e the existing building, an upper structure (US), steel braced frame, and an isolation system (ISO) interposed between the two structures. To select the design value(s) of the dynamic properties of the extension, a preliminary parametric response spectrum analysis (RSA) is carried out varying the isolation period T_{ISO} (namely the *IIS design spectra*). Having set the number of new floors (i.e., three) and the structural solution for floor structure (composite), the value of mass ratio μ (see Eq. (2.23)) is set. Also, the lateral stiffness of the US is not varied.

The RSA is carried out on lumped mass model, 3DOF, representing the LS, ISO, US (Figure 8.3a), with acceleration response spectrum prescribed by Italian seismic design code [94] for the case study site assumed to be the same as the site of the case study introduced in chapter 3 (a_g = 0.162 g, F_0 = 2.347, T_C^* = 0.333 s, S = 1.47, ξ = 0.05, Figure 8.3b). SDOF model of the LS is also considered for comparison.

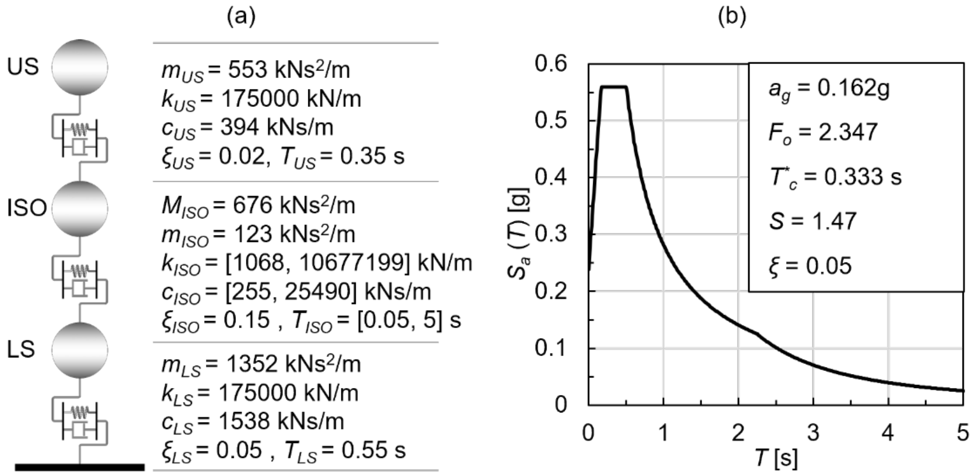

Figure 8.3. (a) 3DOF IIS model, (b) acceleration spectrum (10% probability of exceedance in 50 years).

The base shear in the 3DOF IIS model (i.e., $V_{b,3DOF\ IIS}$) is evaluated and normalized to the existing structure counterpart (i.e., $V_{b,SDOF\ LS}$); this base shear ratio, $\bar{v}$ = $V_{b,3DOF\ IIS}$ /$V_{b,SDOF\ LS}$, is plotted in Figure 8.4 varying T_{ISO} for a preliminary test of the effectiveness of the isolated vertical extension working as mass damper for the LS. In the chart, three points are identified and appointed as 1, 2, 3. The solution 1 corresponds to T_{ISO} = 0.84 s and the minimum $\bar{v}$ value, equal to 0.69, which means a base shear reduction of 29% thanks to the mass damping effect. The solution 3, instead, is characterized by quite long period, 4.7 s, and base shear ratio value that, clearly tending to 1 at increasing T_{ISO}, is here equal to 0.95; this behaviour is related to an almost perfect isolation, i.e., dynamic decoupling of the LS and US, testified by base shear of the structural complex tending to the LS value. The solution 2 is intermediate, with a certain mass damping effect.

The above observations are confirmed by the vibration characteristics of the three solutions (Figure 8.5). For IIS 1, the modal interaction typical of mass damping mechanisms can be observed: the first mode involves the isolated US but also the LS, as demonstrated by participation mass ratio Γ equal to 62%, larger than the ratio between the isolated mass and the total mass, $R_m = \mu / (1+\mu)$, that for $\mu = 0.5$ gives $R_m = 33\%$. For IIS 3, instead, almost no dynamic interaction can be observed between the US and LS: the first mode only involves the isolated upper structure, with no appreciable deformation in the LS and Γ very close to R_m. The behaviour of IIS 2, as already noticed, is intermediate between the two. In all solutions, IIS 1, IIS 2, IIS 3, the second mode involves the LS, while the third mode, corresponding to the second mode of the isolated US, always has null participation mass ratio.

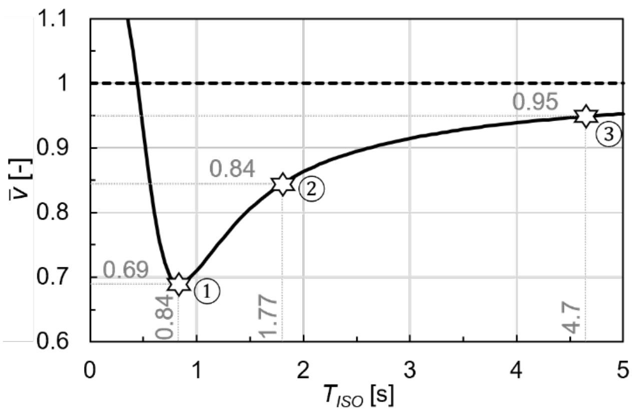

Figure 8.4. IIS design spectrum: IIS 1 (T_{ISO} = 0.84 s); IIS 2 (T_{ISO} = 1.77 s); IIS 3 (T_{ISO} = 4.70 s).

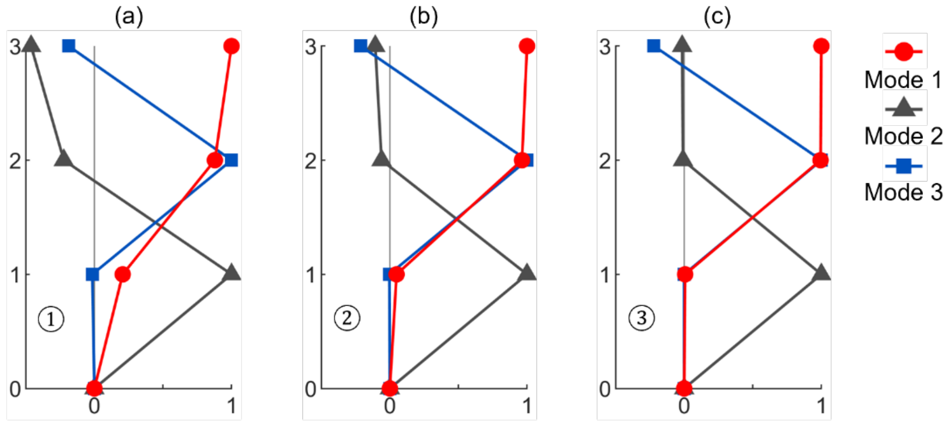

(a)	1	2	3
T [s]	1.01	0.49	0.14
Γ [%]	62	38	0
η [%]	9	10	17

(b)	1	2	3
T [s]	1.84	0.54	0.15
Γ [%]	40	60	0
η [%]	13	7	8

(c)	1	2	3
T [s]	4.72	0.55	0.15
Γ [%]	34	66	0
η [%]	15	6	7

Figure 8.5. Vibration modes of 3DOF models: (a) IIS 1 (T_{ISO} = 0.84 s); (b) IIS 2 (T_{ISO} = 1.77 s); (c) IIS 3 (T_{ISO} = 4.70 s).

8.3 Design configurations for US and ISO

Two design configurations for each solutions IIS 1, IIS2 and IIS3 are defined, which, for the same stiffness of isolation system (i.e., same isolation period), only differ for the single isolators' stiffnesses and the relevant centre position. In Figure 8.6, the schematic isolation plans of all design configurations are depicted. The left column corresponds to configurations with centre of isolator stiffnesses, $\mathbf{K}_{\mathbf{ISO}}$, coincident with the mass centres of both LS and US, **G**, i.e. $\mathbf{G} \equiv \mathbf{K}_{\mathbf{ISO}}$; this approach matches the BIS design strategy for regularizing the response of an irregular structure through isolators arrangement. Configurations with $\mathbf{G} \not\equiv \mathbf{K}_{\mathbf{ISO}}$, depicted in the right column, have also been considered. For both configuration types, 3D FEM models are created, and modal analyses are executed. The results are synthetically shown in Figure 8.7 and Figure 8.8 for the cases $\mathbf{G} \equiv \mathbf{K}_{\mathbf{ISO}}$ and $\mathbf{G} \not\equiv \mathbf{K}_{\mathbf{ISO}}$, respectively. The figures provide four rows: the second, third and fourth show the vibration characteristics of three triplets of modes, in terms of direction of translation modes (either diagonal, i.e. coupled modes; or orthogonal, i.e. uncoupled) and values of periods and participating masses. In each row, the first mode triplet corresponds to the US isolated at its base, appointed as US+ISO; the second and third triplets corresponds to the first and second triplets of modes of IIS. The first row gives vibration data of LS.

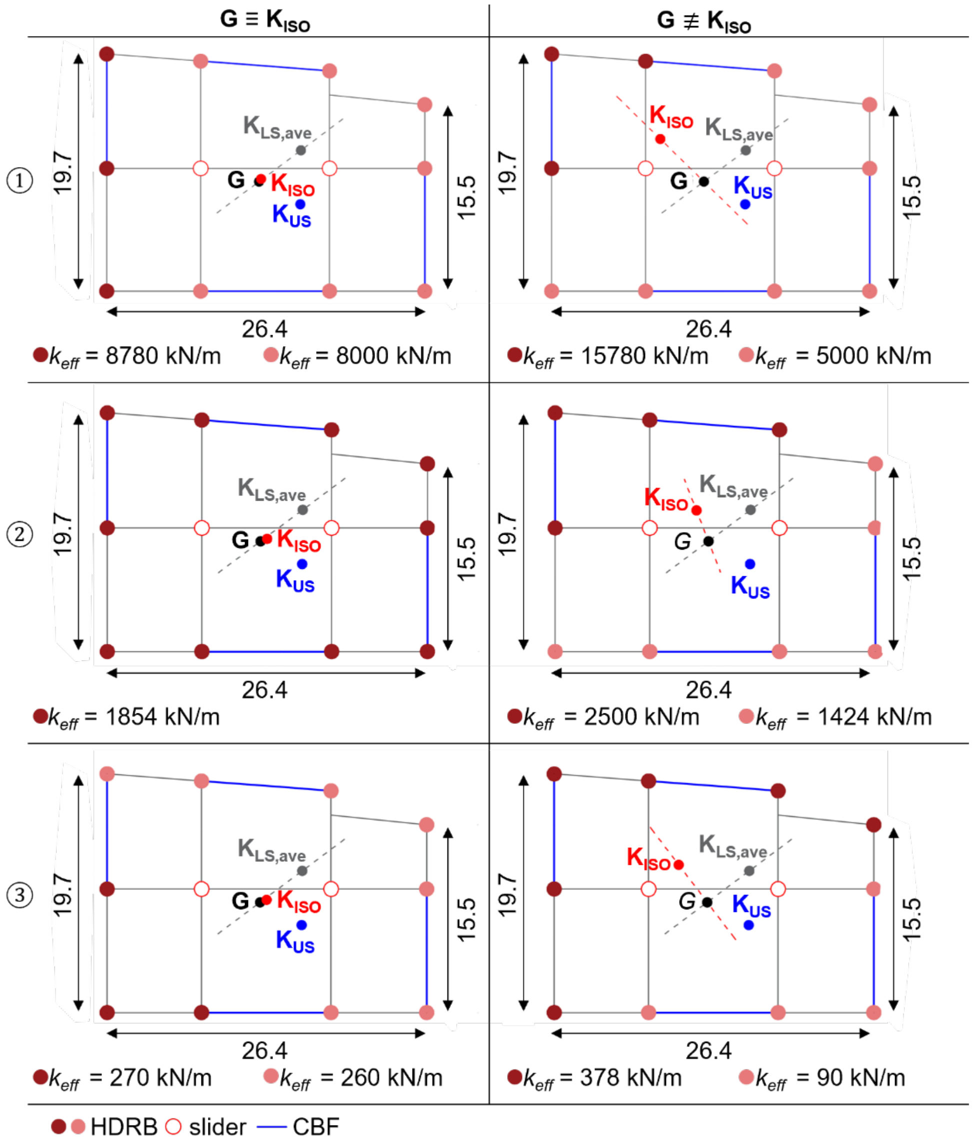

Figure 8.6. Mass and stiffness centroids of the three solutions ① - ③; left: design configurations with G ≡ K_{ISO}; right: design configurations with G ≢ K_{ISO}.
Key: $\mathbf{K_{LS,ave}}$ = average of stiffness centroids for LS floors.

It can be observed that, to have a whatever effect on the response of the LS, the isolation period should not be very long; in such case, indeed, the LS and US are completely decoupled from the dynamic point of view. Solutions IIS 3 for the second modes' triplet show the same values of periods and mass participating in the two cases of **G** ≡ **K**ISO and **G** ≢ **K**ISO; this mode triplet is the LS one and is identical to the LS one considered as standalone structure. The first triplet is the isolated US one, and in fact periods and masses are very close to the US+ISO counterparts.

The regularizing effect of the isolation system is maximum for the period corresponding to the maximum interaction, i.e., for solutions IIS 1, for which: in the case **G** ≡ **K**ISO, though the fundamental mode triplet shows diagonal modes, the modes of the second triplet, that affects the LS, are simple translations in the two orthogonal directions; for **G** ≢ **K**ISO, the modes of the first and second triplets, both involving the LS mass, are decoupled; in this case the midpoint of the line joining **K**ISO e **K**US, i.e. average position of US and ISO stiffness centres, matches the position of **G**.

In Figure 8.9 the percentage of LS mass participating to 1st and 4th modes ($U^{3D\ FEM\ IIS}_{1^{st}\ mode,LS}$, $U^{3D\ FEM\ IIS}_{4^{th}\ mode,LS}$) is given for 1, 2, 3, both cases **G** ≡ **K**ISO and **G** ≢ **K**ISO; the sum of percentage values, and the 1st mass of the LS as standalone (3D LS model), $U^{3D FEM\ LS}_{1^{st}\ mode,LS}$, are also given. The max $U^{3D\ FEM\ IIS}_{1^{st}\ mode,LS}$, and the min $U^{3D\ FEM\ IIS}_{4^{th}\ mode,LS}$, are obtained for IIS 1, in both configurations. On the contrary, min $U^{3D\ FEM\ IIS}_{1^{st}\ mode,LS}$, and max $U^{3D\ FEM\ IIS}_{4^{th}\ mode,LS}$, are obtained for IIS 3.

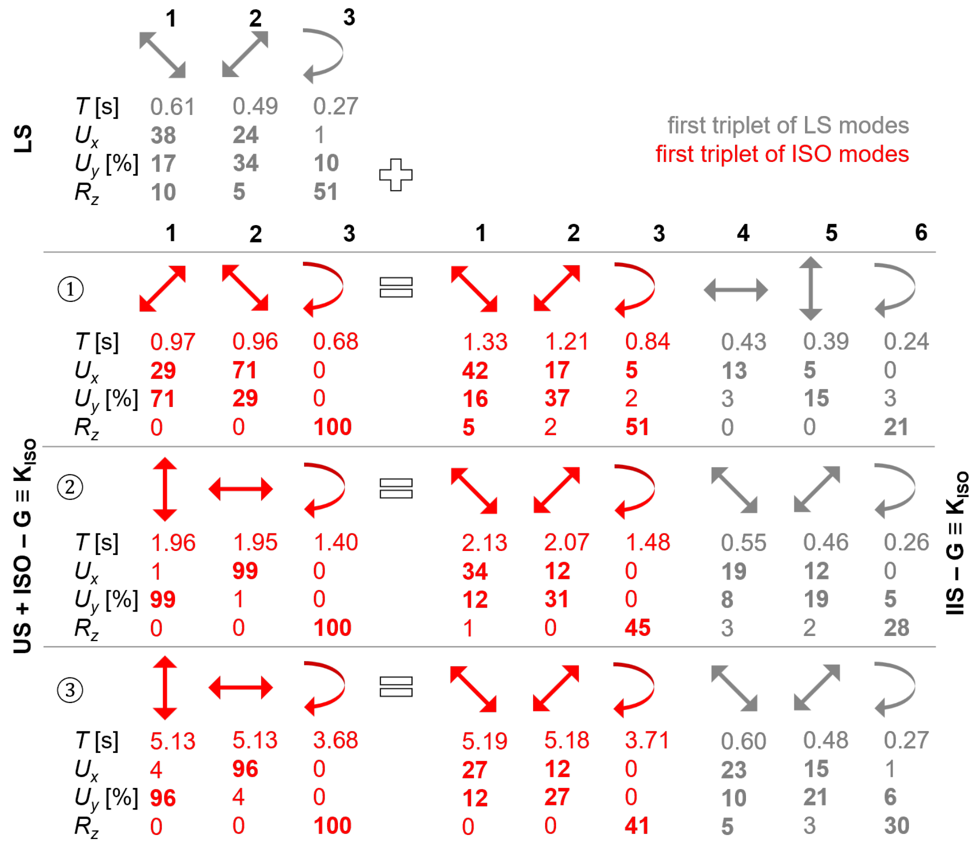

Figure 8.7. Vibration modes of 3D FE models: LS, US+ISO, IIS. Configurations with **G** ≡ **K**ISO.

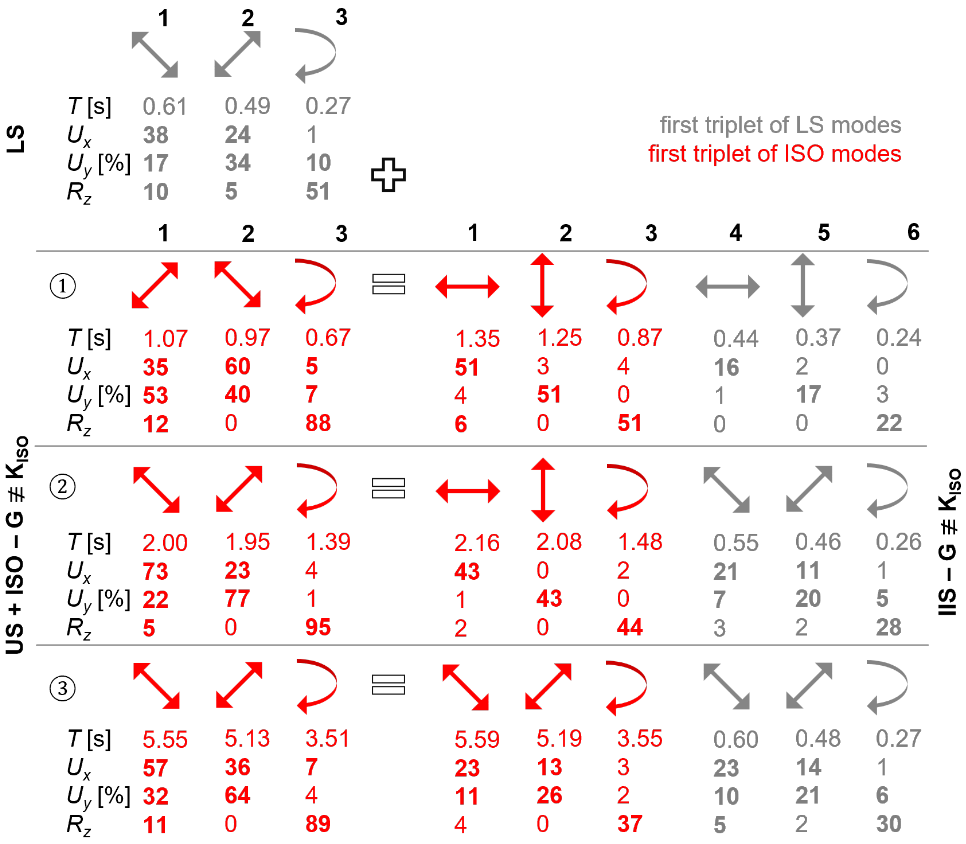

Figure 8.8. Vibration modes of 3D FE models: LS, US ISO, IIS. Configurations with $G \not\equiv K_{ISO}$.

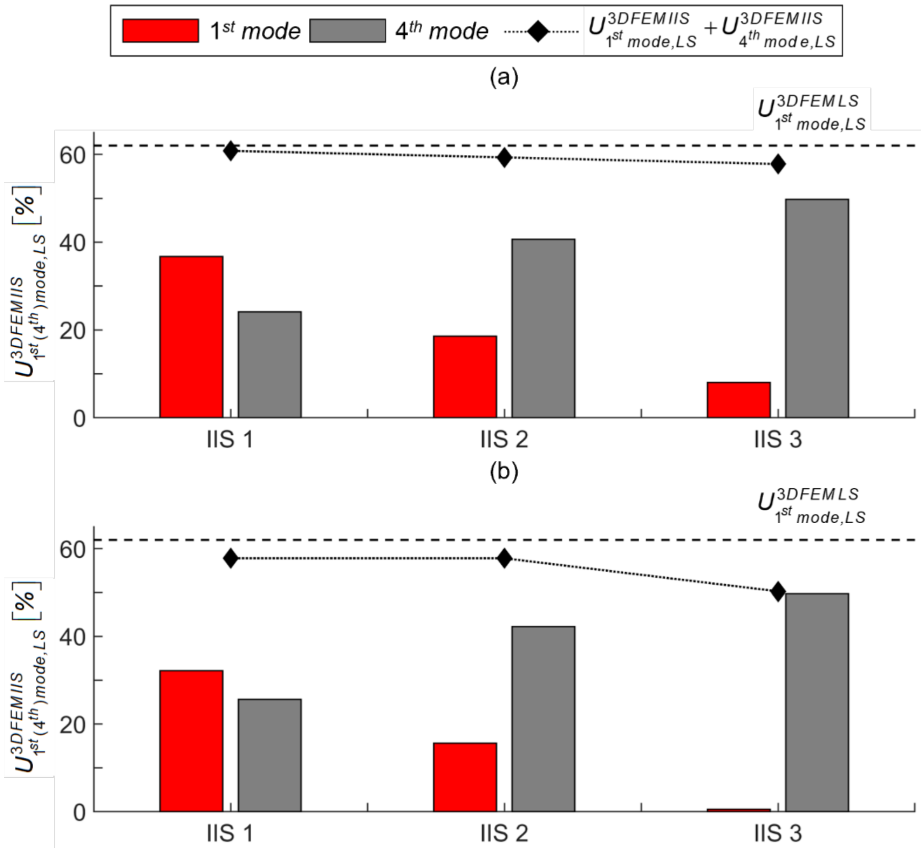

Figure 8.9. LS participating masses, 1st and 4th modes of IIS models ① - ③: (a) **G ≡ K**ISO, (b) **G ≢ K**ISO.

8.4 Time History analyses

Time History Analyses (THA) are carried out on the 3D FEM models of the various solutions, in the two design configurations, with a set of seven acceleration records, already selected in subsection 3.2.2.3, which match averagely the code design spectrum. In Figure 8.10 the peak story values of acceleration and displacement are provided. For the accelerations, the reduction in the LS is maximum for IIS1 and minimum for IIS3, while the opposite occurs for the US. The LS experience almost the same displacement in the three cases, while clearly emerges the difference in the isolation drifts. Interestingly, though obtained with different models, the THA results match the RSA predictions in terms of base shear ratio, with some slight scatters on the safe side, as shown in Figure 8.11.

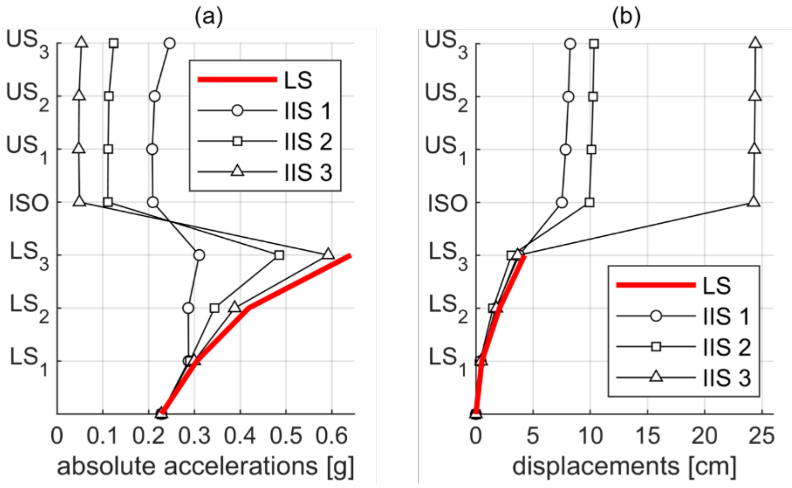

Figure 8.10. Peak values of: (a) accelerations, (b) displacements. IIS 1, 2, 3 – **G** ≢ $\mathbf{K}_{ISO}$.

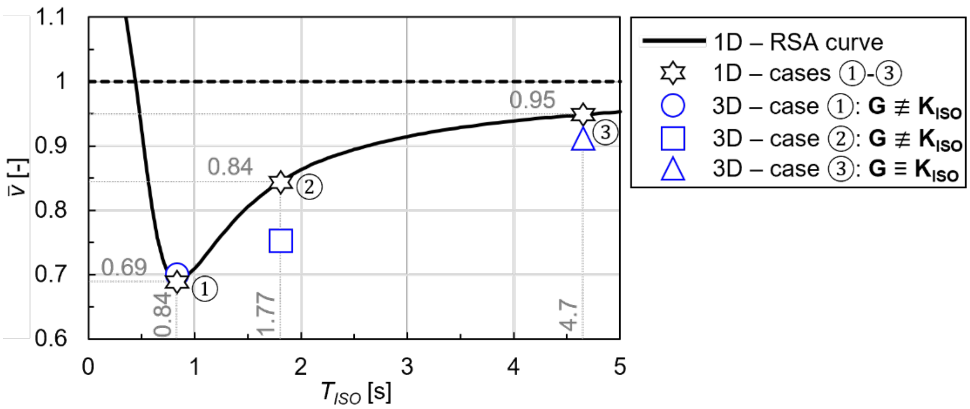

Figure 8.11. Base shear ratio: comparison between the results of the 3DOF and 3D IIS models.

Chapter 9

Conclusions

9.1 General remarks

This thesis is focused on investigating the interesting vibration control strategy based on the use of intermediate isolation system (IIS). This system is realised by means of an isolation (ISO) layer placed along the height of the building, dividing it into two distinct structural parts, i.e. a lower structure (LS) and an upper structure (US) located below and above the isolation layer, respectively.

The deformable layer placed between the two parts of the building (i.e. the ISO system) gives rise to a relative displacement between the LS and the US during the seismic shaking. This movement, if adequately controlled through the choice of mechanical properties of the ISO system, can lead the US to become a very large mass damper for the LS. Therefore, the IIS can be seen as an evolution of the well-known base isolation strategy (BIS), although it shows considerable differences with the BIS. In fact, in the case of the BIS the aim is the dynamic decoupling, as perfect and total as possible the motion of the building from the ground motion; on the contrary, in the case of IIS, the dynamic coupling between the motion of the isolated upper structure (ISO+US) and the LS ensures the arising of mass damping effect. It is worth observing that the IIS has the feature of exhibiting different dynamic behaviours according to the deformability of the ISO system (i.e. changing of T_{ISO}). Indeed, it is possible to identify two limit behaviours of the system: the first, for $T_{ISO} \rightarrow 0$, is representative of the conventional vertical extension behaviour and the second, for $T_{ISO} \rightarrow \infty$, is representative of the perfect (or ideal) isolation, with the motion of the ISO+US perfectly decoupled from the motion of the LS.

Due to these dynamic characteristics, IIS is widely known and employed in Japan for both the construction of new buildings and the seismic retrofitting of existing buildings. In the first case, the strategy of IIS is generally used for the construction of buildings above existing railway stations or lines, or for tall buildings with a strong variation in geometry along the height; whereas, in the second case, IIS is realised by first cutting the building into two parts at a certain level and then reconnecting the two parts through a ISO layer. Less popular is the practice of using IIS for vertical extension and retrofitting of existing buildings. In the latter case, however, IIS could be an attractive solution for several aspects, such as sustainability and easy execution, as the existing building is preserved and, by working outside the building, it is possible to avoid disruption to internal activities.

Obviously, the high interest for IIS buildings in Japan is supported by wide scientific research and by standards and design guidelines that facilitate designers in the realisation of this type of intervention. The general indication provided by the Japanese standards suggests to first define the values of the main IIS design parameters through a simple response prediction method and then develop nonlinear time history analyses (NTHAs). On the other hand, in European (and Italian) regulations, the IIS strategy is never mentioned, thus providing no indication regarding the design method for such systems. The absence of specific standard references as well as clear guidelines has led to a low use of IIS in Europe.

In this context, the aim of the thesis is to provide a clear and detailed framework for the design of IIS buildings, with focus on the use of IIS for the vertical extension and retrofitting of existing buildings. In order to achieve this goal, the dynamic behaviour of the IIS has been initially analysed by identifying the main design parameters of the system and their influence on the structural response. Next, a design procedure for the vertical extension and retrofitting of existing buildings by means of IIS divided into 5-Block has been proposed. The entire procedure is centred around an important preliminary design tool called the *IIS design spectrum*, which provides the prediction of the IIS response by means of linear response spectrum analyses, i.e. without using time-consuming and laborious time-history analyses in the preliminary design phase. The proposed procedure has the advantage of using the *IIS design spectra* to predict the IIS response also when the LS shows non-linear behaviour. This latter feature of the proposed design procedure is very important, because when intervening on existing buildings, their inelastic behaviour cannot be excluded *a priori*.

In order to demonstrate the feasibility and effectiveness of IIS for the retrofitting and vertical extension of an existing building, the proposed procedure has been applied to a real case study. The existing building chosen is a two-storey unreinforced tuff masonry building, a structural typology widely used in southern Italy. The system with intermediate ISO layer is completed by adding an isolated one-storey steel braced structure on the roof of the existing building. Analyses conducted on 3D FE models of the case study demonstrate both the effectiveness of the whole design procedure and the reduction, or at least a non-increase, of the seismic response of the existing building. Furthermore, it is shown how the main design parameters for this intervention type are the mass ratio and the isolation period, which can determine a greater or lesser reduction of the LS seismic response.

Subsequently, the influence of the non-linear behaviour of ISO and LS on the IIS structural response has been evaluated and the accuracy of the response prediction offered by the *IIS design spectra* has been tested by considering additional case studies. Specifically, the design procedure proposed in Block 2 includes a *stepwise sub-procedure* to identify the *IIS design spectra* when the LS has non-linear behaviour. This *stepwise procedure* is based on the possibility of identifying two IIS limit behaviours (i.e. for $T_{ISO} \rightarrow 0$, conventional vertical extension; and for $T_{ISO} \rightarrow \infty$, perfect isolation between LS and US) and on the empirical consideration that when an existing structure experiences inelastic phenomena and structural damage, it exhibits a response softening, quantified by reduction of the global stiffness and elongation of the fundamental period. At the end of the *stepwise procedure*, at most two RSA curves corresponding to the two elongated periods of the two IIS limit behaviours are identified. Consequently, the comparison between the RSA curve results and the non-linear TH analysis showed that the behaviour of the IIS system with non-linear LS is within the two RSA curves corresponding to the two IIS limit behaviours.

Finally, a closed-form relationship obtained through the application of the pole allocation method has been provided, which allows the consideration of *IIS* and *ISO design spectra* without performing complex analyses, as required for the RSAs of IIS, a non-classically damped system. In more general terms, through the application of the pole allocation method, useful closed-form relationships are derived between the modal parameters and the design parameters of IIS, referred to as *target* and *controller* respectively.

Figure 9.1 shows the flowchart summarising the whole proposed design procedure. The starting point are the useful closed-form relationships obtained through the PAM which allow, once known the mechanical characteristics of the existing building ($T_{AS\text{-}IS}$, $\xi_{AS\text{-}IS}$), mass ratio (μ) and consequently its seismic response ($y_{AS\text{-}IS}$), to identify the IIS design spectrum in the case of linear LS response or the IIS inelastic behaviour zone in the case of non-linear LS. It is noted that at the end of the procedure the AS-IS seismic response ($y_{AS\text{-}IS}$) is compared with the IIS seismic response (y_{IIS}) and only if the reduction of the LS seismic response is considered acceptable the design process ends, otherwise it is possible to return to the closed-form relationships and modify the target parameters by varying the IIS design parameters.

The main results obtained in each chapter of this thesis are reported in the following section.

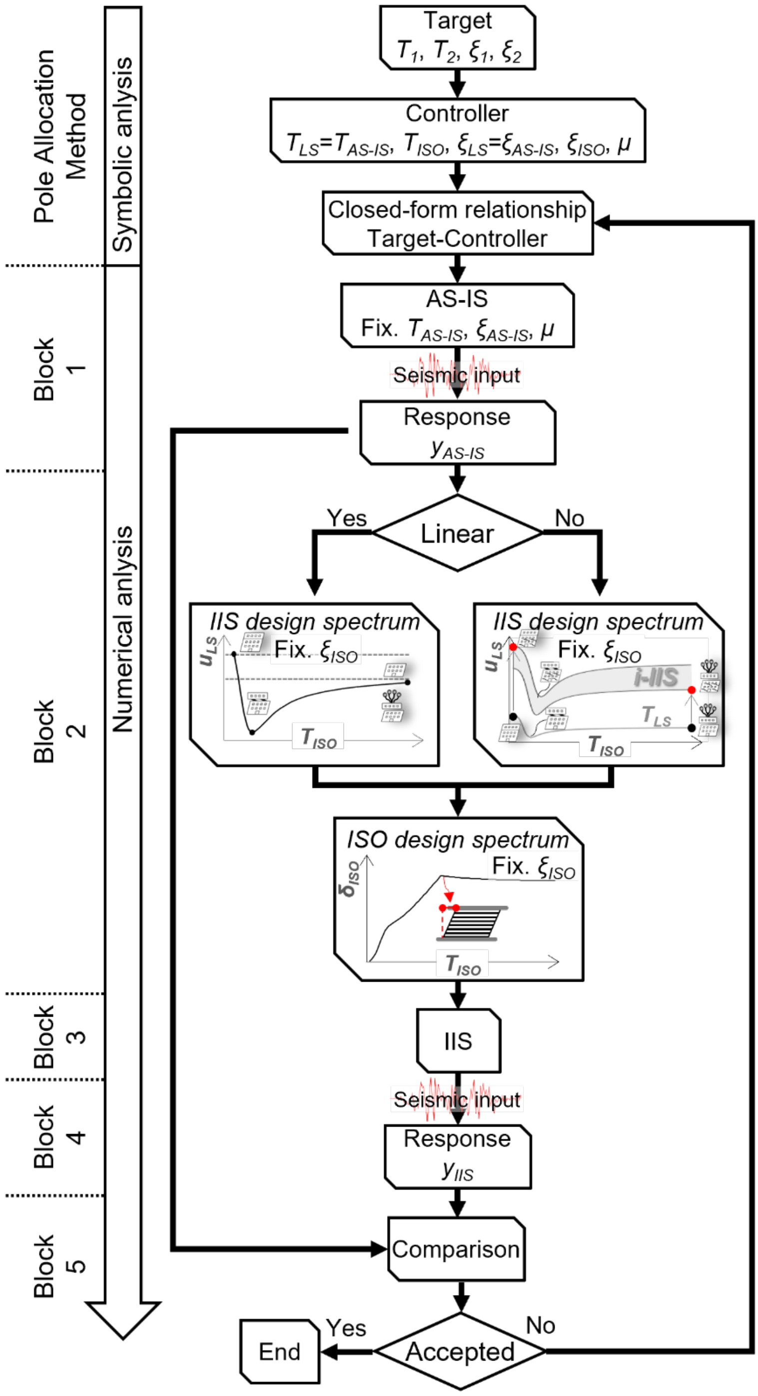

Figure 9.1. flowchart of the proposed design procedure.

9.2 Main outcomes

Chapter 2: *"Dynamic behaviour of IIS"*. In this chapter, the IIS dynamic behaviour is analysed with reference to a reduced-order model, first at 3DOF and then at 2DOF. The main observations that emerged are listed below.

- It is possible to study the dynamic behaviour and thus predict the response of the IIS by means of a 2DOF model if the isolated upper structure (ISO+US) can be considered as a rigid block on the isolation system and the amplification effect of the US response due to the higher mode coupling is avoided.
- The main design parameters for a building with IIS are the mass ratio (a function of the number of floors and structural type of US) and the isolation period (T_{ISO}).

Chapter 3: *"General 5-Block design procedure for IIS in existing building retrofit"*. In chapter 3 is examined the fascinating perspective of utilizing IIS to meet simultaneously the requirement of seismic retrofit of existing masonry buildings and the need for vertical extensions. A procedure, described by 5-Block, is proposed for addressing the design problem and for assessing the effectiveness of IIS. This approach is then applied to a case study, a two-story masonry aggregate located in Pozzuoli, a town near Naples (South Italy), for which a wide plan of reconstruction of rooftop volumes, previously demolished, has been recently issued. Linear parametric analyses are firstly carried out on simplified 3DOF lumped mass models for: (i) verifying the feasibility of the approach, (ii) understanding the dynamic behaviour of the system, and (iii) selecting the properties of isolated vertical additions that minimize the seismic response of the overall building. Then, the selected solutions are designed and assessed through nonlinear time history analyses on more refined 3D FE models, with a particular focus on the effect of the masonry nonlinearities on the structural response. The case of conventional vertical extension, without the isolation system, is also considered for comparative purpose.

From the results of the linear parametric analyses, it emerges that:

- the isolation layer can be designed either for completely disconnecting the existing aggregate and the new vertical addition, thus not varying the seismic demand, or for properly connecting the two structural parts and transforming the isolated superstructure into a large mass damper, thus leading to a reduction of the seismic demand with respect to the AS-IS configuration;

- by adopting an isolation period slightly larger than the period of the lower structure (i.e. T_{ISO}/T_{LS} = 0.5 – 3), the *mass damping effect* is emphasized, leading to the maximum reduction of the top displacement of the existing building with respect to the AS-IS configuration;
- by adopting an isolation period much larger than the period of the lower structure (i.e. T_{ISO}/T_{LS} > 6), the *isolation effect* is emphasized, nearly without any variation of the top displacement of the existing building with respect to the AS-IS configuration.

From the results of the linear and nonlinear dynamic analyses carried out on the 3D model of the design configurations, it can be stated that:

- the reduced order model, 3DOF IIS, is able to predict the dynamic behaviour of the whole 3D IIS structure, both considering or neglecting the hysteretic behaviour of the masonry structure;
- when a vertical extension of the building is to be realized, the insertion of the isolation layer between the new addition and the existing building improves the seismic response of the original structural part as compared to the conventional extension case~~;~~
- the major reductions of the top displacement in the existing masonry structure are obtained for low-medium isolation periods (mass damping effect) when the masonry structure works in the elastic field;
- also when the masonry nonlinearities are accounted for, the lower inelastic engagement of the existing structure is obtained for low-medium isolation periods, both in terms of top displacement and cumulated hysteretic energy;
- though the effectiveness in terms of displacement reduction is not as significant as in the elastic range, the accumulated damage in the masonry structure is remarkably mitigated.

Chapter 4: *"Influence of LS and ISO nonlinear behaviour on IIS response"*. In this chapter, time history analyses have been carried on the 3D FEMs of the existing masonry building introduced in chapter 3, selected as case study, and on some design configurations of the same building, consisting in vertical extensions through IIS. The aim was assessing the validity and accuracy of the prediction derived from response spectrum analyses on lumped mass models for preliminary design purpose (i.e. IIS design spectra). Conventional extension has been also considered for comparison.

Based on the results of the linear and nonlinear THA, the following conclusions can be derived.

- The dynamic behaviour of the 3D FE model of the extended building can be reasonably estimated through the simplified 3DOF IIS model.
- Based on the results of linear THA, the peak displacement demand in the lower structure is reduced for low-medium values of T_{ISO} (zone 2, *mass damping effect*).
- Considering the nonlinear behaviour either for the masonry structure only, or for the isolation system only, a reduced response in the existing building is still obtained for low-medium values of T_{ISO} (zone 2, *mass damping effect*).
- Considering the hysteretic behaviours of both the masonry structure and the isolation system, some reductions in the displacement response are obtained, with the minimum value of $\bar{u}$ reached for T_{ISO} = 1s, in contrast to that observed for LTHAs, where the minimum value of $\bar{u}$ is obtained for T_{ISO} = 0.5s.
- When a building should be vertically expanded, the adoption of an isolation interface between the existing and the new structures usually enhances the seismic performance of the existing structural portion with respect to the case of a vertical extension conventionally realised (without isolation system).
- However, fully nonlinear analyses, accounting for the hysteretic behaviour of both masonry structure and isolation system, have highlighted that design solutions that maximize the mass damping effect for linear system can

lead to an amplification, rather than a reduction of the seismic response.

- The results have also highlighted a remarkable influence of the modal damping values adopted in nonlinear THA on the structural response. When the lower structure exhibits significant inelastic deformations, the design of isolated vertical extension in the mass damping zone seems not advisable.

Chapter 5: *"A diagram-based design procedure for IIS in existing buildings with inelastic behaviour"*. The IIS spectrum, obtained from parametric Response Spectrum Analysis (RSA), does not account for the inelastic behaviour that possibly arises in existing buildings. For this reason, the design framework and the *stepwise procedure* proposed in this chapter allow for utilising IIS design spectra also in the case of existing buildings with inelastic behaviour. In order to validate the *stepwise procedure* three different existing buildings have been considered as case studies with twenty-one different configurations of the isolated vertical extension. For each case study, the *stepwise procedure* is applied to identify the *inelastic IIS behaviour zone*. Subsequently, the effective response of the case studies derived through NLTHA on 2DOF IIS models is compared with the prediction of the IIS response offered by the *IIS design spectra* (i.e. the *inelastic behaviour zone of IIS*).

Some observations and conclusive remarks are briefly reported in the following.

- The procedure allows to construct the so-called *i-IIS behaviour zone* without several NTHAs to account for the inelastic structural response.
- The convenience of the procedure consists in avoiding the execution of several NTHAs to explore the response of the system, varying the isolation period. Only two models, representative of two limit behaviours arising for very short and very long isolation periods, should be analysed in nonlinear field.
- The procedure has a solid and sound conceptual foundation, since it stems from the definition and study of the two models,

representative of two limit behaviours arising for very short and very long isolation periods.

- The accuracy of the procedure is confirmed by the application to some case studies and comparison with NTHA results.
- Of course, the procedure can be applied to building characterised by elastic behaviour and adapted to cover the case of IIS for new buildings, as well.
- The second case study analysed (i.e. T_{LS} = 0.63s) is a special case since the equivalent period of the damaged lower structure for the two limit cases is the same (i.e. $T_{P'0} = T_{P'\infty}$), consequently the *inelastic IIS behaviour zone* degenerates into a single RSA curve, which, again, provides a good prediction of the IIS response.

Chapter 6: *"Generalization of the 5-Block design procedure for IIS"*. In this chapter, an extension and generalisation of the 5-Block design procedure is proposed by means of several design charts assessed for different code design spectra. Two useful tools are suggested, i.e. the *IIS design spectrum* and *ISO design spectrum*. The former allows to explore possible IIS design solutions by varying the isolation period; the latter allows to design the isolation system, by calculating the ISO displacement at the design value of the isolation period. Finally, several design guidelines are provided that can simplify decision-making processes at a preliminary stage of the design.

Some observations are reported in the following.

- Extension and generalization of the procedure are possible, considering different code design spectra; as an example, set the Type 1 spectrum of the Eurocode 8, the design charts can be obtained by varying the design ground acceleration, a_g (on soil type A), the soil type (soil factor S), the structure damping ratio.
- The extension and generalisation of the procedure by means of design charts has proven to be quick and easy to use, as it can be applied both to the case of buildings with inelastic and elastic behaviour and adapted to include the case of IIS for new buildings.

- The chart-based design procedure avoids the development of several complex RSA analyses on reduced-order models to predict the IIS response.

Chapter 7: *"IIS and ISO design spectrum: close-form relationship through Pole Allocation Method (PAM)"*. In this chapter, the Pole Allocation Method (PAM) has been applied to a 2DOF model in order to obtain the *IIS design spectrum* and the *isolator displacement spectrum* in closed-form, both of which can be used as preliminary design tools for IIS. The comparison between the analyses results and the spectra shows good agreement, both in terms of drift in the lower structure (*IIS design spectrum*) and of isolator deformation (*isolator dis-placement spectrum,* or *ISO design spectrum*). The closed-form solution allows for an extension of the application field of these design spectra for the preliminary design of any building with IIS.

The research results obtained in this chapter are summarised below:

- The pole allocation method is used for deriving in closed form the values of damping ratio at the first two modes of vibration for 2DOF model (Eqs. (7.18) and (7.26)), as a function of five dynamic parameters of IIS, i.e., ω_{LS}, ω_{ISO}, ξ_{LS}, ξ_{ISO} and μ. Considering that in the case of seismic retrofitting of existing buildings the value of ω_{LS}, ξ_{LS} and μ are set *a priori*, or are variable within a small range of values, then ξ_1 and ξ_2 only depend on ω_{LS} and ξ_{LS}.
- *IIS design spectra* have been introduced as the core of the IIS design procedure for the extension and seismic retrofitting of existing buildings. However, the strong limitation to the applicability of this design tool was the complicated analytical procedure to be performed, which required complex analysis by applying the modified CQC modal superposition method [83]. With the closed-form solution for deriving the *IIS design spectrum*, the complex analysis is avoided and the classical CQC method is used.
- The use of a classic CQC instead of a modified CQC does not lead to great variations in the calculation of IIS design spectra if ξ_{ISO} is less than 0.30, where the percentage change (Δ)

between the RSA curves assessed with the classical or modified CQC is less than 10%.

- The same approach of the *IIS design spectrum* is used to derive the *isolator displacement spectrum* in closed form, which is another useful preliminary design tool. It provides, indeed, a good estimate of the isolator design displacement that implicitly considers the effect of mass damping and the flexibility of the lower structure.
- The *IIS design spectrum* evaluated using the target spectrum as input show good agreement with the results of the LTHAs.
- The ISO design spectrum evaluated using the target spectrum underestimates the isolation displacement in the range of periods 2 - 4s, therefore it is advisable to calculate it using the average spectrum of records as input, although identification of the ISO design spectrum will be more onerous.

Chapter 8: *"IIS for existing irregular buildings"*. In this chapter the regularizing potential of IIS on LS with stiffness eccentricity has been studied. Selected a case study, different solutions have been considered and analysed. Some preliminary conclusions based on the analyses results are:

- though some analogies with BIS can be found, it is erroneous reasoning as with BIS when IIS is adopted, especially with reference to regularizing effect;
- at isolation period ensuring maximum dynamic interaction of LS and US (i.e. max reduction of LS response), complete regularization can also be obtained;
- at this isolation period, differently from BIS, the US does not contribute only as a mass, but with its stiffness as well, therefore the midpoint of the line joining $\mathbf{K}_{\mathbf{ISO}}$ e $\mathbf{K}_{\mathbf{US}}$, i.e. the average position of US and ISO stiffness centres, should match the position of the mass centroid **G**;
- at long isolation periods, no interaction arises between the LS and US, whichever is the relative position of stiffness and mass centroids, therefore, no regularizing effect is obtained in addition to no response reduction effect;
- it is worth remembering that the above results are obtained in a preliminary phase of study, and with reference to one single case study.

Appendix A: “Examples of IIS”. In this appendix, several case studies of IIS buildings are analysed in order to show the variety of structural solutions that can be achieved with IIS, highlighting which problems arise in design and how they are solved in different design scenarios.

Below are some general remarks on the case studies investigated:

- The ISO layer is usually formed by NRB isolators combined with different types of dampers (i.e. oil dampers, U-shaped steel dampers, lead dampers, etc.) in order to divide the seismic isolation and energy dissipation functions concentrated in the ISO layer.
- The design of buildings with IIS follows the two theoretical approaches introduced in Chapter 2, i.e. the seismic isolation approach and the mass damping approach; where, generally a long isolation period (say 4 s) denotes the adoption of the first approach, conversely shorter periods indicate the taking advantage of the mass damping effect as well.
- The IIS is an excellent vibration control strategy for tall buildings, for which the adoption of a BIS is not very efficient in reducing the seismic response in the upper structure, and thus guaranteeing a continuity of building functionality after a rare earthquake.
- The IIS is very popular for retrofitting existing buildings because it significantly increases the seismic efficiency of the system, it allows no disruption of activities within the existing building, and no excavation operations around the building that would be necessary in the case of the ISO layer at the base.
- In areas with a high risk of flooding, the adoption of an IIS is preferred to BIS, since, in the latter case, the impact of water and/or objects could compromise the correct performance of the isolation layer.
- In the case of IIS for tall buildings in the ISO layer a locking mechanism is generally installed to prevent a large displacement of isolation device under high wind loads; however, this locking mechanism is removed when an earthquake occurs.

Appendix B: “The non-proportional damped system”. This appendix briefly describes the procedure adopted to evaluate the complex modal characteristics and maximum relative displacement response of a system classified as *non-classically damped* or with *non-proportional damping*. In particular, the modified CQC modal superposition method is described, which compared to the classical CQC modal superposition method takes into account the whole damping matrix of the system, and consequently, provides a more accurate system response when there is a coupling effect of the damped modes.

Appendix C: “The Pole Allocation Method (PAM)”. An application of the pole allocation method to a closed-loop system is described in the appendix, where the feedback control process through control gains allows the controlled system to obtain fixed target eigenvalues.

Appendix D: *“Suggested value of ISO damping ratio”*. In this appendix, the influence of the ISO damping ratio (ξ_{ISO}) on the structural response is first investigated by varying several structural parameters such as tuning ratio and mass ratio, and finally, a suggested value of the ISO damping is proposed and compared with several optimal ξ_{ISO} values proposed in the literature. The research results obtained in this appendix are summarised below.

- As the damping ratio of the isolation system increases, the sensitivity of the IIS response to variations of the main frequency of the seismic wave decreases.
- A damping ratio of the ISO system as the mass ratio changes is suggested in order to obtain an IIS response that is insensitive to the variation of the main frequency of the seismic wave.

Bibliography

[1] Reggio A. & De Angelis M., (2014), Optimization of a non-Conventional TMD implemented via Inter-story Isolation. In: *Proceedings of the EURODYN 2014 – IX International Conference of Structural Dynamics, Porto, Portugal, 30 June – 2 July 2014, 1713–20*. https://hdl.handle.net/11573/697261.

[2] Chey M., Chase J.G., Mander J.B. & Carr A.J., (2013), Innovative seismic retrofitting strategy of added stories isolation system. *Frontiers of Structural and Civil Engineering*, 2013;7(1):13–23. https://doi.org/10.1007/s11709-013-0195-9.

[3] Wang S.J., Lee B.H., Chuang W.C., Chiu I.C. & Chang K.C., (2019), Building mass damper design based on optimum dynamic response control approach. *Engineering Structures*, 187:85–100. https://doi.org/10.1016/j.engstruct.2019.02.053.

[4] Argenziano M., Faiella D., Fraldi M. & Mele E., (2019), Optimum tuning frequency and damping ratios in Inter-story Isolation Systems (IIS): a closed form solution. In: *Proceedings of the XVIII Convegno Anidis, Ascoli Piceno, Italy, 15-19 settembre*.

[5] Reggio A. & De Angelis M., (2015), Optimal energy-based seismic design of non-conventional Tuned Mass Damper (TMD) implemented via inter-story isolation. *Earthquake Engineering & Structural Dynamics.* 2015; 44:1623–1642. https://doi.org/10.1002/eqe.2548.

[6] Faiella D. & Mele E., (2019), Vibration characteristics and higher mode coupling in Intermediate Isolation Systems (IIS): a parametric analysis. *Bulletin of Earthquake Engineering,* 17:4347–4387, https://doi.org/10.1007/s10518-019-00637-w.

[7] Faiella D. & Mele E., (2020), Insights into inter-story isolation design through the analysis of two case studies. *Engineering Structures*, 215: 110660. https://doi.org/10.1016/j.engstruct.2020.110660.

[8] Argenziano M., Faiella D., Carotenuto A. R., Mele E. & Fraldi M., (2022), Generalization of the Den Hartog model and rule-of-thumb formulas for optimal tuned mass dampers. *Journal of Sound and Vibration*, 538, 117213. https://doi.org/10.1016/j.jsv.2022.117213.

[9] Holmes D. (1995). Listing of installations. *Engineering Structures*, 1995;17(9):676–78. https://doi.org/10.1016/0141-0296(95)90027-6.

[10] Kaynia A.M. & Veneziano D., (1981), Seismic effectiveness of tuned mass dampers. *Journal of the Structural Division*, 1981, ASCE;107(8):1465–84. https://doi.org/10.1061/JSDEAG.0005760.

[11] Soto-Brito R. & Ruiz S.E., (1999), Influence of ground motion intensity on the effectiveness of tuned mass dampers. *Earthquake Engineering &*

Structural Dynamics, 1999;28(11):1255–71. https://doi.org/10.1002/(SICI)1096-9845(199911)28:11<1255::AID-EQE865>3.0.CO;2-C.

[12] De Angelis M., Perno S. & Reggio A., (2012), Dynamic response and optimal design of structures with large mass ratio TMD. *Earthquake Engineering & Structural Dynamics.* 2012; 41:41–60. https://doi.org/10.1002/eqe.1117.

[13] Tsuneki Y., Torii S., Murakami K. & Sueoka T. (2009) Middle-story isolated structural system of high-rise building. *Journal of Disaster Research* 4 (3), 229-238. https://doi.org/10.20965/jdr.2009.p0229.

[14] Tsuneki Y., Torii S., Murakami K. & Sueoka T. (2008) Middle-story isolated structural system of high-rise building. In: *Proceedings of the 14th World Conference on Earthquake Engineering, Beijing, China.*

[15] ONU Homepage, https://population.un.org/wup/Publications/Files/WUP2018-Highlights.pdf, last accessed 28/01/2024.

[16] Urban Flows Observatory - The University of Sheffield Homepage, https://urbanflows.ac.uk/vertical-extension-sustainable-future/, last accessed 28/01/2024.

[17] GOV.UK Homepage, https://www.gov.uk/government/news/new-laws-to-extend-homes-upwards-and-revitalise-town-centres, last accessed 28/01/2024.

[18] Dutta A., Sumnicht J.F., Mayes R.L., Hamburger R.O. & Citipitioglu A., (2009), An innovative application of base isolation technology. In: *Proceedings of the ATC & SEI Conference on Improving the Seismic Performance of Existing Buildings and Other Structures, San Francisco, CA, USA*, pp. 841–854. https://doi.org/10.1061/41000(315)13

[19] Sumnicht J., (2008), On the Grid-Seismic Isolators, Sandwiched between Two Steel Grids, Separate an Existing San Francisco Building from Its Vertical Addition, *Modern steel construction*, *American Institute of Steel Construction*, Inc.: Chicago, IL, USA.

[20] Faiella D., Calderoni B. & Mele E., (2022), Seismic retrofit of existing masonry buildings through Inter-story Isolation System: a case study and general design criteria. *Journal of Earthquake Engineering*; 26:2051-2087. https://doi.org/10.1080/13632469.2020.1752854.

[21] Argenziano M., Faiella D., Bruni F., De Angelis C., Fraldi M. & Mele E., (2021), Upwards - Vertical extensions of masonry built heritage for sustainable and antifragile urban densification. *Journal of Building Engineering*; 44:102885. https://doi.org/10.1016/j.jobe.2021.102885.

[22] Faiella D., Argenziano M., Esposito F., Brandonisio G., Fraldi M. & Mele E., (2023), Effectiveness of isolated vertical extension of masonry buildings as nonconventional TMD. *Soil Dynamics and Earthquake Engineering*; 165:107675. https://doi.org/10.1016/j.soildyn.2022.107675

[23] Ryan K. L. & Earl C. L., (2010), Analysis and design of inter-story isolation systems with nonlinear devices. *Journal of Earthquake Engineering*, 14(7), 1044-1062. https://doi.org/10.1080/13632461003668020.
[24] Nakamizo D., Kimura S. & Koitabashi Y., (2020), Safety studies in seismic design of a mid-story isolated over track building. In: *Proceedings of the 17th World Conference on Earthquake Engineering, 17WCEE. Sendai, Japan, 13-18 September.*
[25] Okumura Corporation (2017), book on seismic isolation system (**In Japanese**).
[26] Kintetsu Group (2011), Directly connected to Kyoto Station! New hotel specialising in accommodation directly above the Kintetsu Line. Homepage, https://www.kintetsu.jp/news/files/kyoutohoteru0516.pdf. last accessed 28/01/2024. (**In Japanese**).
[27] Mitsuhiro D., (2014), Kintetsu Kyoto Station platform expansion and hotel construction work, Construction machinery construction = Journal of JCMA: Journal of the Japan Construction Machinery and Construction Association, 66 (5), 20-25.
[28] Wang S.J., Chang K.C., Hwang J.S., Hsiao J.Y., Lee B.H. & Hung Y.C., (2012), Dynamic behaviour of a building structure tested with base and mid-story isolation systems. *Engineering Structures*, 42:420–433. https://doi.org/10.1016/j.engstruct.2012.04.035.
[29] Murakami K., Kitamura H., Ozaki H. & Teramoto T. (2000) Design and analysis of a building with the middle-story isolation structural system. In: *Proceedings of the 12th World Conference of Earthquake Engineering, Auckland, New Zealand, Volume 857, pp. 1–8*.
[30] Okada K. & Yoshida S., (2014), Structural design of Nakanoshima festival tower. *International journal of high-rise buildings*, 3(3), 173-183. https://doi.org/10.21022/IJHRB.2014.3.3.173.
[31] Zhou Q., Singh M.P. & Huang X.Y., (2016), Model reduction of mid-story isolation systems. *Engineering Structures* 2016;124:36–48. https://doi.org/10.1016/j.engst ruct.2016.06.011.
[32] Kobayashi M. & Sasaki D., (2009), Making a Seismic Design Database of Mid-story Isolated Buildings and Structural Property Evaluation Based on Response Prediction Method. *Journal of Technology and Design, AIJ*, No.29, pp.65-70. https://doi.org/10.3130/aijt.15.65. (**In Japanese**).
[33] Kawamura S., Sugisaki R., Ogura K., Maezawa S., Tanaka S. & Yajima A., (2000), Seismic isolation retrofit in Japan. In: *Proceedings of 12th World Conference on Earthquake Engineering* (Vol. 8). Auckland, New Zealand.
[34] Association for Seismic Isolation Structures (JSSI), (2002), JIA Architects - Planning seismically isolated housing. Homepage, https://www.jssi.or.jp/wordpress/wp-

content/uploads/2022/06/keikaku.pdf. last accessed 26/01/2024. (**In Japanese**).

[35] Kuroda M., Narita I., Tanaka S., Kawamura S., Ogura K. & Yajima A., (1997), Seismic Isolation Retrofit At Mid-story and Base: Planning and Outline of Works. *Journal of Technology and Design*, *AIJ*, No.5, pp.18-22. https://doi.org/10.3130/aijt.3.18. (**In Japanese**).

[36] Ishizu H. & Furuhashi T., (1999) Seismic isolation retrofit of Kudan Post Office and Kudan Accommodation, *The Japan Society of Seismic Isolation (JSSI), Menshin, No. 26 1999.11.* Homepage, https://jssi.actibookone.com/content/detail?param=eyJjb250ZW50TnVtIjoyMzY0OTgsImNhdGVnb3J5TnVtIjoyMTcxNn0=&pNo=1, last accessed 26/01/2024. (**In Japanese**).

[37] Sera S., Saruta M. & Fujinami K., (2002), Kudan Post Office Building and Kudan Accommodation, *The Japan Society of Seismic Isolation (JSSI), Menshin, No. 38 2002.11.* Homepage, https://jssi.actibookone.com/content/detail?param=eyJjb250ZW50TnVtIjoyMzY1MTcsImNhdGVnb3J5TnVtIjoyMTcxN30=&pNo=1, last accessed 26/01/2023. (**In Japanese**)

[38] Sueoka T., Torii S. & Tsuneki Y. (2004) The application of response control design using middle-story isolation system to high-rise building. In: *Proceedings of the 13th World Conference on Earthquake Engineering, Vancouver, BC, Canada*.

[39] Nakagawa K., Shimazaki D., Yoshida S. & Okada K., (2015), Application of seismic isolation systems in Japanese high-rise buildings. *International journal of high-rise buildings*, 36–38.

[40] Tamari M., Yoshihara T., Miyashita M., Ariyama N. & Nonoyama M., (2017), Structural design and performance evaluation of a mid-story seismic isolated high-rise building. *International journal of high-rise buildings*, 6, 227–235. https://doi.org/10.21022/IJHRB.2017.6.3.227.

[41] Tsuneki Y., Torii S. & Sueoka T., (2004), High-rise buildings with intermediate-level seismic isolation. *The Japan Society of Seismic Isolation (JSSI), Menshin, No. 46 2004.11.* Homepage, https://jssi.actibookone.com/content/detail?param=eyJjb250ZW50TnVtIjoyMzY1MjgsImNhdGVnb3J5TnVtIjoyMTcxN30=&pNo=1, last accessed 26/01/2023. (**In Japanese**).

[42] The Japan Society of Seismic Isolation (JSSI) Homepage, https://www.jssi.or.jp/webmembers/english/doc/9-FFG.pdf, last accessed 20/07/2023.

[43] Murakami K., Kitamura H., Ozaki H. & Yamanishi T. (1999) Design of a Building with Seismic Isolation System at the Mid-story, *Journal of Technology and Design*, AIJ, No.7, pp.51-56. https://doi.org/10.3130/aijt.5.51_1. (**In Japanese**)

[44] Seibu Realty Solutions Homepage, https://www.seiburealsol.jp/ikebukuro/, last accessed 26/01/2024.

[45] Chuo Nittochi Homepage, https://www.chuo-nittochi.co.jp/business/building/office/uploads/edogrand.pdf, last accessed 26/01/2024.
[46] Architectural Institute of Japan., (2016)., Design Recommendations for Seismically Isolated Buildings.
[47] The Japan Society of Seismic Isolation (JSSI), (2020), Construction procedure standard for seismic isolation structure.
[48] Kobayashi M. & Koh T., (2005) Earthquake Response Prediction and Rationalization of Dynamic Design of Mid-story Isolated Buildings, *Journal of Structural and Construction Engineering*, AIJ, No.592, pp.51-57.
[49] Murakami K., Kitamura H. & Matsushima Y., (2001), The Prediction for Seismic Responses of the Two-mass Model with the Mid-story Isolation System, Journal of Structural and Construction Engineering, AIJ, No.549, pp.51-58.
[50] European Committee for Standardization, (2005), Eurocode 8: Design of structures for earthquake resistance-part 1: general rules, seismic actions and rules for buildings. Brussels: European Committee for Standardization.
[51] Murakami K. & Suoeka T., (2004), Proposal of a seismic design method for mid-story isolated structural system using a two-mass analysis model. In: *Proceedings of the International Symposium of Network and Center-Based Research for Smart Structures Technologies and Earthquake Engineering, Osaka, Japan, 6–9 July 2004; SE04-075*.
[52] Tasaka M., Mori N., Yamamoto H., Murakami K. & Sueoka T., (2008), Applying seismic isolation to buildings in Japan—Retrofitting and middle-story isolation. In: *Proceedings of the Structures Congress 2008: 18th Analysis and Computation Specialty Conference, 24–26 April 2008; pp. 1–11.* https://doi.org/10.1061/41000(315)12.
[53] Akiyama H., (1985), Earthquake-Resistant Limit-State Design for Buildings; *University of Tokyo Press: Tokyo, Japan*; ISBN 978-0-86008-377-1.
[54] Faiella D. & Mele E., (2022), Innovative mass-damping approaches for sustainable seismic design of tall buildings. Book Chapter In: *Sustainable High-Rise Buildings: Design, Technology, and Innovation*. The Institution of Engineering and Technology, 2022; 345 – 410.
[55] Wang S.J., Chang K.C., Hwang J.S. & Lee B.H., (2011), simplified analysis of mid-story seismically isolated buildings. *Earthquake engineering & structural dynamics*, 40(2):119–133. https://doi.org/10.1002/eqe.1004.
[56] Moriizumi E. & Kobayashi M., (2012), A study on earthquake response considered vibration characteristics of superstructure and substructure

of seismically isolated buildings. In: *Proceedings of the 15th World conference on earthquake engineering, Lisboa, paper 1792.*

[57] Kobayashi M. & Koh T., (2008), Modal coupling effects of mid-story isolated buildings. In: *Proceedings of the 14th World Conference on Earthquake Engineering, 2008, 2 - 17 October. Beijing, China, paper 05-01-0230.*

[58] Wang S.J., Hwang J.S., Chang K.C., Lin M.H. & Lee B.H., (2013), Analytical and experimental studies on midstory isolated buildings with modal coupling effect. *Earthquake engineering & structural dynamics*, 42(2):201–219. https://doi.org/10.1002/eqe.2203.

[59] Villaverde R, (1985), Reduction seismic response with heavily-damped vibration absorbers. *Earthquake Engineering & Structural Dynamics,* 1985;13(3):33–42. https://doi.org/10.1002/eqe.4290130105.

[60] Sadek F., Mohraz B., Taylor A. W. & Chung R. M., (1997), A method of estimating the parameters of tuned mass dampers for seismic applications. *Earthquake Engineering & Structural Dynamics*, 26(6), 617-635. https://doi.org/10.1002/(SICI)1096-9845(199706)26:6%3C617::AID-EQE664%3E3.0.CO;2-Z.

[61] Miranda J.C., (2013), a method for tuning tuned mass dampers for seismic applications. *Earthquake Engineering & Structural Dynamics*, 2013; 42: 1103–1110. https://doi.org/10.1002/eqe.2271.

[62] Basili M. & Angelis M.D., (2022), experimental Dynamic Response of a Multi-Story Frame Structure Equipped with Non-Conventional TMD Implemented via Inter-Story Isolation. *Applied Sciences*. 2022, 12, 9153. https://doi.org/10.3390/app12189153.

[63] Tan P., Zhang Y. & Zhou F., (2008), Optimal design and control mechanism study on story isolation system. In: *proceedings of the 14th World Conference on Earthquake Engineering; Beijing, China, October 2008, paper 0060*.

[64] Wang S.J., Lee B.H., Chuang W.C. & Chang K.C., (2018), optimum dynamic characteristic control approach for building mass damper design. *Earthquake Engineering & Structural Dynamics*. 2018, 47, 872–888. https://doi.org/10.1002/eqe.2995.

[65] Donà M., Bernardi E., Zonta A., Minotto M., da Porto F. & Tan P., (2019), Effectiveness and optimal design of fluid-viscous dampers for inter-storey isolated buildings. In: *Proceedings of the XVIII Convegno Anidis, Ascoli Piceno, Italy, 15-19 settembre*.

[66] Donà M., Bernardi E., Zonta A., Tan P. & Zhou F., (2021), Evaluation of optimal FVDs for inter-storey isolation systems based on surrogate performance models. *Bulletin of Earthquake Engineering*, 19(11), 4587-4621. https://doi.org/10.1007/s10518-021-01134-9.

[67] Bernardi E., Donà M., Sut S., Saler E., Caprino A. & da Porto F., (2023), Evaluation of the inter-story isolation system applied to an existing masonry school building. In: Proceedings of the *COMPDYN 2023 - 9th*

ECCOMAS Thematic Conference on Computational Methods in Structural Dynamics and Earthquake Engineering. Athens, Greece, 12-14 June 2023.

[68] Bernardi E., Donà M., Ceresara M., Gaspari M. & da Porto F. (2023), Evaluation of the inter-story isolation system applied to an existing rc school building. In: *Proceedings of the COMPDYN 2023 - 9th ECCOMAS Thematic Conference on Computational Methods in Structural Dynamics and Earthquake Engineering. Athens, Greece, 12-14 June*.

[69] Bernardi E., Donà M. & Tan P., (2023), multi-objective optimization of the inter-story isolation system used as a structural TMD. *Bulletin of Earthquake Engineering*, 21, 3041–3065. https://doi.org/10.1007/s10518-022-01592-9.

[70] Ikeda Y., (2021), Fundamental equation based on pole allocation for interstory seismic isolation of buildings. *Structural Control and Health Monitoring*, 28(3), e2687. https://doi.org/10.1002/stc.2687.

[71] Ikeda Y. & Matsumoto Y., (2022), Unified description of passive vibration control for buildings based on pole allocation applied to three-degree-of-freedom model. *Structural Control and Health Monitoring*, 29(9), e2995. https://doi.org/10.1002/stc.2995.

[72] Lukkunaprasit P. & Wanitkorkul A., (2001), Inelastic buildings with tuned mass dampers under moderate ground motions from distant earthquakes, *Earthquake Engineering & Structural Dynamics*, 2001;30(4), 537-51. https://doi.org/10.1002/eqe.22.

[73] Pinkaew T., Lukkunaprasit P. & Chatupote P., (2003), Seismic effectiveness of tuned mass dampers for damage reduction of structures. *Engineering Structures*, 2003;25(1):39–46. https://doi.org/10.1016/S0141-0296(02)00115-3.

[74] Wong K.K.F. & Chee Y.L., (2004), Energy dissipation of tuned mass dampers during earthquake excitations. *The structural design of tall and special buildings*, 2004;13(2):105–121. https://doi.org/10.1002/tal.244.

[75] Miranda J.C., (2005), On tuned mass dampers for reducing the seismic response of structures. Earthquake engineering & structural dynamics, 2005;34(7): 847–65. https://doi.org/10.1002/eqe.461

[76] Wong K.K.F., (2008), Seismic energy dissipation of inelastic structures with tuned mass dampers. *Journal of engineering mechanics*, 2008;134(2): 163-172. https://doi.org/10.1061/(ASCE)0733-9399(2008)134:2(163).

[77] Wong K.K.F. & Johnson J., (2009), Seismic energy dissipation of inelastic structures with multiple tuned mass dampers. *Journal of engineering mechanics*, 2009;135(4):265-75. https://doi.org/10.1061/(ASCE)0733-9399(2009)135:4(265).

[78] Sgobba S. & Marano G.C., (2010), Optimum design of linear tuned mass dampers for structures with nonlinear behaviour. *Mechanical Systems*

and Signal Processing, 24(6): 1739–55. https://doi.org/10.1016/j.ymssp.2010.01.009.

[79] Zhang Z. & Balendra T., (2013), Passive control of bilinear hysteretic structures by tuned mass damper for narrow band seismic motions. *Engineering Structures*. 54: 103–11. http://dx.doi.org/10.1016/j.engstruct.2013.03.044.

[80] Saha A. & Mishra S. K., (2021), amplification of seismic demands in inter-storey-isolated buildings subjected to near fault pulse type ground motions. *Soil Dynamics and Earthquake Engineering*. 147 (2021) 106771. https://doi.org/10.1016/j.soildyn.2021.106771.

[81] Quaranta G., Mollaioli F. & Monti G., (2016), Effectiveness of design procedures for linear TMD installed on inelastic structures under pulse-like ground motion. *Engineering Structures*. 2016; 10(1): 239-60. https://doi.org/10.12989/eas.2016.10.1.239.

[82] Domizio M., Garrido H. & Ambrosini D., (2022), single and multiple TMD optimization to control seismic response of nonlinear structures. *Engineering Structures*. 2022; 252:113667. https://doi.org/10.1016/j.engstruct.2021.113667.

[83] Sinha R. & Igusa T., (2012), CQC and SRSS methods for non-classically damped structures. *Earthquake Engineering & Structural Dynamics*, 24:615–619. https://doi.org/10.1002/eqe.4290240410.

[84] Den Hartog, J. P. (1947). Mechanical Vibrations, Third Edition. McGraw-Hill Book Company, Inc., New York.

[85] Warburton G. B., (1982), Optimum absorber parameters for various combinations of response and excitation parameters. *Earthquake Engineering & Structural Dynamics*, 10(3), 381-401. https://doi.org/10.1002/eqe.4290100304.

[86] Tsai H. C., & Lin G. C., (1993), Optimum tuned-mass dampers for minimizing steady-state response of support-excited and damped systems. *Earthquake Engineering & Structural Dynamics*, 22(11), 957-973. https://doi.org/10.1002/eqe.4290221104.

[87] Feng M.Q. & Mita A., (1995), Vibration control of tall buildings using mega subconfiguration. *Journal of engineering mechanics.* 1995; 121:1082-1088. https://doi.org/10.1061/(ASCE)0733-9399(1995)121:10(1082).

[88] Hoang N., Fujino Y. & Warnitchai P., (2008), Optimal tuned mass damper for seismic applications and practical design formulas. *Engineering Structures*, 2008;30(3):707–15. https://doi.org/10.1016/j.engstruct.2007.05.007.

[89] Yahyai M., Zebarjad L., Head M. & Shokouhian M., (2019), Optimum Parameters for Large Mass Ratio TMDs Using Frequency Response Function. Journal of Earthquake Engineering. https://doi.org/10.1080/13632469.2019.1624228.

[90] Moutinho C., (2012), An alternative methodology for designing tuned mass dampers to reduce seismic vibrations in building structures. *Earthquake engineering & structural dynamics*, 41:2059–2073. https://doi.org/10.1002/eqe.2174.
[91] Kelly J. M., (1990), Base isolation: linear theory and design. *Earthquake spectra*,*6*(2): 223-244. https://doi.org/10.1193/1.1585566.
[92] Kelly J. Earthquake resistant design with rubber. Berlin: Springer; 1997. 1997. https://doi.org/10.1007/978-1-4471-3359-9
[93] Naeim F. & Kelly J. M., (1999), Design of seismic isolated structures: from theory to practice. *John Wiley & Sons*.
[94] Consiglio Superiore dei Lavori Pubblici, (2018), Circolare del Ministero delle infrastrutture e dei trasporti 21 gennaio 2019 "Istruzioni per l'applicazione dell'«Aggiornamento delle "Norme tecniche per le costruzioni"» di cui al decreto ministeriale 17 gennaio 2018". *Gazzetta Ufficiale della Repubblica Italiana, n. 42 del 20/02/2018* (**In Italian**).
[95] De Luca A. & Guidi L. G., (2019), State of art in the worldwide evolution of base isolation design. *Soil Dynamics and Earthquake Engineering*. https://doi.org/10.1016/j.soildyn.2019.105722.
[96] De Luca A. & Guidi L. G., (2020), Base isolation issues in Italy: Integrated architectural and structural designs. *Soil Dynamics and Earthquake Engineering*, *130*, 105912. https://doi.org/10.1016/j.soildyn.2019.105912.
[97] Esposito F., Faiella D., Ikeda Y. & Mele E., (2023), Design spectra for Intermediate Isolation Systems: closed-form relationship based on application of pole allocation method. In: *Proceedings of the 18th World Conference on Seismic Isolation, Energy Dissipation, and Active Vibration Control of Structures (18WCSI). 2023, 6-10 November. Antalya, Turkey*.
[98] Meirovitch L., (1990), Dynamics and Control of Structures. *John Wiley & Sons*.
[99] Meirovitch L., (2001), Fundamentals of vibrations. *McGraw-Hill Book Co*.
[100] Li C., (2000), Performance of multiple tuned mass dampers for attenuating undesirable oscillations of structures under the ground acceleration. *Earthquake Engineering & Structural Dynamics*, 29(9), 1405-1421. https://doi.org/10.1002/1096-9845(200009)29:9<1405::AID-EQE976>3.0.CO;2-4.
[101] Chen X., Ding H. & Li C., (2022), A quasi-tuned-mass-damper design concept for mitigating the dynamic displacement demand of tall piers. *Soil Dynamics and Earthquake Engineering*, 155, 107172. https://doi.org/10.1016/j.soildyn.2022.107172.
[102] Iervolino I., (2021), Dinamica delle strutture e ingegneria sismica: Principi e applicazioni. *HOEPLI EDITORE*. (**In Italian**).
[103] Consiglio Superiore dei Lavori Pubblici, (2019), Circolare del Ministero delle infrastrutture e dei trasporti 21 gennaio 2019, n. 7

Istruzioni per l'applicazione dell'«Aggiornamento delle Norme tecniche per le costruzioni» di cui al decreto ministeriale 17 gennaio 2018. *Gazzetta Ufficiale della Repubblica Italiana, n. 35 del 11/02/2019*. (**In Italian**)

[104] Fajfar P. & Gašperšič P., (1996), The N2 method for the seismic damage analysis of RC buildings. *Earthquake engineering & structural dynamics*, 25.1: 31-46. https://doi.org/10.1002/(SICI)1096-9845(199601)25:1<31::AID-EQE534>3.0.CO;2-V.

[105] Dowell O. K., Seible F. & Wilson E. L., (1998), Pivot hysteresis model for reinforced concrete members. *ACI structural journal*, 95: 607-617.

[106] Pasticier L., Amadio C. & Fragiacomo M., (2008), Non-linear seismic analysis and vulnerability evaluation of a masonry building by means of the SAP2000 V. 10 code. *Earthquake engineering & structural dynamics*, 37(3), 467-485. https://doi.org/10.1002/eqe.770.

[107] Ozturk B., (2017), Seismic behavior of two monumental buildings in historical Cappadocia region of Turkey. *Bulletin of Earthquake Engineering*, 15, 3103-3123. https://doi.org/10.1007/s10518-016-0082-6.

[108] Magenes G. & Calvi G. M., (1997), In-plane seismic response of brick masonry walls. *Earthquake engineering & structural dynamics*, 26(11), 1091-1112. https://doi.org/10.1002/(SICI)1096-9845(199711)26:11%3C1091::AID-EQE693%3E3.0.CO;2-6.

[109] Veletsos A.S. & Ventura C.E., (1986), Modal analysis of non-classically damped linear systems. *Earthquake engineering & structural dynamics*, 14: 217–243. https://doi.org/10.1002/eqe.4290140205.

[110] Connor J. & Laflamme S., (2014), Structural motion engineering. *Springer International Publishing: Switzerland*, 2014. 619 p.

[111] Brandonisio G., Toreno M., Grande E., Mele E. & De Luca A., (2012), Seismic design of concentric braced frames. *Journal of Constructional Steel Research*, Volume 78, November 2012, Pages 22-37. https://doi.org/10.1016/j.jcsr.2012.06.003.

[112] Bosco M., Brandonisio G., Marino E., Mele E. & De Luca A., (2017), Ω* method: An alternative to Eurocode 8 procedure for seismic design of X-CBFs. *Journal of Constructional Steel Research*, Volume 134, July 2017, Pages 135-147. https://doi.org/10.1016/j.jcsr.2017.03.014.

[113] COMPUTERS AND STRUCTURES, INC., (2009), SAP2000 linear and nonlinear static and dynamic analysis and design of three-dimensional structures.

[114] P.U.A. 2015. Piano Urbanistico Attuativo del Comune di Pozzuoli. Ricomposizione volumetrica degli edifici parzialmente demoliti c/o crollati a seguito ai fenomeni bradisismici in coerenza con il P.R.G. art. 26 della L.R. n°16 del 22/12/2004 I° Stralcio. Delibera n. 84 del 24/06/2015. (**In Italian**)

[115] Ghersi A., Lenza P. & Calderoni B., (2020), Edifici in muratura; alla luce della nuova normativa sismica. *Dario Flaccovio Editore*. (**In Italian**)
[116] Quagliarini E., Maracchini G. & Clementi F., (2017), Uses and limits of the Equivalent Frame Model on existing unreinforced masonry buildings for assessing their seismic risk: A review. *Journal of Building Engineering*, 10, 166-182, https://doi.org/10.1016/j.jobe.2017.03.004
[117] Cattari S., Calderoni B., Caliò I., Camata G., de Miranda S., Magenes G., Milani G. & Saetta A., (2022), Nonlinear modeling of the seismic response of masonry structures: critical review and open issues towards engineering practice. *Bulletin of Earthquake Engineering*, 20(4), 1939-1997, https://doi.org/10.1007/s10518-021-01263-1.
[118] Manzini C. F., Magenes G., Penna A., da Porto F., Camilletti D., Cattari S. & Lagomarsino S., (2018), Masonry Italian code-conforming buildings. Part 1: case studies and design methods. *Journal of Earthquake Engineering*, 22(sup2), 54-73. https://doi.org/10.1080/13632469.2018.1532358.
[119] Tomaževič M., (2009), Shear resistance of masonry walls and Eurocode 6: shear versus tensile strength of masonry. *Materials and structures*, 42, 889-907. https://doi.org/10.1617/s11527-008-9430-6.
[120] Iervolino I., Galasso C. & Cosenza E., (2010), REXEL: computer aided record selection for code-based seismic structural analysis. *Bulletin of Earthquake Engineering*, https://doi.org/10.1007/s10518-009-9146-1.
[121] Smerzini S. & Paolucci R., (2013), SIMBAD: A database with selected input motions for displacement based assessment and design – 3rd release, *Research Project DPC - RELUIS 2010-2013*.
[122] Argenziano M., (2022), Mass damping-based solutions for reducing the seismic response of new and existing buildings analytical methods and optimization criteria. *Ph.D. thesis, University of Naples Federico II, Italy*.
[123] FIP industriale, (2018), Isolatori elastomerici serie SI. Homepage, https://www.fipmec.it/assets/Uploads/FIP-MEC_SI.pdf, last accessed 28/01/2024.
[124] Wilson E. L. & Penzien J., (1972), Evaluation of orthogonal damping matrices. *International Journal for numerical methods in engineering*, 4(1), 5-10, https://doi.org/10.1002/nme.1620040103.
[125] Chopra A. K. & McKenna F., (2016), Modeling viscous damping in nonlinear response history analysis of buildings for earthquake excitation. *Earthquake Engineering & Structural Dynamics*, 45(2), 193-211, https://doi.org/10.1002/eqe.2622.
[126] Esposito F., Argenziano M., Faiella D. & Mele E., (2023), Intermediate Isolation System with Nonlinear Lower Structure and Isolation System. *Applied Sciences*; 13:4590. https://doi.org/10.3390/app13074590.

[127] Consiglio Nazionale Delle Ricerche (CNR) - Commissione di studio per la predisposizione e l'analisi di norme tecniche relative alle costruzioni. (2013). Istruzioni per la valutazione affidabilistica della sicurezza sismica di edifici esistenti. (**In Italian**)

[128] Esposito F., Faiella D. & Mele E., (2024), A diagram-based design procedure for Intermediate Isolation System in existing buildings with inelastic behavior. *Earthquake Engineering & Structural Dynamics,* 1-17. https://doi.org/10.1002/eqe.4079.

[129] Esposito F., Faiella D. & Mele E., (2023), Intermediate Isolation System for adding floors in existing buildings: chart-based design. In: *Proceedings of the 18th World Conference on Seismic Isolation, Energy Dissipation, and Active Vibration Control of Structures, Antalya, Turkey, 6-10 November 2023*.

[130] DM. 20 November. 1987. Norme Tecniche per la progettazione, esecuzione e collaudo degli edifici in muratura e per il loro consolidamento. Gazzetta Ufficiale della Repubblica Italiana 285 (18). (**In Italian**)

[131] Heyman J., (1966), The stone skeleton. *International Journal of solids and structures*, 2(2), 249-279. https://doi.org/10.1016/0020-7683(66)90018-7.

[132] Faiella D., (2018), The intermediate-isolation system for new and existing buildings: seismic behaviour and design criteria. *Ph.D. thesis, University of Naples Federico II, Italy*

[133] Tanaka T., Tsubaki E. & Yamane I., (2002), Umeda DT Tower, The Japan Society of Seismic Isolation (JSSI), *Menshin, No. 37 2002.8*. Homepage, https://www.jssi.or.jp/bussiness/shuppan_detail/kaishiback/37.pdf, last accessed 29/01/2024. (**In Japanese**).

[134] Takenaka. Homepage, https://www.takenaka.co.jp/solution/needs/earthquake/service20/index.html, last accessed 29/01/2024. (**In Japanese**).

[135] Shinji G., Nakashima K., Yamamoto T., Kabuto K., Ono S., Nakagawa K., Awano M., Yoshida S., Okada K. & Ezoe S., (2013), Nakanoshima Festival Tower, *NIKKEN JOURNAL14, Nikken sekkei LTD.*

[136] Faiella D., Argenziano M., Esposito F. & Mele E., (2023), Coupling of Structural Additions for the Mitigation of Seismic Response in Existing Buildings. In: *Proceedings of the Seismic Isolation, Energy Dissipation and Active Vibration Control of Structures: 17th World Conference on Seismic Isolation (17WCSI), pp. 632-642. Cham: Springer International Publishing, Turin, Italy*. https://doi.org/10.1007/978-3-031-21187-4_53.

[137] Esposito F., Faiella D., Argenziano M., Brandonisio G. & Mele E., (2023), The Effect of Nonlinear Response of the Primary System in Nonconventional TMDs. In: *Proceedings of the Seismic Isolation,*

Energy Dissipation and Active Vibration Control of Structures: 17th World Conference on Seismic Isolation (17WCSI), pp. 546-556. Cham: Springer International Publishing, Turin, Italy. https://doi.org/10.1007/978-3-031-21187-4_46.

[138] Faiella D., Argenziano M., Brandonisio G., Esposito F. & Mele E., (2022), Intermediate isolation system for the seismic retrofit of existing masonry buildings. In: *Proceedings of the Current Perspectives and New Directions in Mechanics, Modelling and Design of Structural Systems, pp. 1895-1900. CRC Press, Cape Town, South Africa*. https://doi.org/10.1201/9781003348443.

[139] Warburton G.B. & Soni S.R., (1977), Errors in response calculations for non-classically damped structures. *Earthquake Engineering & Structural Dynamics*, 5: 365-376.https://doi.org/10.1002/eqe.4290050404

[140] D'Amato M., Laguardia R. & Gigliotti R., (2020), Seismic retrofit of an existing rc building with isolation devices applied at base. Frontiers in Built Environment. 6:82 doi:10.3389/fbuil. 2020.00082.

[141] De Luca A., Mele E., Molina J., Verzeletti G. & Pinto AV., (2001), Base isolation for retrofitting historic buildings: evaluation of seismic performance through experimental investigation. *Earthquake Engineering & Structural Dynamics*, 44(10), 1623-1642. https://doi.org/10.1002/eqe.2548.

[142] Cuomo G., De Luca A. & Mele E., (2008), Design aspects in seismic isolation: application to retrofit churches. *International Journal of Architectural Heritage*, 2(3), 247-273. https://doi.org/10.1080/15583050802063741.

[143] Darama H., Zekioglu A., Rees S., Pope C. & McGowan R., (2017), Seismic isolation of an asymmetric structure: Taipei Performing Art Center. *16WCEE. Chile, Jan 9-13. Paper N. 371*.

[144] Faiella D., Esposito F. & Mele E., (2023), Vertical extension with Intermediate Isolation System for existing irregular buildings. In: *Proceedings of the 10th European Workshop on the Seismic Behaviour of Irregular and Complex Structures (10EWICS), Catania, Italy, 5-6 October.*

[145] Bridgestone (2022), Seismic Isolation Product Line-up. Hompage https://www.bridgestone.com/products/diversified/antiseismic_rubber/pdf/catalog_202210.pdf, last accessed 29/01/2024.

[146] Taisei Corporation. (2000), Hompage: https://www.taisei.co.jp/MungoBlobs/518/963/K00H16.pdf last accessed 29/01/2024. (**In Japanese**).

[147] Torii T., Otake H. & Minoru O., (2002), Seismic reinforcement of the Shinjuku Station West Exit Bookshop Building, The Japan Society of Seismic Isolation (JSSI), *Menshin, No. 37 2002.8.* Homepage,

https://www.jssi.or.jp/bussiness/shuppan_detail/kaishiback/37.pdf, last accessed 29/01/2024. (**In Japanese**).

[148] Sony Corporation - Sony City Osaki, The Japan Society of Seismic Isolation (JSSI). Homepage, https://www.jssi.or.jp/wordpress/wp-content/uploads/2022/10/aw-13kai-design1.pdf, last accessed 2023/01/08. (**In Japanese**).

[149] Kohno T., (2013), Sony City Osaki - Transpiration Louvers and Variable Seismic-isolated Structures. Steel construction today & tomorrow, No. 38 April 2013. https://www.jisf.or.jp/en/activity/sctt/index.html, last accessed 29/01/2024.

[150] Mita Berge Building, Minato Ward, Tokyo - Vibration control by the weight of the houses on the upper floors. 2012/09/10. https://xtech.nikkei.com/kn/article/nad/mag/20120830/581266/, last accessed 29/01/2024. (**In Japanese**).

[151] Takenaka Corporation (2012), Construction of the Mita Berge Building, with a seismic isolation layer 114 m above ground, completed. - The building's seismic isolation layers effectively reduce shaking of the entire building, ensuring safety and security. https://www.takenaka.co.jp/news/2012/05/01/index.html, last accessed 29/01/2024. (**In Japanese**).

[152] Mita Bellju building - Skyscraper complex with the residence as a damper (2013), *Takenaka Design Works, vol. 25 - Cities and nature - spaces to live in. p.6 – 9*.

[153] Komuro T., Watanabe T., Tatsuno S., Kawamoto S. & Kawaik., (2013), Ochanomizu Sola City - application of Existing Pile Reuse Technology and Structural Frame High Technology, *03 - report of Taisei technology center No.46 2013.* (**In Japanese**).

[154] Komuro T., Korenaga T., Kawai K., Tatsuno S., Soya K., Kawamoto S. & And Kai T., (2012), Design and Construction of Structure of Three-dimensional Urban Plaza - Creating an Underground Space that Can Accommodate Large Gatherings of People during Disasters, *05 - report of Taisei technology center no.45 2012*.

[155] Watanabe T., Ishizaki S., Tomita N., Kawamoto S. & Tatsuno S., (2016), Reuse of existing bored piles for high-rise building foundation. *Japanese Geotechnical Society Special Publication. 2. 158-161*. https://doi.org/10.3208/jgssp.ESD-09.

[156] Nihonbashi Dia building, (2014), *Japan Federation Of Construction Contractors*. Homepage, https://www.nikkenren.com/kenchiku/sb/pdf/308/13-031.pdf. last accessed 29/01/2024. (**In Japanese**).

[157] Nihonbashi Dia Building, Homepage, https://www.mitsubishi-logistics.co.jp/english/estate/office/office01.html. last accessed 29/01/2024.

[158] Takeuchi S., Kato G. & Saito T., (2018), Nihonbashi Dia Building, The Japan Society of Seismic Isolation (JSSI). Homepage, https://jssi.actibookone.com/content/detail?param=eyJjb250ZW50TnVtIjoyMzY1OTcsImNhdGVnb3J5TnVtIjoyMTcyMH0=&pNo=1. last accessed 29/01/2024. (**In Japanese**).
[159] Mitsubishi Logistics Corporation. Homepage, https://www.mitsubishi-logistics.co.jp/english/esg_sdgs/pdf/csr2020e.pdf. last accessed 29/01/2024.
[160] Wakabadai No. 1 Apartment 3-7, (2014), *Japan Federation Of Construction Contractors*. Homepage, https://www.nikkenren.com/kenchiku/qp/pdf/59/058.pdf. Last accessed 17/01/2024. (**In Japanese**).
[161] Intermediate storey seismic isolation retrofitting on residential floors in housing complexes - Construction while living in the house and restoration of its function as a residential floor, (2017), *Sumitomo Mitsui Construction Co.* Homepage, https://www.smcon.co.jp/topics/2017/040518674/. Last accessed 17/01/2024. (**In Japanese**).
[162] Tamari M., Yoshihara T., Miyashita M., Ariyama N. & Nonoyama M. (2017), Structural design and performance evaluation of a mid-story seismic isolated high-rise building. *Int. J. High-Rise Build*, *6*(3), 227-235.
[163] Kyobashi Edogrand, Chuo-Nittochi Group Co. https://www.chuo-nittochi.co.jp/business/building/office/uploads/edogrand.pdf. last accessed 29/01/2024.
[164] Yamano Y., Yoshida K. & Fukushima T., (2017), Kyobashi Edogran - Design and construction of intermediate-layer seismic isolation in high-rise buildings, The Japan Society of Seismic Isolation (JSSI), Menshin, No. 95 2017.1. Homepage, https://jssi.actibookone.com/content/detail?param=eyJjb250ZW50TnVtIjoyMzc1MzIsImNhdGVnb3J5TnVtIjoxOTk5MH0=&pNo=1, last accessed 29/01/2024. (**In Japanese**).
[165] Koitabashi Y., Asakawa T. & Nakamizo D., (2016), Roppongi 3-chome East Urban Area Redevelopment Project Type 1 - Sumitomo Fudosan Roppongi Grand Tower, The Japan Society of Seismic Isolation (JSSI), Menshin, No. 93 2016.7. Homepage, https://jssi.actibookone.com/content/detail?param=eyJjb250ZW50TnVtIjoyMzY1OTAsImNhdGVnb3J5TnVtIjoiMTk5OTAifQ==&pNo=16, last accessed 16/01/2024. (**In Japanese**).
[166] Nakamizo D. & Koitabashi Y. (2018). Structural design of mid-story isolated high-rise building-Roppongi Grand Tower. *International Journal of High-Rise Buildings*, 7(3), 233-242. https://doi.org/10.21022/IJHRB.2018.7.3.233.
[167] Diamond Gate Ikebukuro (2022), Association for Seismic Isolation Structures, 23rd Japan Association of Seismic Isolation Structures

Award. Homepage, https://www.jssi.or.jp/wordpress/wp-content/uploads/2022/08/aw-23kai.pdf. Last accessed 24/01/2024. (**In Japanese**).

[168] Porter B. & Crossley R., (1972), Modal control: theory and applications. *London: Taylor and Francis*.

Author’s publications

1. Esposito F., Faiella D. & Mele E., (2024), Steel vertical extension of existing buildings with isolation system: diagram-based design approach and validation through a case study. Submitted in: *Proceedings of the 11th International Conference on the Behaviour Of Steel Structures In Seismic Areas (STESSA2024), Salerno, Italy, 8 July – 10 July 2024.*

2. Ascione F., Esposito F., Iovane G., Faiella D., Faggiano B. & Mele E., (2023), Sustainable and efficient structural systems for tall buildings: exploring timber and steel-timber hybrids, *Buildings*, 14(2), 524. https://doi.org/10.3390/buildings14020524.

3. Esposito F., Faiella D. & Mele E., (2024), A diagram-based design procedure for Intermediate Isolation System in existing buildings with inelastic behavior. *Earthquake Engineering & Structural Dynamics;1-17.* https://doi.org/10.1002/eqe.4079.

4. Esposito F., Faiella D. & Mele E., (2023), Intermediate Isolation System (IIS) for existing buildings: a design procedure. Submitted in: *Proceedings of the 18th World Conference on Earthquake Engineering (WCEE2024), Milan, Italy, 30 June – 5 July 2024*.

5. Esposito F., Faiella D. & Mele E., (2023), Intermediate Isolation System for adding floors in existing buildings: chart-based design. In: *Proceedings of the 18th World Conference on Seismic Isolation, Energy Dissipation, and Active Vibration Control of Structures, Antalya, Turkey, 6-10 November 2023*.

6. Esposito F., Faiella D., Ikeda Y. & Mele E., (2023), Design spectra for Intermediate Isolation Systems: closed-form relationship based on application of pole allocation method. In: *Proceedings of the 18th World Conference on Seismic Isolation, Energy Dissipation, and Active Vibration Control of Structures, Antalya, Turkey, 6-10 November 2023.*

7. Faiella D., Esposito F. & Mele E., (2023), Vertical extension with Intermediate Isolation System for existing irregular buildings. In: *Proceedings of the 10th European Workshop on the Seismic Behaviour of Irregular and Complex Structures (10EWICS), Catania, Italy, 5-6 October 2023.*

8. Esposito F., Faiella D. & Mele E., (2023), Structural design of tall buildings - 20 years since the collapse of WTC. In: *Proceedings of the V convegno di ingegneria forense, VIII convegno su crolli, affidabilità strutturale, consolidamento. Università di Bologna, 15-17 giugno 2023*. (**In Italian**)

9. Esposito F., Argenziano M., Faiella D. & Mele E., (2023), Intermediate isolation system with nonlinear lower structure and isolation system, *Applied Sciences*, https://doi.org/10.3390/app13074590.

10. Faiella D., Argenziano M., Esposito F., Brandonisio G., Fraldi M. & Mele E., (2023), Effectiveness of isolated vertical extension of masonry buildings as nonconventional TMD, *Soil Dynamics and Earthquake Engineering*, 165, 107675. https://doi.org/10.1016/j.soildyn.2022.107675.

11. Faiella D., Argenziano M., Esposito F. & Mele E., (2023), Accoppiamento di addizioni strutturali per la mitigazione della risposta sismica in edifici esistenti. *Ingenio*. https://www.ingenio-web.it/articoli/accoppiamento-di-addizioni-strutturali-per-la-mitigazione-della-risposta-sismica-in-edifici-esistenti/. Last accessed 2023/15/01.

12. Esposito F., Faiella D., Argenziano M., Brandonisio G. & Mele E., (2023), The Effect of Nonlinear Response of the Primary System in Nonconventional TMDs. In: *Proceedings of the Seismic Isolation, Energy Dissipation and Active Vibration Control of Structures: 17th World Conference on Seismic Isolation (17WCSI)* (pp. 546-556). Cham: Springer International Publishing. https://doi.org/10.1007/978-3-031-21187-4.

13. Faiella D., Argenziano M., Esposito F. & Mele E., (2023), Coupling of Structural Additions for the Mitigation of Seismic Response in Existing Buildings. In: *Proceedings of the Seismic Isolation, Energy Dissipation and Active Vibration Control of Structures: 17th World Conference on Seismic Isolation (17WCSI)* (pp. 632-642). Cham: Springer International Publishing. https://doi.org/10.1007/978-3-031-21187-4

14. Faiella D., Argenziano M., Esposito F. & Mele E. (2022). New life to old buildings in seismic area through structural steelwork. *In Atti del 28° congresso CTA, giornate italiane della costruzione in acciaio (Vol. 1, pp. 907-914). CTA*.

15. Faiella D., Argenziano M., Brandonisio G., Esposito F. & Mele E., (2022), Intermediate isolation system for the seismic retrofit of existing masonry buildings. In: *Proceedings of the Current Perspectives and New Directions in Mechanics, Modelling and Design of Structural Systems* (pp. 1895-1900). CRC Press. https://doi.org/10.1201/9781003348443.

16. Esposito F., Faiella D. & Mele E., (2021), Structural design of tall buildings - 20 years after wtc collapse, *Costruzioni Metalliche, n. 4/2021*. (**In Italian**).

Appendix A: Examples of IIS

For the sake of simplicity, the four Intervention Types (IT) with IIS described in the first chapter and shown in Figure 1.1 are denoted in the following as IT1, IT2, IT3 and IT4 respectively for the intervention types of Figure 1.1 a, b, c and d.

In the following appendix, several buildings with IIS vibration control strategy are described. As mentioned in the introduction chapter, almost all the buildings with IIS realised are located in Japan and were found only one case of IIS application realised outside Japan, i.e. the vertical extension and seismic retrofit of one building at 185 Berry Street, in the China Basin area of San Francisco.

The aim of this appendix is to show the different options for the application of IIS to new and existing buildings, therefore forty-two buildings with IIS will be shown. In particular, for twenty-two buildings, only an external view of the building and its name is shown, while for the remaining twenty buildings will be described in detail in the next sections.

The first twenty-two IIS buildings are listed below: Akasaka Trust Tower (Figure A.1a), Building T&T III (Figure A.1b), White Canvas (Figure A.1c), Sumitomo Fudosan Tamachi (Figure A.1d), Yokohama City Hall (Figure A.1e), Tsutenkaku (Figure A.1f), JA Kyosai Building Hirakawacho Residence (Figure A.1g), Shin-Tokyo Takeda Building (Figure A.1h), Otemachi Financial City Grande Cube (Figure A.1i), Konan Building (Figure A.1l), Yokohama Grand Gate (Figure A.1m), Gamagori Shinkin Bank head office (Figure A.1n), Kochi Autonomy Hall (Figure A.1o), New government building of the new city of Shinden (Figure A.2a), Ishinomaki Municipal Hospital (Figure A.2b), Okaya Fire Department Building (Figure A.2c), New Shibuya Ward Office building (Figure A.2d), Terrace Shibuya Mitake Shibuya (Figure A.2e), Ocean Gate Minato Mirai (Figure A.2f), Kochi Castle History Museum Kyoto Station es (Figure A.2g), Kochi New Library and other complex (Figure A.2h), Kyoto Station building (Figure A.2i),

Figure A.1. (a) Akasaka Trust Tower [license: Copyright © 2022 NTT Urban Development All Rights Reserved.]; (b) Building T&T III [license: © Shinjuku Convention & Visitors Bureau], (c) White Canvas [license: © 2021 Yasuda Real Estate Co., Ltd.]; (d) Sumitomo Fudosan Tamachi [license: Copyright(C)2014 Sumitomo Realty & Development Co.,Ltd All Rights Reserved.]; (e) Yokohama City Hall [license: https://creativecommons.org/licenses/by-sa/4.0/]; (f) Tsutenkaku [license: https://creativecommons.org/licenses/by-sa/4.0/]; (g) JA Kyosai Building Hirakawacho Residence [license: Copyright © NIHON SEKKEI, INC.]; (h) Shin-Tokyo Takeda Building [license: https://creativecommons.org/publicdomain/zero/1.0/]; (i) Otemachi Financial City Grande Cube [license: https://creativecommons.org/licenses/by-sa/4.0/]; (l) Konan Building [license: Copyright © HATO BUS CO.,LTD.]; (m) Yokohama Grand Gate [license: https://creativecommons.org/licenses/by-sa/4.0/]; (n) Gamagori Shinkin Bank head office [license: https://creativecommons.org/licenses/by-sa/4.0/]; (o) Kochi Autonomy Hall [license: © Nishikawa Photograph co.,Ltd.].

Figure A.2. (a) New government building of the new city of Shinden [license: https://creativecommons.org/licenses/by-sa/4.0/]; (b) Ishinomaki Municipal Hospital [license: https://creativecommons.org/licenses/by-sa/4.0/]; (c) Okaya Fire Department Building [license: https://creativecommons.org/licenses/by-sa/3.0/]; (d) New Shibuya Ward Office building [license: https://creativecommons.org/publicdomain/zero/1.0/]; (e) Terrace Shibuya Mitake Shibuya [license: © 2024 PLAZA HOMES, LTD.], (f) Ocean Gate Minato Mirai [license: https://creativecommons.org/licenses/by-sa/4.0/]; (g) Kochi Castle History Museum [license: https://creativecommons.org/licenses/by/3.0/. Attribution: z tanuki]; (h) Kochi New Library and other complex [license: https://creativecommons.org/licenses/by-sa/4.0/]; (i) Kyoto Station building (license: Image © 2024 Google, Data SIO, NOAA, U.S. Navy, NGA, GEBCO. Image Landsat/Copernicus. Data Japan Hydrographic Association).

In Section A. 21, in order to facilitate smoother reading, key information is compared in Tables A.1 – A.7 for the buildings described in sections A.1 – A.20. In these tables, for each building are provided: type of intervention, destination of use, address, year of intervention, companies involved in the design and/or construction, structural type, maximum floor plan dimensions (d_1 x d_2), building height (H), ISO system height (H_{ISO}), number of storeys (n_{floors}) of LS and US, floor area (A_{floors}) of LS and US, mass ratio μ, isolation period (intended as the period of the upper base isolated structure for a 100% shear displacement of the isolator), ISO system displacement (if preceded by the symbol "≤" it is intended as the design limit value), type of isolators/dampers installed in the isolation level. The information just mentioned has been summarised for the twenty buildings in Table A.1 - Table A.7. However, information regarding the mass ratio or isolation period is generally not clearly stated in the scientific literature and has been derived through simplified procedures. For the mass ratio, realistic values for the building weight have been set as a function of the structural building type, i.e. for steel frame (S), reinforced concrete frame (RC), steel and reinforced concrete frame (SRC), a value of 7 kN/m^2, 10 kN/m^2, 10 kN/m^2 respectively has been considered. For the Isolation period, the value of the isolator shear stiffness for 100% deformation has been derived from the catalogue [145], and known the mass of the isolated upper structure, T_{ISO} has been derived from $T_{ISO} = 2\pi(M_{ISO}/k_{ISO})^{0.5}$. The values of μ and T_{ISO} obtained through these simplified procedures, i.e. not reported in the scientific literature, are easily distinguished in Table A.1 - Table A.7 because they are preceded by the symbol "≈".

A.1 Personnel Training Center of Taisei Corporation

All information reported in this section was derived from [33 – 35, 146].

General information on the building is given in Table A.1.

The building analysed in this section is the personnel Training Center of Taisei Corporation Figure A.3a, one of the most important construction companies in Japan; built in the 1964 is located on the Pacific coast in the Shizuoka prefecture. The building is divided into 4 structural parts (Figure A.3b) with different heights as the building is located on a slope of the ground Figure A.4a. The Building A, B and C are 2, 7 and 16 storied steel encased reinforced concrete building, respectively; building D is a 7 storied reinforce concrete building.

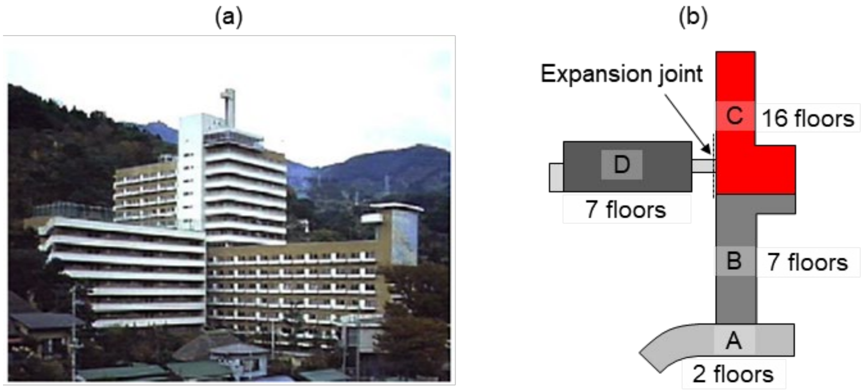

Figure A.3. (a) Personnel Training Center of Taisei Corporation [146]; (b) building layout [redrawn from [33]].

Following the Great Hanshin-Awaji Earthquake of 1995, the "Law on the Promotion of Seismic Repair of Buildings" was promulgated, which favoured the seismic retrofitting of buildings designed in accordance with the pre-1981 standard. For this reason, the building has been subject to retrofit intervention in the 1999. This is the first example of the application of the IIS strategy for the seismic retrofitting of an existing building.

In fact, different interventions have been carried out for the four structural parts. Parts A and B have been reinforced with carbon fiber sheet and reinforced concrete shear walls (SW), part C has been isolated at the intermediate level, i.e. on the seventh floor (Figure A.4), and the in the lower structure in order to avoid torsional motion parallel to the slope and to improve the stability reinforced concrete shear walls were added in some floors, finally part D has been isolated at the base.

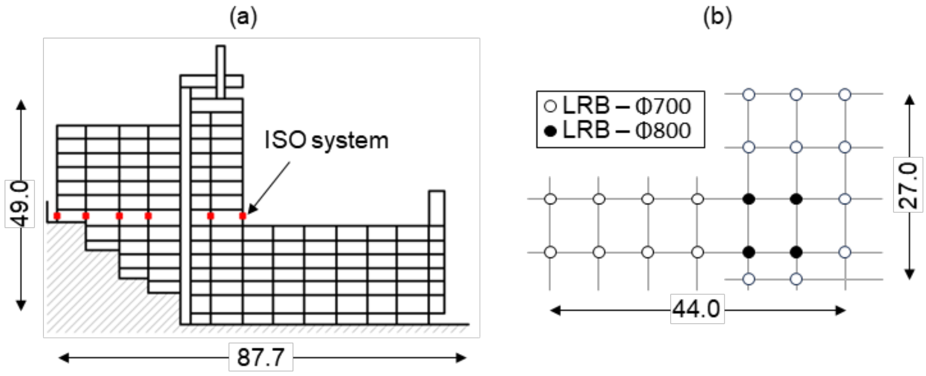

Figure A.4. (a) section of building part B and C; (b) layout of isolators for building part C. [redrawn from [33]].

The Intermediate isolation level in building C has been realised at the first non-underground floor, i.e., the seventh, and is achieved by cutting the existing columns and placing 22 LRB isolators with a diameter of Φ700-800 mm. With this intervention, the vibration characteristics of the building change from a natural fundamental period value of 0.40s and 0.45s to 3s and 2.96s (for an ISO shear deformation of 100%) in the X and Y directions respectively [33].

As reported in [33], from a preliminary linear response analysis the maximum acceleration and shear force (Figure A.5) in the US are reduced to 1/5 - 1/10 compared to the elastic response of the existing building. Moreover, thanks to this type of intervention, no reinforcement was necessary in the US and seismic loads were also greatly reduced in the LS [33].

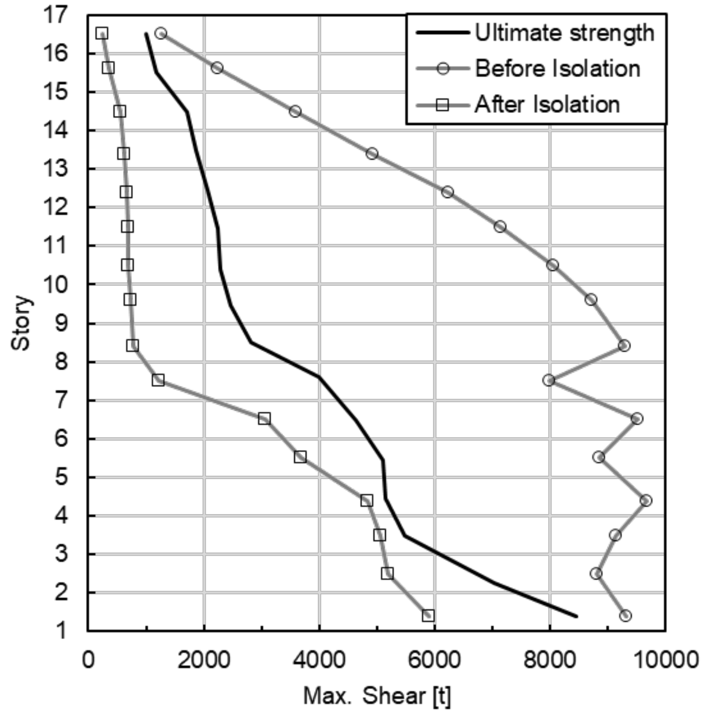

Figure A.5. Personnel Training Center of Taisei Corporation - Maximum shear force vs. story [redrawn from [33]].

The seismic retrofitting was carried out without the use of jacks, but by covering the existing columns with circular steel to expand column and temporarily supported the weight of the upper structure, preventing damage from differential displacements to the structure and keeping the building in operation (Figure A.6). The weight of the US is approximately 65000 KN. With this system, the seismic retrofit intervention was very quick, i.e. 9 months (August 1996 - April 1997).

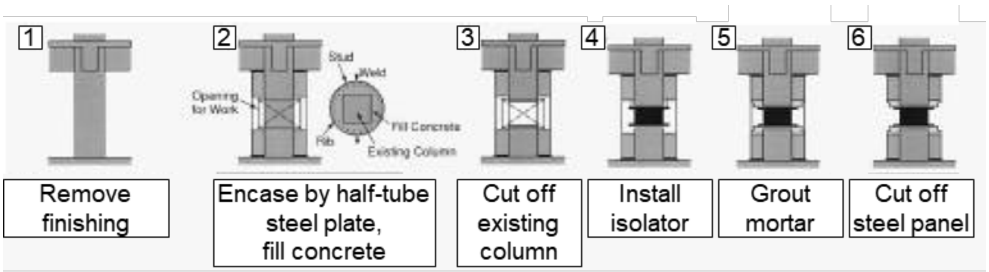

Figure A.6. Process for the realisation of the IIS. [redrawn from [33]].

Further interventions were then carried out on the building to avoid interruption of activities following an earthquake, i.e. special joints were inserted for the pipes passing through the isolation layer and a particular system for the elevator at floors around the isolation system.

A.2 Iidabashi 1st Building

All information reported in this section was derived from [13, 14, 29, 43, 132].

General information on the building is given in Table A.1.

The Iidabashi 1st Building (Figure A.7) is located in Tokyo and is a mixed-use building (Offices, condominiums and retail) with 15 floors above ground and 2 underground, the maximum plan dimensions are about 130 x 40 m for the LS and 130 x 15 m for the US. The isolation system is located between the ninth and tenth floors and is composed by 40 circular Natural Rubber Bearing (NRB) isolators of diameter Φ800 combined with 212 Lead Dampers (LD) of diameter Φ180. The part of the building below the isolation system is realised with steel beams, Shear Walls (SW) in the central bay and Steel Reinforced Concrete (SRC) columns, except for the first floors where there are Concrete-Filled Tube (CFT) columns. The part of the building above the Isolation System is made with reinforced concrete (Figure A.8).

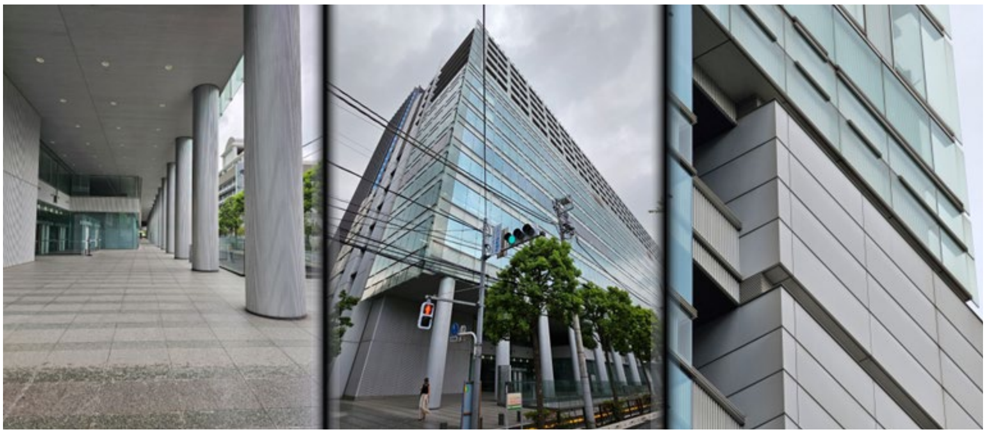

Figure A.7. external view of the Iidabashi 1st Building.

Figure A.9 shows the lumped mass model of the building with the corresponding mass and stiffness values. It can be seen that the mass ratio μ is equal to 0.22 and the equivalent viscous damping ratio for the LS and US is 2%. Consequently, with the mass of the US equal to 14921.2 kNm/s^2 and the stiffness offered by the NRB isolators alone equal to 0.053 GN/m the period of the isolation system is 3.33s.

The design parameter that is introduced for the design of the damping system is the volume of the damper, which is equal to the ratio between the damper yield strength and the weight of the upper floors, α_s, or it can be reported as the ratio between the damper yield strength and the total weight, α'_s. Therefore, a value of α'_s = 0.03 was adopted in the design, as an increase of this value would not lead to a further significant reduction in the maximum deformation of the isolation floor (Figure A.10).

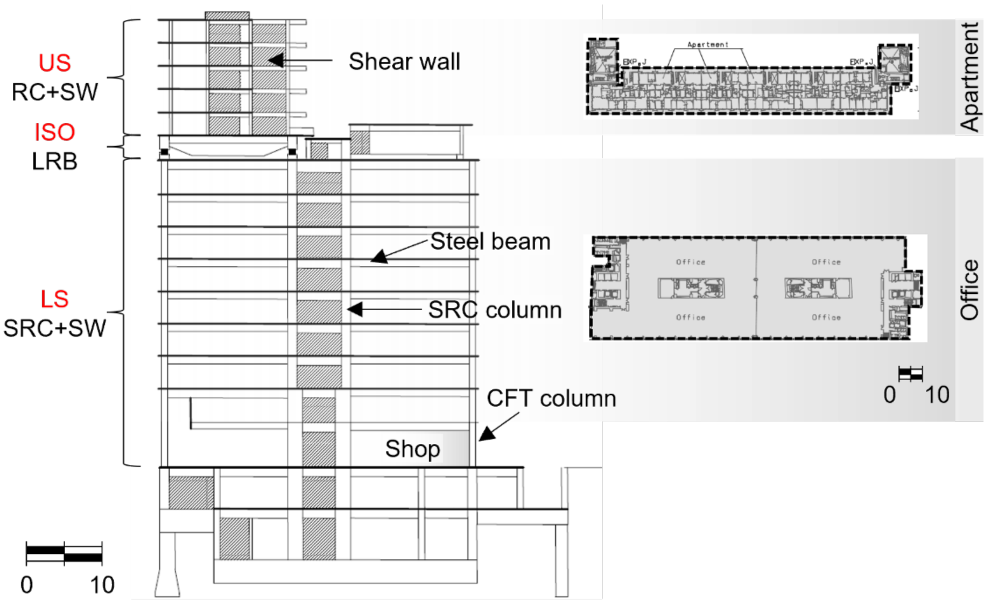

Figure A.8. Elevation View of the Iidabashi 1st Building. [redrawn from [29]].

ISO

Node	Mass [kNs²/m]	Stiffness [GN/m]
15	1657.9	9.4
14	2305.4	16.6
13	2305.4	20.1
12	2315.2	22.9
11	2315.2	34.4
10	4022.1	*
9	12704	7.2
8	4914.8	7.5
7	4914.8	8
6	5091.4	8.5
5	5179.7	9.1
4	5189.5	9.8
3	5209.1	11
2	5532.8	12.8
1	5434.7	12.3

* NRB: 0.0530 GN/m; LD: 1.6251 GN/m.

Figure A.9. concentrated mass model of the Iidabashi 1st Building [redrawn from [132]].

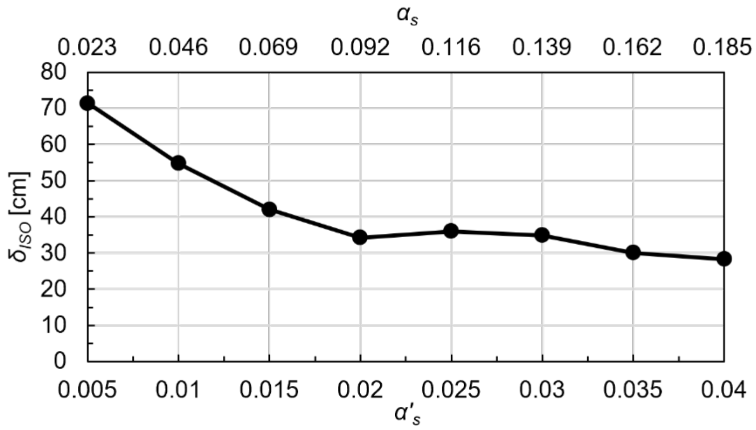

Figure A.10. ISO displacement vs. damper volume [redrawn from [29]].

A.3 Kudan, Post Office and Housing

All information reported in this section was derived from [36, 37].

General information on the building is given in Table A.1.

The building investigated here is a post office and housing building (Figure A.11) located in Tokyo. This building was constructed in 1967 in accordance with the seismic design standard in force at the time. The building has 10 storeys above the ground, the first five of which are in steel reinforced concrete (SRC) and the remaining floors are in reinforced concrete system, with an approximately rectangular floor plan shape with dimensions of 44 x 19 m. In 1995, following a seismic inspection, the building was found to be inadequate for the current seismic regulations and consequently it was decided to retrofit it. However, since this building had a public function, i.e. a post office, an intermediate level of isolation was chosen as the intervention technique, since compared to traditional seismic retrofitting techniques (i.e., installation of shear walls or steel bracings on each floor of the building), it allowed the activities inside the building to continue without disruption. In addition, the use of classical retrofitting techniques also required the retrofitting of existing foundation, which significantly increased the intervention costs. Instead, a base seismic isolation solution involved the problem of excavating around the existing building. However, in the case of IIS, there remains the problem of a high deformation demand of the isolation layer (approximately 50-60 cm), which implies a massive reinforcement of beams and columns on the first floor in order to deal with an increase in stresses due to eccentric loading. Therefore, in order to reduce the displacements of the isolation layer the damping devices are inserted, namely Viscous Damping Walls (VDW) (Figure A.12a). This system made it possible to significantly reduce the displacement of the isolation system, which for a level 2 earthquake defined by Japanese standards led to a displacement less than 25 cm.

The design of the intervention started in September 1998, while retrofitting works started in March 1999 and was completed in November 1999. Making the building one of the first examples in Japan of a building with IIS.

In order to obtain a building with IIS, all 30 columns between the first and second floors were cut (Figure A.12b, c) and then an equal number of NRB isolators (28 with diameter Φ600 and 2 with diameter Φ700) were inserted, with a horizontal stiffness at 100% deformation of 0.021 GN/m. As far as damping devices 18 VDW were installed (Figure A.12d). Consequently, it is possible to estimate the isolation period of 3.6 s in a simplified way (i.e. by approximating the mass of the building above the isolation system). In [37] it is reported that the fundamental period of the whole building is 3.4 s for both directions, which is very close to the approximate estimated value for T_{ISO}.

Figure A.11. External view of Kudan, Post Office and Housing [License: Image © 2024 Google, Landsat / Copernicus].

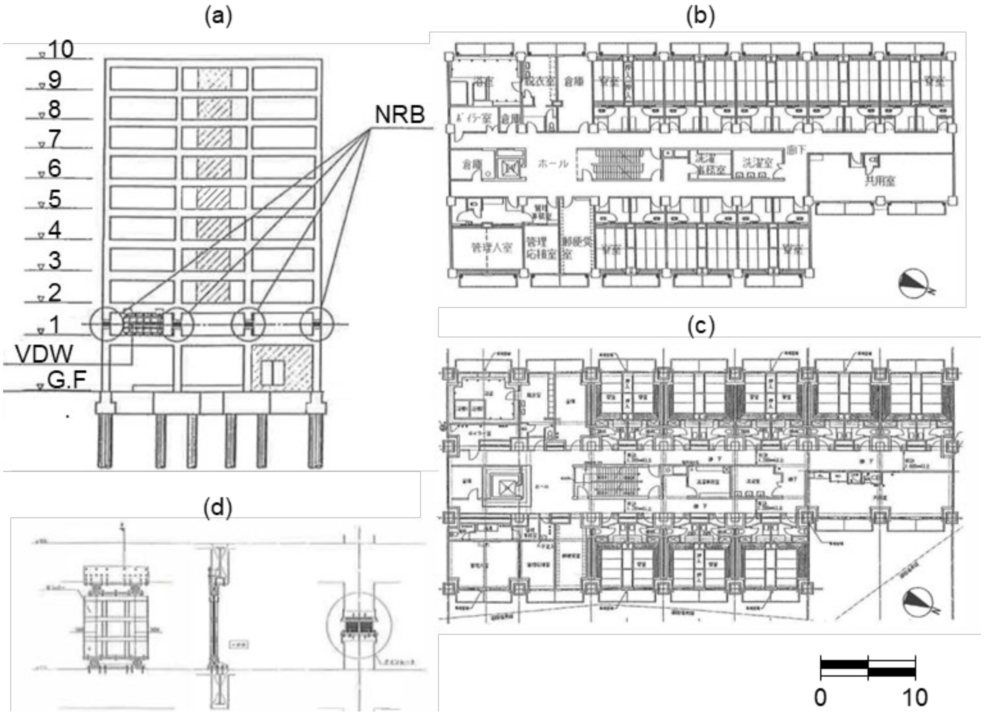

Figure A.12. (a) elevation view; (b) floor plan before intervention; (c) floor plan after intervention; (d) detail of the intervention type. [redrawn from [37]].

A.4 Shinjuku station (West Exit)

All information reported in this section was derived from [147].

General information on the building is given in Table A.2.

The building analysed in this paragraph is located above the west exit of Shinjuku Station in Tokyo. The building in Figure A.13, designed in 1962 and constructed in 1966, is composed by three different blocks, namely A, B and C in Figure A.14. The three different blocks although functionally connected are structurally independent. Building A, analysed in this section, has 9 floors above ground and 2 underground, the ground floor is occupied by the Odakyu line while the upper floors are destined to restaurants and commercial facilities. The building is a reinforced concrete frame system that was later seismically retrofitted by inserting an ISO system between the second and third floors above ground (Figure A.14). The retrofit intervention involved the insertion of 12 natural rubber isolators (NRB), 8 of which with diameter Φ650 and 4 with diameter Φ700, 20 Lead Rubber Isolators (LRB) with diameter Φ650 and 8 oil dampers (OD), four in each principal direction in plan. In addition, the distance between buildings A and B is increased from 8 cm to 40 cm in order to avoid collisions between the two buildings. The steps to carry out the intervention can be summarised in the following steps: 1) removing the finishing layer of the floor near the column; 2) installing a steel plate on the floor near the column and at the base of the column; 3) installing a temporary steel structure at the base of the column; 4) inserting jacks between the temporary supports and the beams at the other end of the column; 5) after the jacks are activated, the existing column is cut; 6) installation of two steel plates above and below the cut zone; 7) installation of the isolator between the two steel plates; 8) removal of the jacks and temporary steel structures.

In [147], the analysis results performed on the 3D FE models of the building are reported, which show an excellent response of the system after the retrofitting with IIS. In fact, it shows a deformation of 14 cm of the ISO layer for a Level 2 earthquake and inter-storey displacements for the US less than 1/500 of the inter-storey height.

Figure A.13. External view of Shinjuku station. [License: Image © 2024 Google, Landsat / Copernicus Data SIO, NOAA, U.S. Navy, NGA, GEBCO Data Japan Hydrographic Association].

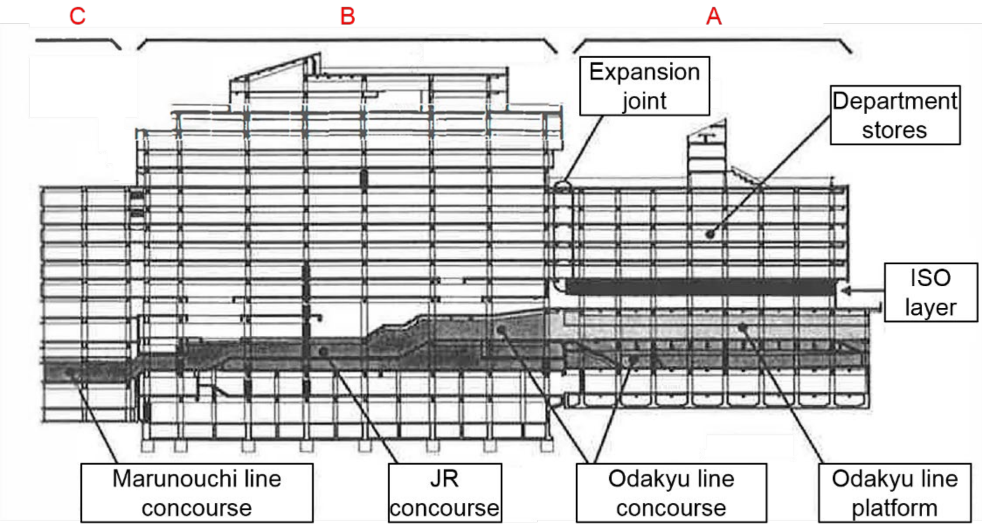

Figure A.14. Elevation View of Shinjuku station. [redrawn from [147]].

A.5 Umeda DT Tower

All information reported in this section was derived from [133, 134].

General information on the building is given in Table A.2.

The building analysed here is the Umeda DT (Figure A.15) located near Osaka station, it has 28 floors above ground and 4 floors below ground (Figure A.16a) for offices and shops. Construction of the building began in 1991 and was interrupted following the Kobe earthquake in 1993. The interruption of the building's construction was necessary in order to revise the initial project with more attention given to the safety of the structure, the reduction of damage to the interior components and the preservation of the building's functionality following the earthquake. Therefore, the initial project was modified, and construction was resumed at the end of 2000 and completed in January 2003. The floor plan of the building is approximately rectangular with dimensions of 56 x 28 m (Figure A.16b).

The building has an ISO system located above the large atrium on the ground floor, at a height of 10.5 m. So, in this case for the Umeda DT, it was decided to adopt an ISO system at an intermediate level to meet the new requirements for buildings after the Kobe earthquake (i.e., reducing damage to structures and internal equipment and maintaining the building's functionality after the earthquake).

The structural system of the above-ground building is a steel frame. Whereas the ISO system is realised with 6 LRB isolators of square shape and variable size between 1100 x 1100 mm and 1350 x 1350 mm associated with 12 linear sliders (LS) and 6 dampers of the Lock-Up Devices type (Figure A.16c). The ISO period evaluated considering the equivalent stiffness of the isolator at 100% deformation is 6 s.

In addition to an accelerometer located above the ISO system, an anemometer is also installed on the roof. The data recorded by the anemometer influence the operation of the Lock-Up Devices dampers. In fact, these dampers have a damping function during an earthquake, behave like normal oil dampers, but when the wind speed exceeds 25 m/s (value intended as the average burst in 10 minutes) the device behaves like a jack, preventing the ISO system from moving.

Finally, to reduce wind-induced vibrations at the top of the building is placed a mass that works as a TMD.

Figure A.15. External view of Umeda DT Tower [Autor: Oilstreet, license: GFDL+creative commons2.5].

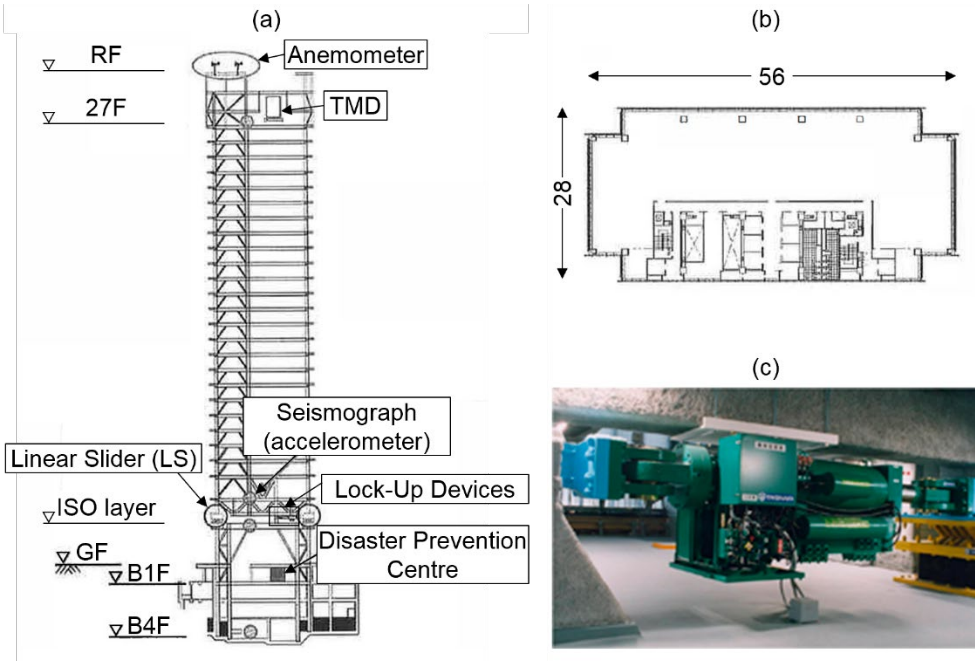

Figure A.16. Umeda DT Tower: (a) Elevation View [redrawn from [133]]; (b) floor plan [redrawn from [133]]; (c) Lock-Up Devices [License: ©Copyright 1995-2023, Takenaka Corporation, source: [134]].

A.6 Shiodome Sumitomo building

All information reported in this section was derived from [13, 14, 38, 132].

General information on the building is given in Table A.2.

The Shiodome Sumitomo building (Figure A.17a) is a 25-storey building constructed in 2004 with maximum plan dimensions of 109.6 x 39.5 m and located near the Shiodome station in Tokyo. The structural system of the building is a steel frame with CFT columns. A distinctive element of the building is the large atrium with a glass façade located at the entrance and approximately 40 m high (Figure A.17b, c). The remaining part of the ground floor plan, where the atrium is located, is destined for a hotel (Figure A.18a, d). Above the atrium, between the tenth and eleventh floors, we find the ISO system, consisting of 41 NRB isolators of which 13 with diameter Φ1300, 19 with diameter Φ1100 and 9 with diameter Φ1000, in addition there are

100 LD and 14 Steel Dampers (SD) (Figure A.18c). Above the ISO layer the destination of use of the building becomes offices (Figure A.18b).

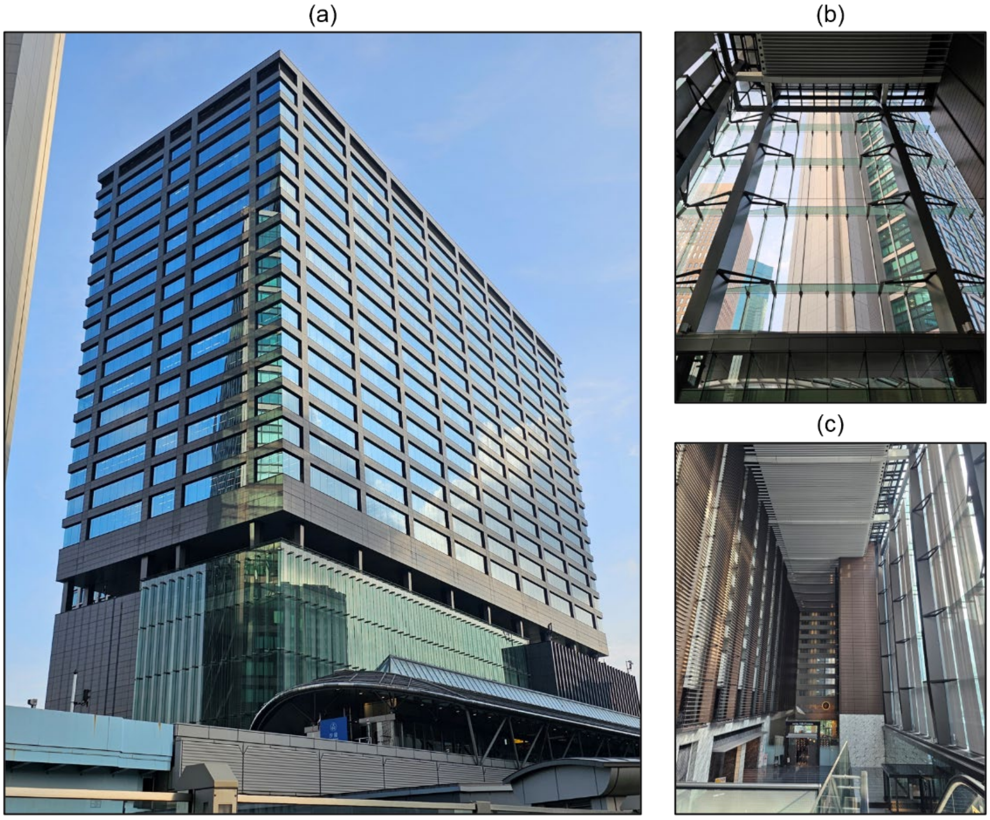

Figure A.17. Shiodome Sumitomo building: (a) External view; (b) façade system; (c) atrium.

In Figure A.19 the concentrated mass model of the building is shown with its mass and stiffness values [38], as a result, it can be seen that the mass ratio μ is equal to 2, while the isolation period is about 5s (considering only the NRB isolators contribution), for a design displacement of 50mm. However, in [38] a modal analysis on the 25-DOF model shows a first mode for the system equal to 6s, thus, slightly higher than T_{ISO}.

The dampers are designed both to provide the most suitable seismic shear force for the response to seismic loads and to prevent severe deformation of the isolation layer under a strong wind load while remaining in the elastic field. Furthermore, the entire building design allowed both US and LS to remain in the elastic field even under a strong earthquake. Finally, the number of dampers was evaluated as a function of the yield capacity of the dampers assessed through the damping volume, α'_s set equal to 0.03 and as a function of the design wind action.

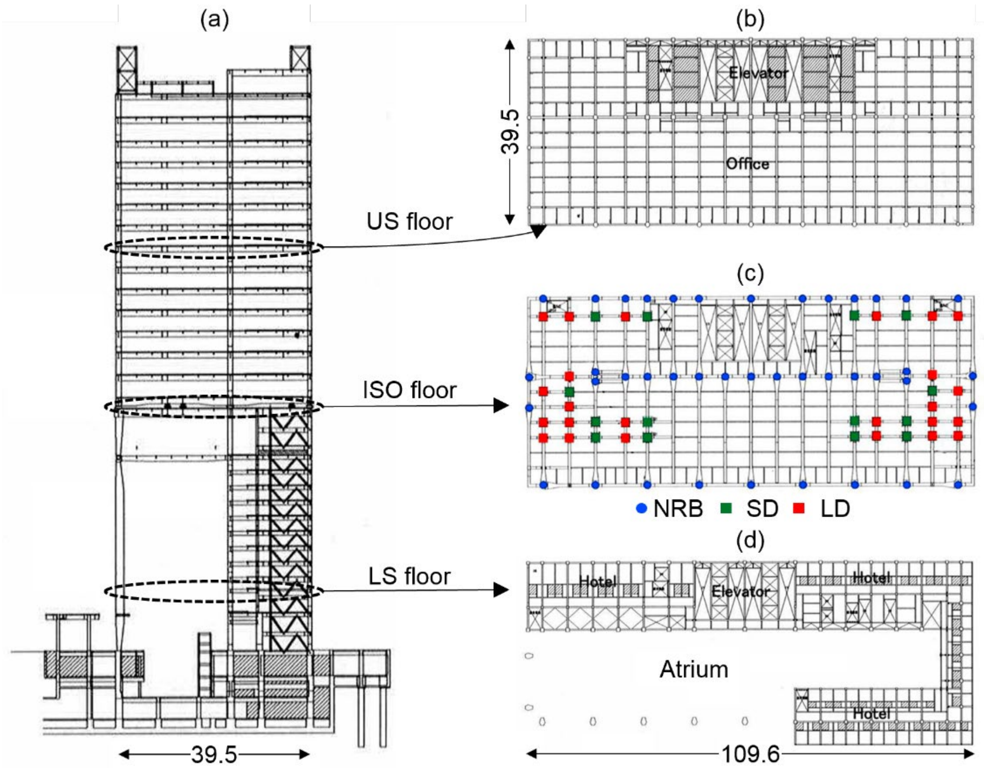

Figure A.18. Shiodome Sumitomo building: (a) elevation view [redrawn from [38]]; (b) upper structure floor plan [redrawn from [38]]; (c) isolation floor plan [redrawn from [132]]; (b) lower structure floor plan [redrawn from [38]].

During a strong earthquake, the storey drift of both US and LS is less than 1/200. While for the glazed façade of the atrium the drift angle is 1/150. The 40 m high atrium columns are designed to remain elastic and only work under gravity loads through a pin connection at the base. In the 26-DOF model shown in Figure A.19, an equivalent viscous damping of 2% was assumed for the LS and US.

In [38], TH analyses are conducted on the 26-DOF model for three different ground motions with a 500-year return period. The results of these analyses show: (i) a maximum displacement of the ISO system is about 30 cm; (ii) the maximum absolute acceleration is occurred at the plane immediately below the ISO system; (iii) the displacement of the LS increases together with the displacement of the ISO system, while the US does not show large displacements; (iv) almost all of the incoming seismic energy (about 70-80%) is dissipated as hysteretic energy in the isolation layer.

Node	Gravity [kN]	Stiffness [kN/mm]
25	56580	1511
24	33950	1734
23	33810	2111
22	30170	2168
21	30250	2240
20	30350	2336
19	30570	2486
18	31070	2484
17	31090	2586
16	30650	2589
15	30720	2652
14	30800	2631
13	31250	2321
12	34990	3106
11	39530	*
Isolation story	30680	1083
10	30670	4452
9	16880	4791
8	16650	4953
7	16850	5204
6	16820	5361
5	16830	5707
4	17000	5923
3	16930	6344
2	25330	2675
1	30210	3178

* NRB:0,0807 GN/m; LD: 2.62 GN/m; SD: 0.0678 GN/m.

Figure A.19. concentrated mass model of the Iidabashi 1st Building [redrawn from [38]].

A.7 China Basin 185 Berry Street Building

All information reported in this section was derived from [18, 19, 132].

General information on the building is given in Table A.3.

The building analysed in this section is the China Basin Landing, 185 Berry Street in San Francisco, USA (Figure A.20); this is one of the few cases of the application of IIS for the vertical extension and seismic retrofitting of an existing building. The retrofit intervention was completed in 2007.

Figure A.20 External view of China Basin
[source: Wikimedia; license: https://creativecommons.org/licenses/by-sa/4.0/]

The existing building is a reinforced concrete building with three storeys above ground level, constructed in 1989 and with a rectangular floor plan shape with dimensions 252 x 33.5 m. Due to the large floor extension, the building is divided into three parts structurally divided by two expansion joints (Figure A.21). The central part of the building is made up of reinforced concrete walls, whereas the remaining two parts have a horizontal load-resistant system consisting in six reinforced concrete frames along each principal plan direction (Figure A.21).

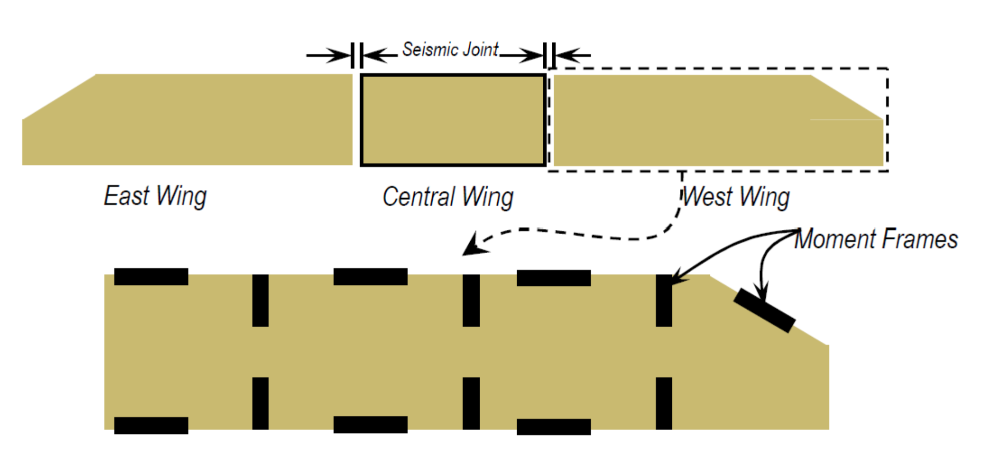

Figure A.21. Floor plan of the China Basin Building. [source: [18]]

The existing building was designed in 1988 in accordance with the 1984 San Francisco Building Code, based on the 1979 Uniform Building Code (UBC). However, the possibility of vertical extend the building by one storey, which corresponds to an increase of 4645 m^2, was already included in the initial design. Thus, the entire structural system had overstrength against both gravity and horizontal loads. Further analysis on the building showed that approximately 8400 m^2 could be added on top of the building without seismic retrofitting of the building. However, the building owner request was to extend the existing building by at least 13500 m^2, which, if realised by means of a conventional vertical extension technique, would have required the construction of new shear walls within the existing building. But the building owner also demanded that during the vertical extension and retrofitting of the existing building, there should be no disruption to the occupant's activity, as the building mainly accommodated the bioscience laboratories of the University of California at San Francisco (UCSF).

The use of the IIS made it possible to add the required 13500 m^2 on the roof of the existing building without having to carry out seismic retrofitting inside the building. In addition, a steel Concentric Braced Frame (CBF) system was used in order to avoid foundation retrofitting for the vertical extension. Therefore, a steel CBF system of two storeys plus a roof deck was built on the roof of the existing building, connected to the existing building by means of a seismic isolation system. In particular, in order to avoid differential seismic inputs on each isolator and to leave active most of the HVAC equipment present on the roof, two girder trusses connecting the ends of each isolator are realised (Figure A.22). In addition, damping devices were placed on the roof at the existing expansion joints to avoid hammering between the different parts of the existing building.

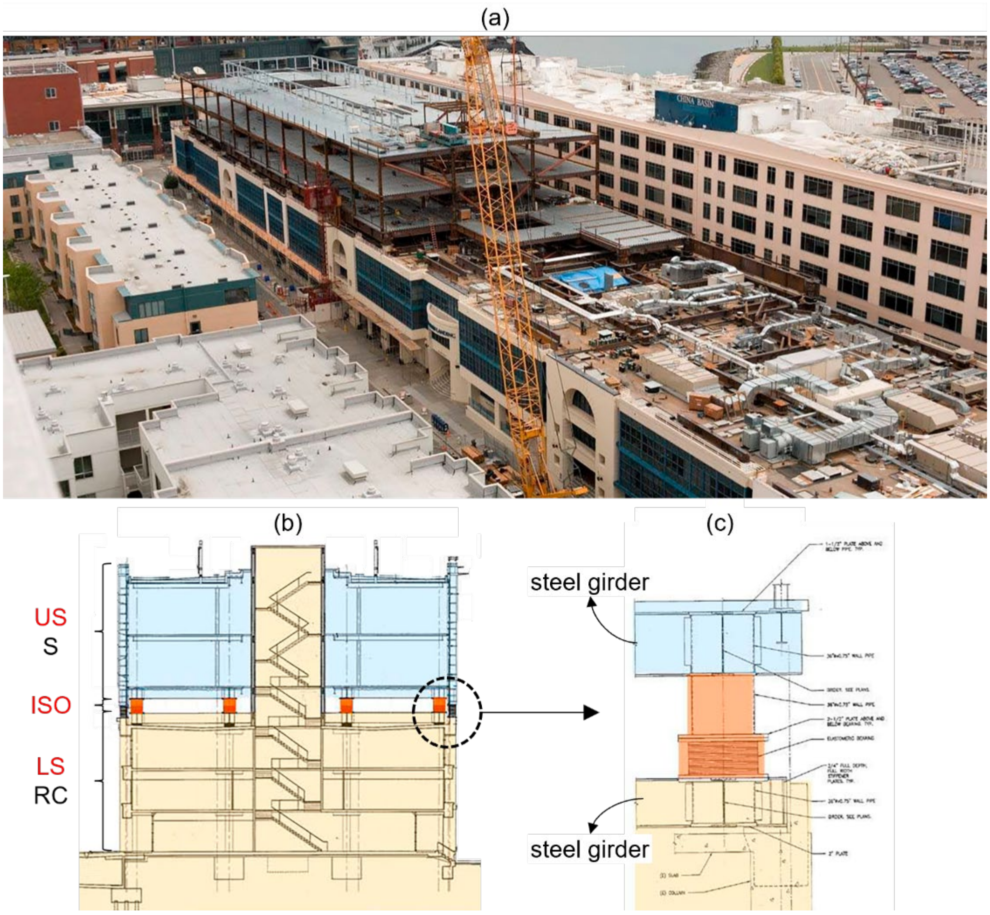

Figure A.22. China Basin: (a) Isolated upper structure under construction; (b) elevation view; (c) Detail of ISO system connection. [redrawn from [19]]

The isolation system consists of 87 isolators, of which 33 LRB isolators with a diameter of Φ1140 mm and 54 elastomeric slider bearings (ESB) made up with LRB isolator (diameter of Φ610 mm and 130 mm lead core) combined in series with 300 mm diameter of Polytetrafluoroethylene (PTFE) sliding surfaces. In this latter solution, the PTFE sliders provide a displacement of +/- 0.76 m, to which is added the additional displacement of 0.38 m, accommodated by the elastomeric isolator, until a displacement of 1.14 m is achieved, equal to 1.5 times the maximum displacement of 0.76 m. Next, in order to achieve the correct balance between stiffness and displacement demand in the isolation layer, the 33 LRB isolators were placed along the exterior alignments to maximise the torsional stiffness/resistance, while the 54 ESB isolators were placed in the interior alignments.

Several analyses conducted on the 3D FE model of the IIS building are reported in [18], the results of which can be summarised as follows: (i) the LS exhibits non-linear behaviour under the seismic design loads; (ii) the reliability level at the collapse prevention or life safety limit state, assessed through Incremental Dynamic Analyses (IDA), is higher than that of a new building designed according to the current regulations; (iii) the absence of adequate damping devices between each part of the LS results in the hammering between the parts.

A.8 Musashino City Disaster Prevention and Safety Center

All information reported in this section was derived from [13, 14].

General information on the building is given in Table A.3.

The Musashino City Disaster Prevention and Safety Center is a building located in the western outskirts of Tokyo and currently has seven storeys above ground. In fact, the building originally had two above-ground storeys (including the roof floor) made of steel reinforced concrete (SRC) with low seismic performance (Figure A.23a). Subsequently, a further four storeys plus one roof floor was added in steel (Figure A.23b), connected to the existing building by an isolation system consisting of, 8 NRB isolators with a diameter of Φ700, 12 elastomeric sliders (ESB) and 8 Steel Dampers (SD). The mass ratio μ for the vertical extension is approximately 1.7.

The building with IIS shows excellent seismic performance such that it can maintain its function as a disaster prevention centre even in the occurrence of a strong earthquake. In addition, the installation of an isolation system between the existing building and the new part made it possible to limit retrofitting work on the existing building, without disrupting activities within it.

(a) (b)

Figure A.23. External view of Musashino City Disaster Prevention and Safety Center: (a) before vertical extension; (b) after vertical extension. [redrawn from [13]].

Figure A.24 shows the elevation view of the building with IIS, where it can be seen that compared to the as-is configuration of the building, an upgrade of the foundations and an increase in the thickness of the shear walls was also carried out.

A ratio between the yield strength of the damper and the total mass of the building, α'_s, equal to 0.04 was adopted for the design of the damping devices. In addition, TH analyses were conducted in [13] on an 8-DOF model of the building with IIS, where equivalent viscous damping value of 2% and 3% was adopted for US and LS respectively. The results of the TH analyses confirmed the excellent seismic performance of the building with IIS, showing that the maximum shear force at each floor is reduced by ½ to ¼ of the forces evaluated in the absence of ISO system between the LS and US, and both the LS and US remain in the elastic field under all seismic waves considered.

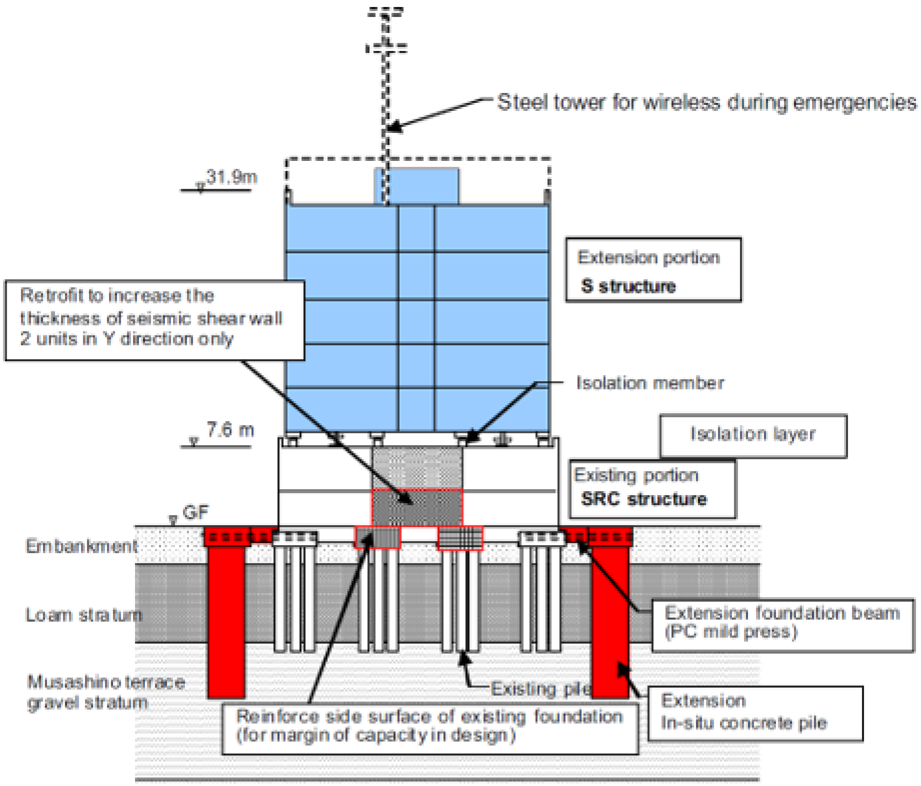

Figure A.24. Elevation view of Musashino City Disaster Prevention and Safety Center. [redrawn from [13]].

A.9 Fukuoka Financial Group Headquater

All information reported in this section was derived from [13, 42].

General information on the building is given in Table A.3.

The Fukuoka Financial Group Headquater is an 86 m high building located in the city of Fukuoka in Japan, characterised by a large open plaza at the base about 16 m high. The building has a regular floor plan shape with 40 x 52.2 m and is designed to accommodate offices.

The structural system is divided into two parts by the ISO system located at 22.5 m height, above the large open plaza, i.e. the LS and the US. The two parts of the building are steel frame system. A rough estimate of the mass ratio showed a value of 6 as a result. The ISO system is realised by means of 16 NRB isolators with a diameter of Φ1100, 4 ESB isolators and 4 dampers (it was not possible to determine the type of dampers). The isolation period for an isolator deformation of 200% is 4 s. Non-linear TH analyses on the building with IIS showed for the US a maximum displacement angle at each floor of 1/258 for the 40.0 m side direction and 1/318 for the 52.2 m side direction.

Figure A.25. External view of Fukuoka Financial Group Headquater [source: Wikimedia; license: https://creativecommons.org/licenses/by-sa/4.0/]

A.10 NBF Osaki building

All information reported in this section was derived from [13, 148, 149].

General information on the building is given in Table A.4.

The NFB Osaki building (Figure A.26) is a 24-storey building above ground level, with a maximum height of 134.1 m, completed in 2011 in Tokyo and has an isolation system on the first level above ground level (orange layer in Figure A.27), at a 5.1 m height. The structural system below the ISO system is reinforced concrete, while the structure above the ISO system is a steel frame. The building has a rectangular floor plan with dimensions of 131.4 x 50 m for the LS, which is reduced to 131.4 x 39 m for the US. Consequently, a mass ratio μ can be estimated at approximately 15. Furthermore, the fundamental period of the building without ISO is 3.5 s.

Figure A.26. External view of NBF Osaki Building [source: Wikimedia; license: https://creativecommons.org/licenses/by-sa/4.0/]

However, for the NBF Osaki Building, the ISO system on the first level achieved a large reduction in displacements (drift angle less than 1/200) and accelerations (less than 250 cm/s^2) along the height of the building compared to the case of an earthquake-resistant building without an ISO system. Furthermore, due to the large floor plan extension of the building and the presence of the ISO system on the first floor, the wind loads are greater than the seismic loads for the building. Therefore, in the design of the structural system to provide sufficient safety against both types of natural actions, oil dampers with a locking mechanism in the dominant wind direction controlled by anemometers located at the top of the building, ISO system strain and velocity measuring devices along the height were used. In particular, the locking system is activated when a strong wind speed or a high displacement of the ISO system is registered, whereas it is released when an earthquake is detected. The isolators placed in the building are NRB with a diameter varying between Φ1100 and Φ1500 coupled with steel dampers (SD). In addition, V-shaped visco-elastic members are added to the short side of the building to improve the vibration damping capacity in the US.

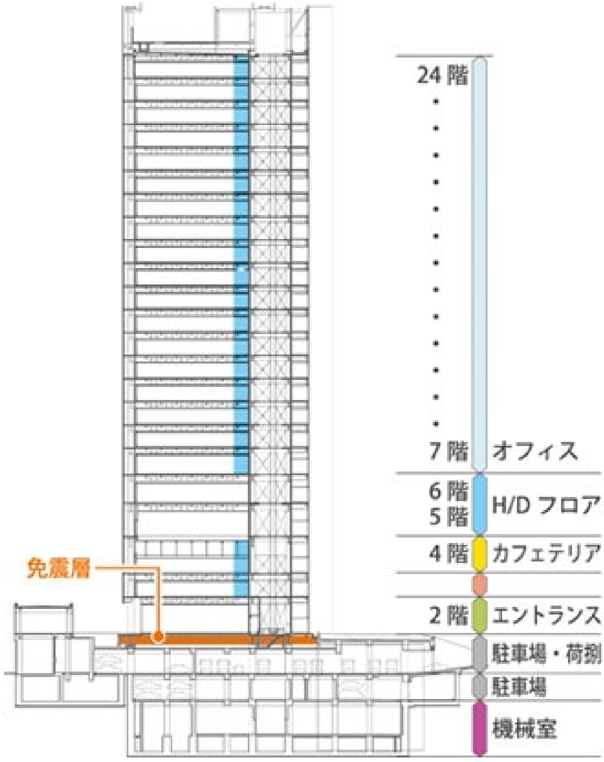

Figure A.27. Elevation view of NBF Osaki Building. [license: Copyright (C) 1995–2024 KAJIMA CORPORATION All Rights Reserved].

A.11 Mita Bellju building

All information reported in this section was derived from [13, 150 – 152].

General information on the building is given in Table A.4.

The Mita Bellju building (Figure A.28a) is located in Tokyo near the JR Tamachi station and is composed by 33 floors above ground plus 4 basement floors, the maximum height reached by the structural system of the building is 152.1 m (Figure A.28b). The building was completed in 2012 and has different destinations of use such as shops on the first levels, office space on the intermediate floors and housing on the upper floors. Consequently, the floor plan dimensions also vary along the height, showing a dimension of 39 x 39 m for the intermediate floors and a dimension of 25 x 25 m for the upper floors. The plan changes dimensions at the ISO layer located at 114 m height, between the 24th and 25th floors (Figure A.28b). This ISO system is composed by 23 NRB isolators (Figure A.29a) combined with 12 oil dampers (Figure A.29b) whose function is to cancel any residual displacement in the isolation layer following earthquakes or strong winds. The structure under the ISO system, i.e. the LS is a steel frame with CFT columns, while the US is a reinforced concrete frame. Therefore, the isolation period can be estimated to be approximately 4 s [150] and the mass ratio to be approximately 0.4.

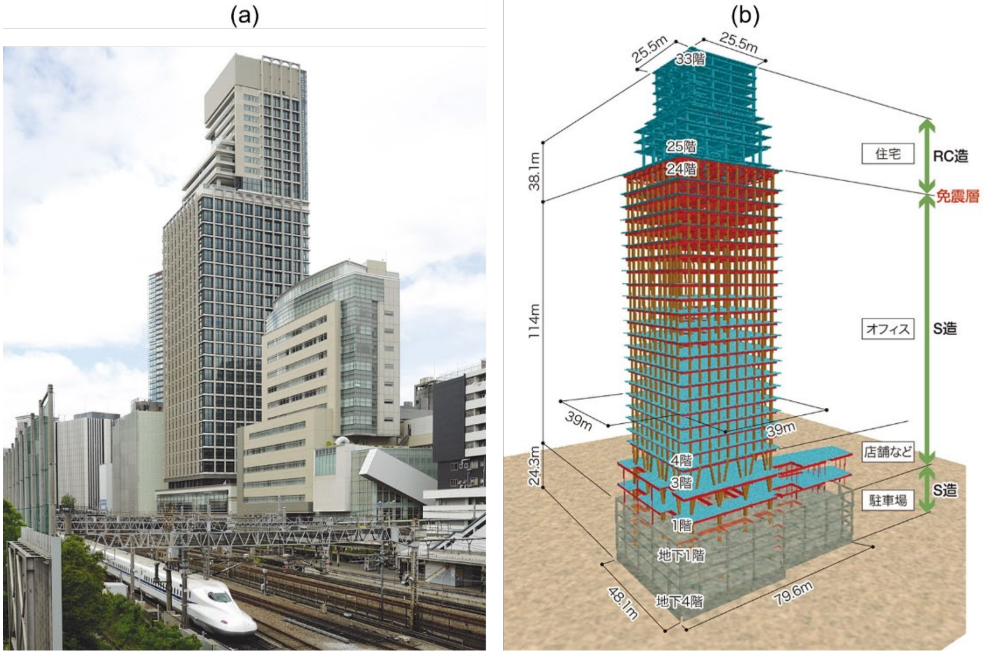

Figure A.28. Mita Bellju building: (a) external view [Autor: Nikkei Architecture; source: [150]; license: Copyright © Nikkei Business Publications, Inc. All Rights Reserved]; (b) structural layout [Autor: Nikkei Takenaka Corporation; source: [150]; license: Copyright © Nikkei Business Publications, Inc. All Rights Reserved].

As indicated in [150], the choice of using a reinforced concrete frame for the US was due to the need to reduce vibrations induced by natural actions and to obtain greater living comfort. On the other hand, the choice of placing a layer of ISO between the 24th and 25th floor had a twofold positive effect, i.e. it regularised the structural behaviour as the building had a strong geometry variation along the height and used the mass of the isolated US as a mass damper for the LS. Considering a damping ratio in the ISO layer of 23%, the seismic analyses reported in [150] show that the maximum drift angle of the story response is approximately 1/125. Furthermore, the solution with IIS compared to the solution with seismic isolation at the base was more economical as it avoided the need to perform the tolerance excavation around the large underground parking structure.

Great attention, as usual for IIS systems, was given to the design of the elevator, which was connected to the LS structural system (Figure A.29c), leaving a tolerance of 60 cm with the US, equal to 1.4 times the maximum displacement induced by a level 2 earthquake.

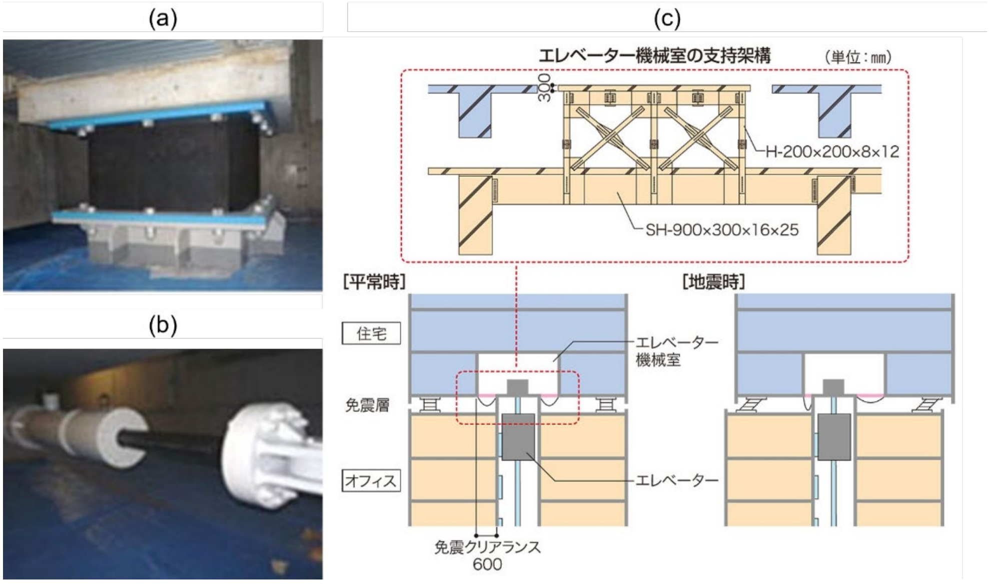

Figure A.29. Mita Bellju building: (a) isolator device [source: [150, 151]; license: ©Copyright 1995-2024, Takenaka Corporation]; (b) oil damper [source: [150, 151]; license: ©Copyright 1995-2024, Takenaka Corporation]; (c) detail of the connection of the elevator in the IIS [source: [150]; license: Copyright © Nikkei Business Publications, Inc. All Rights Reserved].

A.12 Nakanoshima Festival Tower

All information reported in this section was derived from [13, 30, 39, 132, 135].

General information on the building is given in Table A.4.

The Nakanoshima Festival Tower (Figure A.30a) accommodates the new Osaka Festival Hall (Figure A.30b). The old building of the Festival Hall was constructed in 1958 and demolished in 2008, after 50 years of activity. The construction of the current building began in 2010 and was completed in 2012, reaching a height of approximately 200 m with 39 storeys above the ground. The building has a mixed use, i.e. in addition to the reconstruction of the Festival Hall, the basement floors are used for shops, on the 12th floor above the ground there is a sky lobby (Figure A.30c), on the top floors there are rooftop restaurants, and the floors between the sky lobby and the rooftop restaurants are used for offices (Figure A.31). Floor plans of the different storeys of the building and an architectural section are shown in Figure A.31, where it can be seen that a isolation system is located above the Festival Hall. The ISO system divides the building into two parts, the LS, realised with reinforced concrete shear walls associated with a SRC structure and the US realised with a steel structure (Figure A.32a). In particular, in order to obtain a large hall without columns, first an ISO system and then a mega steel transfer beam was placed above the festival hall, as shown in Figure A.32b. While the US structural system is composed by a central system in steel moment resisting frame (MRF) with braces and viscous damper and a perimeter system in steel moment resisting frame. In addition, there is a hat-truss at the top of the building, while at the base of the US there is a belt-truss whose function is to collect the gravity load of the entire perimeter system and transfer it to the 16 principal columns with a cross-section of 3 x 1.5 m.

Figure A.30. Nakanoshima Festival Tower: (a) external view; (b) Festival Hall entrance; (c) Sky Lobby.

Another feature of the Nakanoshima Festival Tower is the mega-truss: a 20 m high three-dimensional steel structure that transfers the load of the central columns of the US to principal columns (Figure A.32a).

The ISO system is obtained by means of 66 LRB isolators of which 32 with a square section of 1500 x 1500 mm and 34 with a circular section of Φ800÷1000, combined with 24 oil dampers (OD), 12 for each principal direction of the plan (Figure A. 30c). From Figure A. 30c, it can be observed that two square-section isolators are located under each principal column, supporting 95% of the weight of the entire building. Consequently, the circular isolators support the remaining 5% of the building's weight. Furthermore, it can be seen from Figure A. 29 and Figure A. 30a that the ISO system follows the shape of the lower festival hall and is placed on different levels. Therefore, in order to avoid contact between the isolated structural elements and the fly tower of the festival hall (Figure A. 30c), a tolerance of 750 mm was insert.

From the above considerations, it is possible to estimate both the mass ratio of the building with IIS (i.e., μ) equal to 2.6 and the isolation period equal to approximately 3.6 s.

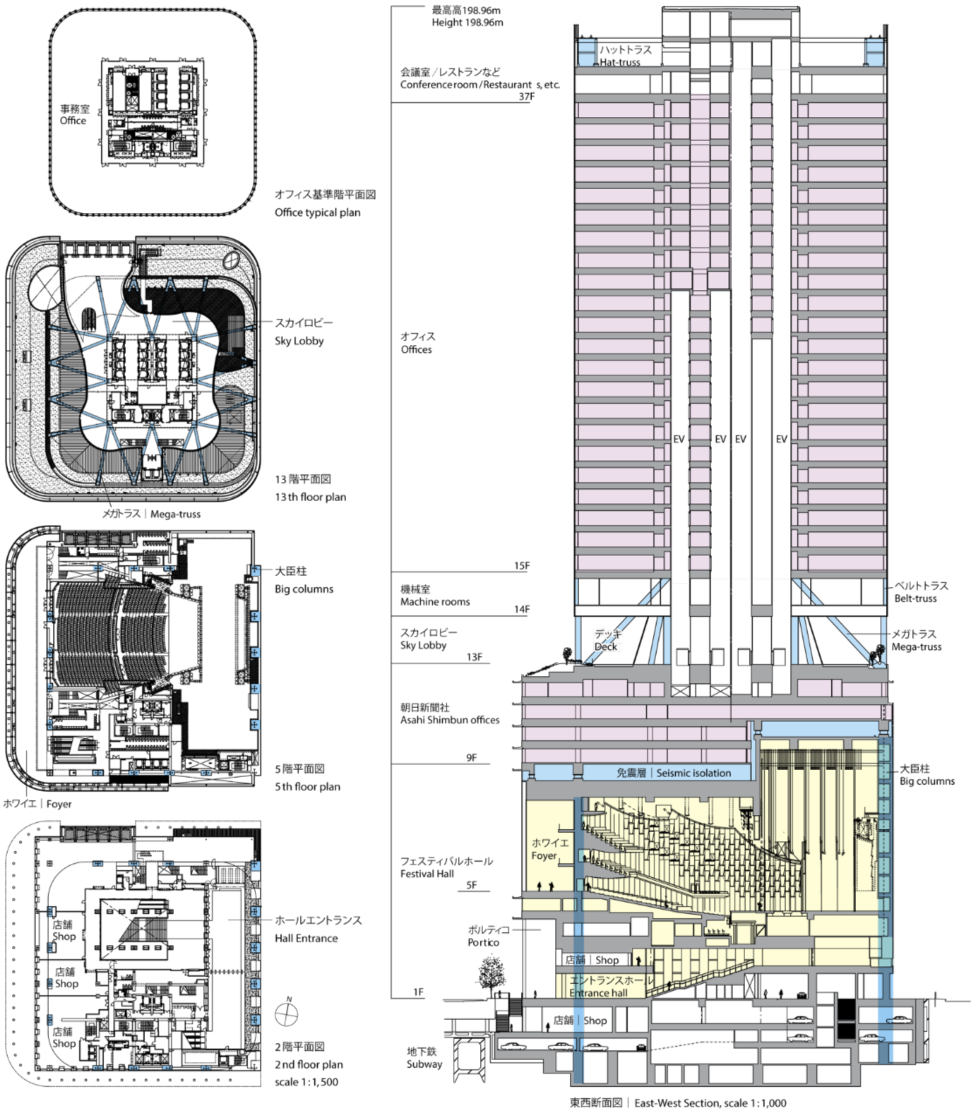

Figure A.31. Cross section of Nakanoshima Festival Tower [redrawn from [135]].

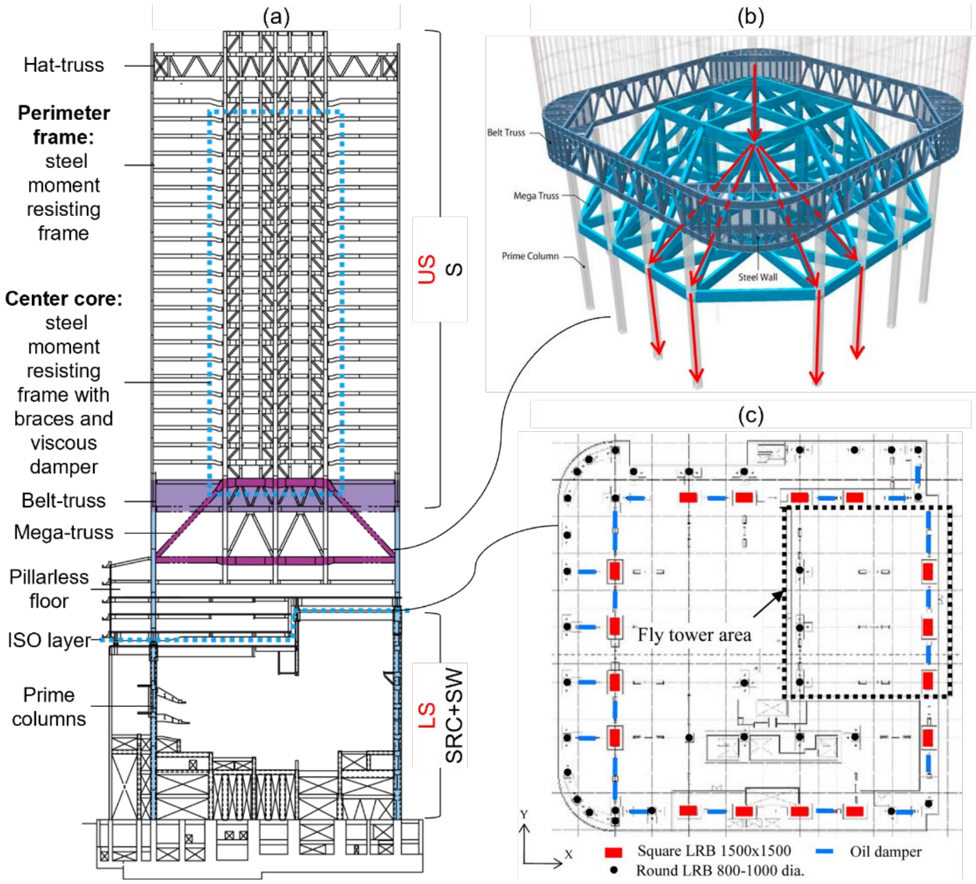

Figure A.32. Nakanoshima Festival Tower: (a) Cross-section of the frame [redrawn from [135]]; (b) 3D model of mega-trusses and belt trusses [redrawn from [30]]; (c) isolation floor plan [redrawn from [30]];

In order to evaluate the seismic behaviour of the building with IIS, non-linear TH analyses were performed in [20] on the 3D FE model of the building under a rare earthquake for level 1 and extremely rare earthquake for level 2, as defined in Japanese standard. Recall that, for level 1 earthquakes, a maximum storey drift angle of 1/300 for US and 1/800 for LS was considered as limit values in the design, whereas, for level 2 earthquakes, a maximum storey drift angle of 1/150 for US and 1/400 for LS was considered. Furthermore, for level 2 earthquakes, the maximum deformation of the ISO system considered is 400 mm. The results of these analyses can be summarised as follows: (i) the LS being an SRC structure is rather rigid, therefore, the seismic response is strongly amplified in the upper part of the hall; (ii) the IIS allows to reduce the acceleration at the upper floors approximately 25%; (iii) the maximum storey drift angle in the US is more than 30% lower than other office buildings; (iv) earthquakes classified as extremely rare by Japanese standards induce stresses in the structural elements that are lower than the permissible short-term stresses of the materials; (v) the use of the mega-truss prevents tensile stresses on the rubber bearings as a result of the overturning moment and the vertical seismic force.

A.13 Ochanomizu Sola City

All information reported in this section was derived from [153 – 155].

General information on the building is given in Table A.5.

The Ochanomizu Sola City (Figure A.33) is a 23-storey above-ground building, 110 m high, located near the JR Ochanomizu station in Tokyo. The building has a regular prismatic shape with a floor plan dimension of 79.2 x 48 m and has replaced a previous 78 m high building of 30 years old. In the construction of the new building, the project involved the construction of new foundation piles and the reuse of existing ones as there was no space for additional piles around the Chiyoda subway line located under the building. In fact, the building is built above two railway lines, the Marunouchi subway line and the Chiyoda subway line.

The building has a mixed use, where on the underground floors there is a car park and going upwards there are shops, a conference centre, educational facilities and offices (Figure A.34).

Figure A.35 shows the structural system of the multi-storey urban square in front of the building, where the level indicated as the ground floor is an artificial ground with a weight of 20 kN/m^2 obtained with a very high strength reinforced concrete (compressive strength of beams: 100 MPa, compressive strength of columns 250 MPa). Instead, the structural system of the tall building is a steel frame with CFT columns (Figure A.36a) that is divided above the second level by an ISO system. This system consists of 14 NRB isolators, 30 LRB isolators and 8 oil dampers (Figure A.36b). In this project, an IIS was chosen instead of a BIS because the complex shape and size of the square in front of the building made it complex to achieve the isolation gap. Furthermore, the adoption of an IIS made it possible both to reduce the seismic response of the US, leaving the structural members in the elastic field even under a very severe level 2 earthquake, and to reduce the stress on the foundation.

Figure A.33. External view of Ochanomizu Sola City [https://creativecommons.org/publicdomain/zero/1.0/]

Figure A.36a shows the typical floor plan of the office floors, which has a large column-free space with a maximum span of 21.6 m. The CFT columns are made of square tube sections with sides 800 -1000 mm, where a high strength concrete, i.e. 100 MPa, was used for the columns under the ISO system.

From the previous mentioned, the mass ratio and isolation period was estimated to be 10.5 and 4.1 s, respectively.

In [153], the results of seismic analysis conducted on the building model under a level 2 earthquake can be summarised as follows: (i) the maximum response acceleration above the ISO layer is less than 3 m/s2; (ii) the storey drift angle is less than 1/200; (iii) all structural members remain in the elastic range; (iv) the maximum deformation of the ISO layer is 34 cm (less than the design limit of 50 mm).

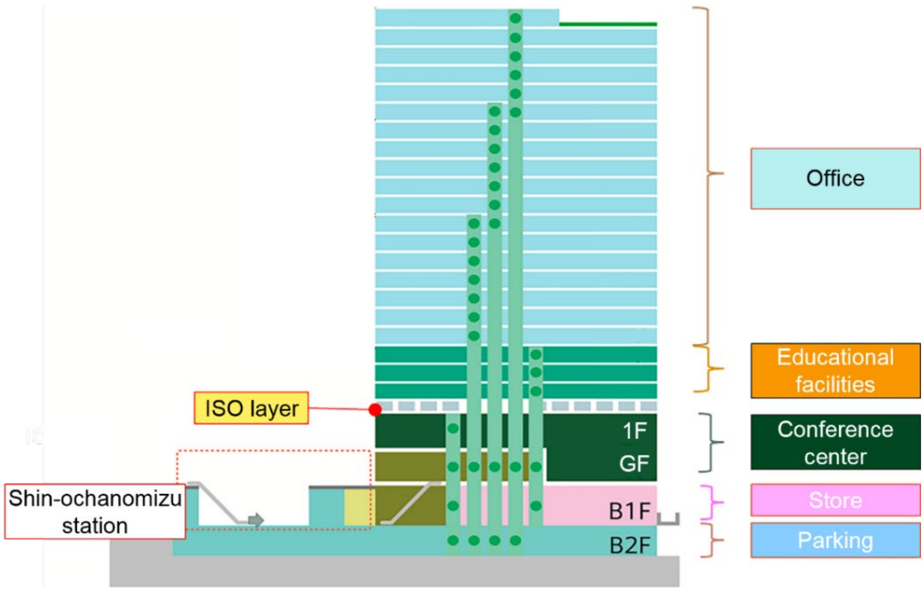

Figure A.34. Destination of use for the Ochanomizu Sola City [Source: [153]; license: Copyright © 2013 TAISEI Corporation. All rights reserved].

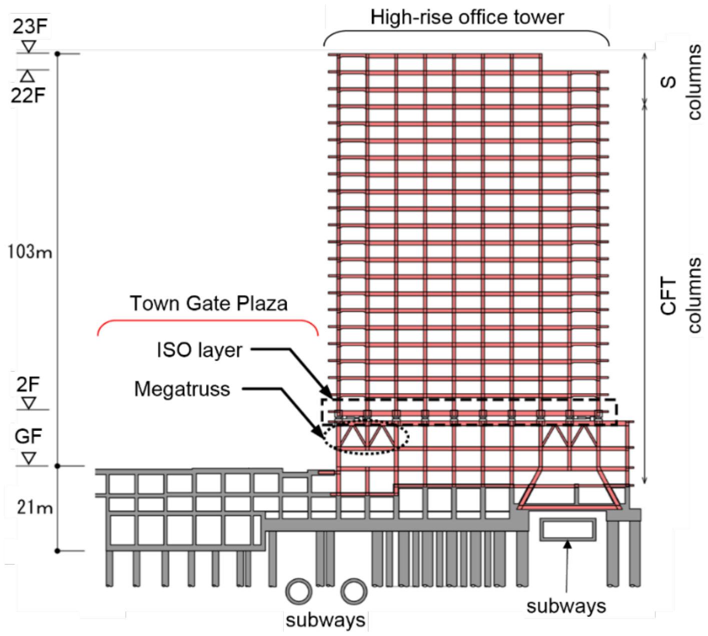

Figure A.35. Elevation view of Ochanomizu Sola City [Source: [154]; license: Copyright © 2012 TAISEI Corporation. All rights reserved].

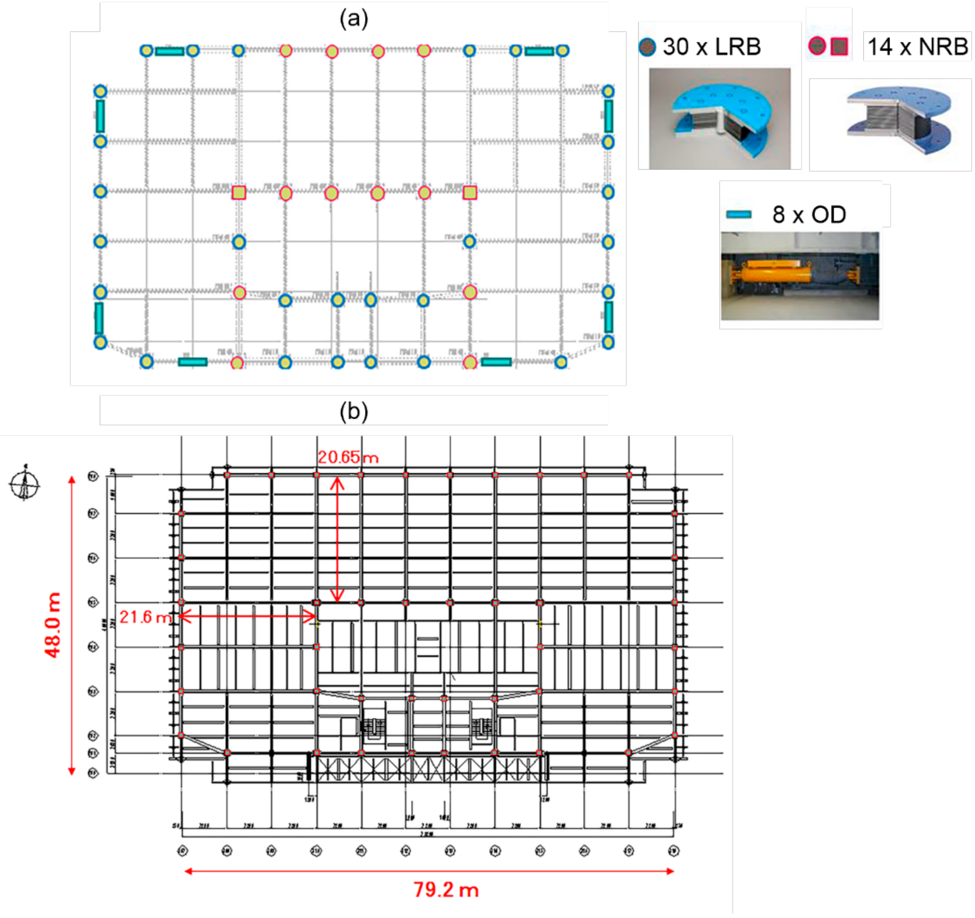

Figure A.36. Ochanomizu Sola City: (a) isolation floor plan; (b) typical floor plan of office [Source: [153]; license: Copyright © 2013 TAISEI Corporation. All rights reserved].

A.14 Nihonbashi dia building

All information reported in this section was derived from [156 – 159].

General information on the building is given in Table A.5.

The construction project analysed here involved first the partial demolition of the historic Mitsubishi Logistics Edobashi Warehouse building, constructed in 1930 in reinforced concrete beside the Nihonbashi River, with 5 storeys above ground level (Figure A.37a) and then, the construction of a new building, named Nihonbashi Dia Building completed in 2014. In this new building, 40% of the existing building was preserved (Figure A.37b) as this building had been designated as a historic building by the Tokyo Metropolitan Government.

(a) (b)

Figure A.37. External view of Nihonbashi Dia Building: (a) under construction [redrawn from: [156]; license: © 2024 Japan Federation of Construction Contractors]; (b) as built [source: wikipedia; license: https://creativecommons.org/licenses/by-sa/4.0/].

The Nihonbashi Dia Building has 18 floors above the ground and one underground for a height of about 90 m, and is located in the Chūō district of Tokyo, its use is office and warehouse. The structural system of the building is characterised by an ISO system above the sixth floor that divides the building into an LS and US (Figure A.38a). The LS is an SRC system with a floor plan dimension of approximately 59.2 x 36.8 m, while the US is a steel frame (SF) system with CFT columns used for offices with a floor plan dimension of 43.3 x 31 m (Figure A.38b). In addition, 5 kN/m^2 was assumed as the floor load in the design, with the exception of heavy load zones for which the floor load is 10 kN/m^2. Consequently, it is possible to estimate the mass ratio of the system to be 0.8.

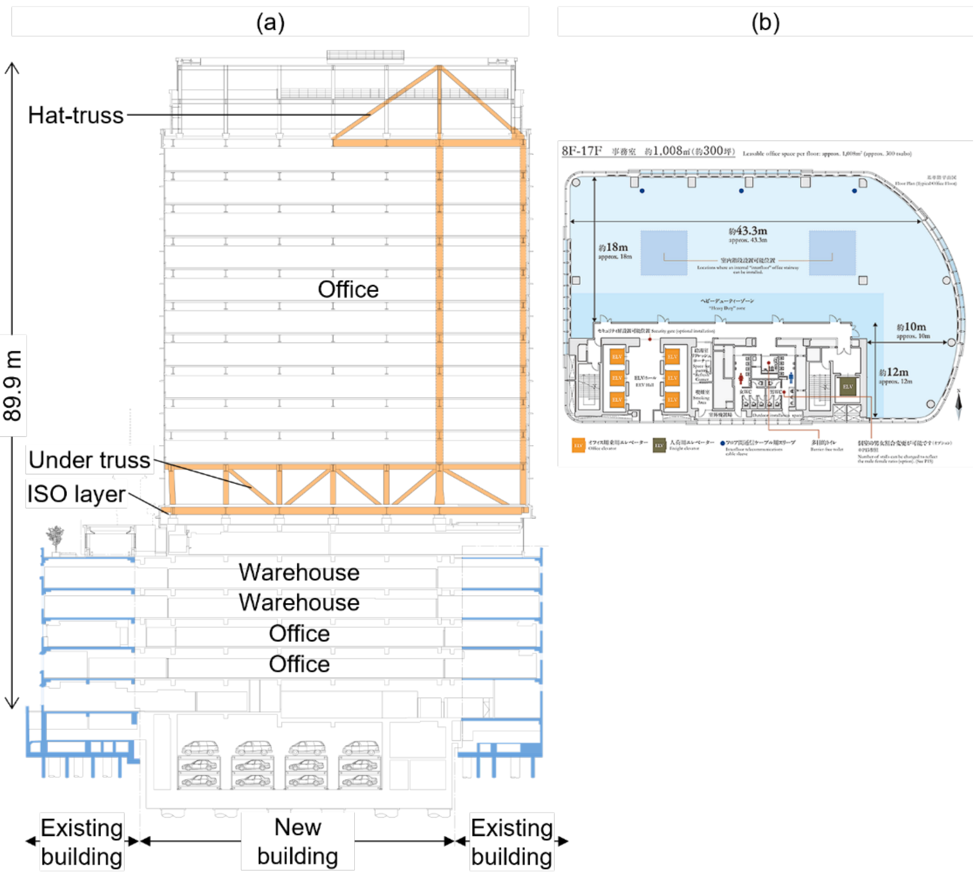

Figure A.38. Nihonbashi Dia Building: (a) elevation view [redrawn from: [156]; license: © 2024 Japan Federation of Construction Contractors]; (b) office floor plan [source: [157]; License: Copyright © Mitsubishi Logistics Corporation All Rights Reserved.]

The ISO system, composed of LRB isolators, also regularises the structural behaviour of the building; in fact, from Figure A.39 it can be seen that the new building constructed inside the existing building presents a strong variation in geometry along the height. In particular, the US has one more bay than the LS and in order to prevent a part of the gravity load of the US falling on the existing building, a hat-truss and an under-truss are placed at the top and base of the US respectively.

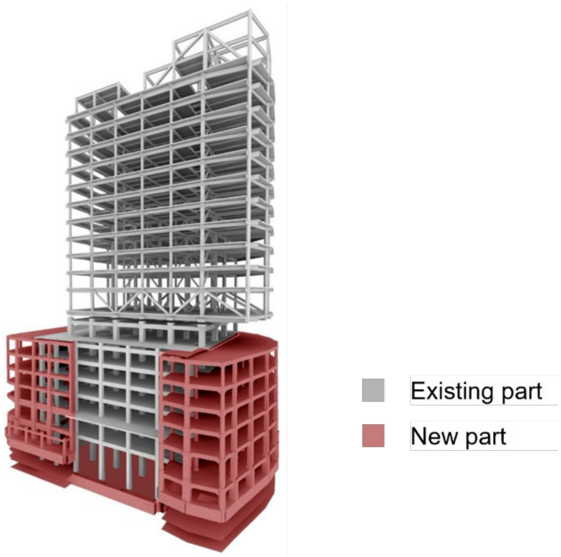

Figure A.39. 3D model of Nihonbashi Dia Building [redrawn from [158]; License: Copyright © The Japan Society of Seismic Isolation. All Rights Reserved.]

A.15 Wakabadai No.1 Apartment Building

All information reported in this section was derived from [160].

General information on the building is given in Table A.5.

The building analysed in this paragraph is part of a residential building complex constructed in 1983 in the Asahi Ward near Yokohama city and designed in accordance with the earthquake-resistant standards in force at the time.

In 2011, a seismic assessment analyses on the Wakabadai 3-7 building (Figure A.40a) showed the need of retrofitting. However, since the building accommodates shops up to the second floor and 60 residential units from the third floor to the thirteenth, these works had to be carried out without interrupting the functionality of the building.

Thus, it was decided to retrofit by placing a layer of ISO at the change of destination of use and geometry of the building along the height, i.e. the 3rd floor (Figure A.40b). The retrofit project was completed in 2013, while all the work was finished in 2014.

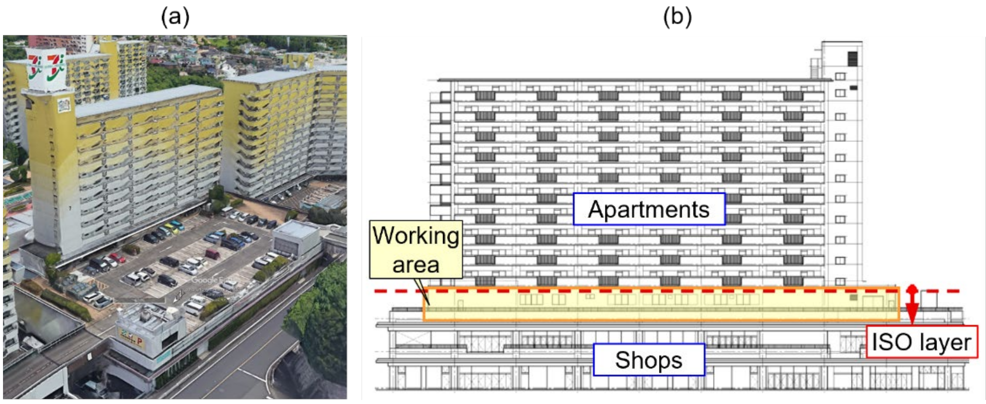

Figure A.40. Wakabadai No.1 Apartment Building, 3-7: (a) bird's-eye view [License: Image © 2024 Google, Data SIO, NOAA, U.S. Navy, NGA, GEBCO, Landsat/Copernicus, Data LDEO-Columbia, NSF, NOAA]; (b) elevation view [redrawn from: [160], license: © 2024 Japan Federation of Construction Contractors].

The building has a floor plan with dimensions of 78 x 80 m for the lower floors and 60 x 10 m for the residential floors. The structural system is reinforced concrete, so the IIS retrofit project required all the building columns on the 3rd floor to be cut. Therefore, a total of 16 NRB and HDRB type isolators were placed in the middle of each column (Figure A.41 a, b) coupled with 4 oil dampers (Figure A.41 c), two for each main direction of the plan.

In order to verify the effectiveness of the designed IIS solution, TH analyses were carried out in [160] for an extremely rare earthquake, the results of which can be summarised as follows: (i) the maximum deformation angle of US floor is 1/400; (ii) the maximum ISO deformation is 40.5 cm, lower than the maximum value assumed in the design of 45 cm; and (iii) the maximum acceleration in US was reduced by 50% compared to the maximum acceleration at the base of the building.

In conclusion, it can be observed that an intervention similar to the one just described was completed in 2016 on another building in the same residential complex, Wakabadai 3-5 (Building highlighted with a dashed rectangle in Figure A.42). The only information found on the latter intervention is reported in [161] and shows that the intervention methodology is the same as the one described above, i.e. the ISO system is located on the third floor at the change of use and geometry of the building. Furthermore, from the air photo shown in Figure A.42, it is also possible to note the strong similarity between the two aforementioned buildings.

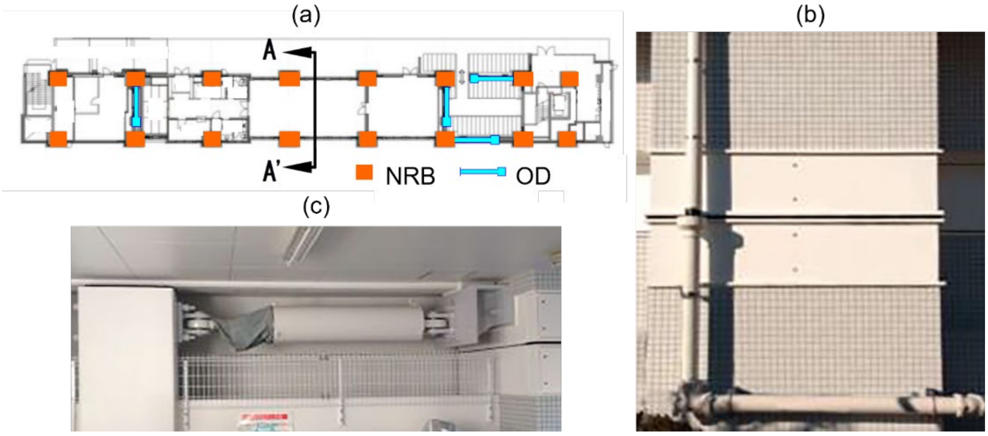

Figure A.41. Wakabadai No.1 Apartment Building: (a) Isolation system layout; (b) photo of the isolation layer; (c) photo of oil damper. [redrawn from: [160], license: © 2024 Japan Federation of Construction Contractors].

Figure A.42. Wakabadai Apartment Building: (a) bird's-eye view [License: Image © 2024 Google, Data SIO, NOAA, U.S. Navy, NGA, GEBCO].

A.16 Tekko Building - Main Building

All information reported in this section was derived from [162].

General information on the building is given in Table A.6.

The Tekko building is located near the Tokyo station and is a typical example of an IIS building that has a strong variation of geometry along the height (i.e., IT4). From Figure A.43, it can be seen that the building has a large floor plan extension at the base, with dimensions of approximately 183 x 35.7 m, for shops; while, in the elevation we find two towers, called the south tower and the main tower, destined for hotels and offices respectively (Figure A.43b). The two towers share the lower floors of the building becoming structurally separated by an expansion joint from the third floor (Figure A.43b, c). However, in order to simplify the discussion, the two towers will be analysed separately, with the main building being investigated in this section and the south building in the next section.

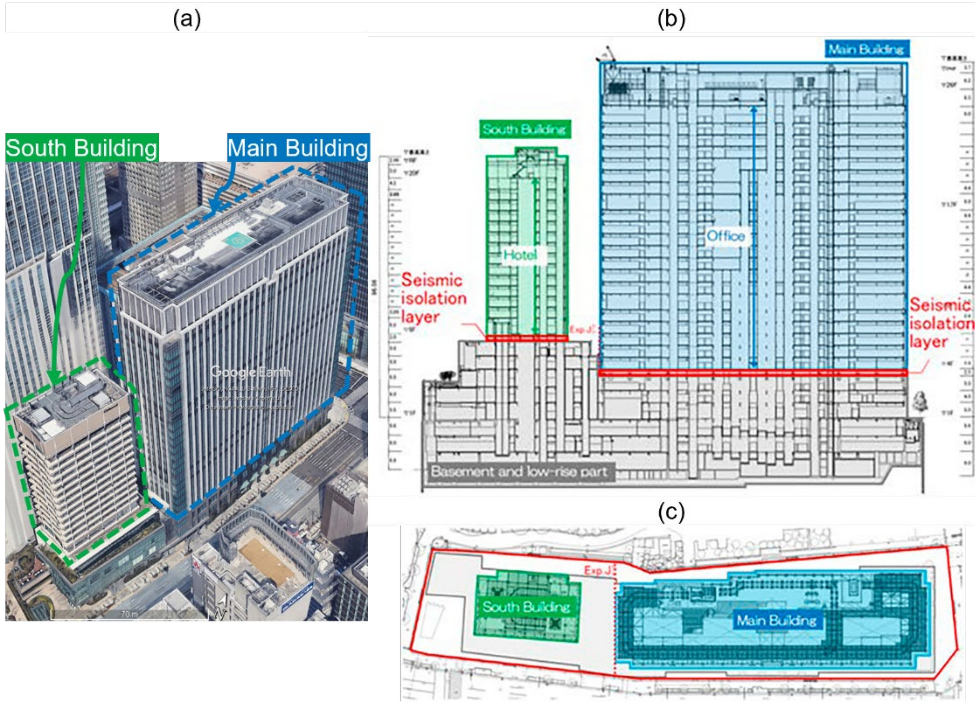

Figure A.43. Tekko Building: (a) External view [License: Image © 2024 Google, Data SIO, NQAA, U.S. Navy, NGA, GEBOC, image Landsat/Copernicus, Data Japan Hydrographic Association]; (b) elevation view [redrawn from [162]]; (c) floor plan [redrawn from [162]].

The main building of the Tekko building has 26 above-ground storeys (136.5 m high) with a roughly rectangular plan form, measuring 114.5 x 33.5 (aspect ratio greater than 4). In addition, an ISO system is located between the third and fourth floors and divides the entire building into an LS and US (Figure A.44a). The structural system of LS and US is a steel frame with CFT columns. In US there is an 18 m span without columns and in the floors with higher heights there are braces to increase the stiffness of the floor (Figure A.44a). Figure A.44b shows the layout of the ISO system, where it can be seen that 48 NRB isolators with diameters varying between 1000 - 1500 mm, associated with 30 “U-shaped steel dampers (U-SD)”, 8 oil dampers and 32 oil dampers with locking mechanism, are installed. These dampers are used to prevent excessive deformation of the ISO system under strong winds and to allow the elevator to continue operating; therefore, they are only inserted in the direction of the short side of the building. The locking mechanism is set to activate when the anemometer positioned at the top of the building detects a wind speed greater than 25 m/s, corresponding to a wind load with a return period of 4-5 years; in addition, if an earthquake occurs when the damper is locked, there is a system, connected to an accelerometer installed in the building, which allows the damper to be unlocked.

In [162] several analyses on a concentrated mass model were performed where the main building and the south are rigidly coupled at the first 3 levels. A modal analysis on such system showed a fundamental period for the main building with initial stiffness of the ISO system equal to 4.24s, while considering a deformation of 30 cm of ISO and the consequent equivalent stiffness the period is 5.38 s. However, a simplified evaluation of the ISO period for a 100% deformation of ISO shows a value of approximately 5.3 s. Finally, the results of the seismic response analysis can be summarised as follows: (i) the maximum drift angle of the floor under a Level 2 earthquake is 1/184; (ii) the maximum displacement of the ISO system is 376 mm, with a shear strain of 185%; (iii) the maximum vertical pressure on the isolator is 27.7 MPa, while the minimum is -0.1 MPa, which is an acceptable tensile stress for the isolator.

In addition to seismic loads, the building is also subject to strong wind loads due to its very extended shape in one direction. Therefore, wind loading response analyses were conducted, the results of which are shown in [162] and can be summarised as follows: (i) oil dampers with a locking mechanism prevent the isolators from exceeding the elastic limit under a Level 2 wind load; (ii) the maximum deformation of the ISO system for a Level 2 wind load is 98 7mm; (iii) the maximum building displacement for a Level 2 wind load is less than 20mm; (iv) the steel dampers do not exceed the elastic limit for a Level 1 wind load; (v) the maximum and minimum surface pressure on the isolators is 26 MPa and 0.5 MPa respectively.

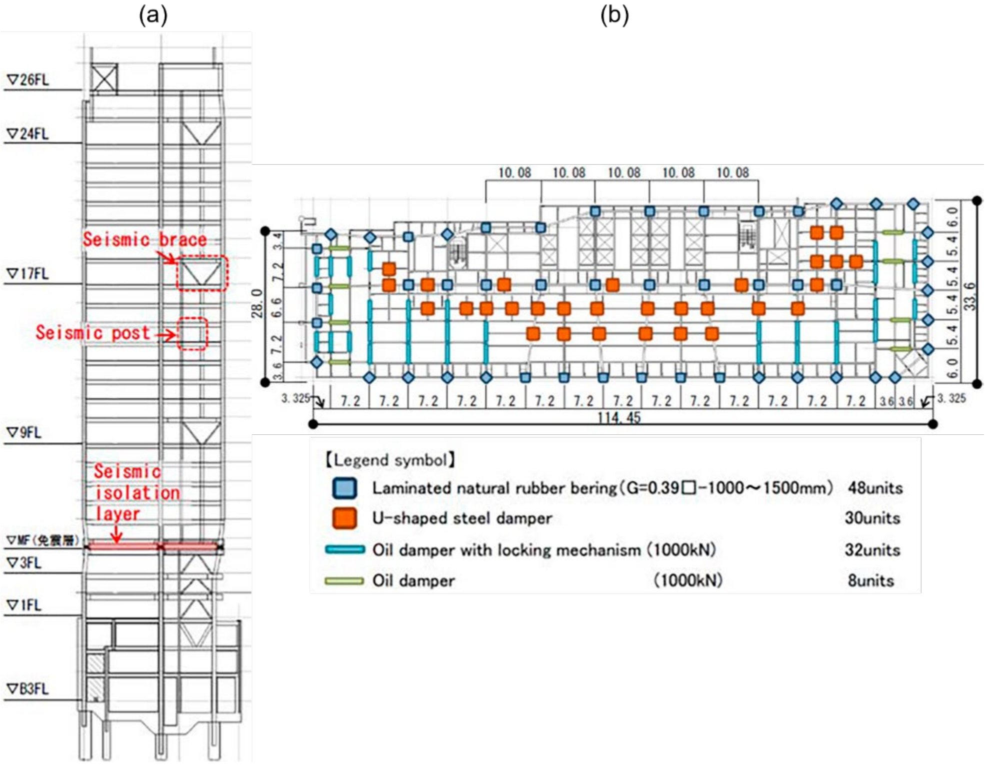

Figure A.44. Tekko Building – Main building: (a) cross section [redrawn from [162]]; (b) Isolation system layout [redrawn from [162]].

The building has several accelerometers installed inside, including accelerometers located at the base of the building (basement, floor -3), on the floor immediately below the ISO system (third floor), on the floor immediately above the ISO system (fourth floor) and at the top (twenty-third floor). However, following the completion of the building in 2015, two major seismic events occurred at the site. The first one is the 16 May 2016 earthquake of M5.5 with epicentre to the south of Ibaraki Prefecture, where an acceleration at the base of the building of 0.101 m/s^2 was recorded, which amplified to 0.322 m/s^2 below the ISO system; while it reduced to 0.099 N/m^2 on the floor immediately above the ISO system, and is approximately the same on the 23rd floor of US (0.094 N/m^2). These records demonstrate the excellent seismic behaviour of the IIS system, with a maximum acceleration at the floor immediately above the ISO system equal to 31% of the maximum acceleration recorded below the ISO system. The second earthquake recorded was on 22 November 2016 with an epicentre in the sea near Fukushima Prefecture with M7.4, where the maximum accelerations recorded at the base, below and above the ISO system are 0.057 m/s^2, 0.18 m/s^2 and 0.114 m/s^2 respectively, with the ISO system leading to a reduction in acceleration in the US although of a lower intensity than the previous earthquake. This effect is probably due to a lower effectiveness of the ISO system due to a greater influence of the long-term component of the seismic wave.

Finally, accelerometer measurements recorded during windstorms exceeding 25 m/s at the top of the building confirmed the excellent behaviour of the oil dampers with locking mechanism.

A.17 Tekko Building - South Building

All information reported in this section was derived from [162].

General information on the building is given in Table A.6.

The south tower of the Tekko building in Tokyo, as shown in Figure A.43a and Figure A.45a, has an ISO system between the fifth and sixth floors. As described in the previous paragraph, the south tower shares a part of LS with the main tower, while the US is a steel frame with CFT columns that reaches a maximum height of 98.5 m (21 storeys above the ground), with a rectangular floor plan measuring 38.3 x 28 m. The building consists of commercial facilities in the lower part, with a rest area for users waiting for the transfer to Haneda Airport on the ground floor and hotels on the US floors. There is also a TMD on the top of the building to increase living comfort in the case of high wind loads.

The ISO system consists of 6 NRB isolators with a size Φ800 ÷ 1000 with a rubber shear modulus of 0.39 MPa and 4 NRB isolators with a size Φ1000 ÷ 1200 and a rubber shear modulus of 0.60 MPa combined with 8 oil dampers (Figure A.45b).

Similarly, as done for the main building (Section A.16), the results of the modal analysis and the response analysis for seismic loads described in [162] are also reported for the south building. In particular, the modal analysis showed a fundamental period of the south building equal to 5.68 s, which is higher than the isolation period of 4.6 s evaluated in a simplified way from the information available on the building considering only the contribution of the NRB isolators. In addition, the results of the seismic response analysis showed that: (i) the maximum storey drift angle is 1/173 and (ii) the maximum deformation of the isolation layer is 285 mm with shear strain of 183%.

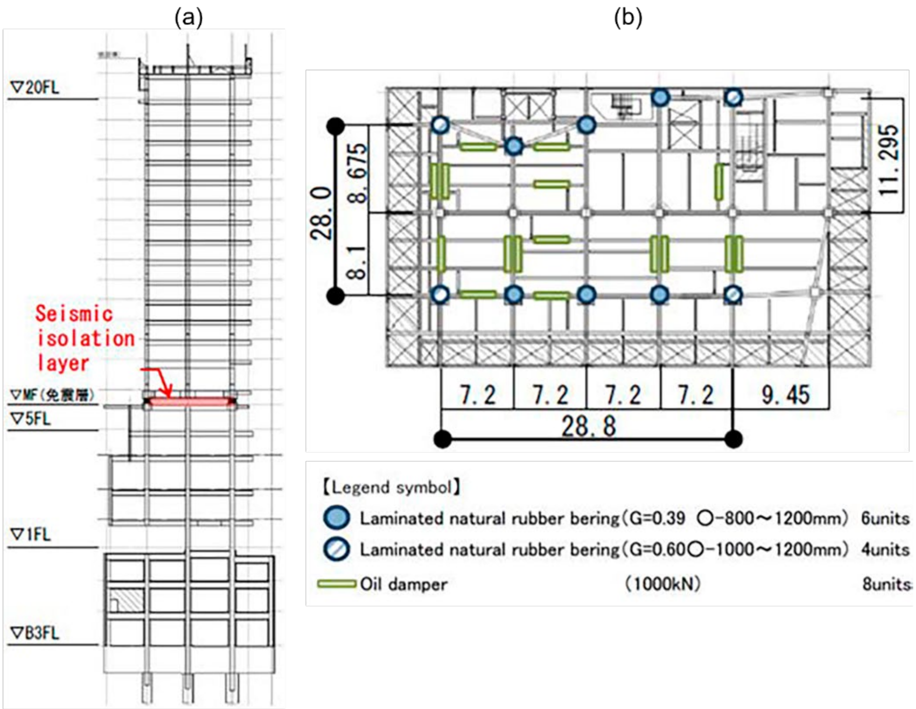

Figure A.45. Tekko Building – South building: (a) cross section [redrawn from [162]]; (b) Isolation system layout [redrawn from [162]].

Accelerometers were also installed for the south building on the several floors which allowed the system response to be recorded during the two seismic events already mentioned in the previous paragraph with reference to the main building. During the M5.5 earthquake of 16 May 2016, a maximum acceleration at the base of 0.101 m/s^2 and a maximum acceleration below and above the ISO system of 0.295 m/s^2 and 0.049 m/s^2, respectively, was recorded, showing a strong effectiveness of the ISO system. Finally, at the second M7.4 earthquake on 22 November 2016, the records of the accelerations above and below the ISO system showed a maximum acceleration of 0.192 m/s^2 and 0.062 m/s^2, respectively. Thus, even in the latter case there is a strong effectiveness of the ISO system in reducing the response in terms of accelerations in the isolated upper building.

A.18 Kyobashi Edogrand

All information reported in this section was derived from [163, 164].

General information on the building is given in Table A.6.

The Kyobashi Edogrand (Figure A.46) is a building with 32 floors above ground and 3 basement floors with a maximum height of 170 m located near Tokyo Central Station. The building is composed of a tower that stands on three buildings at its base, this type of architecture allows to have an urban square that runs across the entire building on the ground floor (Figure A.47). However, it should be pointed out that the construction of the Kyobashi Edogrand involved the demolition of all the existing buildings on the site with the exception of a historic building that is structurally independent of the new building (Figure A.47).

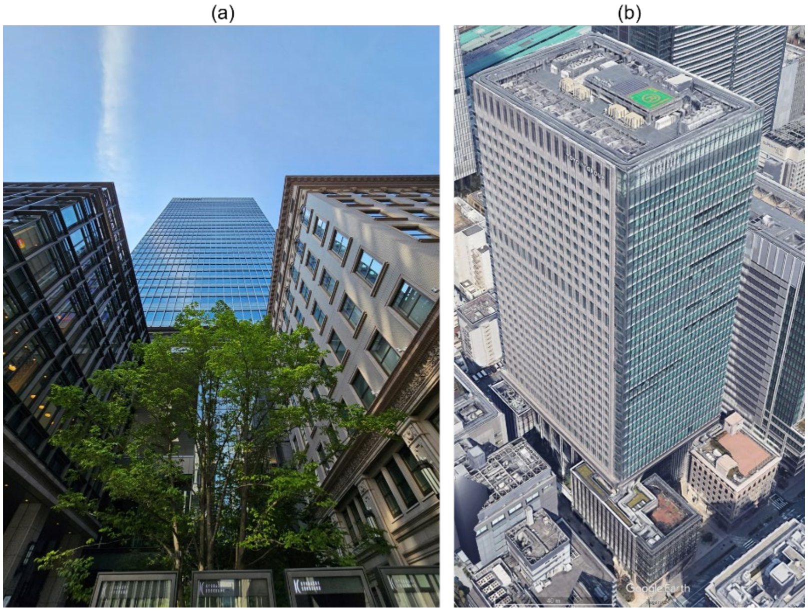

Figure A.46. Kyobashi Edogrand: (a) external view; (b) bird's-eye view [License: Image © 2024 Google, NASA].

In Figure A.47a, it can be seen that on the lower floors, up to the seventh, there are shops, while the floors of the tower are destined for offices. At the floor where the office tower connects to the three buildings at the base, 31 m above ground level, an ISO system is positioned, thus allowing the definition of an LS and a US (Figure A.48a). The LS is composed of the three steel reinforced concrete buildings, which appear to be architecturally separate but are functionally and structurally connected to each other on the third and fifth floors by means of an rigid floor (Figure A.47b). The maximum external plan dimension of the LS is 66 x 98.5 m. The US has a plan dimension of 50 x 75 m with a core for the services on the north side; while the structural system is a steel frame with CFT columns (750 x 1100 mm) and welded square hollow section beams, moreover, braces are inserted in the central bays.

The ISO system is realised by means of 34 NRB isolators (10Φ1300, 2Φ1400, 14Φ1500 and 4Φ1500 in pairs of two) associated with 48 oil dampers, 6 ESBs and 4 Elastic sliding (Figure A.48b). In addition, since the building is high to avoid significant deformations in the ISO layer under windstorms, mechanical locking systems are inserted that fail after a certain shear action allowing the ISO layer to work during an earthquake but at the same time blocking the deformation of the ISO layer under strong wind actions.

Then, from an approximate assessment of the US mass and the type and number of isolators used in the building, it is possible to roughly calculate the isolation period adopted in the design, which is approximately 6.1 s.

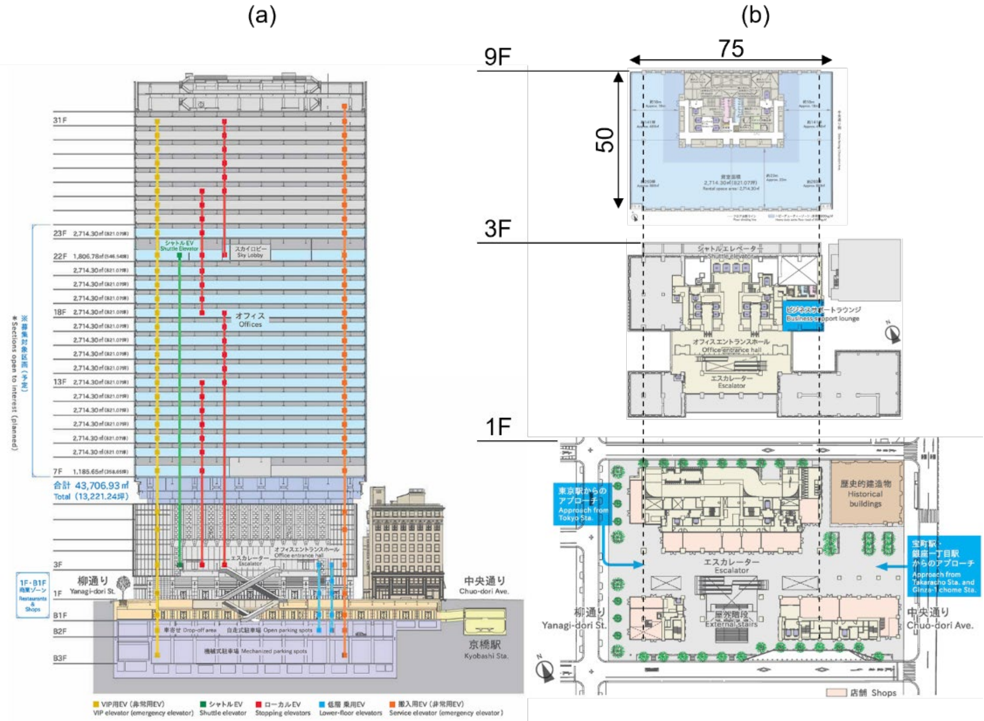

Figure A.47. Kyobashi Edogrand: (a) elevation view [redrawn from [163]]; (b) floor plan layout [redrawn from [163]].

From the above, it can be seen that large diameter insulators were used in the building (the smallest diameter used is Φ1300); since, although the maximum acceptable displacement from the ISO layer is set at 50 cm for a level 2 earthquake, the isolators must also be able to accommodate greater displacements.

Furthermore, the layout of the ISO devices in the isolation layer is due to the need to have the centre of the stiffnesses of the ISO layer coincide as much as possible with the centre of the masses of the US in order to avoid torsion motions at the ISO layer (Figure A.48b). On the other hand, the four elastic sliding devices were placed in the centre of the plan where the gravitational load is lowest. Finally, the Oil Dampers (OD) have the function of absorbing the vibration energy in the ISO layer.

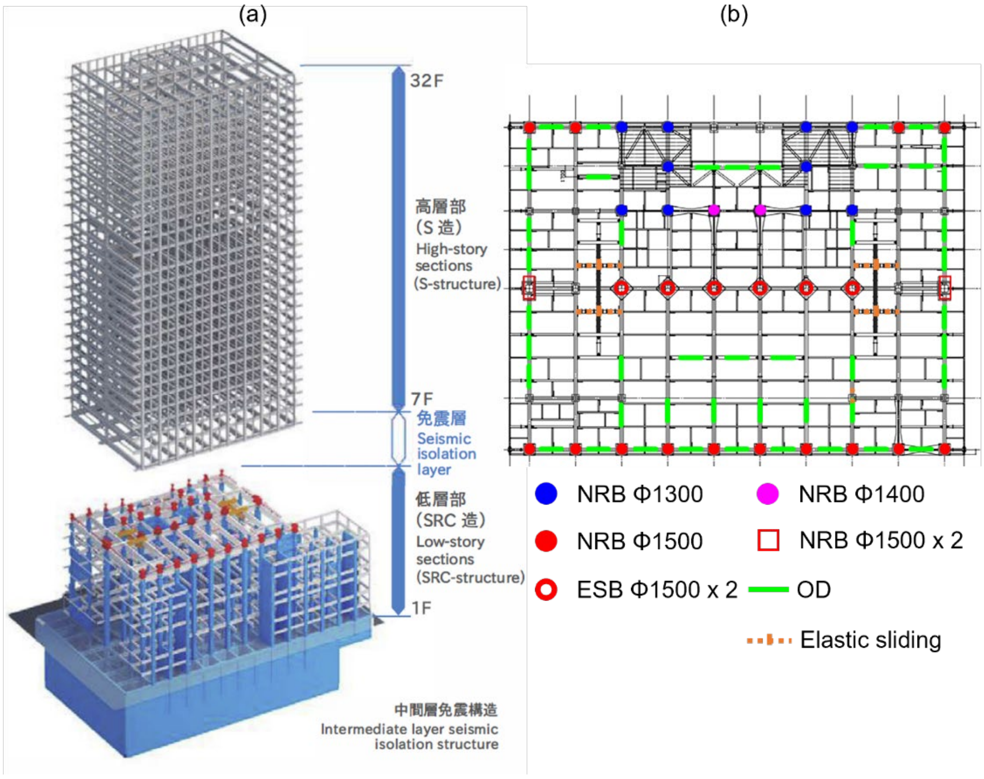

Figure A.48. Kyobashi Edogrand: (a) 3D model [redrawn from [163]]; (b) Isolation system layout [redrawn from [164]].

In [164], the results of the system response analysis assumed as a concentrated mass model with 3DOF assigned to each mass are reported. The results can be summarised as follows: (i) maximum storey deformation angle equal to 1/231 (lower than the limit of 1/150); (ii) maximum ISO deformation equal to 37.5 cm (lower than the limit of 50 cm).

A.19 Roppongi Grand Tower

All information reported in this section was derived from [165, 166].

General information on the building is given in Table A.7.

The Roppongi Grand Tower (Figure A.49a) is located in the luxury district of Roppongi in Tokyo and was constructed between June 2013 and October 2016. The building reaches a height of 230 m (40 storeys above ground and three below) with a floor plan measuring approximately 65 x 65 m whose longest bay is 17 m. The destination of use of the tower is offices (Figure A.49b).

(a) (b)

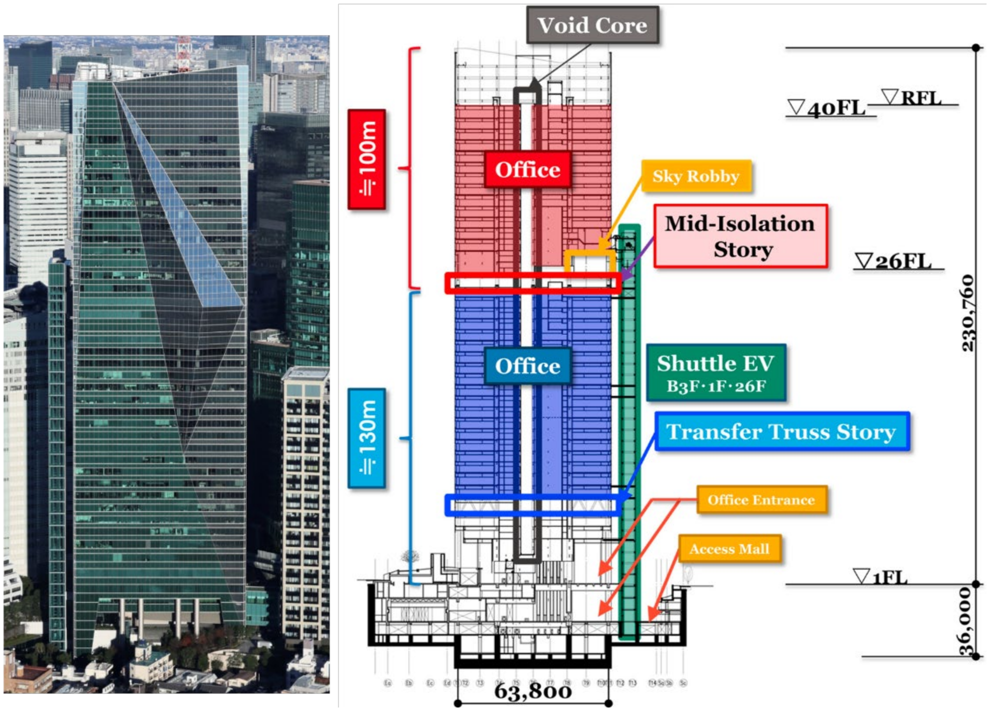

Figure A.49. Roppongi Grand Tower: (a) elevation view [source: Wikimedia; license: https://creativecommons.org/licenses/by-sa/4.0/]]; (b) elevation view [redrawn from [166]].

The building was initially designed as a system with vibration control through plasticizing aseismic braces in the central core, and after the 2011 Tohoku earthquake it was decided to switch to an isolated system at the intermediate level to allow a higher performance and liveability during an earthquake. The building is also characterised by a large transfer beam on the 7th floor that transfers the gravity load from the upper part of the building to the CFT columns located on the lower floors, allowing a large atrium on the ground floor (Figure A.50). These CFT columns have a circular cross-section of 1800 mm (steel ultimate strength: 550 MPa; concrete strength: 60 MPa) and are one of the largest CFT columns in Japan. In addition, aseismic braces and Viscous Damping shear Wall (VDW) are inserted in the central core of the building to reduce the response in terms of accelerations in LS (Figure A.50).

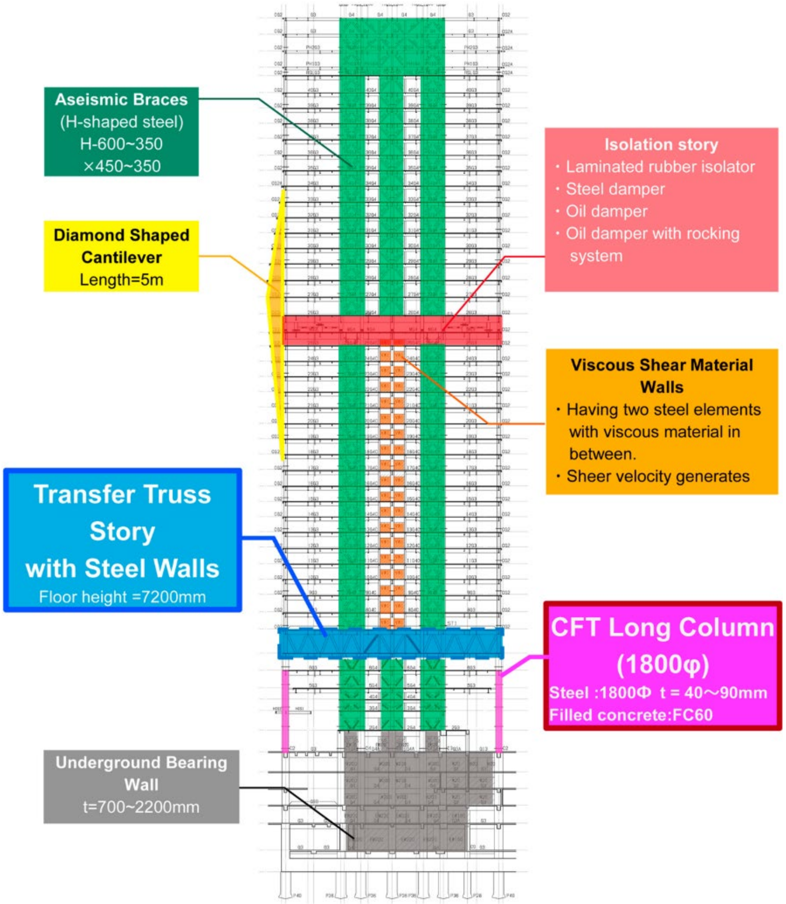

Figure A.50. Structural system of the Roppongi Grand Tower [redrawn from [166]].

As mentioned above, the building was initialy designed to include only vibration control with VDW and only after the 2011 earthquake was it included a layer of ISO along the height of the building. However, the design of the ISO system had to respect the following four points: (i) maximum number of storeys above ISO; (ii) avoid tensile forces in the isolator; (iii) provide sufficient resistance to vertical loads of the isolator; and (iv) do not alter the architectural design of the building. With regard to satisfying points (ii) and (iii), it has been seen that the maximum number of floors to be considered above the ISO system is 30 (20th floor of the building). Whereas, in order to satisfy point (iv), the location of the sky lobby planned on the 26th floor and connected to the ground by a direct elevator must not change. Consequently, it was decided to locate the ISO system immediately below the floor of the sky lobby, connecting the US and the elevator structure with an expansion joint. The other elevators inside the building do not pass through the ISO system except for an emergency elevator.

To achieve the structural system shown in Figure A.50, the designers conducted parametric analyses by modifying the stiffness of the LS and US and also compared the response of the building model with classical vibration control (i.e. without IIS). The results of this parametric analysis, conducted on a concentrated mass model of the building, are shown in [166] and demonstrate both the effectiveness of IIS compared to the system without IIS and how for a building with IIS, a lower stiffness of the LS increases the effectiveness of the ISO system in reducing accelerations, displacements and shear forces at the different floors.

Figure A.51a shows the layout of the ISO system where it can be seen that the following devices are positioned in the isolation layer: 33 NRB isolators Φ1300, 4 NRB isolators Φ1400, 4 NRB isolators Φ1500, 56 steel dampers (SD) and 64 oil dampers (OD) of which 4 are with locking mechanism. The resistance force offered by the steel dampers and the locking mechanism of the 4 ODs (two in each direction) is evaluated in relation to the wind load. The maximum deformation of the ISO layer under a very rare earthquake is set at 40 cm, while elements at risk of collapse or collision, such as the expansion joints between tower and elevator are designed for a displacement equal to 1.5 times the maximum displacement of 40 cm. In addition, the isolators are placed symmetrically in plan in order to avoid torsional motion of the system.

Figure A.51b shows the layout of the installation of the oil and steel dampers in the ISO layer. In particular, it can be seen that in order to reduce the number of struts required for the installation of the ODs and SDs, a staggered system has been realised, where an SD is placed on a strut connected to the LS and one on a strut connected to the US and finally the two struts are connected to each other through an oil damper. Thus, in the case of a strong earthquake, the ODs installed between two struts exhibit a reaction force as a function of the velocity of the floors, whereas, the SDs exhibit a resistance force as a function of the deformation of the ISO layer. A photo of the system *in situ* is shown in Figure A.51c.

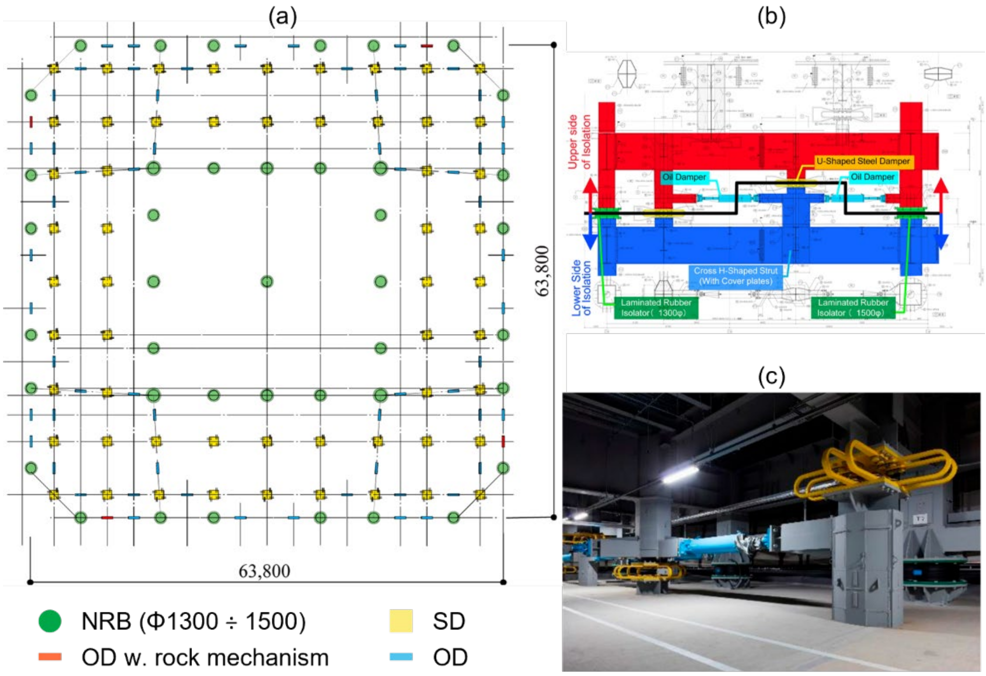

Figure A.51. Isolation system of Roppongi Grand Tower: (a) layout; (b) detail; (c) photo [redrawn from [166]].

A.20 DaiyaGate Ikebukuro

All information reported in this section was derived from [24, 167].

General information on the building is given in Table A.7.

The building investigated in this section is the DaiyaGate (Figure A.52a) built above the tracks of Ikebukuro Station, Tokyo (Figure A.52c). The construction of the building was completed in 2019 and represented the first case in Japan of a building more than 60 m high built above the tracks. The design of the building is oriented to *Transit-Oriented Development* (*TOD* is a new method of planning development with public transport), which involves the construction of new buildings over existing train stations without changing their route or interrupting their activity during the construction of the building.

The building has been constructed to become the new headquarters of the Seibu Group and reaches a height of approximately 100 m with 20 storeys above ground and 2 storeys below ground (Figure A.53) and on the third floor there is an open deck (Figure A.52b).

(a) (b) (c)

Figure A.52. DaiyaGate Ikebukuro: (a) external view; (b) open deck; (c) bird's-eye view [License: Image © 2024 Google, Data SIO, NOAA, U.S. Navy, NGA, GEBCO].

The building has a steel tripod structure on the lower floors, where V-shaped elements make it possible to cross the tracks of the existing railway line. Next, at a height of 20 m above ground level, there is an ISO system that structurally divides the building into two distinct parts, the LS and the US. The US has a typical floor plan with dimensions of 65 x 47 m, with a services core eccentrically placed with respect to the geometric centre of gravity of the plan, resulting in two column-free bays of 18.3 m and 10.8 m in the X and Y directions of the plan respectively (Figure A.54). The decision to reduce the number of columns in the plan, in addition to having an obvious architectural benefit, leads to a smaller number of ISO devices to be adopted and therefore a greater gravitational load on each isolator, which leads to larger isolators able to accommodate greater displacements. In particular, the ISO layer is composed of 20 NRB isolators of which 16 have a diameter Φ1000 and 4 a diameter Φ1500 combined with 4 U-shape steel dampers (Figure A.55).

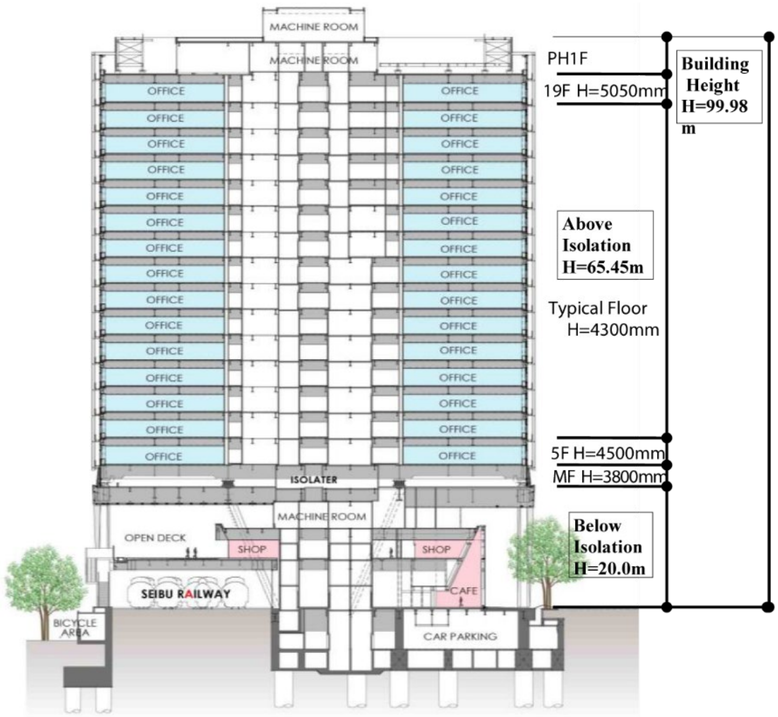

Figure A.53. Cross section of DaiyaGate Ikebukuro [redrawn from [24]].

The US consists of a steel frame with CFT columns and a diagrid on the external façade made of H-shaped hot-dip galvanised steel elements. The use of the diagrid system makes it possible to obtain a high horizontal stiffness for the US such that the steel frame can be considered to have only the function of transmitting gravity loads. In addition, inertial seismic forces are transferred to the diagrid through horizontal steel plates that connect the steel frame to the diagrid itself (Figure A.54).

However, the choice of adopting structural systems with high horizontal stiffness for both US and LS demonstrates the designers' intention to emphasise more the seismic isolation aspect in the building with IIS instead of mass damping aspect (see Chapter 2); in fact, a simplified calculation has identified an isolation period for the US+ISO of approximately 6 s. In addition, the layout of the isolators allows torsional motions of the insulated upper structure to be avoided

(Figure A.55). The isolators were designed for a maximum displacement of 495 mm, under an extremely rare earthquake, corresponding to a 250% shear deformation of the rubber, and for a limit value of the surface pressure equal to 18 N/mm^2.

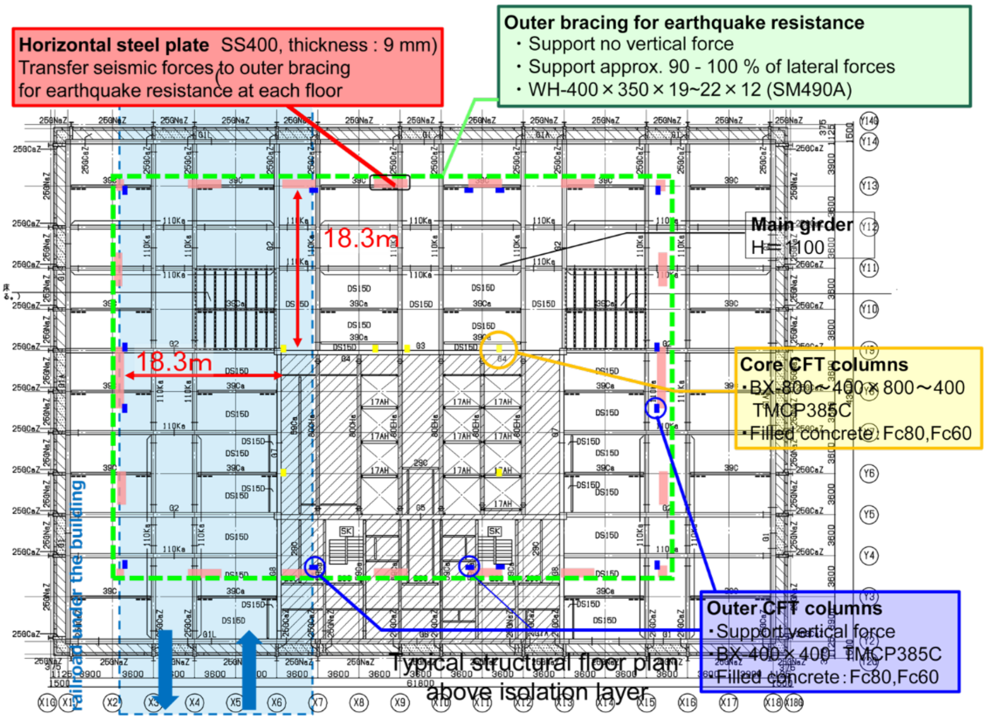

Figure A.54. Typical floor plan above ISO layer of DaiyaGate Ikebukuro [redrawn from [24]].

The design of the DaiyaGate Ikebukuro has several unique features, such as the absence of substructures crossing the train line, and thus connecting the parts of the building that are located at the end of this track line. Therefore, differential seismic inputs at the base of the two building parts have been considered in the building analysis, and a total differential displacement about 30 mm has been evaluated under a design earthquake. A further push-over analysis on the building showed that the collapse of the system occurred for a differential displacement of 200 mm, i.e. approximately 7 times the value of the system response to the design earthquake.

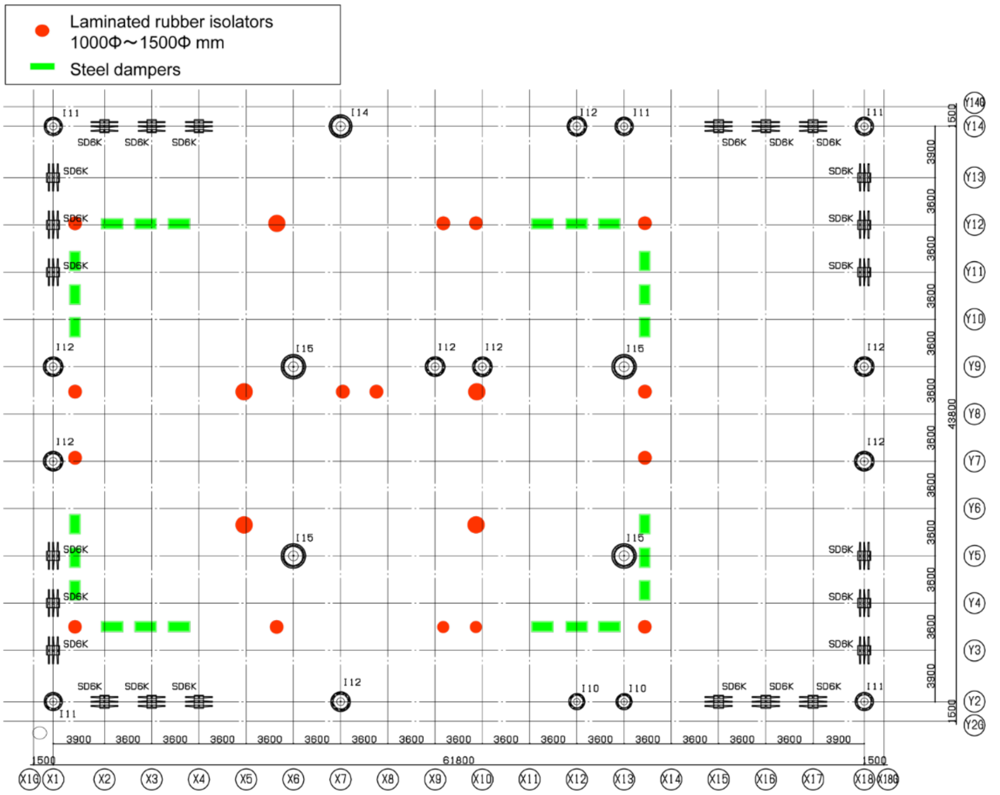

Figure A.55. Isolation system of DaiyaGate Ikebukuro [redrawn from [24]].

In [24] are reported the results of TH analyses performed on a 57-DOF lumped mass model, in which at each plane is assigned a mass with 3-DOF, excited by three different wave shapes of extremely rare earthquakes. The results of these analyses can be summarised as follows: (i) the maximum drift angle in the X- and Y-direction is approximately 1/700 and 1/400 respectively; (ii) the US diagrid system exhibited strong horizontal stiffness; (iii) the maximum displacement of the ISO layer is 41.4 cm, below the limit of 50 cm; and (iv) each structural element remains in the elastic field. In addition, an analysis on the same 57-DOF model under a pulse ground motion was also carried out. The results of this analysis showed a good response of the IIS, with a displacement of the isolation layer that although exceeding 50 cm remains less than 70 cm, a value over which the load-bearing capacity of the isolators is lost, and the maximum drift angle in the US remains 1/700 in the X direction.

A.21 Overview tables

The following Tables A.1 – A.7 show the general information obtained about twenty IIS buildings.

Table A.1. Data of: Personnel Training Center of Taisei Corporation, Iidabashi 1st Building, Kudan, Post Office and Housing.

Name	Personnel Training Center of Taisei Corporation		Iidabashi 1st building		Kudan, Post Office and Housing	
Photo						
Intervention type	Retrofit		New Building		Retrofit	
Destination of use	Personnel Training Center		Office + Condominiums + Retail		Post Office + Housing	
Address	Atami, 413-0001 Shizuoka, Japan		Bunkyo City, Tokyo 112-0004, Japan		Chiyoda City, Tokyo 102-0074, Japan	
Year	1997		2000		2000	
Designer/Constructor	Taisei Corporation		Nikken Sekkei		Shimizu Corporation + Maeda Corporation	
Sub-structure	LS	US	LS	US	LS	US
Building type	SRC	RC	SRC	RC	SRC	SRC+RC
d_1 x d_2 [m]	87 x 27	44 x 27	130 x 40	130 x 15	44 x 19	44 x 19
H [m]	49		59		29.85	
H_{ISO} [m]	22.0		38.0		4.5	
n_{floors}	7	9	9	6	1	9
A_{floors} [m^2]	4852	5281	46800	11700	772	6951
μ [-]	1.1		0.2		9.0	
T_{ISO} [s]	3		≈ 3.3		≈ 3.6	
δ_{ISO} [cm]	≤ 40		≤ 40		≤ 25	
ISO system	22xLRB (18Φ700 + 4Φ800)		40xNRB (Φ800) + 212LD		30xNRB (28Φ600 + 2Φ700) + 18VDW	

Table A.2. Data of: Shinjuku station (West Exit), Umeda DT Tower, Shiodome Sumitomo building.

Name	Shinjuku station (West Exit)		Umeda DT Tower		Shiodome Sumitomo building	
Photo					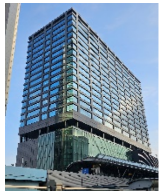	
Intervention type	IT3		IT4		IT4	
Destination of use	Station + Retails		Office		Hotel	
Address	Shinjuku City, Tokyo 160-0023, Japan		Kita Ward, Osaka, 530-0001, Japan		Minato City, Tokyo 105-0021, Japan	
Year	≤ 2002		2003		2004	
Designer/Constructor	Takenaka Corporation + Odakyu Construction Co		Takenaka Corporation		Nikken Sekkei	
Sub-structure	LS	US	LS	US	LS	US
Building type	RC	RC	SF	SF	SF	SF
d_1 x d_2 [m]	n.a.	25 x 55	28 x 56	28 x 56	110 x 40	110 x 40
H [m]	31[*1]		130		126.1	
H_{ISO} [m]	-		10.5		50.0	
n_{floors}	2	6	1	26	10	15
A_{floors} [m^2]	n.a.	8250	4497	38974	32543	65085
μ [-]	n.a.		8.7		2.0	
T_{ISO} [s]	≈ 3.1		≈ 6		≈ 5	
δ_{ISO} [cm]	14		≤ 40		≤ 50	
ISO system	20xLRB (Φ650) + 12xNRB (8Φ650 + 4Φ700) + 8xOD		6xLRB (1100x1100÷1350x1350 w. LΦ155÷190) + 12xLS + 2xLU + TMD		41xNRB (13Φ1300 + 19Φ1100 + 9Φ1000) + 100xLD + 14xSD	

[*1]Isolated building height

Table A.3. Data of: China Basin 185 Berry Street Building, Musashino City Disaster Prevention, Fukuoka Financial Group Headquater.

Name	China Basin 185 Berry Street building		Musashino City Disaster Prevention and Safety Center		Fukuoka Financial Group Headquater	
Photo						
Intervention type	IT1		IT1		IT4	
Destination of use	Office		Office		Office	
Address	185 Berry St, San Francisco, CA 94107, USA		Musashino, Tokyo 180-8777, Japan		Chuo Ward, Fukuoka, 810-0074, Japan	
Year	2007		≤ 2008		2009	
Designer/Constructor	Simpson, Gumpertz & Heger		Nikken Sekkei		MHS Planners,Architects & Engineers	
Sub-structure	LS	US	LS	US	LS	US
Building type	RC	SF	SRC	S	SF	SF
d_1 x d_2 [m]	252 x 33.5	244 x 33.5	29 x 25	29 x 25	40 x 52.2	40 x 52.2
H [m]	25		31.9		86	
H_{ISO} [m]	13.0		7.6		22.5	
n_{floors}	3	3	2	6	1	12
A_{floors} [m^2]	20067	13935	1450	3611	4176	25056
μ [-]	0.5		1.7		6.0	
T_{ISO} [s]	n.a.		n.a.		4	
δ_{ISO} [cm]	≤ 114		n.a.		≤ 40	
ISO system	33xLRB (Φ1200) + 54xESB (Φ1900)		8xNRB (Φ700) + 12xESB + 8xSD		16xNRB (Φ1100) + 6xESB + 4xD	

Table A.4. Data of: NBF Osaki Building, Mita Bellju Bldg., Nakanoshima Festival Tower.

Name	NBF Osaki building		Mita Bellju building		Nakanoshima Festival Tower	
Photo						
Intervention type	IT4		IT4		IT4	
Destination of use	Office + Retails		Office + Retail + Housing		Office + Theatre + Retail	
Address	Shinagawa City, Tokyo 141-8610, Japan		Minato City, Tokyo 105-0014, Japan		Kita Ward, Osaka, 530-0005, Japan	
Year	2011		2012		2012	
Designer/Constructor	Nikken Sekkei + Kajima Corporation		Belju Co., Ltd. + Takenaka Corporation		Nikken Sekkei + Takenaka Corporation	
Sub-structure	LS	US	LS	US	LS	US
Building type	RC	SF	SF	RC	SRC	SF
d_1 x d_2 [m]	131.4 x 50	131.4 x 39	39 x 39	25 x 25	76 x 76	62 x 62
H [m]	134.1		152.1		198.96	
H_{ISO} [m]	5.1		114.0		46.6	
n_{floors}	1	23	24	9	9	30
A_{floors} [m^2]	6570	117866	39167	11705	30680	115320
μ [-]	15.0		0.4		2.6	
T_{ISO} [s]	n.a.		4		≈ 3.6	
δ_{ISO} [cm]	n.a.		≤ 50		≤ 40	
ISO system	NRB (Φ1100 ÷ Φ1500) + OD + SD		23xNRB + 12 OD		66xLRB (32 – 1500x1500 + 34 - Φ800 ÷ Φ1000) + 24xOD	

Table A.5. Data of: Ochanomizu Sola City, Nihonbashi dia building, Wakabadai No.1 Apartment Building

Name	Ochanomizu Sola City		Nihonbashi dia building		Wakabadai No.1 Apartment Building	
Photo			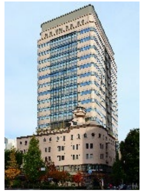			
Intervention type	IT4		IT4		IT3	
Destination of use	Office + Retails + Education-related facilities + Cultural exchange facilities		Office + Storage		Office + Retail + Housing	
Address	Chiyoda City, Tokyo 101-0062, Japan		Chuo City, Tokyo 103-0027, Japan		Yokohama, Kanagawa 241-0801, japan	
Year	2013		2014		2016	
Designer/Constructor	Taisei Corporation		Mitsubishi Warehouse Co. + Takenaka Corporation		Sumitomo Mitsui Construction Co., Ltd.	
Sub-structure	LS	US	LS	LS	LS	LS
Building type	SF + CFT	SF + CFT	SRC	SRC	SRC	RC
d_1 **x** d_2 **[m]**	79.2 x 48	79.2 x 48	78 x 80	78 x 80	78 x 80	60 x 10
H **[m]**	110		89.9		42	
H_{ISO} **[m]**	13.2		29.0		10	
n_{floors}	2	21	3	3	2	11
A_{floors} **[m²]**	7603	79834	18720	18720	12480	6600
μ **[-]**	10.5		0.8		0.5	
T_{ISO} **[s]**	≈ 4.1		n.a.		n.a.	
δ_{ISO} **[cm]**	34 (<50)		n.a.		40.5 (≤ 45)	
ISO system	14xNRB + 30xLRB + 8xOD		LRB		16xNRB + OD	

Table A.6. Data of: Tekko Building – Main and South Building, Kyobashi Edogrand.

Name	Tekko Building - Main Building		Tekko Building - South Building		Kyobashi Edogrand	
Photo					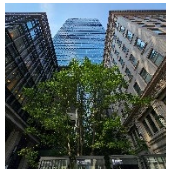	
Intervention type	IT4		IT4		IT4	
Destination of use	Office + hotel + Retail		Office + hotel + Retail		Office + Retail	
Address	Chiyoda City, Tokyo 100-0005, Japan		Chiyoda City, Tokyo 100-0005, Japan		Chuo City, Tokyo 104-0031, Japan	
Year	2015		2015		2016	
Designer/Constructor	Mitsubishi Estate Company, Ltd + Taisei Corporation + Permasteelisa Group		Mitsubishi Estate Company, Ltd + Taisei Corporation + Permasteelisa Group		Nikken Sekkei + Shimizu Corporation	
Sub-structure	LS	LS	LS	LS	LS	US
Building type	SF	SF	SRC	SRC	SRC	SF + CFT
d_1 x d_2 [m]	114.5 x 33.6	68.5 x 35.7	66 x 98.5	66 x 98.5	66 x 98.5	50 x 75
H [m]	136.5		98.5		170	
H_{ISO} [m]	16.0		30.0		31.5	
n_{floors}	3	5	5	5	5	26
A_{floors} [m^2]	12222	10055	18750	18750	32505	97500
μ [-]	7.7		1.3		2.7	
T_{ISO} [s]	≈ 5.3		≈ 4.6		≈ 6.1	
δ_{ISO} [cm]	33.6		28.5		37.5 (<50)	
ISO system	48xNRB (Φ1000 ÷ Φ1500) + 30xU-SD + 40xOD		10xNRB (Φ800 ÷ Φ1200) - 8xOD		10xNRB (Φ1300) + 2xNRB (Φ1400) + 14xNRB (Φ1500) + 4xNRB (Φ1500 x 2) + 6 ESB (Φ1500)+ 48xOD + 4 Elastic sliding	

Table A.7. Data of: Roppongi Grand Tower, DaiyaGate Ikebukuro.

Name	Roppongi Grand Tower		DaiyaGate Ikebukuro	
Photo			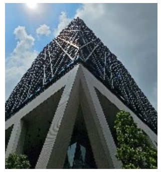	
Intervention type	IT4		IT4	
Destination of use	Office		Office + Retail	
Address	Minato City, Tokyo 106-0032, Japan		Toshima City, Tokyo 171-0022, Japan	
Year	2016		2019	
Designer/Constructor	Nikken Sekkei + Taisei Corporation + Obayashi Corporation		Nikken Sekkei + Obayashi Corporation + Seibu Construction & Engineering Co.	
Sub-structure	LS	LS	LS	US
Building type	SRC+SF (w. VDW)	SRC+SF (w. VDW)	SF	SF
d_1 **x** d_2 **[m]**	65 x 65	65 x 65	46.8 x 64.8	46.8 x 64.8
H **[m]**	230.76		100	
H_{ISO} **[m]**	130.0		20.0	
n_{floors}	25	25	3	16
A_{floors} **[m²]**	105625	105625	9098	48522
μ **[-]**	0.53		5.3	
T_{ISO} **[s]**	≈ 4.4		≈ 6	
δ_{ISO} **[cm]**	≤ 40		≤ 49.5	
ISO system	41xNRB (33Φ1300 + 4Φ1400 + 4Φ1500) + 56xSD + 64xOD (4 with rock mechanism)		20xNRB (16Φ1000 + 4Φ1500) + SD	

Appendix B. The non-proportional damped system

The equation of motion for a general *n*DOF system (*n* = system DOF) can be written in matrix form as:

$$\boldsymbol{M}\ddot{\boldsymbol{u}} + \boldsymbol{C}\dot{\boldsymbol{u}} + \boldsymbol{K}\boldsymbol{u} = -\boldsymbol{M}\mathbf{r}\ddot{\boldsymbol{u}}_{\boldsymbol{g}} \tag{B.1}$$

where the matrices $\boldsymbol{M}$, $\boldsymbol{C}$, $\boldsymbol{K}$ are respectively the mass, damping and stiffness n x n matrices, while the vectors $\ddot{\boldsymbol{u}}$, $\dot{\boldsymbol{u}}$, $\boldsymbol{u}$ contain respectively the n-values of acceleration, velocity and relative displacement with respect to the base of each DOF of the system. Eq. (B.1) is given by considering as input on the system an acceleration $\ddot{\boldsymbol{u}}_g$ applied to the individual DOFs through the vector $\mathbf{r}$.

In design practice, the assumption commonly adopted is that the frequencies and vibration modes of a system can be evaluated from Eq. (B.1) by excluding the contribution of damping, i.e. $\boldsymbol{C}$ = 0. This assumption leads to decoupled equations of motion and thus frequencies and vibration modes expressed by real numbers. However, it is also possible to force decoupling of the motion equations even considering the damping matrix, but it must be assumed that the equivalent viscous damping in the system is proportional to the masses and/or stiffnesses of the system. However, this latter condition can only be satisfied if the distribution of the equivalent viscous damping within the structure is proportional to the distribution of masses and/or stiffnesses in the system. Consequently, such systems are called *non-proportional damped systems* or *non-classically damped systems*.

Therefore, a system with intermediate isolation level showing a large difference between the damping ratio of the isolation storey and the remaining storeys is classified as a *non-proportionally* (or *non-classically*) damped system, for which a fully populated damping matrix should be considered to provide an accurate response prediction [90]. In general, as suggested by [139], the following parameter (e_{ij}) can be used to quantify modal coupling:

$$e_{ij} = \mathbf{\Phi}_{0i}^{T} \boldsymbol{C} \mathbf{\Phi}_{0j}^{T} \omega_{0i} \Big/ \left| \omega_{0i}^{2} - \omega_{0j}^{2} \right| \tag{B.2}$$

where, ω_{0i}, ω_{0j} and $\mathbf{\Phi}_{0i}^{T}$, $\mathbf{\Phi}_{0j}^{T}$ are the undamped natural frequency and mode shapes for the i and j mode. The modal coupling occurs if e_{ij} is larger than unity for all mode pairs $i \neq j$ and if else the natural frequency of each undamped mode ω_0 is close to dominant input frequency (ω).

A non-proportionally damped system has a complex-valued natural modes and does not satisfy the Caughey and O' Kelly identity:

$$\boldsymbol{C}\boldsymbol{M}^{-1}\boldsymbol{K} = \boldsymbol{K}\boldsymbol{M}^{-1}\boldsymbol{C} \tag{B.3}$$

Consequently, since the whole damping matrix $\boldsymbol{C}$ must be considered and the motion equations cannot be decoupled for analytical convenience, it is advisable to rewrite Eq. (B.1) in the first-order state space form as follows:

$$\dot{\mathbf{u}}(t) = \boldsymbol{A}\mathbf{u}(t) + \boldsymbol{b}x(t) \rightarrow \begin{Bmatrix} \dot{u}_1 \\ \vdots \\ \dot{u}_n \\ \ddot{u}_1 \\ \vdots \\ \ddot{u}_n \end{Bmatrix} = \begin{bmatrix} \boldsymbol{0} & \boldsymbol{I} \\ -\boldsymbol{M}^{-1}\boldsymbol{K} & -\boldsymbol{M}^{-1}\boldsymbol{C} \end{bmatrix} \cdot \begin{Bmatrix} u_1 \\ \vdots \\ u_n \\ \dot{u}_1 \\ \vdots \\ \dot{u}_n \end{Bmatrix} + \begin{bmatrix} \boldsymbol{0} \\ \boldsymbol{M}^{-1} \end{bmatrix} \cdot \begin{Bmatrix} 0 \\ \vdots \\ 0 \\ -1 \\ \vdots \\ -1 \end{Bmatrix} \cdot \ddot{\boldsymbol{u}}_g \tag{B.4}$$

where, $\mathbf{u}$ is the state vector of dimension n, $\boldsymbol{A}$ is the state matrix and $\boldsymbol{b}$ are coefficient matrices and have dimensions of $2n$ x $2n$ and $2n$ x n respectively, $x(t)$ is the input control vector of dimension n.

The *i-th* complex-conjugate eigenvalue λ_i, $\bar{\lambda}_i$ and *i-th* ($2n$x1) complex-conjugate eigenvector $\mathbf{\Phi}_i$, $\bar{\mathbf{\Phi}}_i$ can be derived by solving the $2n$ homogeneous algebraic system ($\boldsymbol{A}$- $\lambda_i\boldsymbol{I}$) $\mathbf{\Phi}_i$ = $\mathbf{0}$; the *i-th* natural frequency is $\omega_i = |\lambda_i|$ and the *i-th* modal damping ratio is $\eta_i = \mathbf{Re}(\lambda_i)/|\lambda_i|$. The lower half part of the eigenvector $\mathbf{\Phi}_i$ gives the mode shapes, $\boldsymbol{\psi}_i$.

After evaluating the complex modal characteristics, the total peak response of the system with non-proportional damping can be calculated using a modal superposition rule, square root of the sum of the squares SRSS (R_{SRSS}), or complete quadratic combination CQC (R_{CQC}), as suggested in [83]:

$$R_{SRSS} = \sqrt{\sum_{1}^{n} B_i^2 R_i^2} \tag{B.5}$$

$$R_{CQC} = \sqrt{\sum_{i=1}^{n}\sum_{j=1}^{n} B_i B_j \rho_{ij,mod} R_i R_j} \tag{B.6}$$

where: R_i, is the maximum relative displacement response of SDOF model with natural frequency ω_i and damping ratio η_i, or in other words is the spectral displacement of the oscillator just mentioned; B_i, is a real-valued participation factor and $\rho_{ij,mod}$ are correlation coefficients.

In particular, B_i is equal to:

$$B_i = \sqrt{a_i^2 + \omega_i^2 c_i^2} \tag{B.7}$$

in which $a_i = -2\mathrm{Re}\left(b_i \bar{\lambda}_i\right)$ and $c_i = -2\mathrm{Re}\left(b_i\right)$ are the real valued coefficients, while $b_i = \left(\mathbf{q}^{\mathbf{T}}\mathbf{\Phi}_i\right)\left(\mathbf{\Phi}_i^T \boldsymbol{M}\mathbf{r}\right)\left(-\lambda_i \mathbf{\Phi}_i^T \boldsymbol{M}\mathbf{\Phi}_i + \lambda_i^{-1}\mathbf{\Phi}_i^T \boldsymbol{M}\mathbf{\Phi}_i\right)^{-1}$. The matrix $\mathbf{q}^{\mathbf{T}}$ = diag($\boldsymbol{I}$) is used to consider the relative displacements of the system.

Both Eqs. (B.5) and (B.6) provide the maximum system displacement to a response spectrum analysis with the difference that Eq. (B.5) is evaluated using the SRSS modal combination rule and does not take into account the correlation between modal responses. However, this effect can considerably change the response of the system when two or more natural frequencies are close to each other. Thus, it is recommended to employ the modal superposition rule CQC in the latter case.

The correlation effect between the modal responses is taken into account in Eq. (B.6) through the correlation coefficient $\rho_{ij,mod}$:

$$\begin{aligned}\rho_{ij,mod} &= \rho_{ij} \cdot ce_{ij} \\ &= \left[\frac{8\sqrt{\xi_i \xi_j}\left(\beta_{ij}\xi_i + \xi_j\right)\beta_{ij}^{3/2}}{\left(1-\beta_{ij}^2\right)^2 + 4\xi_i\xi_j\beta_{ij}\left(1+\beta_{ij}^2\right) + 4\left(\xi_i^2+\xi_j^2\right)\beta_{ij}^2}\right]\cdot\left[\frac{a_i a_j + \omega_i\omega_j c_i c_j}{B_i B_j}\right]\end{aligned} \tag{B.8}$$

where β_{ij} is the ratio between the frequencies at modes i and j. Furthermore, it can be seen that the first square brackets of Eq. (B.8) (i.e. ρ_{ij}) shows the correlation term already suggested by several standards [50, 94] for classically damped systems, whereas the term ce_{ij} takes into account the phase difference between the modal response coefficients and thus considers the correlation effect of the phase.

It should be pointed out that non-classically damped systems can be analysed within the framework of time-history analyses by considering the whole damping matrix, which requires a direct integration analysis, again excluding the assumption of proportional damping to masses or stiffnesses.

Appendix C. The Pole Allocation Method (PAM)

C.1 Open-loop vs. closed-loop system

Before introducing the pole allocation method, it is important to define the difference between an open-loop controlled system and a closed-loop controlled system.

In general, a system excited through an input signal responds with an output signal, such as the case of a building under ground motion that will oscillate according to its dynamic characteristics yielding an output signal, following the *processes* (or *plants*) in Figure C.1.

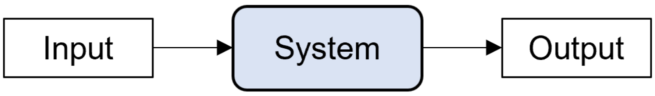

Figure C.1 Plants.

Generally, in engineering problems, the operation that is performed is to calculate the output, through so-called *analysis*, since the characteristics of the system and the input are known data of the problem. However, in some cases the known data of the problem could be the input and output and the goal become the identification of the system properties, in this case the task is called *system identification*. In addition, it could also happen that the working conditions of a system are known, but the system has not yet been defined; in that case, the aim will be the *system design*.

In a system control problem, all three of the above-mentioned tasks are involved; where, the characteristics of the *processes* (input - system - output) may not all be known exactly, but there may be uncertainties that need to be managed by means of a mechanism guaranteeing that certain requirements are met.

The system shown in Figure C.1 is a typical case of an *uncontrolled system*, where the input acting on the system gives an output in accordance with the mechanical characteristics of the system. Instead, a process where the input acting on the system is provided by a controller set to allow a desired output to the system is called a *controlled system* (Figure C.2). In the latter case, the controller is pre-programmed to provide a certain output (i.e. the system input) that is not affected by the effective output; therefore, this type of control is called *open-loop control*. A classic example of a process with open-loop control in building management concerns lighting or air-conditioning system that switches on or off at a certain time independently of ambient conditions, i.e. low light or deviation from the comfort temperature.

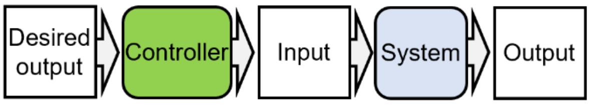

Figure C.2 block diagram of the open-loop control processes.

However, if to the process just described, tasks are added that allow the variation of the input into the system as a function of the output, the efficiency of the whole process increases. Indeed, returning to the example of the lighting or air-conditioning system, sensors can be installed that detect the variation of lighting or temperature with respect to target values and adjust the input accordingly to achieve these target values of lighting and temperature. This type of control can be simplified with the block diagram in Figure C.3 and is called *feedback control* or *closed-loop control*.

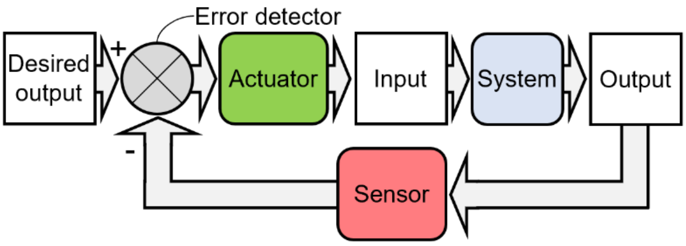

Figure C.3. block diagrams of the closed-loop control processes.

Let us now take as an example the 2DOF IIS system under a ground motion analysed in the chapter 2 (Figure 2.2b). From the aforementioned, if the mechanical characteristics of the system (i.e. m_{LS}, c_{LS}, k_{LS} and M_{ISO}, c_{ISO}, k_{ISO}) are known, the output can be evaluated by writing the equations of motion, and after some analytical manipulations we have seen how the transformed input (i.e. $\ddot{U}_g(s)$) and the transformed output (i.e. U_{LS} (s)) can be connected to each other through the transfer function G (s). Finally, it is possible to calculate the response of the system by means the inverse Laplace transform. Therefore, the block diagram in Figure C.1 becomes the diagram in Figure C.4 for the *uncontrolled system*. However, since control of the systems response is not possible, an unstable system response may occur.

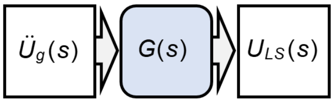

Figure C.4. block diagrams for open-loop control processes with transfer function.

As known from the literature [98, 99], the stability of the system response depends on the position of the system poles in the Laplace domain. In fact, if the poles are located on the right-hand side of the s-plane the response of the system will be unstable, conversely, if the poles are located on the left-hand side of the s-plane the response of the system will be stable (Figure C.5). For each degree of freedom of the system, we obtain a set of poles (λ_i and its conjugate λ_i^*) associated with the corresponding i-th mode of vibration of the system, thus, in Figure C.5 with ξ_i and ω_i have been denoted, respectively, the damping ratio of the i-th mode and the circular natural frequency of the i-th mode.

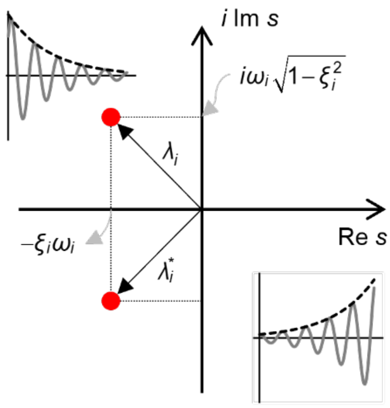

Figure C.5. Laplace plane for a system with viscous damping.

There are several system control techniques to achieve only a stable system response, i.e. the poles are placed on the left side of the *s*-plane. One of the most widely used techniques in the engineering field is the Pole Allocation Method (PAM).

The PAM is generally applied for the closed loop control systems. Only recently, Ikeda [70, 71] has proposed an application of PAM to passive vibration control systems, i.e., systems with open-loop control. So, in order to highlight the differences between the two approaches in the following, the application of PAM to closed-loop systems will be briefly analysed, and then PAM will be applied to the 2DOF IIS, i.e., an open-loop system.

C.2 PAM for closed-loop systems

The approach of the PAM has been developed in the late 1960s and is essentially a time domain approach, based on the state-space description of the dynamic behaviour of the lumped-parameter systems [98]. In particular, the PAM control strategy is the methodology used to calculate the control gains required to move the poles of the closed-loop system associated with the controlled modes; hence, this approach is also known as *modal control* (Figure C.6).

Now, let us first describe PAM in general following the time domain approach proposed by Porter and Crossley in [168].

Let us consider a 2DOF concentrated mass system, where ***M***, ***C***, ***K*** denote the mass, damping and stiffness matrix of the system, respectively. The state equation is as follows:

$$\dot{\mathbf{u}}(t)=\boldsymbol{A}\mathbf{u}(t)+\boldsymbol{b}x(t)\rightarrow\begin{Bmatrix}\dot{u}_1\\\dot{u}_2\\\ddot{u}_1\\\ddot{u}_2\end{Bmatrix}=\begin{bmatrix}\boldsymbol{0} & \boldsymbol{I}\\-\boldsymbol{M}^{-1}\boldsymbol{K} & -\boldsymbol{M}^{-1}\boldsymbol{C}\end{bmatrix}\cdot\begin{Bmatrix}u_1\\u_2\\\dot{u}_1\\\dot{u}_2\end{Bmatrix}+\begin{bmatrix}\boldsymbol{0}\\\boldsymbol{M}^{-1}\end{bmatrix}\cdot\begin{Bmatrix}x_1\\x_2\end{Bmatrix} \quad \text{(C.1)}$$

where $\mathbf{u}(t)$ is the state vector of dimension $2n$ (n = system DOF), ***A*** (plant matrix of uncontrolled system) and ***b*** are coefficient matrices and have dimensions of $2n$ x $2n$ and $2n$ x n respectively, $u(t)$ is the input control vector of dimension n.

Eq. (C.1) is representative of the dynamic behaviour of an open-loop system, for which it is possible to calculate the eigensolutions [98, 168]: eigenvalue λ_1, λ^*_1 and λ_2, λ^*_2, right eigenvector $\mathbf{x}_1$ e $\mathbf{x}_2$ and left eigenvector $\mathbf{v}_1$ and $\mathbf{v}_2$. It can be shown that if the left and right eigenvectors are normalised, they satisfy the following condition:

$$\mathbf{v}_j^T \mathbf{x}_i = \delta_{ij} \quad \forall i, j = 1,2 \tag{C.2}$$

where δ_{ij} denotes the kronecker delta; thus, this means that the eigenvectors of $\boldsymbol{A}$ and $\boldsymbol{A}^{\mathrm{T}}$ corresponding to different eigenvalues are orthogonal.

However, it is possible to control m modes of the system; in fact, if all elements of the state vector $\mathbf{u}(t)$ are measured by appropriate sensors, it will be possible to combine these read outputs to generate a control signal provided by the expression:

$$s_j(t) = \sum\nolimits_{k=1}^{n} v_{jk} u_k = \mathbf{v}_j^T \mathbf{u}(t) \quad \forall j = 1,\ldots,m \tag{C.3}$$

where the measured vector can be chosen equal to $\mathbf{v}_j$, to allow an appropriate selection of m eigenvectors of $\boldsymbol{A}^{\mathrm{T}}$. Indeed, with this position, as demonstrated in [168] the eigenvalues λ_j change to some new values ρ_j and the eigenvectors $\mathbf{x}_j$ to some corresponding new vectors $\mathbf{w}_j$; while leaving unchanged the (n - m) eigenvalues and eigenvectors of the uncontrolled system plant matrix. Thus, there are m proportional controllers having as modal control gain, g_j, which provides an input control force $x(t)$ equal to:

$$x(t) = -\sum\nolimits_{j=1}^{m} g_j \mathbf{v}_j^T \mathbf{u}(t) \tag{C.4}$$

By substituting Eq. (C.4) into Eq. (C.1), is obtained:

$$\dot{\mathbf{u}}(t) = \boldsymbol{A}\mathbf{u}(t) - \boldsymbol{b}\sum\nolimits_{j=1}^{m} g_j \mathbf{v}_j^T \mathbf{u}(t) \tag{C.5}$$

Thus, the plant matrix $\boldsymbol{A}$ of the uncontrolled system becomes the plant matrix $\boldsymbol{C}$ of the controlled system, where $\boldsymbol{C}$ is equal to:

$$\boldsymbol{C} = \boldsymbol{A} - \boldsymbol{b}\sum\nolimits_{j=1}^{m} g_j \mathbf{v}_j^T \tag{C.6}$$

Hence, Eq. (C.5) can be rewritten as:

$$\dot{\mathbf{u}}(t) = \boldsymbol{C}\mathbf{u}(t) \tag{C.7}$$

Eq. (C.7) is the equation for the closed-loop system, and it can be observed that:

$$\boldsymbol{C}\mathbf{x}_j = \boldsymbol{A}\mathbf{x}_j = \lambda_j \mathbf{x}_j \quad \forall j = m+1,\ldots,n \tag{C.8}$$

From Eq. (C.8) it can be seen that eigenvalues and eigenvectors of the open-loop system are equal to eigenvalues and eigenvectors of the closed-loop system, for modes m + 1 to n (i.e. uncontrolled modes).

The procedure just described can be summarised by the block diagram in Figure C.6, where it can be seen that the system described by the coefficient matrix ***A*** belongs to an open-loop system; whereas the system described by the matrix ***C*** is evaluated through the modal control gains defined within the closed-loop system.

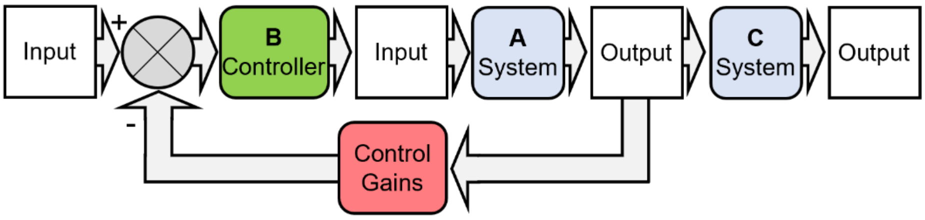

Figure C.6. Block diagram for pole allocation method.

The whole analytical procedure to identify the algorithm for computing modal control gains can be found in [98, 168]; where it can be seen that the PAM provides a "*feedback control*" relationship, making the structural response less sensitive to variation in structural parameters. Therefore, this approach is classified as "modern control theory" and is applied for the systems with active or semi-active control.

Appendix D: Suggested value of ISO damping ratio

In chapter 2 has been analysed the influence of design parameters f and μ on system response for a fixed value of ξ_{LS} and ξ_{ISO}. However, while the parameter ξ_{LS} is usually fixed in practical applications and therefore its influence on the systems response is not very important, the influence of the parameter ξ_{ISO} on the IIS response is very important.

In the literature, there are several works that assess under certain positions the optimal value of f and ξ_{ISO}, i.e. f_{opt} and $\xi_{I,opt}$, for a classical TMD system. Consequently, this appendix aims to provide a suggested ξ_{ISO} value for a system with non-classical TMD such as the IIS. To achieve this goal, we first analyse the influence of ξ_{ISO} on the IIS response and then suggest a value of ξ_{ISO} to be used in practical design.

D.1 Influence of design parameters on IIS structural response

The system response has been analysed in the chapter 2 through the *Dynamic Magnification Factor* evaluated for both support excitation ($DMF_{ug,\ 2DOF\ IIS}$) and an applied force on the first mass ($DMF_{FE,\ 2DOF\ IIS}$), whose equations are given below for simplicity.

$$\begin{aligned}
&DMF_{ug,2DOF\,IIS} = \frac{u_{LS}}{\ddot{u}_g} = \left| -\frac{2\xi_{ISO}\lambda f + 2\mu\xi_{ISO}\lambda f - \mu f^2 i - f^2 i + \lambda^2 i}{\omega_{LS}^2\left(b_1 f^2 + b_2 f + \lambda^2 i - \lambda^4 i - 2\lambda^3\xi_{LS}\right)} \right| \\
&b_1 = \left(2\xi_{LS}\lambda - i + \lambda^2 i + \mu\lambda^2 i\right) \\
&b_2 = \left(-2\xi_{ISO}\lambda^3 + 2\xi_{ISO}\lambda - 2\mu\xi_{ISO}\lambda^3 + 4\xi_{LS}\xi_{ISO}\lambda^2 i\right)
\end{aligned} \tag{D.1}$$

$$DMF_{F_E,2DOF\,BIS} = \left|\frac{u_{LS}}{u_{st}}\right| = \sqrt{\frac{\left(2\xi_{ISO}\lambda^2\right)^2 + \left(\lambda^2 - f^2\right)^2}{\left(2\xi_{ISO}\lambda\right)^2\left(\lambda^2 - 1 + \mu\lambda^2\right)^2 + \left[\mu f^2\lambda^2 - \left(\lambda^2 - 1\right)\left(\lambda^2 - f^2\right)\right]^2}} \tag{D.2}$$

As reported in section 2.2, the Eq. (D.1) is a function of the following design parameters: tuning ratio, f, forced frequency ratio, λ, mass ratio, μ, LS damping ratio, ξ_{LS} and ISO damping ratio, ξ_{ISO}. The Eq. (D.2) is a function of the same design parameters just mentioned except for the LS damping ratio, which for simplicity is set equal to zero.

Starting from Eq. (D.2), In order to evaluate the influence of the design parameter ξ_{ISO} on the structural response of the 2DOF IIS model, in Figure D.1 are reported five different curves obtained for five value of ξ_{ISO} = [0, 0.1, 0.2, 0.3, ∞]. In particular, Figure D.1 shown the ratio between the LS mass displacement amplitude u_{LS}, divided by the static displacement of the same mass, u_{st}, versus the forced frequency ratio, λ = [0.5 – 2]; for a fixed value of forced frequency ratio, f = 1 and several value of damping ratio, ξ_{ISO}, and mass ratio, μ = [0.05, 0.20, 1, 2]. Therefore, it is observed that as the damping ratio varies, there are two limiting solutions, i.e. ξ_{ISO} = 0 and ξ_{ISO} = ∞; for the first solution there are two vertical asymptotes, for the second limit solution only one peak is shown as the mass of the isolated upper structure is fixed to the LS mass. However, if we consider values of ξ_{ISO} with more practical interest, i.e. ξ_{ISO} = [0.1, 0.2, 0.3], we observe that the amplitude at resonance frequency is only limited by the variation of the damping ratio. Moreover, the range of λ values for which it is interesting to study the system response includes the frequency values at the two vibration modes of the 2DOF IIS model where is a response amplification due to the resonance effect, i.e. $0.5 \leq \lambda \leq 1.5$. Finally, it is interesting to note that low mass ratios bring the system response peaks closer to each other, with the result that the system is very sensitive to the input frequency, *vice versa* with high mass ratios the two system response peaks move away from each other, and the absorber provides greater robustness against input frequency variation.

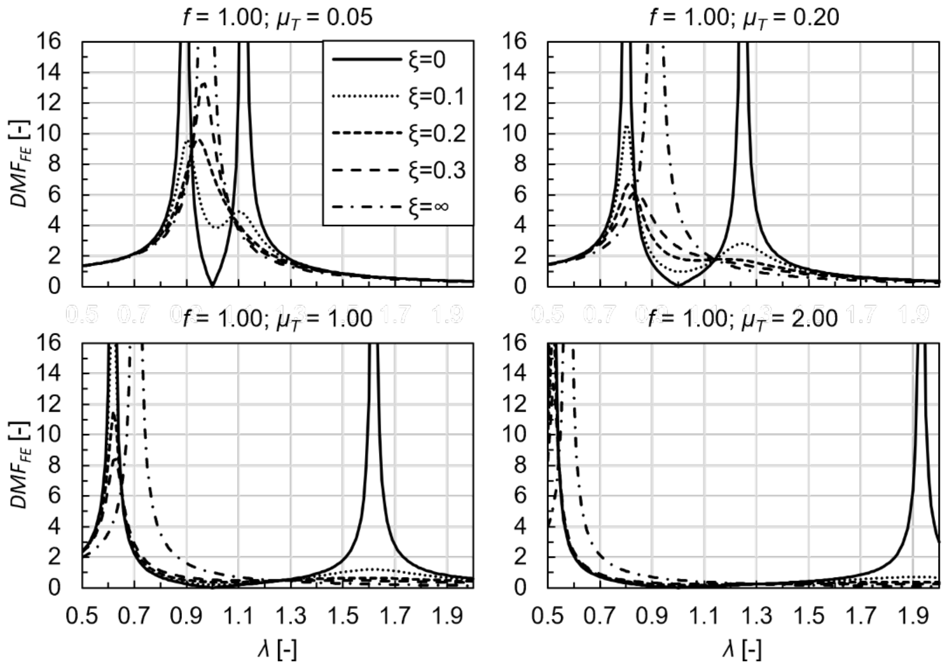

Figure D.1. Main mass displacement amplitude vs. forced frequency ratio for f = 1 and μ_T = [0.05, 0.20, 1, 2].

Next, we assess the influence of the five design parameters (i.e., f, λ, μ, ξ_{LS} and ξ_{ISO}) on the response of the 2DOF IIS model given by Eq. (D.1) through a parametric analysis.

First, we consider the response of the system (Figure D.2) by varying the following design parameters: μ = [0.01, 1], where the first value is representative of a system with classical TMD, while the second value, i.e. 1, can be assumed as representative an IIS solution; λ =[0 - 3], this range of values can identify both the first and second vibration mode response peaks; ξ_{ISO} = [0 - 0.5], where the upper limit, i.e. 0.5, has been assumed as the maximum value obtainable in practical applications; ξ_{LS} = 0.05, is a typical value used for reinforced concrete and masonry structures; f = (0.5, 1), which are the optimal tuning value for μ = 0.01 and 1, respectively, evaluated thought a Den Hartog's formula $f_{opt} = (1/1+\mu)^{0.5}$ [84].

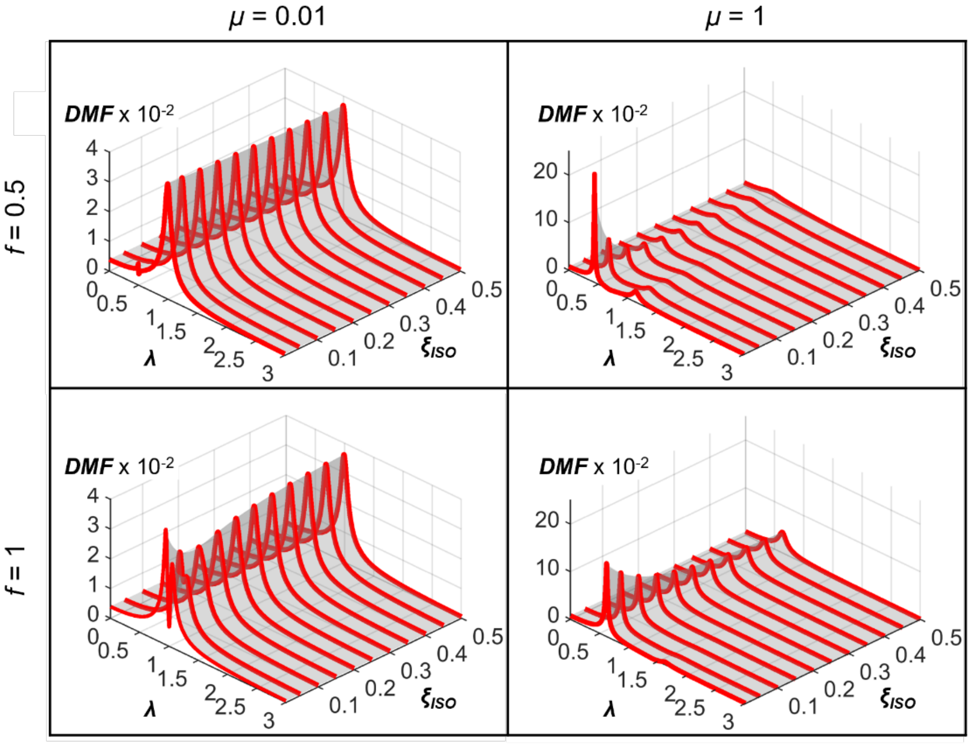

Figure D.2. *DMF*-λ-ξ_{ISO} surface plots for λ = [0 - 3], ξ_{ISO} = [0 – 0.5], f = [0.5, 1], μ = [0.01, 0.1].

The results of this parametric analysis are shown in Figure D.2, where it is observed that: (i) as the mass ratio μ increases, the distance between the two peaks of the response increases; (ii) the adoption of the optimal tuning ratio is necessary when low mass ratios are considered, i.e. μ = 0.01, in fact, if $f \neq f_{opt}$ even an increase in the damping ratio of the isolation system (i.e. absorber damping) does not lead to an appreciable reduction of the *DMF* parameter; (iii) for large mass ratios, i.e. μ = 1, and for very small values of ξ_{ISO} the use of an optimal tuning ratio, $f = f_{opt}$, leads to a greater reduction in the system's response than the case of f = f_{opt} =0.5, but for ξ_{ISO} values equal to or greater than 0.1, the *DMF* value evaluated for both values of f is approximately equal; (iv) the range of λ values of greatest interest is between 0.5 and 1.5.

Subsequently, in order to investigate, in more detail, the influence of the tuning ratio on the 2DOF IIS model response, a parametric analysis has been conducted; where the tuning ratio, *f,* is varied within the range of values 0 - 3, for three fixed values of forced frequency ratio, i.e. λ = [0.5, 1, 1.5] and four fixed values of the mass ratio, i.e. μ = [0.01, 0.1, 0.5, 1]. For the LS and ISO damping ratio, the same values adopted in the previous analysis have been considered, i.e. ξ_{LS} = 0.05 (typical value used for reinforced concrete and masonry structures) and ξ_{ISO} = [0 – 0.5]. The results of this analysis are reported in Figure D.3 and Figure D.4 that show several surface plots depicting the *DMF* values when *f* and ξ_{ISO} vary, for fixed values of μ and λ.

For low values of mass ratio, i.e. μ = 0.01, it can be observed from Figure D.3 that the tuning ratio has a considerable influence on the system response. Indeed, for λ = 1 (i.e. $\omega = \omega_{LS}$), a tuning ratio equal to 1 (i.e. $\omega_{LS} = \omega_{ISO}$) leads to a considerable reduction in the system response, which decreases as the value of ξ_{ISO} increases, since the increase in the damping ratio of ISO tends to increase the DMF value in the area between the two response peaks. For comparison, the surface plots are also considered for the case of λ equal to 0.5 and 1.5, where an insensitivity of the *DMF* value to both *f* and ξ_{ISO} can be seen, indicating that outside the λ region where the response amplification peaks occur, the efficiency of the system drops. In addition, for the mass ratio μ = 0.1 (Figure D.3) the same considerations just made are still applicable except that for λ equal to 0.5 and 1.5, where *f* starts to have a small influence on the *DMF* value. However, as the mass ratio increases, the two response peaks identified in Figure D.2 move away from each other and thus *f* also influences the response for λ equal to 0.5 and 1.5, although the increase of DMF when *f* is changed can be managed by increasing the damping ratio of the isolation system.

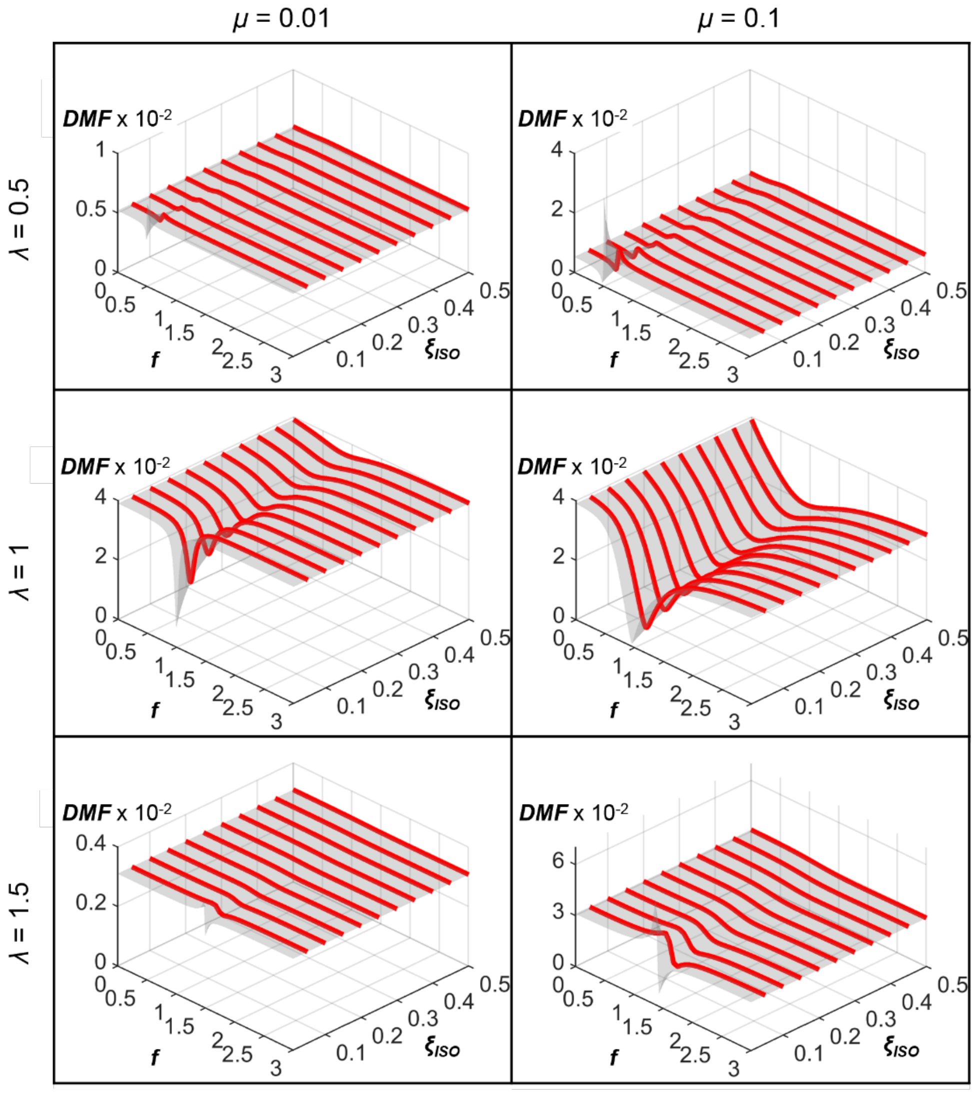

Figure D.3. *DMF-f-* ξ_{ISO} surface plots for λ = [0.5, 1, 1.5] and μ = [0.01, 0.1]

Furthermore, in Figure D.3 and Figure D.4 for λ = 1, as μ increases, it can be seen that after a certain value of *f*, we could say 0.5, the system response becomes independent of *f*. Finally, the red curves above the surface plots represent the DMF trend as *f* changes for a fixed value of ξ_{ISO} where it is clear that as ξ_{ISO} increases, the curves tend to flatten out and not change. The latter observation occurs for any value of λ.

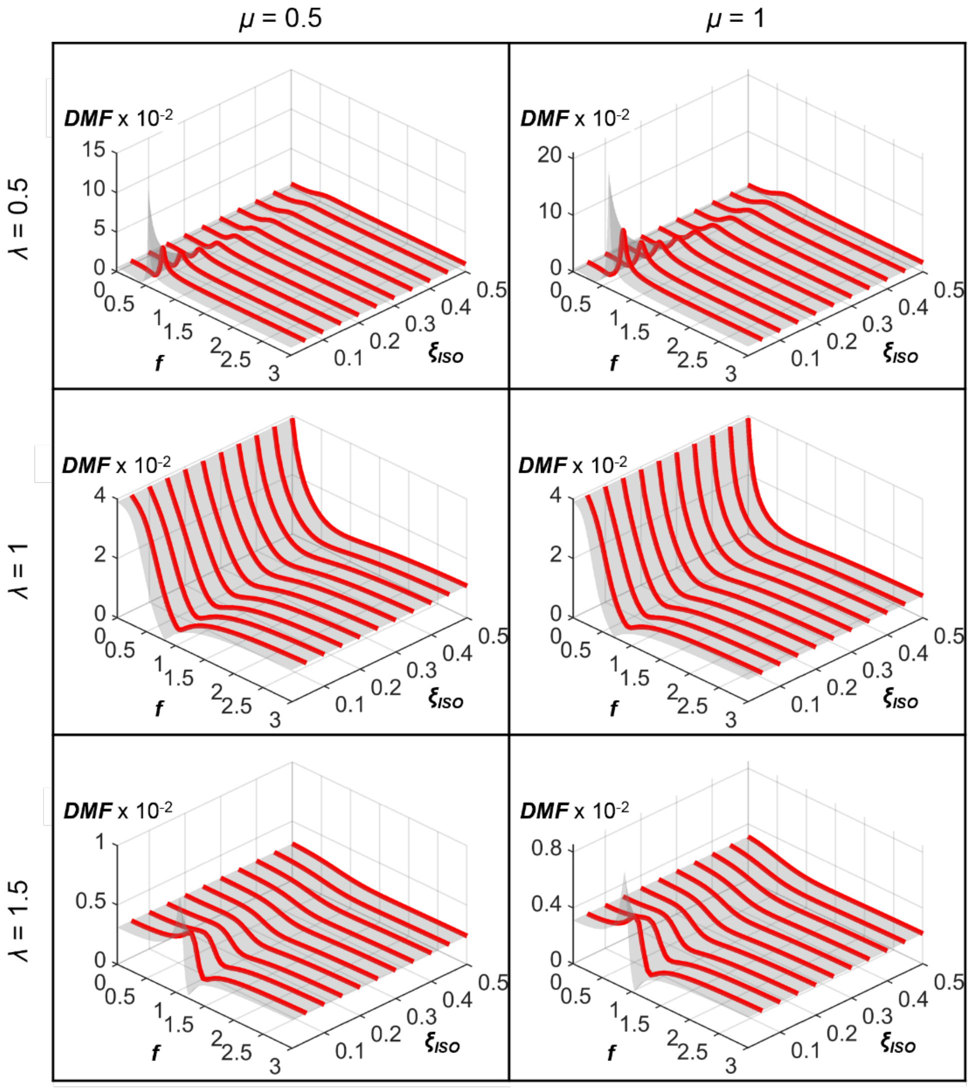

Figure D.4. *DMF-f-* ξ_{ISO} surface plots for λ = [0.5, 1, 1.5] and μ = [0.5, 1].

The considerations just made show that the classical TMD system (i.e. the 2DOF IIS model with low mass ratio) is very sensitivity to the input frequency yields the classical TMD strategy inefficient against the earthquake because the seismic inputs that may be characterised by a considerable frequency content. Instead, for the intermediate isolation system (i.e. the 2DOF IIS model with hight mass ratio) the sensitivity at parameter *f* is lower than the classic TMD system; of consequence, its efficiency against seismic inputs is higher than the classical TMD system. For this reason, it is considered that in the case of IIS, since the absorber vibration system (i.e. the isolated upper structure) may not be tuned to the lower structure, an optimal damping value must be found for the isolation system that does not start from the assumption that there is a tuning between the frequencies of the main system and the absorber.

D.2 Optimal design parameters: conventional TMD vs nonconventional TMD

In literature, there are several relationships that provide the optimal values of f and ξ_{ISO}, respectively indicated as f_{opt} and $\xi_{ISO,opt}$; among the best known relations could be taken into account the ones suggested by Den Hartog [84], Warburton [85] and Tsai and Lin [86], respectively shown in Eqs. (D.3) – (D.5).

$$\begin{cases} f_{opt} = \dfrac{1}{1+\mu} \\ \xi_{ISO,opt} = \sqrt{\dfrac{3\mu}{8(1+\mu)}} \end{cases} \tag{D.3}$$

$$\begin{cases} f_{opt} = \dfrac{\sqrt{(1-\mu/2)}}{1+\mu} \\ \xi_{ISO,opt} = \sqrt{\dfrac{3\mu}{8(1+\mu)(1-\mu/2)}} \end{cases} \tag{D.4}$$

$$
\begin{cases}
f_{opt} = \left(\dfrac{\sqrt{1-\mu/2}}{1+\mu} + \sqrt{1-2\xi_{LS}^2} - 1 \right) \\
\qquad -\left(2.375 - 1.034\sqrt{\mu} - 0.426\mu\right)\sqrt{\mu}\,\xi_{LS} \\
\qquad -\left(3.730 - 16.903\sqrt{\mu} + 20.496\mu\right)\sqrt{\mu}\,\xi_{LS}^2 \\
\xi_{ISO,opt} = \sqrt{\dfrac{3\mu}{8(1+\mu)(1-\mu/2)}} + \left(0.151 h_L - 0.170\xi_{LS}^2\right) \\
\qquad +\left(0.163\xi_{LS} + 4.980\xi_{LS}^2\right)\mu
\end{cases}
\tag{D.5}
$$

In particular, Eq. (D.3) has been derived by considering as input on the system a harmonic force applied to the mass of the main system, i.e. LS, with the displacement amplitude fixed and independent of input frequency; furthermore, the damping of the main system has been assumed null and, so, the procedure for finding f_{opt} and $\xi_{I,opt}$ is based on the well-known fixed point theory developed by Den Hartog in [84]. The Eq. (D.4) has been derived in the same way as Eq. (D.3) with the only difference of considering a harmonic support excitation with acceleration amplitude fixed and independent of frequency. Finally, Eq. (D.5) has been derived similarly to Eq. (D.4), but in addition, the LS damping ratio, ξ_{LS}, has been taken into account; therefore, since it has not been possible to utilise the two fixed points, suggested by Den Hartog's procedure [84], it has been necessary to firstly find the optimum parameters for damped system through numerical searching and then a curve-fitting scheme has been applied to find mathematical expressions of f_{opt} and $\xi_{I,opt}$ with the minimum amount of error [86].

All the above-mentioned relationships (Eqs. (D.3) – (D.5)) have been derived from classical TMD systems; where usually low mass ratios are considered, i.e. of the order of 10^{-1}-10^{-2}, and it is necessary that the natural circular frequency of the absorber is tuned with the circular natural frequencies of the main system, usually the first, because the structural response is greatly influenced by the tuning ratio f (see section D.1). In the case of wanting to mitigate the vibration amplitudes of other modes in addition to the first, it is possible to employ multiple tuned mass dampers [100], or other vibration control techniques for the main system that show great efficiency over a wide range of λ. Consequently, these equations provide the optimal damping ratio values, $\xi_{ISO,opt}$, corresponding to the optimal tuning ratio f_{opt}. However, in the case of IIS, since the mass of the absorber is equal to a building part mass, the resulting mass ratios are much larger than the ones adopted for classical TMD, leading to a lower influence of the tuning ratio, f, on the structural response (see section D.1).

Hence, wanting to suggest an isolation damping ratio value that can be adopted in the design of IIS, it will not be possible to follow any procedures adopted for the computation of Eqs. (D.3) – (D.5)), i.e. to identify an absolute minimum value of ξ_{ISO} for a fixed value of $f = f_{opt}$ and varying μ. But, as already observed from Figure D.3 and Figure D.4 the value of *DMF* tends to become constant after a certain value of ξ_{ISO}, over the whole range of values of f. Hence, with reference to the system described by Eq. (D.1), for a fixed value of λ as the mass ratio μ varies, it is possible to identify a suggested isolation damping value, $\xi_{ISO,sug}$, for the IIS design. In fact, let us consider as the suggested value of ξ_{ISO} a value for which a small increase in the damping ratio does not lead to an appreciable response improvement. The selection condition of $\xi_{ISO,sug}$ just described can be reported in numerical terms by considering in *DMF* - f plane, the value of ξ_{ISO} for which an increase of 0.01 does not lead to a percentage change in the min-max *DMF* values (i.e. the *DMF*-f curve for ξ_{ISO} ed (ξ_{ISO} + 0.01)) greater than 1%. For example, consider the two *DMF*-f curves for μ = 0.5, λ = 1.5 and ξ_{ISO} = 0.22 - 0.23 (analogous to the red curves in surface plots of Figure D.3 and Figure D.4), where the min-max values of *DMF* are 2.025×10^{-3} - 3.131×10^{-3} for ξ_{ISO} = 0.22 and 3.117×10^{-3} - 2.044×10^{-3} for ξ_{ISO} = 0.23; therefore, the percentage change is equal to 0.43% - 0.90%, i.e. $\xi_{ISO,sug}$ = 0.22. The same procedure can be repeated by choosing λ values that most amplify the LS response, i.e. the range of values identified in section D.1, $0.5 \geq \lambda \geq 1.5$. Furthermore, the value of $\xi_{ISO,sug}$ has been limited to 0.5, as higher damping values are considered hard to achieve in design practice.

Figure D.5a shows the values of $\xi_{ISO,sug}$ as μ changes for several λ (black/grey curves) and the corresponding average values for each value of μ (red curve), i.e. $\overline{\xi}_{ISO,sug} = \text{average}\left[\xi_{I,sug(\lambda=0.5)},\ldots,\xi_{I,sug(\lambda=1.5)}\right]$. This average value could be considered as the suggested design value of the isolation damping ratio since generally a ground motion as it is known involves different frequencies with different amplitudes.

It is interesting to note that the curves for the different λ values show a very similar trend, in fact above a μ value around 0.5 the $\xi_{ISO,sug}$ value remains more or less constant; and this same trend is also shown by the $\bar{\xi}_{ISO,sug}$ curve. Thus, in general, there is less influence of the mass ratio on the definition of the suggested isolation damping value as the mass ratio increases.

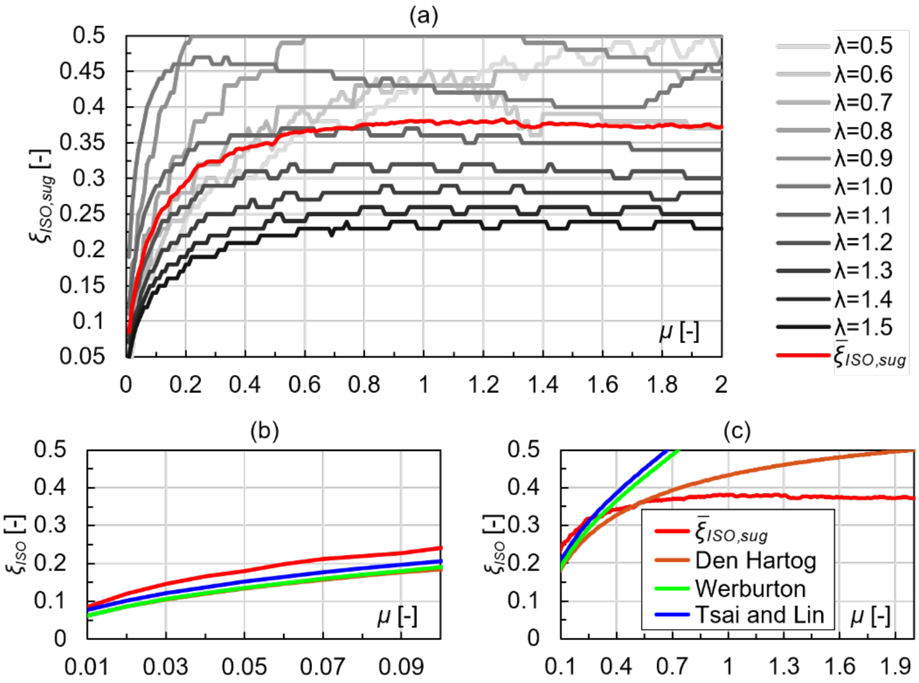

Figure D.5. (a) $\xi_{ISO,sug} - \mu$ for λ = [0.5 - 1.5] and suggested value in design practice $\bar{\xi}_{ISO,sug}$; (b) comparison between several $\xi_{ISO,opt}$ and $\bar{\xi}_{ISO,sug}$ values for μ = 0.01 - 0.1; (c) comparison between several $\xi_{ISO,opt}$ and $\bar{\xi}_{ISO,sug}$ values for μ = 0.1 – 2.

Then, in Figure D.5b compares the values of $\bar{\xi}_{ISO,sug}$ identified by the above procedure and the values of $\xi_{ISO,opt}$ suggested by Eqs. (D.3) – (D.5) in the range of mass ratios for which these equations have been suggested, i.e. $0.01 \leq \mu \leq 0.1$. It can be seen that all curves show the same trend, and the $\bar{\xi}_{ISO,sug}$ curve gives, over the whole μ range, a higher value of ξ_{ISO}; which was predictable because $\bar{\xi}_{ISO,sug}$ was evaluated without taking into account an optimal tuning value. However, the greatest differences between the several curves are recorded in the range of larger mass ratios (Figure D.5c), i.e. the case of systems with *unconventional TMD*. In fact, Eqs. (D.4) and (D.5) provide values of ξ_{ISO} greater than 0.5 for mass ratios greater than 0.7 and thus provide no practical interest results. On the other hand, the curve relating to Eq. (D.3) unlike the curve relating to $\overline{\xi}_{ISO,sug}$, which provides a constant value of ξ_{ISO} for values of μ greater than about 0.5, provides values of ξ_{ISO} that increase as μ increases until reaching the value of 0.5 for a value of μ equal to 2.

In order to investigate the difference, in terms of maximum *DMF*, between design solutions obtained through the use of the optimal parameters and those obtained through the use of the suggested value $\overline{\xi}_{ISO,sug}$, three case studies have been identified: case 1, considers the design solution obtained with $f_{opt(1)}$ and $\xi_{ISO,opt(1)}$ from Eq (D.3) versus the design solution obtained with the same $f_{opt(1)}$ and $\overline{\xi}_{ISO,sug(1)}$; case 2, considers the design solution obtained with optimal design parameters from Eq (D.4) versus the design solution obtained with the $f_{opt(2)}$ and $\overline{\xi}_{ISO,sug(2)}$; finally, case 3, considers the design solution obtained with optimal design parameters from Eq (D.5) versus the solution with $f_{opt(3)}$ and $\overline{\xi}_{ISO,sug(3)}$

The same mass ratio has been considered for all case studies, i.e. μ = 0.5. in addition, it is also recalled that a 5% damping ratio has been considered for the lower structure.

The table in Figure D.6 shows the considered values for several parameters (i.e. μ, f_{opt}, $\xi_{ISO,opt}$, $\overline{\xi}_{ISO,sug}$), while the graphs in Figure D.6 show the three case studies response through *DMF* - λ plots, where the corresponding solutions with ξ_{ISO} = 0 and ξ_{ISO} = 0.5 are shown for comparison.

Figure D.6a shows the results of case study 1, which is a special case because the value of $\xi_{ISO,opt} = \overline{\xi}_{ISO,sug}$, so we can only note the small difference in terms of maximum DMF between the solution with ξ_{ISO} = 0.35 and ξ_{ISO} = 0.50, in fact $DMF_{max,(\xi ISO=0.35)}$ = 0.0141 and $DMF_{max,(\xi ISO=0.50)}$ = 0.0146 with a percentage change of 3%, which in practice may not justify reaching ξ_{ISO} = 0.50. Next, Figure D.6b shows the case study 2 where the values of f_{opt} and $\xi_{ISO,opt}$ obtained with Eq.

(D.4) are 0.58 and 0.41, respectively; on the other hand, the value of $\bar{\xi}_{ISO,sug}$ obtained for μ = 0.5 is always equal to 0.35, so we have two different curves for $\xi_{ISO,opt}$ and $\bar{\xi}_{ISO,sug}$. The curve for $\bar{\xi}_{ISO,sug}$ reaches a higher *DMF* value (i.e. $DMF_{max,(\xi ISO=0.35)}$ = 0.0119) than the analogous curve for $\xi_{ISO,opt}$ (i.e. $DMF_{max,(\xi ISO=0.41)}$ = 0.0114) and the percentage change is equal to 4%, so, again, an increase in ISO damping ratio may not be justified. Finally, Figure D.6c shows the results for case study 3, where the values of f_{opt}, $\xi_{ISO,opt}$ and $\bar{\xi}_{ISO,sug}$ are respectively 0.52, 0.43 and 0.35; while the maximum *DMF* values for the $\xi_{ISO,opt}$ and $\bar{\xi}_{ISO,sug}$ curves are 0.0103 and 0.0106 respectively, with a percentage change of 3%; moreover, in this case the maximum *DMF* value for ξ_{ISO} = 0.5 is higher than the maximum value found for ξ_{ISO} = 0.35.

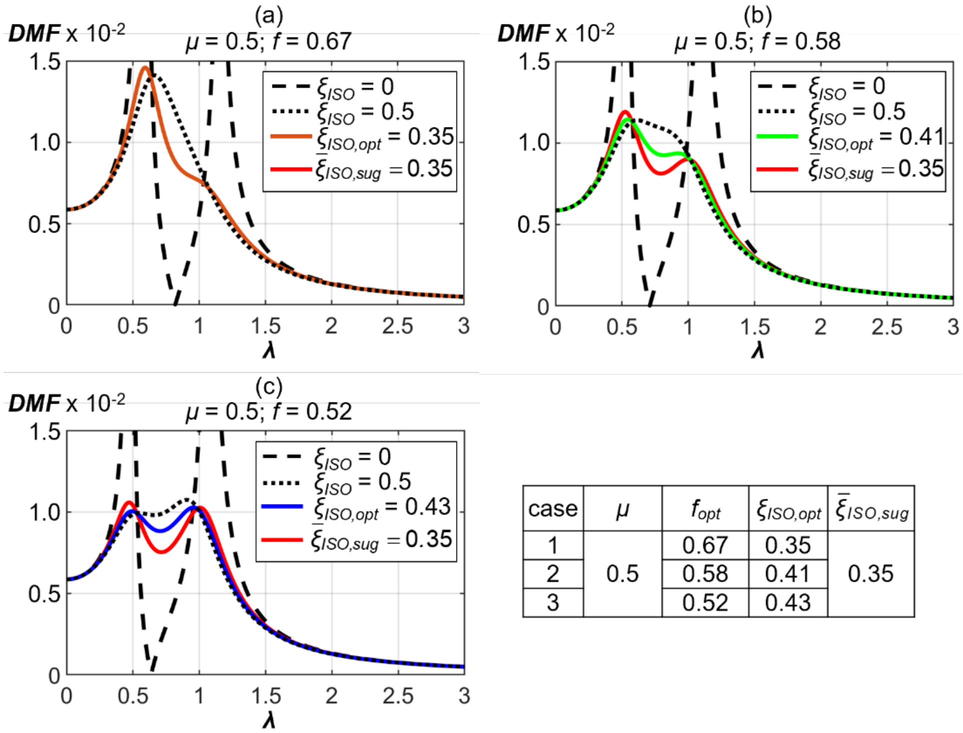

case	μ	f_{opt}	$\xi_{ISO,opt}$	$\bar{\xi}_{ISO,sug}$
1	0.5	0.67	0.35	0.35
2		0.58	0.41	
3		0.52	0.43	

Figure D.6. DMF – λ graphs for three case studies: (a) Case study 1; (a) Case study 2; (c) Case study 3.